ICBSII- 2018

PROCEEDINGS OF THE 4th INTERNATIONAL CONFERENCE ON BIOSIGNALS, IMAGES AND INSTRUMENTATION

DEPARTMENT OF BIOMEDICAL ENGINEERING

IN ASSOCIATION WITH

CENTRE FOR HEALTHCARE TECHNOLOGIES

SSN COLLEGE OF ENGINEERING
OLD MAHABALIPURAM ROAD
KALAVAKKAM- 603110
TAMILNADU, INDIA

22nd-24th MARCH 2018

2018 International Conference on Biosignals, Images and Instrumentation (ICBSII - 2018)

ISBN 978-1-5386-4473-7

Additional copies of this publication are available from Curran Associates, Inc.

57 Morehouse Lane

Red Hook, NY 12571 USA

+1 845 758 0400

+1 845 758 2633 (FAX)

Email: curran@proceedings.com

ISBN 978-1-5386-4473-7

Proceedings of the

4th International Conference on Biosignals, Images and Instrumentation

Department of Biomedical Engineering,

SSN College of Engineering

In association with

Centre for Healthcare Technologies

ICBSII - 2018
(22nd – 24th March 2018)

Editorial Board

Contents

Chief Guest's Profile

Keynote Speakers

Research Papers

Session-I
Image Processing

ISBN 978-1-5386-4473-7

Research Papers

Session-II
Instrumentation

Research Papers

Session-III
Biosignal Processing

Research Papers

Session-IV
Image Processing and Bioscience

Dedicated

to

all Staff and Students

of

the Department of Biomedical Engineering

ISBN 978-1-5386-4473-7

From the Chief Patron

Mrs. Kala Vijayakumar

President, SSN Institutions

SSN College of Engineering (SSN) is primarily focused on promoting cutting-edge research. It encourages and nurtures the novel ideas of the students and faculty members. SSN prides itself on providing holistic education to its students.

I congratulate the Department of Biomedical Engineering for organizing the 4th International Conference on Biosignals, Images and Instrumentation, in association with the Centre for Healthcare Technologies of SSN. This conference will provide the participants and the students a unique opportunity to develop enriching perspectives by interacting with some of the renowned experts from all over the world in these fields. I am certain that the talks by eminent scientists, researchers, industry-experts and the papers presented will stimulate lively discussions and will lay a strong foundation for further advanced research in these fields. I appreciate the untiring, excellent teamwork carried out by the faculty of the Biomedical Engineering department towards organizing this conference.

I am sure all the delegates will find every session interesting and fruitful. I wish the conference all success.

Mrs. Kala Vijayakumar
Chief Patron,
ICBSII – 2018.

From the Patron

Dr. S. Salivahanan

Principal, SSN College of Engineering

I am pleased to mention that SSN College of Engineering is ranked 27th among all engineering colleges and 80th among all educational institution in India Rankings 2017 by NIRF, MHRD. The institution provides quality education to students from all economic strata and it is the best at serving the need of the society by graduating talented, broadly educated engineers with good technical knowledge, conducting high quality research, developing breakthrough technologies, emphasizing on 360 degree development of each and every student which makes them stand out from the crowd in all aspects. The college aims towards not just developing knowledge but also conducts a range of events from social awareness to international programs to impart life skills, competencies and attributes which are greatly valued in today's global work environment.

Biomedical engineering is a multidisciplinary field integrating Engineering and healthcare. It focuses on the advances that improve human health and healthcare at all levels. The department's engagement in wide spectrum of activities with involvement of students and faculty along with strategic planning process has strengthened it.

To add feather to the crown, the department is organizing the 4th International Conference on Biosignals, Images and Instrumentation (ICBSII 2018) in a manner befitting the stream. I congratulate the entire team of Biomedical Department for structuring it to perfection and wish them all success.

Dr. S. Salivahanan,
Patron,
ICBSII – 2018.

ISBN 978-1-5386-4473-7

From the Convener

Dr. A. Kavitha

Professor & Head,
Department of Biomedical Engineering
SSN College of Engineering

Education is a holistic endeavour, creating new paths with endless boundaries and priming minds to orient one to the world. That being said, it gives me immense pleasure to present the Fourth International Conference on Bio-signals, Images and Instrumentation.

Biomedical engineering discipline is one which catalyzes interactions between biologists, physical scientists, and engineers to benefit medicine and human health. This serves society by conducting research that develops quantitative linkages across scales in the human body and uses that development to build new tools to improve human health. The outcomes of research assume a whole new level of importance and significance.

The department is frequently organizing workshops, seminars, project exhibitions and guest lectures on diverse concepts related to the core and interdisciplinary subjects in biomedical engineering to equip the students in gaining a comprehensive knowledge of the industrial requirements to the fullest.

The Centre for Healthcare Technologies, a multidisciplinary research initiative, concentrating on research through innovation in healthcare, in association with the Department of Biomedical Engineering, is organizing the 4th International Conference on Biosignals, Images and Instrumentation, hoping to instil research aptitude in students and provide a great platform for the researchers to showcase their work in various domains of Biomedical Engineering.

It is rightly said, coming together is a beginning, Keeping together is a progress, and Working together is a success. With confidence, we progress towards success!!!

Dr. A. Kavitha
Convener,
ICBSII – 2018.

ISBN 978-1-5386-4473-7

From the Coordinators

Dr. V. Mahesh

Associate Professor,
Department of Biomedical Engineering
SSN College of Engineering

The main objective of this conference is to create professional interactions among eminent personalities, a platform for exchange of ideas and spread of knowledge.

This conference will be a perfect platform for scientists, researchers, academicians to express their innovative thoughts and unique research work at a global level.

It is also aimed at emphasizing the current advancements in the industry to make undergraduate and postgraduate students unite their ideas in terms of project development and provides an opportunity to students to meet and interact with International speakers and scientists of National Importance.

This conference provides scope for various disciplines of medicine, engineering, healthcare and software in a single venue to elevate medical and healthcare industry to generate standards and will provide a wonderful forum to unveil the efforts of researchers, engineers and scholars.

I extend my sincere gratitude to the management of SSN College of Engineering, Mrs.Kala Vijayakumar, President, SSN Institutions and Dr.S.Salivahanan, Principal, SSN College of Engineering for granting the department a wondrous opportunity to organize and conduct this prolific occasion helping us to take it forward to the global level.

Dr. V. Mahesh
Secretary,
ICBSII – 2018.

From the Coordinators

Dr. S. Bagyaraj

Associate Professor,
Department of Biomedical Engineering
SSN College of Engineering

Welcome to the IEEE sponsored fourth International Conference on Biosignals, Images and Instrumentation (ICBSII 2018) on March 22nd to March 24th, 2018 in SSN College of Engineering, Kalavakkam - 603110. The purpose of this Conference is to bring together researchers and industry practitioners to present and discuss novel approaches and solutions as well as recent results in the field of Biological, Medical, Health Care, Pharmaceutical, Biotechnology, Bioinformatics, Computer Science, Information Technology and Communication for creating synergy and supporting Interdisciplinary Research, and to exchange ideas and explore new avenues of collaborations.

This conference collected research papers on the above research issues from India and abroad countries. Papers collected in this international conference were rigorously reviewed by the scientific programme committee members. According to the review results, the program committee members have selected twenty nine high quality papers to be presented in this conference. Many researchers from all over the world have kindly helped us to prepare and organize the ICBSII-2018. The conference turned out to be a forum for scientists and researchers all over the world to share their ideas, experiences, findings, and conclusions of their work in due course of their scientific research.

First of all, I would like to thank the ICBSII-2018 organization and technical program committee for their support, constructive feedback, and timely proposal review. I extend my sincere gratitude to the management of SSN College of Engineering, Mrs.Kala Vijayakumar, President, SSN Institutions and Dr. S. Salivahanan, Principal, SSN College of Engineering for granting the department a wondrous opportunity to organize and conduct this prolific occasion helping us to take it forward to the global level.

Finally, I also would like to take opportunity to thank all external reviewers and contributing authors for producing high quality papers to be presented at ICBSII 2018.

Dr. S. Bagyaraj
Secretary,
ICBSII – 2018.

ISBN 978-1-5386-4473-7

From the Organising Secretary

Ms. M. Dhanalakshmi

Assistant Professor,
Department of Biomedical Engineering
SSN College of Engineering

The international conference aims to create a platform to share knowledge and ideas with the eminent speakers from the world.

It is also focussed on the advancements and current trends in the industry to provide an opportunity for undergraduate students with their ideas in terms of project and project development.

The conference would be a forum for scientists and researchers from various disciplines of medicine, engineering and healthcare in a single venue to discuss and share their ideas, experiences, findings and outcome of their work in due course of their scientific research.

I extend my sincere gratitude to the management of SSN College of Engineering, Mrs. Kala Vijayakumar, President, SSN Institutions and Dr. S. Salivahanan, Principal, SSN College of Engineering for providing the department a great opportunity to organise and conduct this prolific occasion helping us to take forward to the global level. I would like to extend my heartfelt thanks to our HoD, Dr. A. Kavitha for giving me such an opportunity to organize this prestigious event.

Ms. M. Dhanalakshmi
Organising Secretary,
ICBSII – 2018.

ISBN 978-1-5386-4473-7

Conference Organizing Committee

Chief Patron

Ms. Kala Vijayakumar, President, SSN Institutions

Patron

Dr. S. Salivahanan, Principal, SSN College of Engineering

Convener

Dr. A. Kavitha, Professor and HOD/BME

Coordinators

Dr. V. Mahesh

Dr. S. Bagyaraj

Organizing Secretary

Ms. M. Dhanalakshmi

Treasurer

Dr. R. Subashini

Committee Members

Dr. S. Pravin Kumar

Dr. L. Suganthi

Dr. J. Vijay

Dr. S. Arun Karthick

Dr. R. Sivaramakrishnan

Dr. Sachin Gaurishankar Sarate

Dr. B. Geethanjali

Mrs. R. Nithya

Mrs. K. Nirmala

Mrs. B. Divya

Technical Advisory Committee

International Advisory Committee Members

- **Dr. Sriram Balasubramanian, Asso. Prof., Drexel University, USA**
- **Dr. Kong Pui Wah, Asso. Prof., NTU, Singapore**
- **Dr. Teo Ee Chon, Asso. Prof., NTU, Singapore**
- **Dr. M. Murugappan, Asso. Prof., KCST, Kuwait**
- **Dr. Eko Supriyanto, Asso. Prof., Universiti Teknologi Malaysia, Malaysia**
- **Dr. S. Arunachalam, Asso. Prof., JIC, Kingdom of Saudi Arabia**
- **Dr. Tinashe Mutswangwa, Senior Lecturer., UCT, South Africa**
- **Dr. Sekar Raju, Asso. Prof., Xi'an jiaotong-Liverpool University, China**
- **Dr. J. Jesu Christopher, Senior Scientist, ASTRAZENCA, Cambridge, UK**
- **Dr. S. Ramji, Queen's University Belfast, UK**

National Advisory Committee Members

- **Dr. S. Ramakrishnan, Prof., IIT Madras**
- **Dr. S. Muttan, Prof., Anna University**
- **Mr. S. Sivagnanam, Additional Industrial Advisor.,Govt. of India, MSME**
- **Dr. R. Periyasamy, Assistant. Prof., NIT Raipur**
- **Mr. K. Mohanavelu, Scientist E, DEBEL., DRDO, Bangalore**
- **Dr. Niranjan D. Khambete, Biomedical Head., Pune Govt. Hospital, Pune**
- **Dr. Kumar Rajamani, Manager, Robert Bosch Gmbh, Bangalore**
- **Dr. G. Sudhir, Orthopaedic Spine Surgeon., SRMC, Chennai**
- **Dr. G. Kumaramanickavel, Director of Research., Narayana Nethralaya**
- **Dr. B. Minimol, Asso. Prof., Gov. Model Engineering College, Kochi**
- **Dr. C.M. Sujatha, Asso. Prof., Anna University, Chennai**

Review Committee

- **Dr. Vivek Padmanaabhan Indramohan** – Senior Lecturer, Brimingham City University,UK
- **Dr. Kong Pui Wah** – Deputy Head, Associate Professor, Nanyang Technological, University, Singapore
- **Dr. Teo Ee Chon** – Professor, Nanyang Technological University, Singapore
- **Dr. R. Sivaramakrishnan** – Research Scientist, National Institutes of Health, USA
- **Dr. S. Pravin Kumar** – Research Specialist, Palacký University, Olomouc, Czech Republic
- **Dr. Rahuman Sheriff** –Biomodels Project Leader, European Bioinformatics Institute , UK
- **Dr. R. Yuvaraj** – Research Scientist, Nanyang Technological University, Singapore
- **Dr. Aleksandra Kawala-Janik** – Research Scientist, Opole University of Technology, Poland
- **Dr. Eko Supriyanto** – Professor, IJN-UTM Cardiovascular Engineering Centre, UTM, Malaysia
- **Dr. Sriram Balasubramanian** – Associate Professor, Drexel University, USA
- **Dr. M. Murugappan** – Associate Professor, Kuwait College of Science and Technology, Kuwait
- **Dr. S. Arunachalam** – Associate Professor, JIC, Kingdom of Saudi Arabi
- **Dr. T. Prabakar** – Associate Professor, Dept. of. ECE, GMR Institute of Technology, Rajam, AndhraPradesh, India
- **Dr. T.S.Karthik –** Associate Professor, Dept. of ECE, B.V.Raju Institute of Technology, Telengana, India
- **Dr. M. Akila** – Professor, Dept. of ECE, KPR Institute of Engineering and Technology, Coimbatore, India
- **Dr. Balaji.V**– Associate Professor, Dept. of ECE, KPR Institute of Engineering and Technology, Coimbatore, India
- **Dr. B. Jaishankar** – Associate Professor, Dept. of ECE, KPR Institute of Engineering and Technology, Coimbatore, India
- **Dr. O. Uma Maheswari** – Assistant Professor (Senior Grade), Department of ECE, Anna University, Chennai, India

Review Committee

- **Dr. Ravish Rao –** Associate Professor, Department of Medical Electronics, Dr.Ambedkar Institute of Technology, Bangalore, India
- **Dr. S. Prabakar** – Professor & Head, Department of Biomedical Engineering, DRNGP Institute of Technology, Coimbatore, India
- **Dr. R. Periyasamy** – Assistant Professor, Department of Biomedical Engineering, NIT Raipur, India
- **Dr. T. Christy Bobby –** Assistant Professor, Deptartment of ECE, MSRUAS, Bangalore, India.
- **Dr. M. Kayalvizhi** – Associate Professor & Head, Department of Biomedical Engineering Agni College of Technology, Chennai, India
- **Dr. A. Kavitha –** Professor, Department of Biomedical Engineering, SSNCE, Chennai**,** India
- **Dr. C. M. Sujatha** - Assistant Professor, Dept. of ECE, Anna University, India
- **Dr. G. Kavitha** - Assistant Professor (Senior Grade), MIT campus, Anna University, India
- **Dr. A. Mythili** - Associate Professor, Sensor and Biomedical Technology Division, School of Electronics Engineering (SENSE), VIT Vellore campus, India
- **Dr. N. Venkateswaran –** Professor, Department of ECE, SSNCE, Chennai, India
- **Dr. V. Mahesh –** Associate Professor, Department of Biomedical Engineering, SSNCE, Chennai, India
- **Dr. K. Kamalanand –** Assistant Professor, MIT campus, Anna University, India
- **Dr. B. Minimol** – Associate Professor, Department of Electronics & Biomedical Engineering, Model Engineering College, Kerala, India
- **Dr. R. Tamilselvi** – Professor, Department of ECE, Sethu Institute of Technology, Madura
- **Dr. D. Vaithyanathan –** HOD, Department of ECE, NIT, Delhi, India
- **Dr. A. K. Jayanthy –** Professor, Department of Biomedical Engineering, SRM University, Chennai, India
- **Dr. S. Karthiga** – Associate Professor, Department of Information Technology, SSNCE, Chennai, India
- **Dr. P. Rajasekar** – Senior Assistant Professor, Department of Biotechnology, Rajalaksmi Engineering College, Chennai, India
- **Dr. Shoba Narayan –** Senior Assistant Professor, Chettinad University, Chennai, India

ISBN 978-1-5386-4473-7

Review Committee

- **Dr. Jaganathan. M –** Associate Professor, VIT, Chennai, India
- **Dr. K. Adalarsasu –** Associate Prof, School of EEE, Sastra University, Tanjavur, India
- **Dr. Ganesh Vaidhyanathan** – Principal, SVCE, Chennai, India
- **Dr. T. R. Ganesh babu –** Professor, Muthyammal Engineering College, Rasipuram, India
- **Dr. M. C. Jobin Christ** – Associate professor, Department of Biomedical Engineering, Rajalakshmi Engineering College, Chennai, India
- **Dr. K. Vidhya** – Professor, School of ECE, Saveetha University, Chennai, India
- **Dr. E. Priya Beatrice –** Associate Professor, Department of ECE, Sri Sairam Engineering College, Chennai, India
- **Dr.B.Padmapriya –** Associate Professor, Department of Biomedical Engineering, PSG College of Technology, India
- **Dr. Judith Justin** – Professor & Head, Department of Biomedical Instrumentation Engineering, Avinashilingam University, India
- **Dr.D.Balasubramanian –** Professor and Head, Department of ECE, GKM college of Engineering and Technology, India
- **Dr. L. Suganthi** – Associate Professor, Department of Biomedical Engineering, SSN College of Engineering, Chennai, India
- **Dr. S. Bagyaraj –** Associate Professor, Department of Biomedical Engineering, SSN College of Engineering, Chennai, India
- **Dr. J. Vijay –** Associate Professor, Department of Biomedical Engineering, SSN College of Engineering, Chennai, India
- **Dr. S. Arun Karthick –** Associate Professor, Department of Biomedical Engineering, SSN College of Engineering, Chennai, India

Student Organizing Team

Registration:

- Viswanath S. – Third Year, UG
- Praveen Kumar G. – Third Year, UG
- Sangeetha B. – Third Year, UG
- Apurva S. – Third Year, UG
- Abarna R – Third Year, UG
- Kirthana M. – Third Year, UG
- Aravindarajan – Third Year, UG
- Om Prakash S – Third Year, UG

Conference Proceedings:

- Rathi Adarshi R. – Final Year, UG
- Meghna Murali. – Third Year, UG
- Manuj R. –Third Year, UG
- Aparna B. –Third Year, UG
- Harshni V. – Third Year, UG
- Priyadarshini K. – Third Year, UG
- Sreeja P. –Third Year, UG
- Sucharitha S. Prakash. –Third Year, UG
- Viswath Naryanan R. –Third Year, UG

Accommodation:

- Pragadeesh T. – Final Year UG
- Annamalai M. – Final Year, UG
- Sanju Varshini T. – Final Year, UG
- Gomathi S. – Final Year, UG

Food Committee:

- Natarajan A. –Final Year, UG
- Suganraj V. – Final Year, UG
- Vignesh R. – Final Year, UG
- Anjana K R. – Third Year, UG

- Anuharshini K. – Third Year, UG
- Arun Kumar K. – Third Year, UG
- Pavithran P. G. – Third Year, UG
- Sivaranjani M. – Third Year, UG
- Sowmiya M. – Third Year,UG

Hall Arrangements:

- Priyanga T. – First Year, PG
- Kesiya M. – First Year, PG
- Ragapriyadharsini S. – First Year, PG
- Preethi Kurian. – First Year, PG
- Srithaladevi E. – First Year, PG
- Bharathi G. – First Year, PG
- Pragadeesh T. – Final Year, UG
- Sangeetha B. – Third Year, UG
- Apurva S. – Third Year, UG
- Asha R. – Third Year, UG
- Sowmiya M. – Third Year, UG
- Devayani S. –Third Year, UG
- Manuj R. –Third Year, UG

Transport Arrangements:

- Ashok Kumar S. K. – Final Year, UG
- Aniruddh Balaji R. – Third Year, UG
- Bhargav M. – Third Year, UG
- Jerome Jeyakar S. A. – Third Year, UG
- Raviprasad R. V. – Third Year, UG
- Sai Sudan R. – Third Year, UG

Culturals:

- Swetha S. – Final Year, UG
- Manasvi S. – Final Year, UG

ISBN 978-1-5386-4473-7

4th International Conference on Biosignals, Images and Instrumentation ICBSII 2018

CHIEF GUEST PROFILE

ISBN 978-1-5386-4473-7

The Chief Guest

DR. PAUL W. BRANDT-RAUF

Professor and Dean,

School of Biomedical Engineering,

Drexel University.

PROFILE:

Dr. Paul W. Brandt-Rauf is Dean and Distinguished University Professor in the School of Biomedical Engineering, Science and Health Systems at Drexel University. Dr. Brandt-Rauf received his BS, MS, and ScD in Applied Chemistry and Chemical Engineering, his MD, and his MPH and DrPH in Environmental Sciences from Columbia University. He did post-graduate training in anatomic/environmental pathology, internal medicine, and occupational/environmental medicine, and he is certified by the American Board of Internal Medicine and the American Board of Preventive Medicine in Occupational Medicine. He is a Fellow of the American College of Physicians, the American College of Preventive Medicine, the American College of Occupational and Environmental Medicine, and the Royal Society of Medicine.

Dr. Brandt-Rauf has been the recipient of several honors and awards including: the Allan Rosenfield Alumni Award for Excellence in Public Health from Columbia University; the Robert R.J. Hilker Award; the Harriet Hardy Award; the Robert A. Kehoe Award of Merit, the Meritorious Service Award and the Knudsen Lifetime Achievement Award of the American College of Occupational and Environmental Medicine; and a Certificate of Appreciation from the National Institute for Occupational Safety and Health. He has been featured in an award-winning film documentary (Blue Vinyl). He has been ranked among the top twenty Deans and Directors of Public Health and previously was regularly listed among the Top Doctors in Occupational Medicine and the Top Doctors in Preventive Medicine.

ISBN 978-1-5386-4473-7

4th International Conference on Biosignals, Images and Instrumentation ICBSII 2018

KEYNOTE SPEAKERS' PROFILE

ISBN 978-1-5386-4473-7
IEEE sponsored 4th International Conference on Biosignals, Images and Instrumentation, SSNCE, Chennai. ICBSII 2018 – 22nd-24th Mar'18

Lower Limb Exercise Therapy for Runners with Chronic Low Back Pain

Dr. KONG Pui Wah

Abstract:

Chronic low back pain (CLBP) is common and contributes to significant disability and healthcare costs. The mechanism and etiology of cLBP are frequently unclear, and treatment choices vary. Chronic low back pain (cLBP) is common among runners but there is currently no specific protocol for managing runners with cLBP. This study aimed to compare the treatment effect of lower limb (LL) exercises versus conventional lumbar extensor (LE) and lumbar stabilization (LS) exercises in recreational runnerscLBP.

The study involved 84 recreational runners with cLBP, who were allocated to three exercise groups (LL, LE, LS) for an 8-week intervention. Outcome measures included self-rated pain and running capability, lower limb strength, back muscles function, and running gait. Participants were assessed at pre-, mid- and end-intervention; selected outcomes also followed up at three and six months. Generalized estimating equation was adopted to examine group-by-time interaction. The conclusion of this study was that LL exercise therapy could be a new option for cLPB management given its superior effects in improving running capability, knee extension strength, and running gait.

Dr. KONG Pui Wah,
Professor,
NTU Singapore

Dr.Veni Kong graduated from the Department of Sports Science and Physical Education at the Chinese University of Hong Kong in 2000. She went on to study at Loughborough University (UK) to obtain her MSc in Sports Science in 2001, followed by a PhD in Sports Biomechanics in 2005. She started her career as an Assistant Professor in the Department of Kinesiology at the University of Texas at El Paso from 2005 to 2008. She was a visiting faculty member at the Emergency Responder Human Performance Laboratory, University of Pittsburgh, School of Medicine for one year prior to joining the National Institute of Education, Nanyang Technological University, Singapore in July 2009

Dr. Kong's research interests include sports and clinical biomechanics. She has led projects on footwear and gait analysis on athletes, firefighters and older adults. She also worked closely with hospitals and healthcare professionals to address clinical problems such as foot health and low back pain management. Her research on computer simulation models of springboard diving has received international awards including those from the International Sports Engineering Association and British Association of Sport and Exercise Sciences.

ISBN 978-1-5386-4473-7

Design and Development of Smart FES system for physically challenged persons

Dr. Dinesh Bhatia

Abstract:

One of the most exciting recent advances in the neuroprosthetics field has been the application of bio-signals in the design of Functional Electrical Stimulation (FES) devices. Different approaches in the field of Functional Electrical Stimulation (FES) enabling control of human gait to address fundamental perquisites by enabling FES walking systems to become safer, more practical, comfortable and therefore clinically efficacious have been tried over the years.

Several forms of disability in humans due to paralysis, it appears possible to regain some measure of functional control of movement through direct electrical stimulation of paralyzed muscles.

This study provides a comprehensive overview of the advancements in clinical uses of Functional Electrical Stimulation for functional and therapeutic applications in subjects with spinal cord injury or stroke. Weighed opinions of perspectives on future developments and clinical applications of smart FES device developed will also be discussed.

Dr. Dinesh Bhatia,
Professor,
North Hill University,
Shilong, India .

Dr. Dinesh Bhatia pursued his PhD in Biomechanics and Rehabilitation Engineering from MNNIT, Allahabad, India in 2010 with Bachelor's (2002) and Master's degree (2004) in Biomedical Engineering from Mumbai University. He completed his MBA from IMT Ghaziabad in 2007. He is currently working as Associate Professor and Head, Department of Biomedical Engineering, North Eastern Hill University (NEHU), Shillong, Meghalaya, India. He was selected for the "Young Scientist Award (BOYSCAST)" in (2011-12) by Government of India to pursue research in osteoarthritis (OA) for one year at Adaptive Neural Systems Laboratory, Biomedical Engineering Department, Florida International University, Miami, Florida, USA. He is also the recipient of "INAE fellowship award" in 2011 by Indian National Academy of Engineering.

His research focuses on understanding muscle mechanics, joint kinematics and dynamics involved in performing locomotion and routine tasks and undermining it effects during an injury or disease. His interest areas are medical instrumentation, biomechanics and rehabilitation engineering, medical informatics, signal and image processing, marketing and international business.

ISBN 978-1-5386-4473-7

Design/ Material/ Performance Evaluation of Footwear by Gait analysis

Dr. G. Saraswathy

Abstract:

Gait is the medical term to describe our pattern of walking. Footwear design, materials used for footwear fabrication and performance of footwear during various activates of wearer strongly influence the gait and posture. Physiological factors are difficult to control once developed and it involves cost. But prevention of gait changes due to footwear is possible by designing, constructing and evaluating the performance of footwear through gait analysis.

On the other hand, footwear can also act as therapeutic aid to correct and improve gait in case of neuromusculoskeletal disorders. In such cases, design and development of footwear based on individual gait or characteristic gait of particular condition is crucial. Gait analysis helps to design the footwear to accommodate the permanent deformity, to treat the functional deformity and to improve the abnormal gait and also to prevent the foot related complications due to various diseases. Kinetic study of gait wearing footwear will help to choose materials which can increase foot comfort by providing optimal ground reaction force and shock absorption.

Performance of footwear can be evaluated by combined three dimensional gait analysis (3DGA) which includes kinematics, kinetic and electromyographical study.3DGA can give fruitful information regarding the activation of respective muscles at respective phases of gait cycle along with range of motion of limb joints during various phases of gait cycle in three planes of motion. Identification of gait alteration due to footwear by gait analysis will led to design of biomechanically compatible footwear as gender specific, age specific, activity specific and performance specific in future.

Dr. G. Saraswathy,
Scientist, Gait Analysis Laboratory,
CSIR-Central Leather Research Institute,
Chennai, India

Dr. G. Saraswathy, currently working as a scientist in Shoe and Product Design Centre, CSIR, Chennai. She pursued her PhD and Master's degree (2004) in Biomedical Engineering from from Jadhavpur University, Kolkata with an undergrad degree Pharm from Dr.M.G.R Medical University, Tamil Nadu. She has also published numerous papers in national and international conferences and she was granted a patent on her work "A Formulation for the process of taking impression of an object". She has various credentials to her name like UGC fellowship for M.E., Woman Scientist Fellowship, Department of Science & Technology, and Govt. of India.

She also has experience in operating scientific instruments like FTIR & ATR Spectrophotometer, Thermogravimetric Analyzer, 3D Gait and Motion analysis system for complete analysis of kinematic, kinetic and muscle activity on human locomotion. She also has handled plantar pressure measurement systems in shoe and HR Mat for evaluation of static and dynamic pressure distribution under the foot and performance of polymeric insole and sole materials

Advance Post Processing Techniques in Clinical Scenario

Mr. Sunith George

Abstract:

Mr. Sunith George,
Sr. Clinical Education Manager,
GE Healthcare,
India

Sunith George is a seasoned GE professional with more than 20 years in Diagnostic Radiology Technology. With a great educational background in Radiology technology from India's top institutions, Sunith has a track record of exceptional experience in various positions at GE Healthcare.

Currently, Sunith is working as the Clinical Education Manager for Education & Skill development for GE healthcare across Africa, South Asia and ASEAN regions. Sunith's interests are in the areas of Oncology Applications including RT Simulation, CT and MR Cardiac Imaging, Radiation protection and Low dose CT, Silent and Zero TE imaging in MR, Non contrast perfusion and angiograms in MR, Dual Energy and Spectral CT innovations. Apart from work, Sunith has also been a speaker in various radiology forums like IRIA, ISCT, etc and has delivered many lectures and external class room sessions including faculty development programs in leading Engineering and Paramedical institutions across India and south Asia. He has a long list of achievements and has won many awards. Sunith has been closely associated with the Engineering team for the ICFC project, and has played a key role in making GE Healthcare's clinical application team a role model in the industry.

ISBN 978-1-5386-4473-7
IEEE sponsored 4th International Conference on Biosignals, Images and Instrumentation, SSNCE, Chennai. ICBSII 2018 – 22nd-24th Mar'18

ECG Simulation by 2D Whole Heart Modeling

Dr. Minimol. B

Abstract:

Computer vision Simulation of ECG from cardiac models has many potential applications. Whole heart models generally mean a macroscopic model which represents the total function of the heart. Usually they are three-dimensional and are computationally expensive. But a two-dimensional model is computationally more tractable. The formulation of a 2D whole heart cardiac model based on gap junction conductance (GJC) that connects the cells is adopts a microscopic approach as far as the impulse propagation is considered (role of cell to cell connections through GJC, and heterogeneity of action potential duration (APD) variations are explored) and a macroscopic approach as far as the generation of ECG (whole heart approach) is considered. This will help to find a forward relation of propagation of the cardiac impulse to ECG. The major applications of the models are

- Understand the generation of ECG signal and the relationship of its interval, amplitude and duration of each wave to the various GJC and APD.
- Simulate different types of arrhythmias by varying the parameters of the cells defining the model
- Explore the therapeutical effects of drugs and pacing therapies in case of atrial fibrillation. It can also suggest new possible methods of treatment techniques which alter GJC and eliminates atrial fibrillation

Dr. Minimol. B
Professor,
Department of BME,
Govt. Model Engineering College,
Cochin, India

Dr.Minimol.B, currently working as an assistant professor in the department of Biomedical Engineering in Govt.Model Engineering College, Thrikkakara, Cochin, and Kerala completed her Doctorate from IIT Madras with a Masters from College of Engineering, Guindy and an UG degree from Model Engineering College, Kochi. Her areas of research interests include computational modelling of physiological systems, cardiac electrophysiology, Biomedical signal processing and neural networks. She has 23 years of teaching experience in the field of biomedical engineering. She has published two international journals in cardiology.

ISBN 978-1-5386-4473-7

Patient Centered Design

Mr. C. J. Ravisankar

Abstract:

Traditional disease based medicine focused on understanding the biology of the disease and addressing it with practice guidelines. If you followed the practice guidelines for specific conditions, there were specific outcomes. The diagnosis and treatment are standardized for a set of outcomes and do not take into consideration patient related factors like social conditions, behavior, or physiological needs. This has resulted in variation in expected outcomes when patient reaction and behavior are not identical. The variation also results in leakages like sub-optimal outcomes, added cost and patient dissatisfaction. Patient centered design on the other hand considers the patient as an integral part of the diagnosis and treatment. Social factors like literacy, employment, and community access, behavioral factors like norms and beliefs, ability to withstand pain along with co-morbidities play a role. Understanding and designing healthcare - drugs, devices or hospitals, for patients increases the efficiency of the overall system.

A report from the Kaiser Family Foundation estimates that just 10 percent of our health is determined by the care we receive within a clinic's walls. Individual behavior and social circumstances, including where we live, how we make a living, and what services we have access to, contribute about 60 percent. (An individual's genetics make up the remaining 30 percent.) And until our health care system—including the technology that supports it—addresses those factors, we won't see the significant improvements in quality of care or cost savings these investments were supposed to bring. Patient centered design allows for incorporating these social and behavioral factors to allow improved health outcomes.

Mr.C.J.Ravisankar,
Managing Director,
Sagitec Healthcare
and Life Sciences,
India

Mr. Ravi has held several executive positions during his professional tenure in the USA and India including Global Solutions Head at HCL Technologies. He brings extensive business, domain and delivery experience in Healthcare. Ravi is currently focused on building a digital health stack to help enterprises navigate the disruption in healthcare.

Ravi has an undergraduate degree in Electrical Engineering and MBA from University of Arizona.

ISBN 978-1-5386-4473-7

4th International Conference on Biosignals, Images and Instrumentation

ICBSII 2018

RESEARCH PAPERS

.

An Approach to Extract Optic -Disc from Retinal Image using K-means Clustering

N. Kowsalya, A. Kalyani, C. Jasmine Chalcedony, R. Sivakumar, M. Janani*, V. Rajinikanth

Department of Electronics and Instrumentation Engineering,
St. Joseph's College of Engineering,
OMR, Chennai 600119, India.
Email: jananimohan144@gmail.com

Abstract—**generally, retinal picture valuation is commonly executed to appraise the diseases. In this paper, an image examination technique is implemented to extract the Retinal-Optic-Disc (ROD) to assess its condition. An approach based on the combination of Kapur's entropy and K-means clustering is considered here to mine the optic disc region from the RGB retinal picture. During the experimental implementation, this approach is tested with the DRIVE and RIM -ONE databases. Initially, the DRIVE pictures are considered to appraise the proposed approach and later, the RIM-ONE dataset is considered for the testing. After extracting the ROD, comparative analyses with the expert's Ground-Truths are carried out and the image similarity values are then recorded. This approach is then validated against the Otsu's+levelset existing in the literature. All these experiments are implemented using Matlab2010. The outcome of this procedure confirms that, proposed work provides better picture similarity values compared to Otsu's+levelset. Hence, in future, this procedure can be considered to evaluate the clinical retinal images.**

Keywords—Retinal picture; Optic-disc; Kapur's entropy; K-means clustering; validation.

I. INTRODUCTION (*HEADING 1*)

Retinal abnormality is a common disease among humans. Optic Disc Disorder (ODD) is one of the widespread retinal abnormality occurs due to a variety of reasons, like aging, infection, and diabetes [1]. Retinal pictures are commonly used in the diagnosis and healing of various diseases based on the structural and physical distinction in optic disc and blood vessels. Hence, optic-disc extraction is essential to examine the diseases, such as ocular hypertension (OHT), diabetic retinopathy, glaucoma, and papilloedema [2]. Hence, due to its clinical importance, the ODD examination procedures are widely discussed by the researchers [3, 4, 31-33].

Earlier studies on ODD examination procedures attempts to utilize conventional and heuristic procedures to extract and localize Optic-Disc (OD) from retinal images [5]. The work by Sudhan et al. [6] implements a two -step practice based on Otsu's function + level set (OFLS) to mine the optic-disc of RIM-ONE [7,8]. In this approach, images of different ODDs are considered and the extracted disc is evaluated against the ground-truths (GT) in order to compute the similarity metrics. This procedure offered a satisfactory result for all the disease cases adopted in their work. Shree et al. [5] proposed an hybrid technique based on the Shannon's entropy+levelset (SELS) to mine the OD of RIM-ONE [7,8] and validated the performance of levelset (DRLS) segmentation approach with the exiting Chan-Vese (CV) and Water Shed (WS) approaches. This work confirmed that, SELS approach offered superior result compared with the CV and WS. The approach of Sudhan et al. [6] discussed about the recognition of glaucoma using the fundus image segmentation and feature extraction procedure. Amin et al. [9] discussed about the recognition and categorization of diabetic retinopathy by structural predictors of intense injuries. Various procedures based on the optic cup to disc ration also proposed to examine the abnormalities in retinal OD [1-4, 10]. The above said works confirm that, correctness in ODD recognition and evaluation depends principally on the accurateness of image segmentation technique.

The main aim of this paper is to implement a heuristic algorithm assisted ODD evaluation procedure for RGB retinal images. Initially, the Shannon's entropy of Shree et al. [5] is adopted to pre-process the DRIVE [11] and RIM-ONE retinal pictures and found that, the Shannon's approach offered better result only for RIM-ONE pictures. Hence, Kapur's entropy approach is then tried and sufficient result is obtained with both DRIVE and RIM-ONE pictures. The proposed approach implements a tri-level thresholding based on the Firefly Algorithm (FA) driven Kapur's entropy and segmentation of OD based on K -means clustering (KMC). In order to verify the superiority of the proposed procedure, a relative examination is performed among extracted OD and GTs of the chosen test picture and the image similarity measures and the statistical measures are then computed [12-14]. Finally, proposed technique is validated with respect to the recent work based on OFLS discussed in Sudhan et al. [6]. The experimental outcome confirms that, proposed procedures help in attaining the better values of image similarity and statistical approaches.

II. METHODOLOGY

This section briefs about the FA, dataset considered and the methods implemented to examine the retinal OD.

A. Firefly Algorithm (FA)

FA is a bio-inspired technique discussed firstly by Yang by imitating the blinking prototype created by fireflies [15, 16]. .

Let there are two fireflies F_1 and F_2 in optimization search, the movement in fascinated firefly F_1 towards firefly F_2 can be mathematically represented as;

$$X_{F_1}^{t+1} = X_{F_1}^{t} + \beta_0 e^{-\mu d_{xy}^2}(X_{F_2}^{t} - X_{F_1}^{t}) + \alpha_1 . sign(rand - 1/2) \oplus B(s) \quad (1)$$

where $X_{F_1}^{t+1}$ is restructured place of F , $X_{F_1}^{t}$ is beginning setting of firefly, $\beta_0 e^{-\mu d_{F_1F_2}^2}(X_{F_2}^{t} - X_{F_1}^{t})$ the attractive force between fireflies, $B(s) = A.|s|^{\alpha/2}$ is Brownian walk scheme, A is an arbitrary variable, β is spatial supporter and α is temporal supporter. Related details on FA can be found in [17-19].

B. Kapur's Entropy (KE)

KE was implemented in 1985 to evaluate gray scaled pictures according to its histogram's entropy [20]. KE can be utilized to locate optimal threshold of experiment picture by purely scrutinizing its entropy. Due to its superiority, substantial studies on KE are discussed in the literature [21,22].

Mathematical model of the KE is defined below:

Let, $T = [t_1, t_2, ..., t_{L-1}]$ denotes thresholds of the picture, then the overall entropy of KE will be;

$$Cost\ function = J_{max} = J_{Kapur}(T) = \sum_{J=1}^{L} O_j^R \quad for\ R\{1,2,3\} \quad (1)$$

Eqn. 2 presents the maximized-entropy with respected to the chosen threshold value.

In multiple-thresholding assignment, the objective function value is denoted as;

$$O_1^R = \sum_{j=1}^{t_1} \frac{Po_j^R}{\theta_0^R} \ln\left(\frac{Po_j^R}{\theta_0^R}\right),$$
$$O_2^R = \sum_{j=t_1+1}^{t_2} \frac{Po_j^R}{\theta_1^R} \ln\left(\frac{Po_j^R}{\theta_1^R}\right), \quad (2)$$
$$O_k^R = \sum_{j=t_k+1}^{L} \frac{Po_j^R}{\theta_{L-1}^R} \ln\left(\frac{Po_j^R}{\theta_{K-1}^R}\right)$$

where Po_j^R signify likelihood distribution and $\theta_0^R, \theta_1^R, ..., \theta_{L-1}^R$ depicts probability occurrence in L-levels [22]. The major role of the FA is to identify the optimal threshold based on maximized entropy. The FA arbitrarily alters the thresholds of test image till $J_{Kapur}(T)$ is reached.

C. K-Means Clustering (KMC)

A well known unsupervised segmentation technique is the K-means clustering, initially proposed to discover solutions for the clustering difficulty. K-means splits n observations into K groups [23].

Let, (c_1, c_2,..., c_n) are the given set of observations, of dimension 'D'. Then, K-means grouping process attempts to split given n interpretation into K groups; G (G_1, G_2, ..., G_k) for ($k \le n$) in order to reduce the within-cluster sum of squares [24-28].

$$\arg\min_{G} \sum_{i=1}^{k} \sum_{c_j \in G_i} \left\| c_j - \mu_i \right\|^2 \quad (3)$$

where μ is the mean of G_i.

D. Optic Disc Mining

Mining of OD is carried by a two-stage procedure based on the thresholding and segmentation. Thresholding is framed by FA+KE, which clusters the alike pixels based on the selected thresholds and the K-means grouping approach is considered to extract the OD area by separating the picture based on the grouped pixels. In this work, two well known retinal datasets, such as the DRIVE and RIM-ONE are considered for the experimental analysis. DRIVE has 20 train and 20 test RGB pictures of size 565 x 584, recorded by means of a Canon CR5 non-mydriatic 3CCD camera at 45^o field of view [29]. DRIVE pictures are primarily selected to realize the proposed method. Later, segmentation is demonstrated with RIM-ONE dataset. In this paper, release1 version of RIM-ONE is considered and is categorized into five groups, such as deep (14 images), early (12 images), moderate (14 images), normal (118 images) and ocular hypertension (11 images). Along with the test pictures, it also contains the Ground Truths (GT) offered by five experts. In this study, the RIM-ONE test-pictures considered by Sudhan et al. [6] is used to show the advantage of the proposed procedure.

This procedure is applies as follows:

Step 1: FA is initialized with following chosen parameters: number of fireflies=30, dimension of search = 3, maximum iteration =2000, stopping criteria is J_{max} [17].

Step 2: Implement tri-level (T=3) threshold based on Kapur's entropy, to cluster the similar pixel value (this process will eliminate the foremost section of retinal blood vessel and enhances the OD region).

Step 3: Execute K-means grouping to mine the OD section (the cluster numbers are chosen as three, which segments the image in to three groups based on the pixel intensity).

Step 4: Consider the segmented optic disc cluster; apply RGB to gray scale conversion and register the black & white (BW) image.

Step 5: Apply comparison of the OD with GTs and record the image similarity indices such as the Jaccard-Index (JI), Dice-Coefficient (DC), Sensitivity (SEN), Specificity (SPE) and Accuracy (ACC) [13, 14, 30].

III. RESULTS AND DISCUSSIONS

The chief insight behind this research is to construct a computerized tool to evaluate OD of the RGB retinal pictures. The experimentation of this paper is implemented using Matlab 7. Initially, RGB retinal dataset is considered for the examination and the FA+KE procedure is implemented on the chosen picture for tri-level thresholding. This thresholding procedure will eliminate the retinal vessels and enhance the OD of the test picture. Later, the K -means grouping approach is then implemented to extract the OD in order to assess the ODD.

ISBN 978-1-5386-4473-7
IEEE sponsored 4th International Conference on Biosignals, Images and Instrumentation, SSNCE, Chennai. ICBSII 2018 – 22nd-24thMar'18

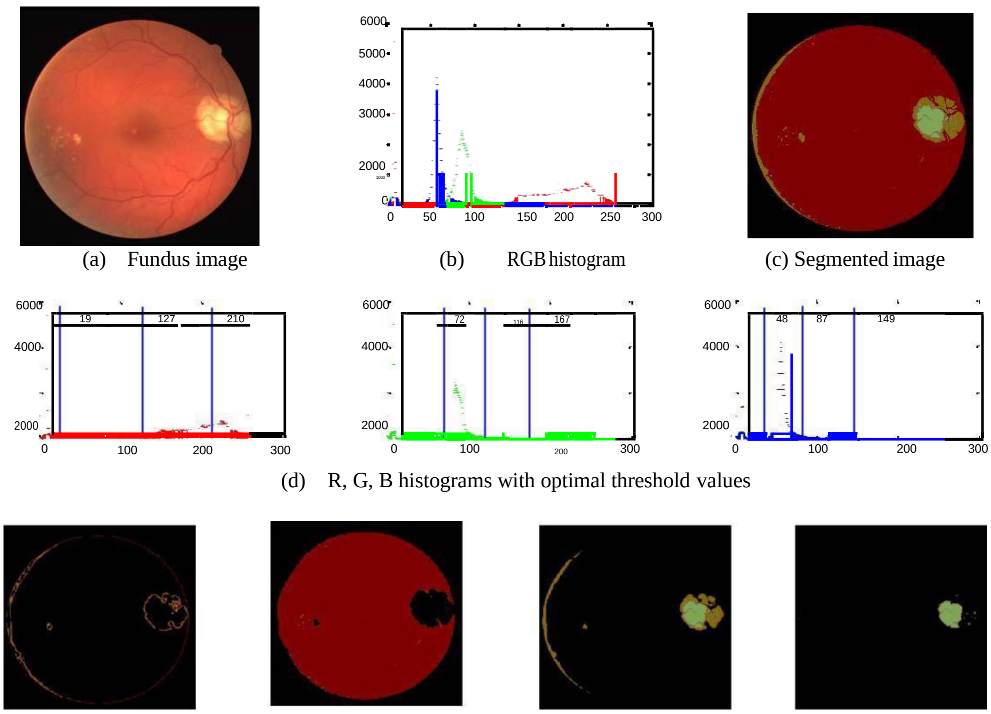

(a) Fundus image (b) RGB histogram (c) Segmented image

(d) R, G, B histograms with optimal threshold values

(e) Boundary (f) Background (g) Extracted section (h) OD

Fig 1. Results obtained with the FA+KE and KMC

Fig.1 depicts the outcome obtained with the FA+KE and three clusters (c_1, c_2 and c_3) of KMC on the chosen DRIVE picture. Fig.1 (a) and (b) shows the test picture and its RGB histogram respectively. From Fig(b), it can be seen that, it has a complex histogram pattern and finding the optimal threshold is a challenging task. Fig.1 (c) and (d) presents the tri-level threshold and its values respectively. Fig.1 (e), (f) and (g) depicts the various layers of outcomes attained with KMC and Fig.1 (h) presents the extracted OD. From these images, it is clear that, proposed tool works well on the DRIVE pictures.

Similar procedure is then repeated using the RIM-ONE pictures. During this, the test pictures discussed in Sudhan et al. [6] based on Otsu's+levelset is considered for the evaluation and validation. Fig. 2 (a) and (b) shows the chosen test picture and thresholded pictures respectively. Fig.2 (c) to (g) presents the GTs and Fig. (h) depicts the mined OD.

Fig .3 presents other images considered in this paper and its related results. This table confirms that, implemented procedure is very efficient in extracting the OD section from the chosen RGB scaled retinal pictures. Later a relative evaluation is implemented among the OD and GTs and the image similarity measures, such as JI, DC, SEN, SPE and ACC are computed and recorded. The values existing in Sudhan et al. [6] is depicted in Table I and the obtained measures with this paper is tabulated in Table II. In order to have a graphical comparison, the average values of the parameters existing in Table I and Table II are considered.

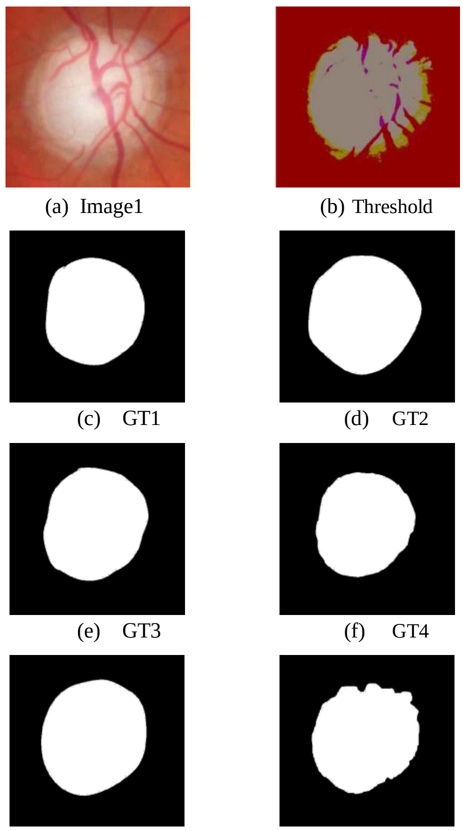
(a) Image1 (b) Threshold

(c) GT1 (d) GT2

(e) GT3 (f) GT4

(g) GT5 (h) Optic-Disc

Fig 2. Experimental results obtained with RIM-ONE image

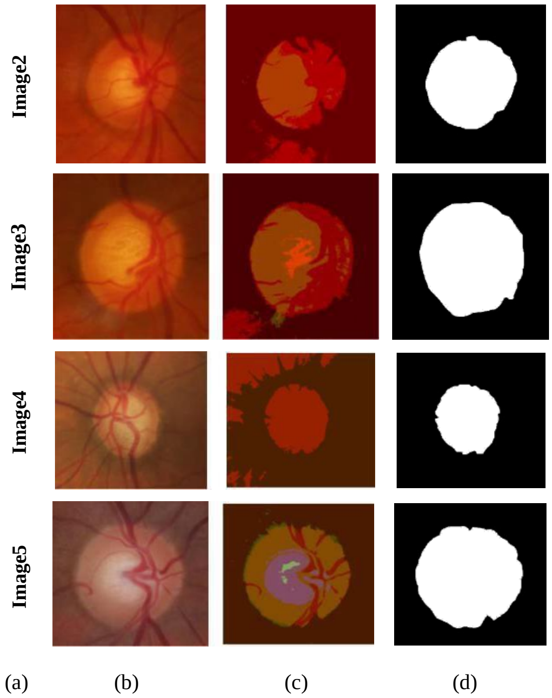

Fig. 3 Sample test pictures of RIM-ONE. (a) Pseudo name, (b) Test image, (c) Thresholded image, (d) Extracted OD

TABLE I IMAGE METRICS CONSIDERED FROM PREVIOUS WORK

Image	JI	DC	SEN	SPE	ACC
1	0.8570	0.9472	0.9659	0.9263	0.9539
2	0.8329	0.9384	0.9774	0.9337	0.9619
3	0.8424	0.9521	0.9430	0.9273	0.9473
4	0.8713	0.9574	0.9594	0.9420	0.9449
5	0.8255	0.9116	0.9822	0.9629	0.9694
Average	0.8458	0.9413	0.9656	0.9384	0.9555

TABLE II IMAGE METRICS OBTAINED IN THIS STUDY

Image	JI	DC	SEN	SPE	ACC
1	0.8518	0.9285	0.9614	0.9279	0.9518
2	0.8402	0.9405	0.9785	0.9361	0.9627
3	0.8416	0.9556	0.9518	0.9311	0.9515
4	0.8698	0.9583	0.9617	0.9461	0.9470
5	0.8316	0.9134	0.9831	0.9636	0.9717
Average	0.8470	0.9393	0.9673	0.9410	0.9569

From Table I and II, it can be noted that, the JI, SEN, SPE and ACC are better in the proposed approach and the DC is very close to the value in Sudhan et al. [6]. Fig 4 presents the graphical pattern obtained during the comparative evaluation with average values of Table I and II. The overall results of proposed FA+KE and KMC is better compared with the Otsu's +levelset procedure.

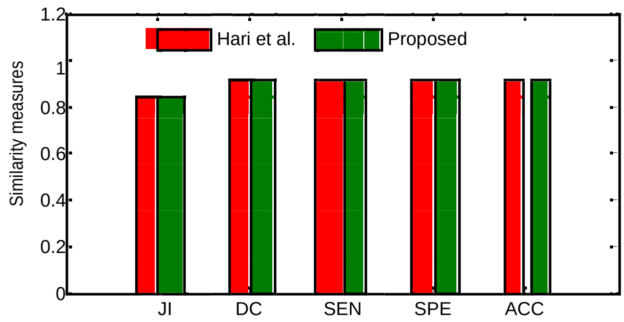

Fig 4. Average image metrics beween the existing values and values of proposed approach

From these results, it is confirmed that, proposed tool works well on the DRIVE as well as the RIM-ONE pictures. Hence, in future, proposed tool can be considered to evaluate the OD of RGB retinal pictures obtained from hospitals.

IV. CONCLUSION

A Firefly Algorithm (FA) guided technique is executed to extract the optic disc from retinal images with KE+KMC. Initially, the optic disc segmentation is employed for DRIVE database and later with RIM- ONE dataset. For the RIM-ONE, an average JI of 84.70%, DC of 93.93%, SEN of 96.73%, SPE of 94.10% and ACC of 95.69% are attained from the proposed technique. In order to confirm the superiority of implemented tool, a comparative analysis is done against the similar approach existing in the literature. This study prove that, proposed two-stage procedure offers better result compared to the existing method considered in this paper. Hence, in future, it can be considered in clinics to examine the real time medical retinal images.

REFERENCES

[1] N. Dey, A.B. Roy, A.Das, and S.S. Chaudhuri, "Optical cup to disc ratio measurement for glaucoma diagnosis using Harris corner," In. Third International Conference on Computing Communication & Networking Technologies (ICCCNT), IEEE, 2012 . Doi: 10.1109/ICCCNT.2012.6395971.

[2] A. Almazroa, R. Burman, K. Raahemifar, and V. Lakshminarayanan, "Optic disc and optic cup segmentation methodologies for glaucoma image detection: A survey," Journal of Ophthalmology, vol.2015, Article ID 180972, 28 pages. Doi: 10.1155/2015/180972.

[3] M.W. Khan, M. Sharif, M. Yasmin, and S.L. Fernandes, "A new approach of cup to disk ratio based glaucoma detection using fundus images," Journal of Integrated Design and Process Science, vol. 20, no. 1, pp. 77-94, 2016. Doi: 10.3233/jid-2016-0004.

[4] G. Kavitha, and S. Ramakrishnan, "An approach to identify optic disc in human retinal images using ant colony optimization method," Journal of Medical Systems,vol..34, no.5, pp. 809–813, 2010. Doi: 10.1007/s10916-009-9295-4.

[5] T.D.V. Shree, K. Revanth, N.S.M.Raja, Raja, V. Rajinikanth, "A hybrid image processing approach to examine abnormality in retinal optic disc," Procedia Computer Science, vol.125, pp. 157-164, 2018. DOI: 10.1016/j.procs.2017.12.022.

[6] G.H.H. Sudhan, R.G. Aravind, K..Gowri, and V. Rajinikanth, "Optic disc segmentation based on Otsu's thresholding and level set," In. International Conference on Computer Communication and Informatics (ICCCI), IEEE, pp.1-5, 2017. Doi: 10.1109/ICCCI.2017.8117688.

[7] F. Fumero, S. Alayon, J. L. Sanchez, J. Sigut, and M. Gonzalez-Hernandez, "RIM-ONE: An open retinal image database for optic nerve evaluation," In. 24th International Symposium on Computer-Based Medical Systems (CBMS), IEEE, pp.1–6, 2011. Doi: 10.1109/CBMS.2011.5999143.

[8] http://medimrg.webs.ull.es/research/retinal-imaging/rim-one/

[9] J. Amin, M. Sharif, M.Yasmin, H. Ali, and S.L. Fernandes, "A method for the detection and classification of diabetic retinopathy using structural predictors of bright lesions," Journal of Computational Science, vol.19, pp. 153-164, 2017.

[10] F. Bokhari, T. Syedia, M. Sharif, M. Yasmin, and S.L. Fernandes, "Fundus image segmentation and feature extraction for the detection of glaucoma: A new approach," Current Medical Imaging Reviews, vol.14, no.1, pp. 77-87, 2018.

[11] http://www.isi.uu.nl/Research/Databases/DRIVE/

[12] N.S.M. Raja, V. Rajinikanth, S.L. Fernandes, and S.C. Satapathy, "Segmentation of breast thermal images using Kapur's entropy and hidden Markov random field," Journal of Medical Imaging and Health Informatics, vol.7, no.8, pp. 1825-1829, 2017.

[13] V. Rajinikanth, S.C. Satapathy, S.L. Fernandes and S. Nachiappan, "Entropy based segmentation of tumor from brain MR images–A study with teaching learning based optimization," Pattern Recognition Letters, vol.94, pp.87-95, 2017. DOI: 10.1016/j.patrec.2017.05.028.

[14] V. Rajinikanth, N.S.M. Raja and K. Kamalanand, "Firefly algorithm assisted segmentation of tumor from brain MRI using Tsallis function and Markov random field," Journal of Control Engineering and Applied Informatics, vol.19, no.3, pp. 97-106, 2017.

[15] X.-S. Yang, "Firefly algorithms for multimodal optimization," Lecture Notes in Computer Science, vol. 5792, pp. 169–178, Springer, 2009.

[16] X.-S. Yang, "Review of meta-heuristics and generalised evolutionary walk algorithm," International Journal of Bio-Inspired Computation, vol. 3, no. 2, pp. 77–84, 2011.

[17] N.S.M. Raja, V. Rajinikanth and K. Latha, "Otsu based optimal multilevel image thresholding using firefly algorithm," Modelling and Simulation in Engineering, vol.2014, paper id.794574, 2014.

[18] V. Rajinikanth, and M.S. Couceiro, "Optimal multilevel image threshold selection using a novel objective function", Advances in Intelligent Systems and Computing, vol. 340, pp 177-186, 2015.

[19] N.S.M. Raja, K.S. Manic, and V. Rajinikanth, "Firefly algorithm with various randomization parameters: An analysis," Lecture Notes in Computer Science , vol. 8297, pp. 110-121, 2013. Doi: 10.1007/978-3-319-03753-0_11.

[20] J. N. Kapur, P. K. Sahoo, and A. K. C. Wong, "A new method for gray level picture thresholding using the entropy of the histogram," Computer Vision, Graphics, and Image Processing, vol. 29, no. 3, pp. 273–285, 1985.

[21] K.S. Manic, R.K. Priya, and V Rajinikanth, "Image multithresholding based on Kapur/Tsallis entropy and firefly algorithm," Indian Journal of Science and Technology, vol.9, no.12, 89949, 2016.

[22] V.S. Lakshmi, S.G. Tebby, D. Shriranjani, and V. Rajinikanth, "Chaotic cuckoo search and Kapur/Tsallis approach in segmentation of T.cruzi from blood smear images," International Journal of Computer Science and Information Security (IJCSIS), vol.14, CIC 2016, pp. 51-56, 2016.

[23] T-W. Chen, Y-L. Chen, and S-Y. Chien, "Fast image segmentation based on K-Means clustering with histograms in HSV color space," 10th Workshop on Multimedia Signal Processing, IEEE, 2008. Doi: 10.1109/MMSP.2008.4665097.

[24] R. Vishnupriya, N.S.M. Raja, and V.Rajinikanth, "An efficient clustering technique and analysis of infrared thermograms," Third International Conference onBiosignals, Images and Instrumentation (ICBSII), IEEE, pp.1-5, 2017. DOI: 10.1109/ICBSII.2017.8082275.

[25] K. Manickavasagam, S. Sutha and K, Kamalanand, An automated system based on 2D empirical mode decomposition and k-means clustering for classification of Plasmodium species in thin blood smear images, BMC Infectious Diseases, vol.14, no.3, pp.1, 2014.

[26] K. Manickavasagam, S. Sutha and K. Kamalanand, Development of systems for classification of different plasmodium species in thin blood smear microscopic images, Journal of Advanced Microscopy Research, vol.9, no.2, pp. 86-92, 2014.

[27] S. Revathy, B. Parvathavarthini, and N. Shajunisha, "Enforcement of rough fuzzy clustering based on correlation analysis," International Arab Journal of Information Technology (IAJIT), vol.14. no.1, pp.91-98, 2017.

[28] S. Revathy, B. Parvathavarthini, and S.S. Caroline, "Decision theory, an unprecedented validation scheme for rough-Fuzzy clustering," International Journal on Artificial Intelligence Tools, vol.25, no.2, pp. 1650003, 2016.

[29] K.S. Sreejini and V.K. Govindan, "Improved multiscale matched filter for retina vessel segmentation using PSO algorithm," Egyptian Informatics Journal, vol.16, pp.253-260, 2015.

[30] V. Rajinikanth, and S.C. Satapathy, "Segmentation of ischemic stroke lesion in brain MRI based on social group optimization and Fuzzy-Tsallis entropy," Arabian Journal for Science and Engineering, pp.1-14, 2018. DOI: 10.1007/s13369-017-3053-6.

[31] N.S.M. Raja, G.Kavitha, S. Ramakrishnan, Analysis of vasculature in human retinal images using particle swarm optimization based Tsallis multi-level thresholding and similarity measures, Lecture Notes in Computer Science, vol.7677, pp. 380-387, 2012.

[32] F. Bokhari, T. Syedia, M. Sharif, M. Yasmin, S.L. Fernandes, Fundus Image Segmentation and Feature Extraction for the Detection of Glaucoma: A New Approach, Current Medical Imaging Reviews, vol.14, no.1, pp.77-87, 2018. DOI. 10.2174/1573405613666170405145913.

[33] R. Zafar, M. Sharif and M. Yasmin, A Survey on the Prevalence of Cataract and its Accompanying Risk Factors, Current Medical Imaging Reviews, vol.14, no.2, pp.251-262, 2018. DOI: 10.2174/1573405613666170331103423.

An Artificial Neural Network Based Approach towards Eye Gesture Classification for Texting

M Anand, V Jeya Maria Jose
Instrumentation and Control Engineering, National Institute of Technology, Tiruchirapalli, Member of Spider, R&D Club Tiruchirapalli, India

J Veejay Karthik, Prasanna Kumar G R
Electrical and Electronics Engineering, National Institute of Technology, Tiruchirapalli, Member of Spider, R&D Club Tiruchirapalli, India

Ashwin Natraj A
Electronics and Communication Engineering, National Institute of Technology, Tiruchirapalli, Member of Spider, R&D Club Tiruchirapalli, India

***Abstract*—The task of typing using the gestures from the eye like left, right, center, blink by obtaining the eye images from a camera feed has been worked on in this research work. A multi-layered neural network is used to recognize the gestures from our eye and an accuracy of 91.6% has been obtained with the image data that were collected and used. With the recognized gestures, an application that aids people to type only using their eye gestures was developed. This method of texting minimizes the muscle movement for paralyzed people or people who suffer from acute illness who would find it difficult to communicate with any other means. The robustness of the application also proves that it can be applied on any handheld device substituting the normal process of texting using keyboard.**

Keywords - Neural Networks; Image Processing; Human-Computer Interaction

I. INTRODUCTION

Human Computer Interaction through gestures [1][2] has been a phenomenon ever since its first inception. Dating back to the early 1950s, the invention of the computer mouse sowed the seeds for the basic gesture recognition in 2-dimensional planes. The relative motion with respect to a stationary surface was estimated and the data was sent to a computer.

Ever since this breakthrough, there has been a steady impetus towards more sophisticated means of sensing gestures and interacting with machines. To put this into a better perspective, stepping into the 21st century, Smart devices began to dominate the field of technology. These devices often rely on the simple gestures made by the hand, converting them into meaningful output. Within a turn of another decade, people began to realize there was vast pool of the gestures, such as those using eyes was left untapped, and these have a great potential, waiting to be explored.

Presently, the major techniques available for tapping the eye gestures are Electro-Oculography [3][4] and Eyeball tracking [5] using Digital Image Processing. The former method uses electrodes and it is not often convenient for practical applications while the latter provides a lot of scope for easy and convenient means of data acquisition. With fast computing methods and quick processors, Digital Image Processing is a more feasible option.

With powerful Machine Learning Algorithms [6] using Neural Networks [7], we have come a very long way from where we actually started. These algorithms, when coupled with high processing speeds, provide a stable and reliable means of sensing these gestures.

The aim of this paper is to describe a method to determine the gestures of the eye through Image processing techniques using neural networks. The subsequent sections comprise of the general algorithm used to determine the position of the eyeball from a digital image. It also describes the implementation details and real-time results.

II. SYSTEM DESCRIPTION

A. Mechanical Design

The proposed design in this paper, consists of a helmet-like cap fitted with a webcam. This camera is placed at a distance of 9 cm to track the position of the pupil to sufficient accuracy. The cap is made of polymerized plastic to provide sufficient strength to hold and bear the weight of the webcam. It is made slightly flexible so that it fits on the user's head without disorienting itself during prolonged use. The material is also light-weight, so as to reduce the mechanical strain on the user. The camera distance can also be made adjustable to an allowable extent based on the comfort of the user. Fig.1 shows the image of the proposed design. The camera specifications are as follows:

Optical resolution - 1280 x 960 1.2MP
Frame rate – 30 fps
Focal length – 4 mm

Fig.1: The hardware design

The system can also be incorporated in a small scale by fixing miniature cameras such as pi cam and fixed onto goggles, thereby enhancing the ease of usability.

B. Neural Network Methodology

The authors of the paper have made use of Multiple-Layer neural network architecture to classify the eye gestures into middle, left and right gestures. The formulae involved in the classification are as follows:

Output of a neuron:

$$z^{(i)} = w^T x^{(i)} + b$$

Where $z^{(i)}$ is the output for i^{th} input
w is the weight of the input b
is the bias added to output

Activation function:

$$sigmoid(w^T x + b) = \frac{1}{1+e^{-(w^T x+b)}}$$

Using feed forward propagation, the output is calculated and the deviation from expected value is calculated using the loss function given by:

$$J = -\frac{1}{m}\sum_{i=1}^{m} y^{(i)}\log(a^{(i)}) + (1-y^{(i)})\log(1-a^{(i)})$$

where J is the calculated loss function,
$y^{(i)}$ is the output for i^{th} input,
$a^{(i)}$ is the activated output for i^{th} input,
m is the number of training examples

The loss function is used to predict the change in the weight and bias of neurons in each hidden layer, required to minimize the output error using back propagation algorithm.

$$\frac{\partial J}{\partial w} = \frac{1}{m}X(A-Y)^T$$
$$\frac{\partial J}{\partial b} = \frac{1}{m}\sum_{i=1}^{m}(a^{(i)} - y^{(i)})$$

The weight and bias parameters of each neuron are updated using the gradient descent algorithm.

$$w = w - t * dJ/dw$$
$$b = b - t * dJ/db$$

Where w is the updated weight
b is the updated bias
t is the learning rate used in gradient descent

Tensorflow API has been used as the backend in python for the implementation. The architecture is composed of input layer of 9, 21,600 inputs (Each image is 640*480*3), 3 hidden layers of 50, 70 and 50 neurons respectively and an output layer. The weight and the bias parameters have been randomly initialized using Xavier's initialization and forward propagation is carried out. The backward propagation and updating of weights is done using Adam Optimizer [8].

C.. Graphical User Interface(GUI)

The GUI part of this project is implemented in python using the PyQT library [9]. The software continuously takes image input from the camera. Based on the gesture, corresponding action is carried out in the GUI. The GUI window is equipped with buttons as shown in Fig.2.
The keys are arranged in a circular manner. When a left gesture is recognized, the cursor moves through the characters in anticlockwise direction and when a right gesture is recognized, the cursor moves in clockwise direction. When the eyes look at the center, the cursor is made not to move. When the user closes his/her eyes, the software starts measuring how long the eyes are closed. When a threshold level is reached, it is considered as an indication for typing the character and the presently selected character will get typed in the text box. The delay in this process is found to be less than 0.2 sec.
The GUI also has keys for space, backspace, clearing entire text and speech conversion in addition to alphabets. When a key is selected, a short beep sound is produced and when a key is typed by closing the eyes, a long beep is produced to indicate that the selected character is typed successfully in the text box. When the speech conversion button is selected, the text present in the text box will be fed to a text to speech conversion engine that converts the typed text into speech. Pyttsx engine is used for text to speech conversion in this project which takes approximately 0.1 sec for conversion. [10].

ISBN 978-1-5386-4473-7

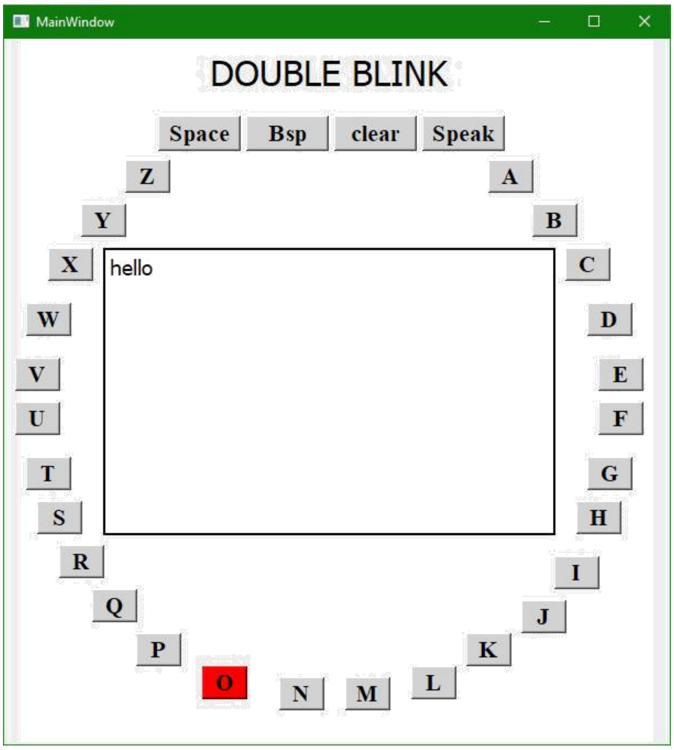

Fig.2: The application screen window

III. ALGORITHM

The eye gesture classification is first done by collecting and using the images that are fed from the camera placed in the helmet. As the camera is fixed at a fixed distance from the eyes according to the design proposed, there are no interferences in the output due to errors caused by mis-alignment of the eyes with respect to the reference frame of camera. The training and testing dataset for the neural network are made by making a python script that collects the images of current frame of the camera. Then, the collected images are classified into four classes manually as follows: blink, center, left and right gestures. Each class can have as many as images as needed for training the network for a high accuracy, but that will proportionately increase the computing time. So, in this project, 250 images from each class has been used for training, thus training a total image of 1000 images and 50 images from each class is used for testing.

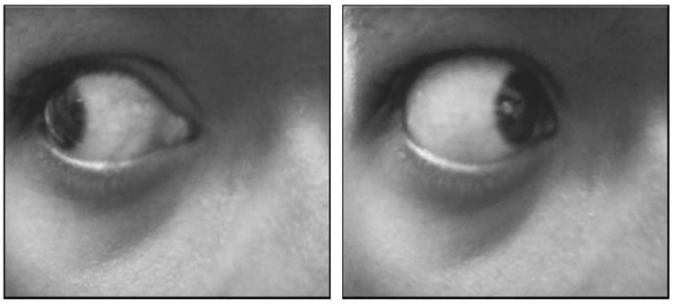

Fig.3 : Example images from dataset belonging to classes Blink, Center, Left , Right gestures respectively from top left to bottom right.

The images are first converted into a vector form by storing the pixel values of it in a single vector that is fed as the input to the neural network. The neural network is built in python with the architecture as described in section II. The training data is fed to the neural network with a learning rate of 0.001 while keeping the number of epochs as 1500. At the end of the training, the weights and the bias matrices of all the layers of the neural network are updated according to the dataset. These numpy matrices are stored into separate files in the .npy format for further usage.

The updated weights and bias matrices were then used for testing the accuracy of the system using the whole dataset. In the script that runs the GUI for texting, these files are loaded into the weights and biases variable matrices. These are used to classify the current frame that is captured in the real-time by the camera into one of those four classes. The classified output is then used for the texting part. A blink is programmed for a click, the right and left gestures of eye are programmed for traversing across the virtual keyboard built. Thus, in the GUI the cursor can be moved and characters printed using eye gestures taken from the camera. The whole algorithm is summarized into a flow chart as shown in Fig. 4.

ISBN 978-1-5386-4473-7

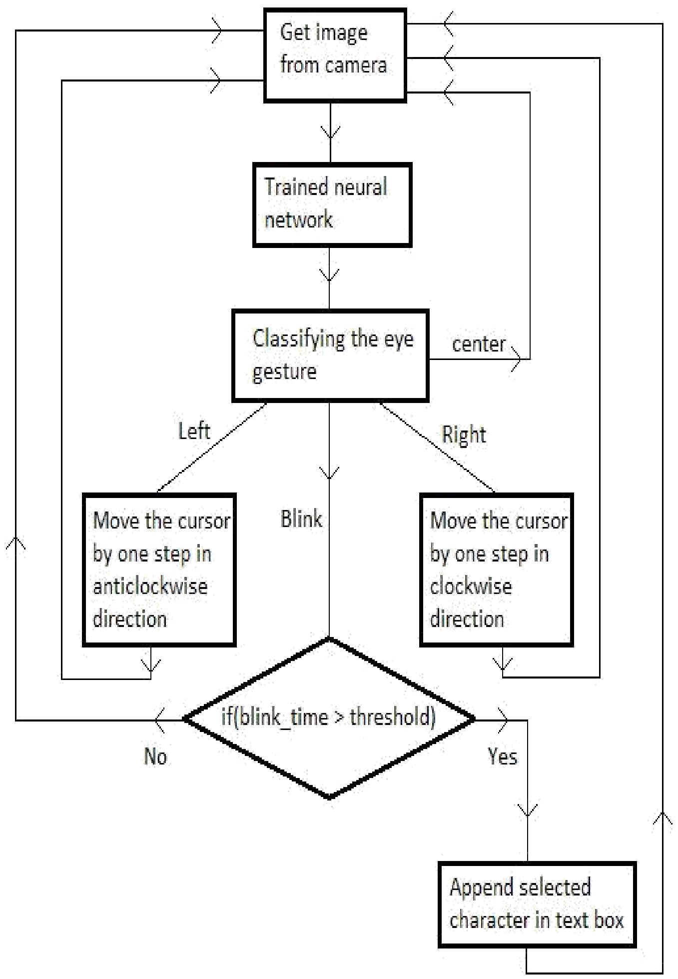

Fig.4: Flow Chart

IV. RESULTS

The output weights and bias matrices that are trained using the neural network are found to be efficient and robust for the classification of eye gestures for texting purposes. The cursor movements are found to be in phase to the change in the eye gestures.

In the experiment, the training accuracy was found to be 100% while the test accuracy was found to be 91.6% for the dataset that was used for the project. Fig.5 shows the decrease in the cost with respect to the number of epochs for the neural network architecture used.

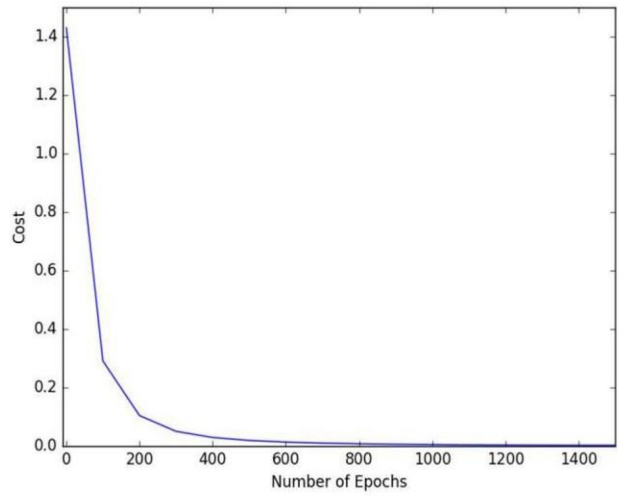

Fig.5 : Relationship between number of epochs and cost. However, these values are subject to change according to the dataset , leaning rate , the network architecture, the activation function, number of epochs and a few other factors.

V. ADVANTAGES

According to the 2011 Indian Census of the Indian Population, around 50% of the total disabled population are paralyzed and cannot move [11]. However, these people can easily move their eyes and hence we can obtain their eye gestures with which they can communicate easily with minimal muscle movement. This approach requires very minimal hardware thus helping even the poor people to use this system. Also, as the system is very adaptive as it trains itself by the user's eye image directly, it is highly user friendly. The unintentional blinks have also been taken into account thus reducing the errors.

VI. FUTURE WORKS

In this work, the eye gesture classification has been used only on a very narrow field of texting. A lot of other fields like home automation and vehicle locomotion can be explored to new depths using the robust eye gesture classification work that is discussed in this paper. A complete system catering the needs of a paralyzed person can be developed with the aid of this technology. A wheelchair moved only using eye movements can be developed using this technology. Moreover, switching on or off of electronic equipments using eye gestures can also be done. Also, this algorithm can be tested and if possible, be incorporated to handheld devices for texting.

VII. CONCLUSION

In this work, various methods of eye gesture classification were discussed and detection using camera and classification using neural networks was found to be the most effective. The mechanical design for the hardware and the GUI built for software was explained. The algorithm was found to be effective and was validated with the trained network for texting. The work was also found to highly useful in health care applications helping in communication for the paralyzed and also has high prospects for further developments in terms robustness and accuracy and can change the whole methodology of texting. The application and source code has also been made available open source for any further developments.

ACKNOWLEDGMENT

The authors of this paper would like to express their gratitude to everyone who assisted us with our work. We would like to express our sincere gratitude to Spider, the R&D Club of NIT Trichy, for mentoring and funding us.

REFERENCES

[1] Z. Ren, J. Meng and J. Yuan, "Depth camera based hand gesture recognition and its applications in Human-Computer-Interaction," *2011 8th International Conference on Information, Communications & Signal Processing*, Singapore, 2011, pp. 1-5.

[2] V. I. Pavlovic, R. Sharma and T. S. Huang, "Visual interpretation of hand gestures for human-computer interaction: a review," in *IEEE Transactions on Pattern Analysis and Machine Intelligence*, vol. 19, no. 7, pp. 677-695, Jul 1997.

[3] T. Yagi, Y. Kuno, K. Koga and T. Mukai, "Drifting and Blinking Compensation in Electro-oculography (EOG) Eye-gaze Interface," *2006 IEEE International Conference on Systems, Man and Cybernetics*, Taipei, 2006, pp. 3222-3226.

[4] D. Kumar and E. Poole, "Classification of EOG for human computer interface," *Proceedings of the Second Joint 24th Annual Conference and the Annual Fall Meeting of the Biomedical Engineering Society] [Engineering in Medicine and Biology*, 2002, pp. 64-67 vol.1.

[5] A. E. Kaufman, A. Bandopadhay and B. D. Shaviv, "An eye tracking computer user interface," *Proceedings of 1993 IEEE Research Properties in Virtual Reality Symposium*, San Jose, CA, USA, 1993, pp. 120-121.

[6] G. B. Huang, H. Zhou, X. Ding and R. Zhang, "Extreme Learning Machine for Regression and Multiclass Classification," in *IEEE Transactions on Systems, Man, and Cybernetics, Part B (Cybernetics)*, vol. 42, no. 2, pp. 513-529, April 2012.

[7] D. F. Specht, "A general regression neural network," in *IEEE Transactions on Neural Networks*, vol. 2, no. 6, pp. 568-576, Nov 1991.

[8] Diederik P. Kingma, Jimmy Ba, Adam:A method of stochastic optimization , arXiv:1412.6980

[9] Computational Materials Science, ISSN: 0927-0256, Vol: 28, Issue: 2, Page: 155-168. Publication Year:2003

[10] D. Klatt, "The klattalk text-to-speech conversion system," *ICASSP '82. IEEE International Conference on Acoustics, Speech, and Signal Processing*, 1982, pp. 1589-1592.

[11] http://censusindia.gov.in/Census_And_You/disabled_population.aspx

Colour Image Segmentation of Fundus Blood Vessels for the Detection of Hypertensive Retinopathy

Anna Latha M, *Assistant Professor, Agni College of Technology, Chennai, India,* Christy Evangeline N, *Assistant. Professor, Agni College of Technology, Chennai, India.,*

SankaraNarayanan S., Research Scholar, National Institute of Technology, Trichy, India.

***Abstract*— Retina is the major part of the human eye. Most of the diabetic and hypertensive problems will initially affect the retinal blood vessels of the eye. Using normal segmentation techniques, we can identify only the blood vessels. Therefore, color image segmentation is the best way to identify the retinal problems, because using color image segmentation we can differentiate the retinal veins and arteries. We have used masking techniques to segment the images of arteries and vein. The proposed technique is evaluated with data from ten patients diagnosed with hypertensive retinopathy. For this process, histogram equalization is performed on the complemented green plane image. From the result, the optic region is removed by morphological operation, after which it is converted into binary image. This output is multiplied with R, G, & B channels of input data and combined to get required segmented region of retinal blood vessels. All this vessels extraction has been done by using image processing techniques.**

***Keywords*—Color, Green plane, masking, hypertensive, image processing, diabetic retinopathy, vessels extraction.**

I. Introduction

Hypertensive retinopathy is the medical term caused by high blood pressure. It mainly affects the retina and the retinal blood circulation. Due to high blood pressure retinal blood vessels such as retinal arteries and retinal veins also affected. So that blood circulation to the retina collapsed. The symptom of hypertensive retinopathy depends on the patient conditions. Some medical conditions may have visual conditions. Hypertensive retinopathy symptoms include blood vessel changes, artery narrowing, vein narrowing, artery vein crossing location angle deviation; this is known as arteriovenous nicking. This arteriovenous nicking mainly affects the arteries and veins crossing locations.

Hypertensive retinopathy leads many problems such as cardiovascular disorders and death. The treatment for hypertensive retinopathy is to reduce the high blood pressure. They are many treatment procedure is available to treat the hypertensive retinopathy. One among the treatment is using Anti-hypertensive drugs. These drugs are used to control the pressure and damage level of retina. Hypertensive retinopathy also leads multiple problems to the eye. AV nicking can be identified with the help of deviations in the artery vein crossing location and angle variations. The early detection of AV nicking can greatly reduce the visual acuity problems.

A. Review on Previous Works on Blood Vessel Segmentation

In general, retinal blood vessel segmentation consists of green channel conversion, optic disk removal, and masking. Joes Staal et al [1] presented the work automatic extraction of blood vessel in Two Dimensional retinal color images. The classification process is applied for the feature vector extraction. The classification is based on Neural Network classifier. Classifier accuracy ranges varies 0.9441 versus 0.9471.

Elisa Ricci [2] presentedautomated digital detection of retinal disorders, using basic morphological line operator and support vector classification.

Xinge You et al [3] presented the radial projection and semi-supervised techniques are used to extract the retinal blood vessels. They experimented and shows the result of detecting the thinner blood vessels and decrease the vessel false detection in the anatomical region of eye and compared to rival solution.

Uyen T. V. Nguyen et al [5] presented an algorithm for detecting the Retinal Arteriovenous nicking. Here the retinal image is used as a input, then the blood vessels are segmented using the multi scale line detection technique.

II. Proposed System for Retinal Blood Vessel Segmentation

Color fundus image blood vessel extraction is mainly proceeded to differentiate the artery and vein. Retinal vascular network extraction can be carried out by using very high resolution fundus colour images. It has some complications such as reflection of central light, artifact present in the input retinal image the proposed system for color retinal blood vessel segmentation consists of combination of morphological processes to identify blood vessels.

III. Methodology

The work flow of the system is processed as given in the Fig.1. Each stage of our project work is described in detail as follows.

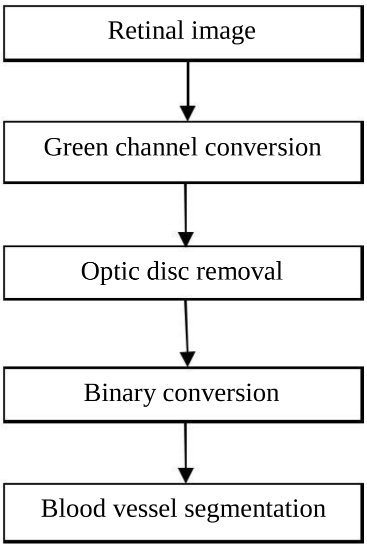

Fig.1. Diagrammatic representation of proposed system

A. Green-channel conversion

From the input color fundus image is the combination of RGB color space and the original retinal image and R, G, B channels can be represented as follows. Fig 2(a) Original image,Fig 2(b) Red-channel, Fig 2(c) Green-channel and Fig 2(d)Blue-channel respectively. It is clear from these images that the green channel image consists of more information compared to red and blue channel images.

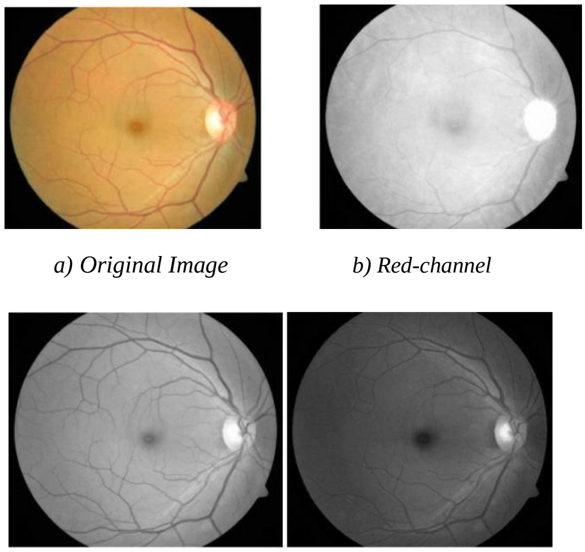

a) Original Image *b) Red-channel*

(c) *Green-channeld)Blue-channel*

Fig.2. Image conversion

B. Optic disc removal

First step of our proposed method is to extract the green-channel components. Next step is to remove the optic disc of the retinal image. The optic removal is the very important step for the retinal blood vessel segmentation. The optic disc size varies depends upon the patient. The diameter always varies between 80-100 pixels this is a standard retinal image. The optic disc removal is not easy task. It is difficult to remove from retinal blood vessels. Because the optic disc boundaries, veins and arteries also connected. The optic disc boundary for some patients is not visible. In this paper we used to remove the optic disc from the retinal blood vessels using three different stages.

Step 1. In this step the complimentary image for the green-channel portion of the input-image is taken. The importance of the Green-channel from the RGB color space is to provide the better contrast of the original image. Local contrast-enhancement technique is used as preprocessing step to improve the detection of low contrast and narrow vessels. In order to obtain enhancement, the image is converted into a complimentary image. Initially, zeros are converted into ones and vice versa. Hence, the black and white pixels are reversed. After that, the complementary image intensity value of an each pixel is subtracted from the maximum pixel value. Then find the difference of that value. That difference value is considered as the pixel value in the output image. The output of this step is, light areas become darkerand dark areas become lighter. Fig 3 (a) depicts the complimentary image.

Step 2. In this step**,** contrast limited Adaptive Histogram Equalization is applied to the complimentary image. This histogram equalization is used to enhance the contrast of the complementary image by transforming the values. In this adaptive histogram equalization the complementary image is split into small data. That small data is called tiles. Each tile is enhanced separately. After that each enhanced tiles are combined with the help of bilinear-interpolation techniques. Because bilinear-interpolation techniques are used to remove the artificial boundaries. This is the way to improve the contrast of the complementary image. Fig 3 (b) depicts the equalized image.

Step 3. In this step themorphological structuring element is used to remove the optic disc of an equalized image. Initially, a non-flat "ball-shaped" structuring element with radius, R and height, H is created. Where, R is a nonnegative integer and H is a real scalar. After creating the morphological structure, the image is dilated and eroded which will result in a optic disc removed image. Fig 3 (c) depicts the optic disc removed image.

C. Binary Image Conversion

The optic disc removed complementary image is then converted into binary image. The binary image only has the two vales. It can be represented by using zeros and ones. Each pixel of the complementary value is converted into binary values. For that binary value conversion initially needs grayscale conversion. Then the converted grayscale images are converted into binary values. The output binary image will be having 0 (Black) for all the pixels in the input image with luminance lesser than the threshold level and 1 (white) for all the other pixels. Fig 3 (d) depicts the binary image.

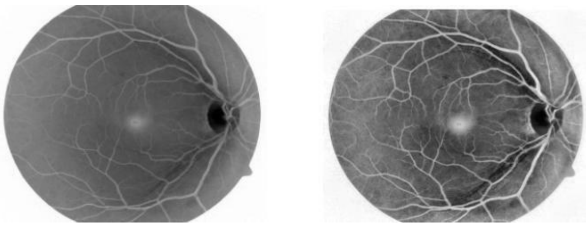

a) Complimentary Image *b) Equalized Image*

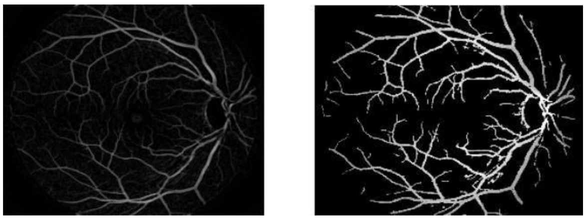

c) Optic disc removed *d) Binary Image*

Fig.3. Optic disc removal

D. Segmentation

The binary image is multiplied individually with R, G and B channels of the original image. It multiplies every element in the array of binary image by the corresponding element in the array of R, G and B channels of the original image and returns the product in the corresponding element of the output array. If both images are real numeric arrays of same size and class, then the output image will have the same size and class as input images.

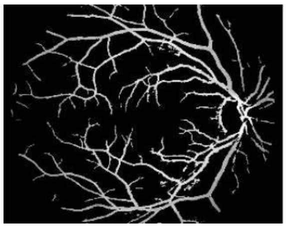

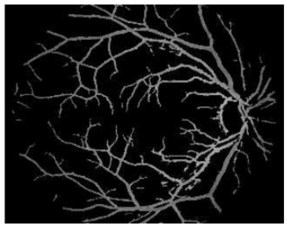

a) Multiplied Red image *b)MultipliedGreen image*

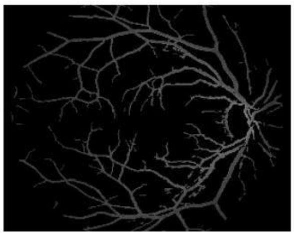

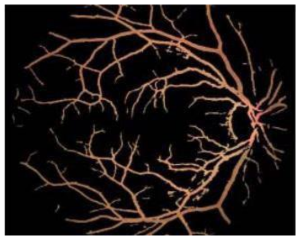

c) Multiplied blue image *d) Segmented Image*

Fig.4. Segmentation process

Finally the concatenation of these three images will give the color segmented retinal blood vessels alone. Image concatenation is the process of joining one or more images to make a new image. The multiplied R, G, B and segmented images are shown in Fig.4 (a), (b), (c) and (d) respectively.

IV Experimental Results

A dataset of retinal images of 7 patients is acquired. Each image has an image matrix of 2438×2112. The original input color image is converted into R, G, & B channel images. For removing optic disc the compliment image of the green-channel image is acquired. The complimentary image is enhanced using morphological structuring element. The image is dilated and eroded which resulted in an optic disc removed image. After that, the optic disc removed image is converted into binary image. The binary image is multiplied with Red, Green and Blue channels of the original image. Finally the concatenation of these three images will give the color segmented retinal blood vessels. So the retinal blood vessels are segmented.

V Conclusion

The aim of this study is to propose a computerized design for automatic color retinal blood-vessels (veins and arteries) segmentation from the retinal input images. Thus the color retinal blood-vessels (veins and arteries) are segmented using morphological operations. The advantage of this project work is the automatic color based extraction of retinal blood vessels.

VI. Acknowledgment

We acknowledge Anna University’s National Hub for Health Care instrumentation Development at Anna University funded by Technology Development and Transfer for supporting this work.

References

[1] Abràmoff, Joes Staal, Michael D. “Ridge-based vessel segmentation in color images of the retina” IEEE transactions on medical imaging, VOL. 23, NO. 4, APRIL 2004.

[2] Elisa Ricci and Renzo Perfetti “Retinal blood vessel segmentation using lineoperators and support vector classification” IEEE transactions on medical imaging, VOL. 26, NO. 10, OCTOBER 2007.

[3] JiajiaLei, Xinge You a, QinmuPeng a, YuanYuan b, Yiu-mingCheung c, “Segmentation of retinal blood vessels using the radial projection and semi-supervised approach” Pattern Recognition 44, 2011.

[4] UyenT.V.Nguyena,n, AlauddinBhuiyan a, LaurenceA.F.Park b, KotagiriRamamohanarao “An effective retinal blood vessel segmentation method using multi-scale line detection” Pattern Recognition 46 (2013) 703–715.

[5] Uyen T. V. Nguyen, AlauddinBhuiyan, Laurence A. F. Park, Ryo Kawasaki, Tien Y. Wong, Jie Jin Wang, Paul Mitchell, KotagiriRamamohanarao “An automated method for retinal arteriovenous nicking quantification from colour fundus images” IEEE transactions on medical imaging, 2013.May 2013.

Computer aided system for Human Blood Cell Identification, Classification and Counting

Christy Evangeline N, *Assistant Professor, Agni College of Technology, Chennai, India.*

Annalatha M, *Assistant Professor, Agni College of Technology, Chennai, India.*

Abstract— **Evaluation of Blood Smear is one of the most basic laboratory procedures in Hematology as deviations of blood cell count from their reference values can be indicators of various disease conditions. Digital Image Processing can help the technologists in the analysis and classification of blood cells and diagnosis of certain health conditions based on the CBC values and their morphology. This project aims at generating software that can identify, classify and count various blood cells from the peripheral blood smear samples. Locating, identifying and counting of Blood cells manually can be tedious, time consuming and inaccurate. On the other hand, Automatic Hematology Analyzers that work on Flow cytometry principle for classification are expensive and can perform only quantitative analysis. Thus taking into consideration, the wide scope of Image processing in the field of medicine, this proposed work aims to generate a preliminary framework of Automatic Analysis of Human Blood smear for identification, classification and counting of blood cells by using various Image processing.**

Keywords – Automatic Analysis, Digital Image Processing, Blood cell Identification, Classification of Blood Cells, Blood Cell counting

I. Introduction

Locating, identifying and counting of Blood cells manually can be tedious and time consuming. And classifications under certain conditions need more expertise and practice. Such manual Blood cell counting can be laborious and as it is a subjective assessment it can cause variation in blood cell counting and classification.

Also, it is difficult to train less-experienced technologists using a light microscope set up. Hence, this proposed software can fulfill the above flaws being faced while using manual counting method

On the other hand, Automatic Hematology Analyzers that work on Flow cytometry principle for classification are expensive. They need periodical maintenances and periodical calibrations. They may also incur recurring expenditure by means of Quality Controls and Reagents for each test. Hence, this software will work as a cost effective (especially for smaller labs) and ideally a low maintenance alternative. Also, using Flow cytometry technique based system, basic classification of blood cells that is quantitative analysis can only be done, while identification of abnormal cells and their count can't be performed. Disease conditions like Malaria, Leukemia, Sickle cell anemia etc., can be easily identified by the cell morphology. By use of this proposed software, we can perform a qualitative assessment of the blood cells as well.

Alongside the above mentioned advantages, the proposed work can enable archiving the digital images of each patient, thereby creating an electronic record of the abnormalities for future references. Also, this help in accessing the images through the Laboratory Information System (LIS) and can be used as an aid in telemedicine technology.

Besides, this framework can help laboratories in consistency of cell identification, accuracy of identification and in reducing labour cost. This method can typically reduce the sample reviewing time by the pathologists.

While there are many works that are related to Human blood cell segmentation and counting, there has been no work found that can process all the three type of blood cell images altogether. Also taking into consideration, the wide scope of Image processing in the field of medicine, this work aims to generate a preliminary framework of an Automated System that can analyse the Human Blood Smear Images to identify, classify and count various types of blood cells – viz., Red blood Corpuscles (RBC), White Blood Corpuscles (WBC) and Platelets (PLT). This work can overcome various drawbacks that are being faced while using Conventional Microscopy Technique or a Flow cytometry technique

II. Proposed Methodology

The proposed work presents an automated method that can classify and count all the three types of Blood cells – RBC, WBC and PLT. This set of values altogether is called the *Complete Blood Count* (CBC) value, which is an essentially useful parameter in various diagnoses. Finding the CBC value is one of the inevitable ways to evaluate the patients' health. While the manual method has various drawbacks like excess time consumption and inaccuracy, the Automatic flow cytometry method has disadvantages of recurring cost, repeated Quality assessments and falls short of Qualitative assessments.

ISBN 978-1-5386-4473-7

This work aims to generate an automated technique for qualitative and quantitative analyses of the blood smear - giving us an information about the count of RBCs, WBCs and PLTs which is the *Quantitative data* and information about different types of WBC cells (Morphological) which is the *Qualitative data*.

A. Block Diagram

This paper presents methodology that aims at finding the Complete Blood Count (CBC) values of the Human blood samples. This is done by use of microscopic images which is processed using certain algorithms which may vary according to the type of blood cell. The Peripheral Blood Smear (PBS) is prepared from the Blood sample in glass slides, whose images are collected through Microscopes with camera of high resolution. The 10x and 40x objectives were used to focus sharply onto the 'body' region of the prepared smear. Images through 10x and 40x objectives were collected.

There are four modules that comprise the proposed work, viz., segmentation and counting of RBCs, segmentation and counting of WBCs, segmentation and counting of PLTs and identification of differential WBC cells. RBC cells are segmented from other cells by taking advantage of the variation in its intensity when compared with other cells' intensity, while WBC and Platelets are segmented based on Area factor. The differential cell identification is done abased on edge detection of the WBC cells' Nuclei. Thus the features like Area and shape are made use of in detection and counting of cells. The following is the overall flow diagram of the proposed work.

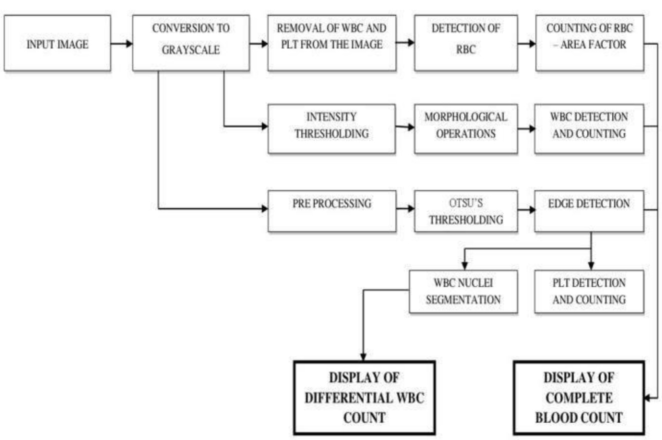

Fig 1. Block Diagram of proposed methods

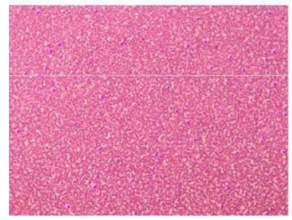

10x Input Image

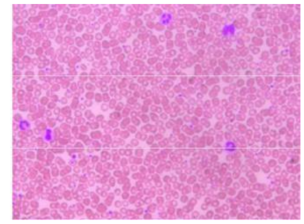

40x Input Image

Fig 2. Input images

B. RBC Segmentation and Counting

The counting of RBC is one of the modules in finding the Complete Blood Count values. The 40x image of the PBS is used in finding the RBC count. This involves using of circular Hough transform to detect the RBC cells among other cell types.

The initial step involves gray scale conversion followed by Image enhancement using Contrast Stretching and Histogram equalisation. After enhancement, images from previous two steps are added, to give image that can help better in segmentation. Then, the image is converted to a binary image by use of thresholding technique. The image after being converted to binary, is subjected toedge detection to trace the edges of segmented RBC Cells

Following the above step is the application of average radius values to detect any overlapping cells or the cells that are almost out of ROI. In case of overlapping, which is a result of improper slide preparation, we may find a circle with radius values more than what is set, however, in case of Out of field cells the radius value will be less than set radius. Thus the RBC cells are detected and counted.

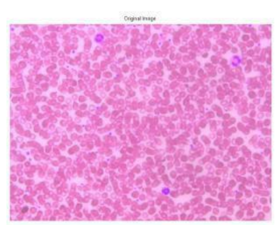

Input Image

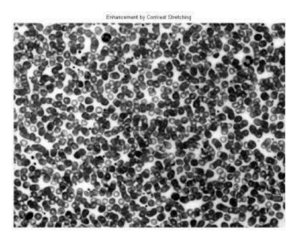

Histogram Equalized Image

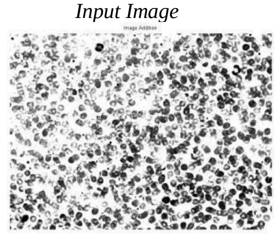

Detected RBCs

Complete RBC Count

Fig 3. RBC Segmentation and Counting

ISBN 978-1-5386-4473-7

C. WBC Segmentation and Counting

The counting of WBC cell is yet another procedure in finding the CBC value of a PBS. The 10x image of the PBS is used for the counting of WBC cells.

For counting of WBC, there is no need of pre-processing as in a 10x image only RBCs and WBCs are visible and platelets being too small aren't visible through a 10x objective. Hence, on conversion to gray scale, there is a vast difference in the intensity ranges that are covered by RBC cells and WBC cells.

Taking advantage of the variations in intensity ranges, Thresholding is applied in order to segment the WBCs out of the PBS Image. Morphological image processing is based on a strong mathematical concept which been used to change the size, shape, structure and connectivity of objects in the image. Thus morphological Opening and closing are done to improve the segmentation of the Cells. Morphological opening removes the stray pixels and protrusions around and on the cell that may cause error while counting. Morphological Closing is then performed on the image to fill and complete broken parts of a cell forming connections between them.

The output at this stage gives completely segmented WBC cells that are ready for counting. The counting of cells is then done and displayed in a separate message box. This procedure is done for 12 images and an average of the WBC count is computed and related to the count that is obtained and confirmed by both manual and Flowcytometry method. This value is taken as reference value for further counting of WBC from other samples. This complete procedure is performed again on samples of unknown values to find the WBC Count based on the reference value.

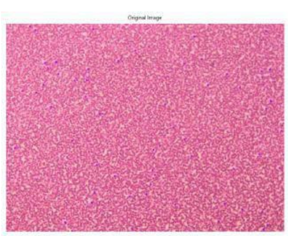

Input Image

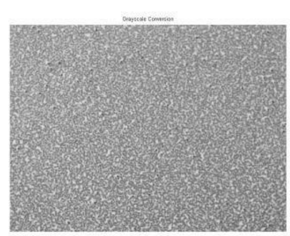

Gray scale converted image

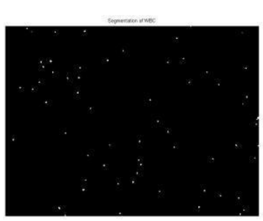

Detected WBCs

Complete WBC Count

TABLE I

ABBREVIATIONS FOR THE TERMS USED

S No	Abbreviation	Acronym
1	PBS	Peripheral Blood Smear
2	RBC	Red Blood Corpuscle/Cell
3	WBC	White Blood Corpuscle /Cell
4	PLT	Platelets

D .Segmentation and counting of WBC Nuclei and Platelets

The segmentation of WBC nuclei and Platelets is done on 40x images. As previously mentioned the platelets are too small to be visible in a 10x image. Hence we take up 40x image for platelet counting. Also, the WBCs are further classified differentially based on their nuclei shape. As the nuclei aren't visible on a 10x image, we again opt for a 40x image that can clearly show the nucleus of a WBC cell.

For segmentation of both WBC and Platelets, the 40x images are used. Initial step being conversion to gray scale image, the segmentation follows a sequence of procedure. The gray scale image is subjected to Contrast Stretching and Histogram Equalization. The Contrast Stretched and Histogram Equalized images are then added and subtracted to and from each other.

The resultant images are then added to get an output which is then subjected to Otsu's thresholding. Otsu's method converts the gray scale image into binary image based on the bimodal histogram of the gray scale image that depicts the foreground and background components of the PBS image. Thus the WBC and PLTs are segmented by the thresholding technique. The edge detection is then performed to find out the proper shape of WBC nuclei. At this point the output image consists of both WBC Nuclei and the PLTs Thus by further step of morphological opening, the platelets are removed to isolate the nuclei for further classification. This stage's output is also retained as a mask that is used to remove WBC nuclei and retain the PLTs. Hence the PLTs are also segmented and the output image can be taken up for further counting of PLTs. As in case with WBC counting, we set a reference value here as well and based on the reference value we can further segment and count the PLTs.

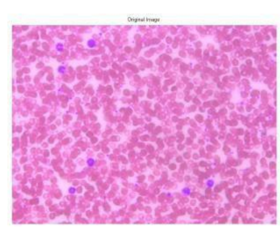

Input Image

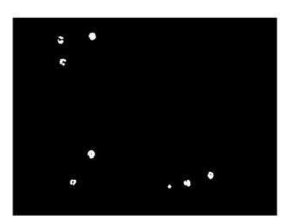

Segmented WBC Nuclei

Detected PLTs

Complete WBC Count

Thus the methodologies to implement RBC, WBC and PLT Classification and counting were discussed as above.

III. Performance Analysis

The proposed framework is a system to automatically segment and count all three types of blood cells and also provides results for differential WBC Analysis. So the system is a combination of three blocks that can give the CBC Value and Differential Analysis of WBC. Our proposed system uses intensity and area factors to segment and count each type of blood cell.

The goal of this work is to provide a cost effective and less time consuming alternative to currently available methods. Also, it eliminates the need for expert lab Technicians to perform CBC and Differential WBC Analysis. The proposed system has a reasonable processing time and the RBC module shows an accuracy of 92.5% while WBC and PLT Module show accuracy of 96.7% and 91% respectively. However as the smears are prepared manually, errors in the staining process and intensity or blurring issue during image capture can significantly affect the results. Through this work, Complete blood count of RBC, WBC and PLTs can been found; and the differential classification of WBC Cells has been done as the WBC Nuclei are of 5 types, that vary in the shapes of their nuclei.

Future work can be extended towards development of automated cell counters using Artificial Neural Networks that includes segmenting WBCs into nuclei and cytoplasm, feature extraction from each region, classifying WBCs into five categories, and accurate disease diagnosis. Texture analysis can be used to quantify intuitive qualities described by terms such as rough, smooth, silky, or bumpy as a function of the spatial variation in pixel intensities by which different WBC Cells and RBC Cells can be counted accurately.

IV. Conclusion

While there are many such works that were conducted on Blood Cell Classifications, they have shown to concentrated only on one type of Blood Cell or only on Differential Classification of WBC. This proposed works aims at both Qualitative and Quantitative Analysis simultaneously there by giving Complete Blood Count and the Differential WBC information at the same time. Thus this work can effectively be used as an alternative to conventional Microscopic studies and the Flow cytometry Methods

V. References

[1] Anjali Gautam and H.S.Badauria (2014), White Blood Nucleus Extraction Using K-Mean Clustering and Mathematical Morphing, IEEE Conference – Confluence – The Next generation Information Technology Summit, Pg: 549 – 554.

[2] Firdaus Ismail Sholey (2013), White Blood Cell Segmentation for Fresh Blood Smear Images – IEEE International Conference on Advanced Computer Science and Information Systems (ICACSIS), Pg: 425 – 429.

[3] Jyoti Rawat, A.Singh and H.S. Badauria (2014), An Approach for Leukocytes Nuclei Segmentation based on Image Fusion – IEEE International Symposium on Signal Processing and Information Technology (ISSPIT), Pg: 000456 –000461.

[4] Mausumi Maitra, Rahul Kumar Gupta and Manali Mukherjee (2012), Detection and Counting of Red Blood Cells in Blood Cell Images using Hough Transform - International Journal of Computer Applications (0975 – 8887) Volume 53– No.16.

[5] P.Maji, A.Mandal and M.Ganguly and S.Saha (2015), An Automated method for counting and characterising Red Blood Cells using mathematical morphology - IEEE International Conference on Advances in Pattern Recognition (ICAPR), Pg:1 – 6.

[6] Ratnadeep Dey and Pramit Ghosh (2015), An Automated system for Segmenting platelets from Microscopic images of Blood Cells – IEEE International Symposium on Advanced Computing and Communication (ISACC), Pg: 230 – 237.

[7] Shubhangi Khobragade, Dheeraj D Mor,Dr. C.Y.Patil (2015), Detection of Leukemia in Microscopic White Blood Cell Images, IEEE International Conference on Information Processing (ICIP)Pg: 435 – 440.

[8] Siti Madihah Mazalan, Nasrul Humaimi Mahmood (2013), Automated Red Blood Cells Counting in Peripheral Blood Smear Image Using Circular Hough Transform - IEEE International Conference on Artificial Intelligence, Modelling & Simulation, Pg: 320 – 324.

[9] S. S. Adagale, Ms. S. S. Pawar (2013), Image Segmentation using PCNN and Template Matching for Blood Cell Counting - IEEE International Conference on Computational Intelligence and Computing Research IEEE International Conference on Computational Intelligence and Computing Research,Pg: 1 –5.

[10] S.S.Savkare and S.P.Narote (2015), Blood Cell Segmentation from Microscopic Blood Images -IEEE International Conference on Information Processing (ICIP), Pg: 502 – 505.

ISBN 978-1-5386-4473-7
IEEE sponsored 4th International Conference on Biosignals, Images and Instrumentation, SSNCE, Chennai. ICBSII 2018 – 22nd-24th Mar'18

Contrast Enhancement of Medical Radiography Images Using Edge Preserving Filters

Lekshmy Sudha Kumari, Rajan Kanhirodan
Department of Physics
Indian Institute of Science
Bangalore, India

***Abstract*—Radiographic medical imaging is a key diagnostic tool for many diseases and has an important role in monitoring treatment and predicting outcome. As in the case with any other medical imaging modality, insufficient image contrast associated with the X-ray images could negatively affect the treatment process. Methods to improve the contrast in X-ray images by intensifying the X-ray dose delivered to the patient is also not advisable due to the harmful effects of the increased intensity radiation on the body. Therefore, the image quality improvement through post processing techniques is an essential part of medical imaging. This paper aims to present an iterative algorithm based on Guided Image Filtering for contrast enhancement of X-ray images.**

Keywords—Medical Imaging; Contrast Enhancement; Histogram Equilization; Adaptive Histogram Equalization; CLAHE; Guided Image Filter.

I. INTRODUCTION

Medical imaging plays a very important role in advancement in diagnosis and treatments of various diseases. Different types of medical imaging procedures are presently in use based on different technologies. Radiography can be considered as one of medical imaging techniques used widely by physicians for diagnosis and treatment of various physical conditions and diseases. Radiography uses X-ray beams for visualizing the internal body parts. The body part which needs to be studied for diagnosis or treatment of a particular physical condition is subjected to an acceptable quantity of X-ray exposure. Based on the internal structure of the body part, a part of the X-ray will be absorbed or scattered. The portion which is neither absorbed nor scattered is made to fall on a detector which helps in recording an image. Evaluation and conclusions are later done based on the recorded image. Radiography is also extensively used in industries for nondestructive testing for verifying the structure and integrity of the manufactured components.

Dynamic range in a digitally acquired images is defined as the ratio between the brightest and the darkest pixel in the image. Even the most advanced cameras fail at capturing the wide dynamic range to accurately represent the radiance of a natural scene, containing several orders of magnitude from light to dark regions. However, several novel techniques have been developed to synthesize HDR images from several low dynamic range images that have been obtained under varying exposures. HDR imaging was introduced to address this problem of low dynamic range in images. These techniques, thus aim at increasing the dynamic range of the captured images. HDR imaging is used in many applications, including biomedical imaging[14], remote sensing[13], and photography[15]. Hence, when compared to the conventional low dynamic range (LDR) images, the features of both the dark and bright areas of a scene are secured well by the HDR images[1]. Advancements in the imaging technology has helped in capturing, synthesizing and storage of the increased dynamic range images possible. But the output limitations of the display methods have not followed the same level of advancement. The conventional display devices have only limited dynamic range and hence cannot faithfully reproduce the captured HDR images. Tone-mapping algorithms scale the large range of luminance information so as to effectively display on a device with much lower dynamic range capability. The tone mapping algorithm, thus, realizes a dynamic rage compression. The goals of these algorithm specifically depend on their applications. In the case of medical imaging, the tone -mapping algorithms aim to provide increased contrast so as to enhance the detail information from the image, as required by a physician examining the medical images to come up with accurate conclusions.

In this paper, we present an iterative algorithm based on a well-known guided image filter for tone mapping and contrast improvement of HDR radiographic medical images. First, the guided image filter is used to bifurcate the image into base layer, i.e., the lower frequency components of the image and detail layer i.e., higher frequency components of the image. Our iterative algorithm selectively boosts the detail layer so that faintest changes in image data are easily perceived. The paper is organized as follows. We review relevant work on the tone mapping and contrast enhancement in section II, whereas Section III presents the overview and image enhancement using edge preserving filters. Further in Section IV we discuss base and detail manipulation techniques using the edge preserving filters. Finally, Section V concludes the paper.

II. BACKGROUND

In image processing, it is important to get contrast enhancement without introducing any artifacts. Various enhancement techniques have been developed to address this[5]. We state here few of the techniques which represents the cutting edge approaches in contrast enhancement of images and which form the basis of various tone mapping algorithms.

ISBN 978-1-5386-4473-7

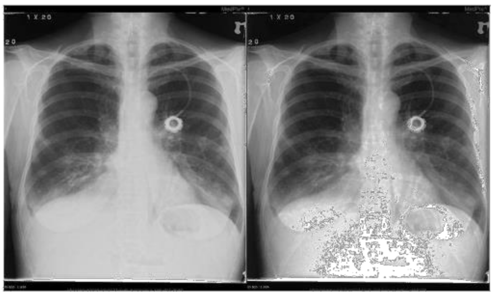

Fig. 1. Image enhancement using histogram equalization.

A. Histogram Equilization

Histogram equalization is a much widely used image enhancement technique. In histogram equalization, the gray levels in the image are redistributed more evenly(for example [0-28-1] levels for an 8 -bit device.)[6]. In order to increase the contrast in an image, the histogram equalization technique spreads out the pixel intensity values along the total range of values. The gray levels in the input image is remapped via a cumulative density function(CDF). This results in the expansion of the interval gray level between high and low histogram components. For an input image I(x,y) composed of discrete gray levels in the dynamic range of [0,L-1], the transformation function C(*rk*) is defined as:

$$S_k = T(r_k) = \sum_{i=0}^{k} P_r(r_i) = \sum_{i=0}^{k} n_i/n \qquad (1)$$

where $0 \leq S_k \leq 1$ and k = 0,1,2,3...L-1, n_i is the number of pixels with gray level r_i, n represents the total number of pixels in the input image, and the Probability Density Function of the input gray level r_i is represented by $P_r(r_i)$. Based on the PDF, the Cumulative Density Function is defined as C(r_k). The level-mapping equation, based on which the histogram equalization operation maps an input level k into an output level, is given by:

$$H_k = (L - 1) \times C(r_k) \qquad (2)$$

This increase in the luminance difference in the image causes the objects in the input image to become clearly distinguishable, thus enhancing the contrast[8]. This method of increasing the contrast using histogram equalization is much useful when an image has close contrast values and hence is often used to achieve contrast enhancement in medical imaging such as digital X-rays. Fig. 1 shows the enhancement achieved using histogram equalization under standard settings, with Fig. 2 showing the histogram of the input and the enhanced images.

However, the basic Histogram Equalization technique might result in unwanted effects, where the highly probable intensity levels become over enhanced and the levels with low probabilities get less enhanced. This results in signal frequencies with low probability to get either reduced or eliminated in the output image. Moreover, false contour might occur in the enhanced image due to the excessive merger of gray levels[9].

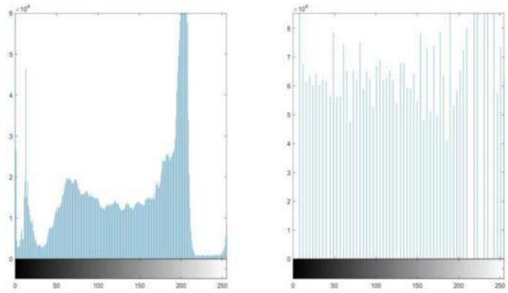

Fig. 2. Image Histogram of the input image(left) and the enhanced image using HE(right

B. Adaptive Histogram Equilization

As mentioned, for images containing local regions of low contrast bright or dark regions, a simple histogram equalization will not give effective enhanced results. In order to address this shortcoming of the simple histogram equalization method, new methods were proposed. One such method called the Adaptive Histogram Equalization (AHE) is a modification of the basic histogram equalization method. Instead of operating on the entire image, the AHE method operates on small data regions called the tiles. Histogram equalization mapping is applied on to each pixel in an image based on its neighboring pixels. This neighboring region is called *contextual region*.

Initially histogram equalization operation is applied on each tile in an image to enhance the contrast. It is followed by combining the contrast enhanced neighboring tiles using a bilinear elimination. This is done to eliminate artificially induced boundaries in the enhanced output image. Fig. 3 shows the enhancement achieved using adaptive histogram equalization under standard settings, with Fig. 4 showing the histogram of the input and the enhanced images using the method. Even though this modified technique is known to produce good contrast enhancement and better detail extraction, AHE also has some disadvantages. The most notable downside of AHE is the enhancement of noise in the image, if any, along with enhancing the image[2]. This causes considerable impact in the accurate examination of medical images by the clinicians

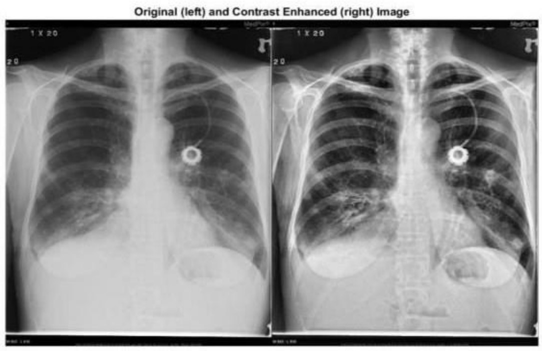

Fig. 3. Image enhancement using adaptive histogram equalization.

ISBN 978-1-5386-4473-7

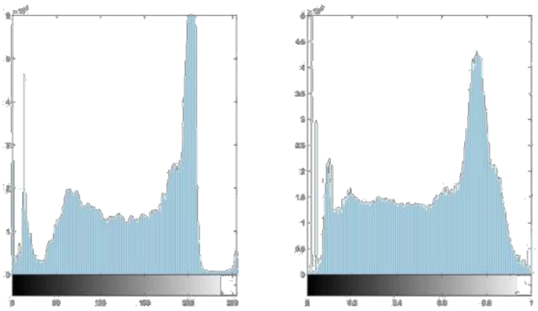

Fig. 4. Histogram of the input image(left) and the enhanced image using AHE(right).

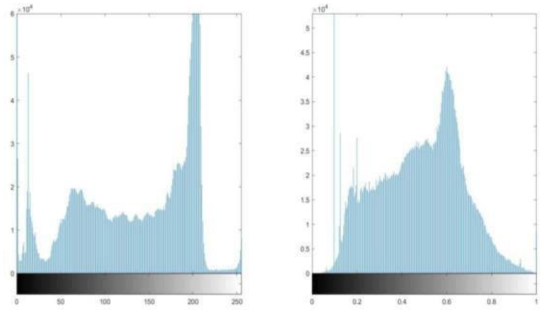

Fig. 6. Histogram of the input image(left) and the enhanced image using CLAHE(right).

.

C. Contrast Limited Adaptive Histogram Equalization

Contrast Limited Adaptive Histogram Equalization(CLAHE) was developed as a solution to the major disadvantage of noise amplification in adaptive histogram equalization. This method is formulated based on dividing the image into different non-overlapping regions. To achieve this, the contrast enhancement of AHE is limited[2].

In CLAHE, histogram of each of the regions is calculated. A clip limit for clipping the histograms is obtained based on a desired limit for contrast enhancement. Each histogram is redistributed such that its height does not go beyond the clip limit, β. The additional counts beyond β are uniformly distributed among the gray scales with counts within β through an iterative process. Further, the cumulative distribution function(CDF) of the contrast limited histograms is calculated for histogram equalization of the gray scale mapping. The pixels are then mapped by linearly combining the results from the mappings of the four nearest regions[10]. Fig. 5 shows the enhancement achieved using adaptive histogram equalization under standard settings(clip limit of 0.02 and Rayleigh distribution of the counts exceeding the clip limit value), with Fig. 5 showing the histogram of the input and the enhanced images using the CLAHA method.

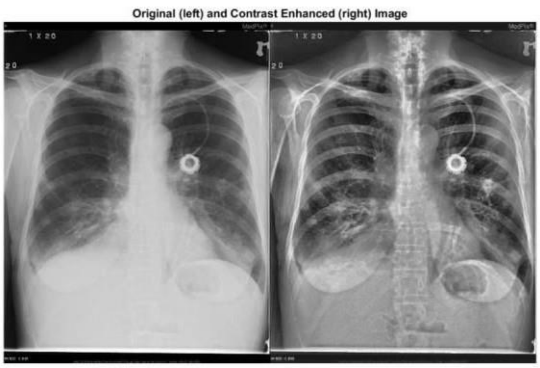

Fig. 5. Image enhancement using Contrast Limited adaptive histogram equalization.

It can be inferred from literature that contrast limited adaptive histogram equalization has made good achievement in producing effective enhancement on medical images. However this technique of histogram equalization based on a clip limit is proved to have the drawbacks of noise amplification in flat region and introduction of ring artifacts at strong edges.

III. IMAGE ENHANCEMENT USING EDGE PRESERVING FILTERING

Edge preserving filters have been well researched and documented since 1990's. In edge-preserving smoothing operation, the image is separated into large-scale layer and detail layer. The detail-scale retains the small variances of the image and large-scale retains the large variance, like edges, of the original image. Such a type of decomposition of the image can be used for tone mapping[11][12]. Several edge preserving smoothing algorithms, including have been developed in the last three decades and they are known to produce better results as tone mapping algorithms and in improving the features of the input images, than the algorithms based on histogram equalization methods. Of the various well developed edge preserving filters, we could observe from our past study that, guided image filter[3] is more consistent in restoring noisy images with excellent edge preserving and image enhancing features.

He et al. [3] proposed a new type of explicit edge preserving image filter - the guided image filter as an alternative to the bilateral filter which is known to introduce gradient reversal like artifacts in filtered images. Derived from a local linear model, the guided filter produces the filtering result (Q) by considering the contents of an input image (I) and guidance image (G). The guidance image can be the input image or another different image, this choice depends on the user's application. The filtering result is locally a linear transform of the guidance image. The filter exhibits good smoothing performance, while suppressing the gradient reversal like

ISBN 978-1-5386-4473-7
IEEE sponsored 4th International Conference on Biosignals, Images and Instrumentation, SSNCE, Chennai. ICBSII 2018 – 22nd-24thMar'18

artifacts. Fig. 7 shows the excellent detail enhancement feature of guided image filtering operation.

The guided filter can be operated with an O(N) computational cost where the number of pixels are N on both gray and color images. The output of the guided filter for a pixel is computed as a weighted averages as follows:

$$Qi = \sum_j W_{i,j}(G)I_i \tag{3}$$

Here, *(i,j)* are our image pixel indices and $W_{i,j}$ is the filter kernel, which, is a function of the guidance image *G*. If *Q* is a linear transform of *G* in a patch centered at the pixel *k* as given below:

$$Qi = a_kG_i + b_k , \forall i \in \omega_k \tag{4}$$

In the above equation, a_k,b_k are linear coefficients, which have been assumed to be constant in ω_k and computed over a small window whose radius is *2r+1 × 2r+1*. This model ensures that *Q* will have an edge only if the guidance image has an edge too. In [3] a_k, b_k have been computed to minimize the following cost function:

$$E(a_k,b_k) = \sum ((a_kG_i + b_k - I_i)^2 + \mathcal{E}a_k^2) \tag{5}$$

Here, $\mathcal{E}$ is a regularization parameter on the linear coefficient *a* for numerical stability. In [3] the importance of the regularization parameter and its relation to the bilateral kernel is given. For our implementation, we have chosen to use $r = 8$ and $\mathcal{E} = 0.01$.

The linear coefficients used to minimize the cost function in 5 are determined by linear regression as follows:

$$a_k = ((1/|\omega|)\sum_{i\in\omega k} G_I I_i - \mu_k I'_k) / (\sigma_k^2 + \mathcal{E}) \tag{6}$$

$$b_k = I'_k - a_k\mu_k \tag{7}$$

$$I'_k = (1/|\omega|) \sum_{i\in\omega k} I_i \tag{8}$$

In the above equation μ_k and σ_k^2 are the mean and variance of *G* in ω_k, $|\omega|$ is the total pixel count in the image patch ω_k, and I'_k is the mean value of *I* again in ω_k patch. The linear coefficients a_k and b_k are computed for all windows ω_k

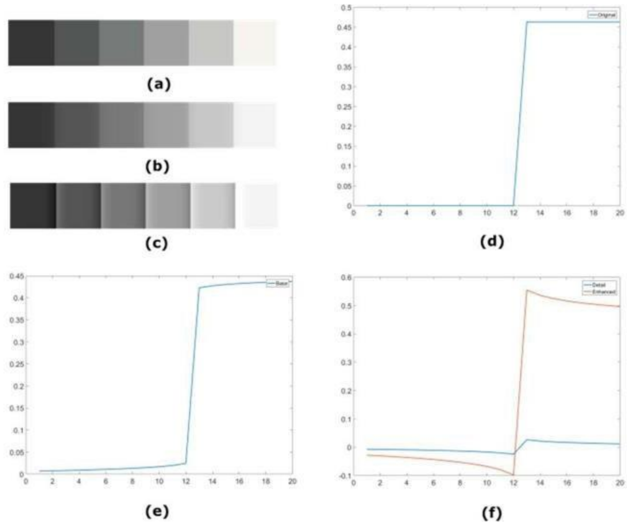

Fig. 7. Detail enhancement using the guided filter \cite{He}. (a) Input (b) Smoothed using guided filter. (c) Edge enhanced (d) Original 1-D edge profile (e) Base layer and (f) Original and enhanced detail.

through the image. However, one pixel *i* is involved in all the above windows ω_k that contains *i* so the value of Q_i in 4 will be different for different windows. So, after taking the average of all the possible value of Q_i, the filtered output is determined as in 9

$$Q_i = (1/|\omega|) \sum_{i\in\omega k} (a_kG_i + b_k) = (a'_iG_i + b'_i) \tag{9}$$

In 9, a'_i and b'_i are computed as follows:

$$a'_i = (1/|\omega|) \sum_{k\in\omega i} a_k , \; b'_i = (1/|\omega|) \sum_{k\in\omega i} b_k \tag{10}$$

With the modifications in 9 we can see that, spatially varying strong edges of G_i are preserved in Q_i, that is $AQ \approx a'_iAQ$, while smoothing all other small changes in intensity.

IV. BASE AND DETAIL MANIPULATION USING EDGE PRESERVING FILTERS

We know from [11] that an image can be decomposed into a base layer (low frequency) which captures the large scale intensity variations and detail layer (high frequency) which captures the smaller textures. Given an input image $I_{j,k}$ the base layer ($base_{i,j}$) can be computed by performing an edge preserving smoothing on *I*, and the resulting image will be composed of only large scale variations. And to obtain a detail layer ($detail_{i,j}$) of the image *I*, we just need to perform the subtraction or division between *I* and *base_layer*, the resulting difference or quotient is the required detail layer depending on the operation we choose.

The base layer (11) and detail layer (12) can be manipulated separately for various applications. For example, in tone mapping the base layer is compressed using some mapping function and enhanced or attenuated detail layer is fused back to obtain a tone-mapped image [16][17]. In computer graphics the base and detail layer have been independently manipulated to realize various applications like video stylization [18] pencil drawing and re-coloring [19].

A. Detail enhancement using guided filter

In our contrast enhancement algorithm, $base_{(i,j)}$ a base layer is computed from 9 as follows:

$$base_{(i,j)} = Qi \tag{11}$$

For a given input image $I(i,j)$, we can define detail layer as the difference between the input image and the guided filtered output image:

$$detail(i,j) = I(i,j) - base(i,j) \tag{12}$$

In our implementation we directly operate on the three channels of the input image using guided filter, we used the same input image as the guidance image. The input image I is decomposed into the low frequency base layer (b) and detail layer (d). The one dimensional edge profile of the input image, base and detail layer are shown in Fig. 7. The detail enhanced image is obtained using the following equation:

$$J = baselayer \times k1 + detaillayer \times 5 \tag{13}$$

The boosted detail layer 1-D profile is shown in Fig. 7. In the above equation we used $0.8 \leq k_1 \leq 1$. This configuration suits the medical radiography images as it leads stronger contrast perception, while highlighting the bone features. In Fig. 8 we present more detail enhanced images for visual inspection. We can easily notice that smaller image data in input images are clearly visible in the output images, we have highlighted the regions of interest with a close up view.

B. Comparison with WLS filter

Farbman[11] proposed a global optimization filter, that makes use of a multi -scale edge-preserving decomposition, based on the Weighted Least Squares (WLS) method. Given an input image I, the algorithm computes a new image R, which is as close as possible to I, and, is as smooth as possible everywhere, except across significant gradient regions(like strong edges) in the input image, I[11]. As a variation, we used WLS filter to construct two layers of the CIELAB luminance channel to compute a multi-scale edge-preserving decomposition of the input image Fig. 9. From the Fig. 9, detail enhancement result obtained using the WLS filter, we notice that, even though the contrast ratio is better in WLS filter detail enhancement method, but the resulting image is prone to gradient reversal (see highlight Fig. 9). It occurs primarily, due to the abrupt changes of the edge caused by the detail enhancement. However, as expected the resulting image obtained from guided filter is cleaner (Fig. 9), as the guided filter gradually erodes the edges without notably distorting the shape of the original signal. From our cursory experiments, we feel that a combined approach could result in more stable and interesting results. For example, a guided filter image can be iteratively enhanced using WLS method for stronger detail manipulation, thus combining the inherent advantages of both the filters, while keeping a check on the accompanying issues that may arise in the pipeline. A few iterations might be required to obtain optimum result.

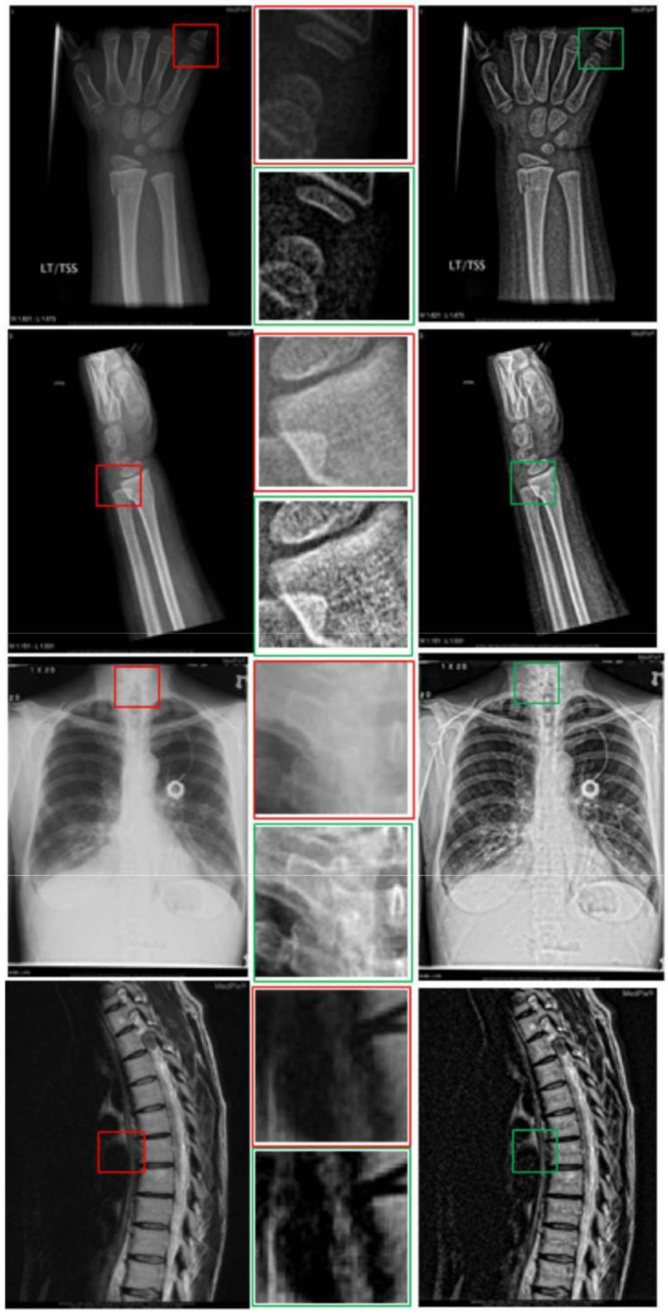

Fig. 8. Visual evaluation of our contrast enhancement algorithm. (Left) Input radiography images. (Center) Corresponding highlights enlarged. (Right) Detail enhanced output images generated.

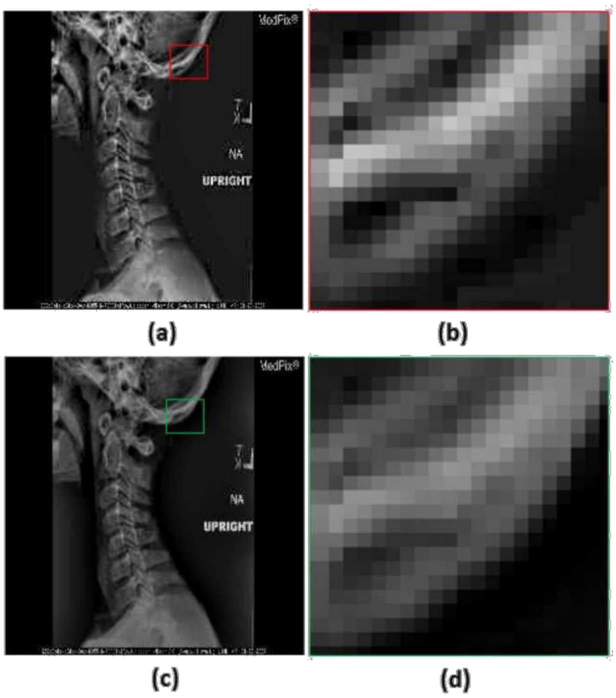

Fig. 9. (a) Detail enhancement using the WLS filter[11]. (b) Appearance of gradient reversal artifacts in WLS filtered image. (c) Detail enhanced using guided filter[3] (d) Artifact less close up of the same patch, while using guided filter.

V. CONCLUSIONS

Radiography images are vital for medical diagnosis and prognosis, however the advancement in radiography instruments are limited by the kind of X-ray dosages that can be delivered to patients. Here, we presented a simple post processing algorithm that manipulates the image details using the well known guided filter. The advantage of using this filter is the delicate balance it provides in suppressing artifacts like gradient reversals while enhancing the useful fine details. As an extension, more iterative detail layers can be enhanced and blended with the current layers to reveal more finer textures. However, a trade-off should be set, to the point where computational time versus the details enhanced tends to become bottleneck.

REFERENCES

[1] Li, Zhengguo, and Jinghong Zheng. "Visual-salience-based tone mapping for high dynamic range images." IEEE Transactions on Industrial Electronics 61.12 (2014): 7076-7082.

[2] Pizer, Stephen M., et al. "Adaptive histogram equalization and its variations." Computer vision, graphics, and image processing 39.3 (1987): 355-368.

[3] He, Kaiming, Jian Sun, and Xiaoou Tang. "Guided image filtering." IEEE transactions on pattern analysis and machine intelligence 35.6 (2013): 1397-1409.

[4] Gu, Bo, et al. "Local edge-preserving multiscale decomposition for high dynamic range image tone mapping." IEEE Transactions on image Processing 22.1 (2013): 70-79.

[5] Debevec, Paul, and Simon Gibson. "A tone mapping algorithm for high contrast images." 13th Eurographics Workshop on Rendering: Pisa, Italy, June 26-28, 2002. Association for Computing Machinery, 2002.

[6] Larson, Gregory Ward, Holly Rushmeier, and Christine Piatko. "A visibility matching tone reproduction operator for high dynamic range scenes." IEEE Transactions on Visualization and Computer Graphics 3.4 (1997): 291-306.

[7] Boschetti, Alberto, et al. "High dynamic range image tone mapping based on local histogram equalization." Multimedia and Expo (ICME), 2010 IEEE International Conference on. IEEE, 2010.

[8] Hum, Yan Chai, Khin Wee Lai, and Maheza Irna Mohamad Salim. "Multiobjectives bihistogram equalization for image contrast enhancement." Complexity 20.2 (2014): 22-36.

[9] Zhu, Youlian, and Cheng Huang. "An adaptive histogram equalization algorithm on the image gray level mapping." Physics Procedia 25 (2012): 601-608.

[10] Reza, Ali M. "Realization of the contrast limited adaptive histogram equalization (CLAHE) for real-time image enhancement." The Journal of VLSI Signal Processing 38.1 (2004): 35-44.

[11] Farbman, Zeev, et al. "Edge-preserving decompositions for multi-scale tone and detail manipulation." ACM Transactions on Graphics (TOG). Vol. 27. No. 3. ACM, 2008.

[12] Tumblin, Jack, and Greg Turk. "LCIS: A boundary hierarchy for detail-preserving contrast reduction." Proceedings of the 26th annual conference on Computer graphics and interactive techniques. ACM Press/Addison-Wesley Publishing Co., 1999.

[13] Gyanesh Chander, Brian L. Markham, and Dennis L. Helder. Summary of current radiometric calibration coefficients for Landsat MSS, TM, ETM+, and EO-1 ALI sensors. Remote Sensing of Environment, 113(5):893–903, May 2009.

[14] Julia H. Jungmann, Luke MacAleese, Jan Visser, Marc J. J. Vrakking, and Ron M. A. Heeren. High Dynamic Range Bio-Molecular Ion Microscopy with the Timepix Detector. Analytical Chemistry, 83(20):7888–7894, 2011.

[15] Christian Bloch. The HDRI Handbook 2.0: High Dynamic Range Imaging for Photographers and CG Artists. Rocky Nook, 2013.

[16] Pattanaik, S. N., Ferwerda, J. A., Fairchild, M. D., \& Greenberg, D. P. (1998, July). A multiscale model of adaptation and spatial vision for realistic image display. In Proceedings of the 25th annual conference on Computer graphics and interactive techniques (pp. 287-298). ACM.

[17] Tumblin, J., \& Turk, G. (1999, July). LCIS: A boundary hierarchy for detail-preserving contrast reduction. In Proceedings of the 26th annual conference on Computer graphics and interactive techniques (pp. 83-90). ACM Press/Addison-Wesley Publishing Co.

[18] DeCarlo, D., \& Santella, A. (2002, July). Stylization and abstraction of photographs. In ACM transactions on graphics (TOG) (Vol. 21, No. 3, pp. 769-776). ACM.

[19] Gastal, E. S., \& Oliveira, M. M. (2011, August). Domain transform for edge-aware image and video processing. In ACM Transactions on Graphics (ToG) (Vol. 30, No. 4, p. 69). ACM.

ISBN 978-1-5386-4473-7
IEEE sponsored 4th International Conference on Biosignals, Images and Instrumentation, SSNCE, Chennai. ICBSII 2018 – 22nd-24thMar'18

Augmentation of Statistical Features in Cytopathology Towards Computer Aided Diagnosis of Oral Precancer/Cancer

Saunak Chatterjee, Debaleena Nawn, Mousumi Mandal, Jyotirmoy Chatterjee
School of Medical Science and Technology
Indian Institute of Technology Kharagpur
Kharagpur, India
E-mail: saunakchatterjee14@gmail.com, jchatterjee@smst.iitkgp.ernet.in

Somdutta Mitra, Mousumi Pal, Ranjan Rashmi Paul
Department of Oral & Maxillofacial Pathology
Guru Nanak Institute of Dental Sciences and Research
Kolkata, India

***Abstract*—Oral cancer is a leading malignancy and a rising concern in India. Early detection of the disease is essential at reducing mortality. In this paper, we propose a computer assisted method for diagnosis of oral pre-cancer/cancer using oral exfoliative cytology. A combination of features were extracted from expert delineated cells and nuclei collected from cytology of patients suffering from oral sub- mucous fibrosis, oral leukoplakia or oral squamous cell carcinoma and subject with no lesion. These features were used to train predictive machine learning models like support vector machine, k nearest neighbor, random forest, etc. These models were verified using validation data set. The verification experiments showed promising results with the random forest classifier having a test accuracy of 90%.**

Keywords—oral exfoliative cytology; oral pre-cancer/cancer; image processing; machine learning.

I. Introduction

Cancer in the lip and oral cavity is a leading cause of cancer which accounts for 11.3% prevalence rate and 10.2% mortality rate among male cancer victims in India [1]. 95% of oral cancer patients are of the form of oral squamous cell carcinoma (OSCC) [2]. OSCC is generally preceded by some form pre-cancers like oral sub mucous fibrosis, oral leukoplakia, oral erythroplakia, etc. [3].Oral leukoplakia (LKP) is the most common premalignant lesion of all other pre-cancers [4]. It has been highly related to smoking and chewing habits. It has been shown that the duration and frequency of usage of tobacco relates to the prevalence of this disease [5]. On the other hand Oral sub mucous fibrosis (OSF) is a condition which predominantly affects the Indian population [6]. Studies have found a rising incidence rate of OSF in the Indian population [7]. The cause of this disease has been attributed to the excessive use of areca nuts which is an ingredient used in gutka and betel quid.

The high mortality rate of oral cancer in India is mainly due to late diagnosis of patients. Histopathological evaluation is the current gold standard for detection of oral cancer or pre-cancer among patients with clinically identifiable lesions [8]. The process of histopathological evaluation begins with a biopsy of the lesion region. This is an invasive process and is only done in extreme cases. However, a number of non-invasive and semi-invasive techniques for early detection of oral cancer and pre-cancer exist [9]. One of the non-invasive procedures for early detection is exfoliative cytology. It is a semi invasive procedure that can be carried out as a preliminary examination [10]. Due to the painless nature of this procedure it has a high compliance among patients. The Papanicolaou staining procedure is a popular staining procedure used in cytological slides. However, this examination is purely qualitative in nature and thus is exposed to subjectivity.

Numerous cytomorphometric studies have been conducted to find the differences in cells and nuclei among disease and normal conditions. Ramaesh et al. found significant difference among the cellular and nuclear diameters in cells from normal mucosa, dysplastic lesions and OSCC lesions [11]. Pektas et al. studied features like nuclear perimeter, area, diameter, etc. revealing statistically significant differences among the disease and control groups [12]. Our literature review suggests that features other than morphology have not been studied in oral exfoliatve cytology.

This study proposes augmentation of statistical features like shape, intensity & color, texture and histogram bins to train predictive machine learning models capable of distinguishing cells in normal subjects or patients with OSCC, LKP and OSF.

II. Methodology

A. Sample Collection and Preparation

Oral smears from patients diagnosed with OSF (n=21), LKP (n=20) or OSCC (n=19) were collected from the Dept. of Maxillofacial Surgery at Guru Nanak Institute of Dental Sciences. As a control group we also collected oral smears from persons with no lesion and no oral habits (n=20). The epidemiological data of the sampled patients are shown in table I. The collected oral smears were fixed on slides and stained using the Papanicolaou staining procedure. The Pap stained slides were imaged using Zeiss Observer.Z1 microscope (Carl Zeiss) under 200x magnification and bright field setting. The resultant images were 3 channels (red, green, blue), 1388 × 1040 pixel resolution with a bit depth of 24. A total of 800 images

ISBN 978-1-5386-4473-7
IEEE sponsored 4th International Conference on Biosignals, Images and Instrumentation, SSNCE, Chennai. ICBSII 2018 – 22nd-24thMar'18

were acquired from all the slides belonging to disease and control group.

TABLE I: Epidemiological data of selected patients in the study

Characteristics		NOM (%)	OSF (%)	LKP (%)	OSCC (%)
Age	21-30	1	3	0	0
	31-40	7	3	4	1
	41-50	7	8	6	4
	51-60	3	5	8	10
	61-70	1	2	1	1
	71-80	1	0	1	3
Sex	M	16	10	19	12
	F	4	11	1	7
Oral Habit	No habit	20	0	0	0
	Smokers	0	5	5	7
	Tobacco chewers	0	8	3	2
	Alcohol	0	3	2	2
	Habits in common	0	5	10	8
Total		20	21	20	19

B. Image Pre-processing

The acquired images were preprocessed to remove noise, enhance edges and normalize the color. Firstly, anisotropic diffusion based noise elimination was adopted. This preserved edges while removing noise from the image. The 2D anisotropic diffusion is given by the (1) and (2).

$$I_t = \mathrm{div}(c(x,y,t)\nabla I) = \nabla c.\nabla I + c(x,y,t)\Delta I \quad (1)$$

$$c(\|\nabla I\|) = \frac{1}{1+(\|\nabla I\|/\kappa)^2} \quad (2)$$

I_t is the smoothened image at t^{th} iteration. ∇I is the gradient of the image and ΔI is the Laplacian of the image. $c(x,y,t)$ is the diffusion coefficient and it controls the rate of diffusion. As discussed, to preserve the edges the coefficient is chosen as a function of the gradient of the image. The function in this case is taken from the work done by Perona & Malik [13].

This was followed by an image sharpening using unsharp masking technique. This process adds a fractional part of the image's high frequency components to the image itself. This enhances those high frequency components like edges. The unsharp masking method is defined by the (3) and (4).

$$I_g = I_0 - (I_0 \star G) \quad (3)$$

$$I_s = I_0 + k \cdot I_g \quad (4)$$

I_0 is the input image and I_s is the resultant sharpened image. G is taken as a Gaussian smoothing kernel convolved ($\star$) with I_0. I_g is an image with the edge or high frequency information.

The sharpened image I_S is obtained by adding a weighted I_g to the input image where k is the weight.

Finally, the images were normalized using the gray world color normalization algorithm. This approach assumes that the mean reflectance in the image is achromatic. The mathematical steps for this method are shown below:

Step 1: Calculate average of individual color channels and grey channel.

$$\bar{R} = \frac{1}{MN}\sum_{x=1}^{M}\sum_{y=1}^{N} I_R(x,y) \qquad \bar{G} = \frac{1}{MN}\sum_{i=1}^{M}\sum_{j=1}^{N} I_G(x,y)$$

$$\bar{B} = \frac{1}{MN}\sum_{x=1}^{M}\sum_{y=1}^{N} I_B(x,y) \qquad \bar{I} = \frac{1}{MN}\sum_{x=1}^{M}\sum_{x=1}^{N} I_{gr}(x,y)$$

Step 2: Calculate ratio of grey channel average with average of individual color channels.

$$\alpha_R = \frac{\bar{I}}{\bar{R}} \qquad \alpha_B = \frac{\bar{I}}{\bar{B}} \qquad \alpha_G = \frac{\bar{I}}{\bar{G}}$$

Step 3: Scale each color channel of original image by calculated ratios.

$$I^*_R = \alpha_R \cdot I_R \qquad I^*_B = \alpha_B \cdot I_B \qquad I^*_G = \alpha_G \cdot I_G$$

The pre-processing steps are shown in Fig. 1.

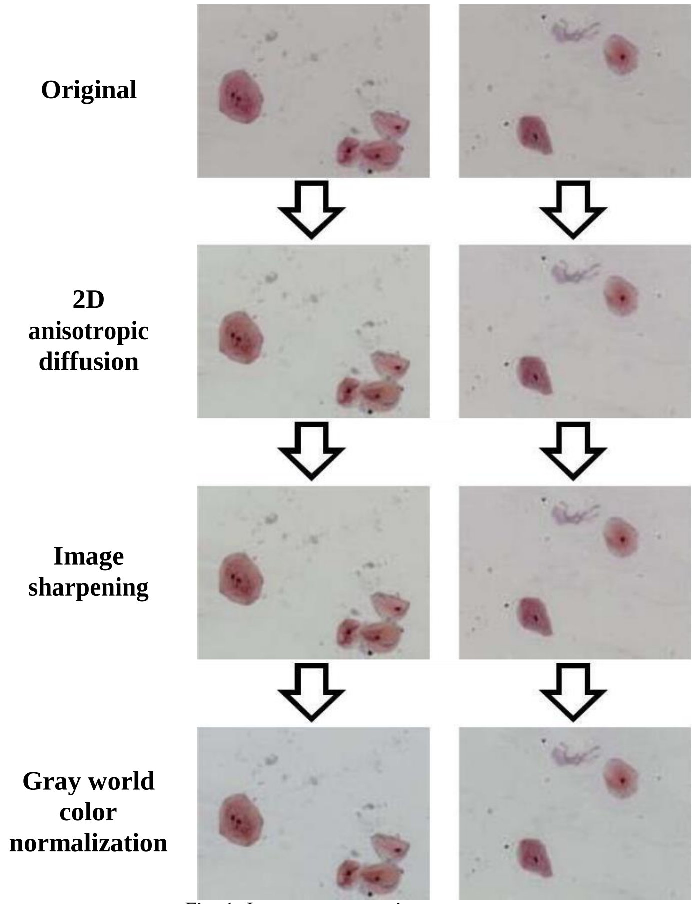

Fig. 1: Image preprocessing steps.

C. Expert Delineation of Cell and Nucleus

The cells and nucleus in the digital images were delineated by expert pathologist. During this process highly overlapping and folded cells were excluded. The cells and nuclei were labeled with the actual diagnosis from histopathological evaluation of the corresponding patient.

D. Feature Extraction

Potential features were extracted from the cells and nuclei delineated by the experts. These features can be broadly classified into morphological, intensity & color, texture and

ISBN 978-1-5386-4473-7

histogram features. Established morphological features like area, perimeter and diameter of cell and nucleus were computed. Apart from area, perimeter and diameter of cell and nucleus eccentricity was also considered which represents the form of the cell or nuclei. For nucleus its irregularity of shape was computed by the area ratio parameter (*ARP*) using (5-7).

$$ARP_p = \frac{1}{Nr} \sum_{k=1}^{N} r_k - \bar{r} \quad p \tag{5}$$

Where, $r_k = \sqrt{(x_k - x_c)^2 + (y_k - y_c)^2}, \quad \forall k \in \{1,2,\ldots N\}$ (6)

And, $\bar{r} = \frac{1}{N} \sum_{k=1}^{N} r_k$ (7)

Intensity and color features included the average intensities and intensity variations within a cell and nucleus. To measure the intensity variation in cytoplasm and nucleus a new approach was used. Concentric ellipses were fit within the cytoplasm or nucleus. Average gray scale values of the image within each concentric ellipses. The variation within these average values was used as the parameter for intensity variation. The average value of hue was also calculated for cytoplasm and nucleus.

In finding a distinguishable feature for cell types, histogram features were computed of the cytoplasm. This was done in a special color space called the HED (hematoxylin, eosin, DAB) color space. This is obtained by a non-linear transform based on the Beer Lambert's law. The parameters for this method were estimated by color deconvolution process [14]. Histogram of the cytoplasm in the eosin channel was extracted from each cell. A total of 8 bins were computed and selected as features. Additionally the number of significant peaks in the histogram was computed to estimate the modality of the histogram.

Gray level co-occurrence matrix (GLCM) features were considered to define nucleus texture. GLCM features of texture energy, correlation, contrast and homogeneity were computed for all nuclei using (8-11) [15].

$$Contrast = \sum_{i,j} |i - j|^2 p(i,j) \tag{8}$$

$$Correlation = \sum_{i,j} \frac{(i - \mu i)(j - \mu j) p(i,j)}{\sigma_i \sigma_j} \tag{9}$$

$$Energy = \sum_{i,j} p(i,j)^2 \tag{10}$$

$$Homogeneity = \sum_{i,j} \frac{p(i,j)}{1 + |i - j|} \tag{11}$$

A total of 31 features were computed for all cells resulting in a labeled data matrix of size 1358x31 comprising of cells from all 4 disease groups. An illustration of the features is shown in Fig. 2. The features are listed in table II.

E. Training and Testing Predictive Machine Learning Models

The extracted data was used to train various machine learning models for disease classification. Five sets of data were created by combining different combinations of the extracted features in order to examine importance of each type of feature for classification. Table III shows the division of feature among these datasets.

TABLE II: Division of analytical features into four groups.

Sl. No	Feature group	Features
1	Morphology	cell area (CA), cell perimeter (CP), cell equivalent diameter (CED), cell eccentricity (C Ecc), nucleus area (NA), nucleus perimeter (NP), nucleus equivalent diameter (NED), nucleus eccentricity (N Ecc), nucleus irregularity (N Irr), nucleus:cytoplasm area ratio
2	Intensity & Color	cell avg hue, cell int. variation, nucleus avg hue, nucleus circular int. variation, nucleus avg int, nucleus int. variation, nuclear hyperchromaticism
3	Nucleus Texture	nucleus texture contrast, nucleus texture correlation, nucleus texture energy, nucleus texture homogeneity
4	Histogram	8 histogram bins, no. of significant peaks in histogram

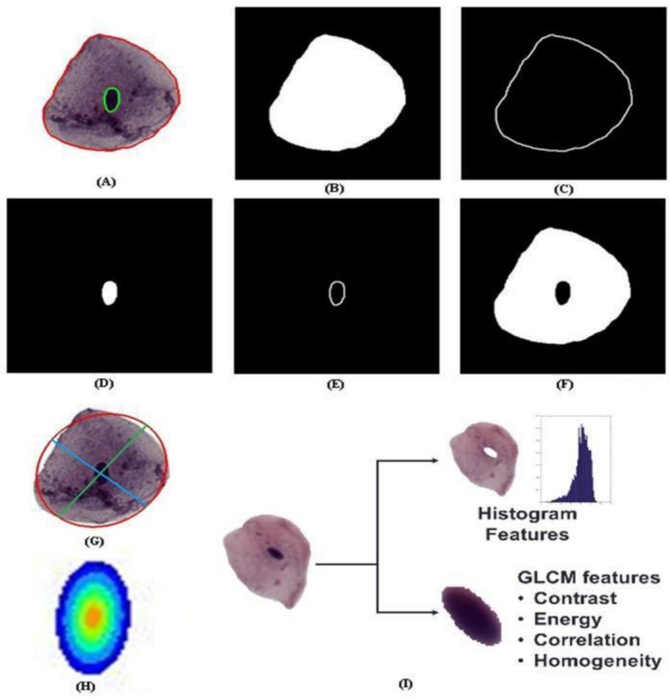

Fig. 2: Proposed features (A) manually delineated outline of cell and nucleus; (B) cell area; (C) cell perimeter; (D) nucleus area; (E) nucleus perimeter; (F) cytoplasm area; (G) fitted ellipse (red) major axis length (green) minor axis length (blue); (H) concentric ellipse fitted inside nucleus, (I) histogram and texture features.

TABLE III: Features groups in data sets.

Data set	Feature set
1	{Morphology}
2	{Morphology, Intensity & Color}
3	{Morphology, Intensity & Color, Nucleus Texture}
4	{Morphology, Intensity & Color, Histogram}
5	{Morphology, Intensity & Color, Nucleus Texture, Histogram}

The labeled data was shuffled and divided into training and testing sets where 30% of the data was reserved for testing. Classifiers like K nearest neighbor (9 neighbors), support vector machine (with radial basis function kernel), multilayer perceptron (with 31 input nodes, two 60 node hidden layer and

4 output nodes), decision tree and random forest (with 100 trees) were trained using the training data as a four class classification problem. The resultant models were tested using the testing data and calculate the average recall and precision scores of the classifiers using (12) and (13).

$$recall = \frac{true\ positive}{true\ positive + false\ negative} \quad (12)$$

$$precision = \frac{true\ positive}{true\ posive + false\ positive} \quad (13)$$

III. Results and Discussions

To examine the separability of classes, the data was visualized. As the dimension of data was 31 so a dimension compression technique called t-distributed stochastic neighbor embedding (TSNE) was used to create a 2 dimensional equivalent of the data. The scatter plot of this embedded data is shown in Fig. 3. It can be observed from the scatter plot that decision surfaces exist to accurately distinguish the classes.

The test accuracies of the classifiers are observed to increase with the addition of proposed features. This suggests that the augmentation of the proposed features increase the distinguishability of the classification models. Table IV shows the classification accuracies of the different classifiers used.

TABLE IV: Comparative efficiency of the classifier models for different data sets.

Classifier	Metric	Data set				
		I	*II*	*III*	*IV*	*V*
K nearest neighbours	Recall	61.71	78.57	78.71	79.23	81.15
	Precision	62.36	78.71	78.91	79.54	81.43
Support vector machine	Recall	78.27	78.35	78.35	78.35	78.35
	Precision	59.94	79.09	79.45	80.63	81.29
Multi layer perceptron	Recall	56.11	83.58	82.55	93.08	93.44
	Precision	54.93	83.75	82.70	93.06	93.42
Decision tree	Recall	83.87	89.69	89.76	90.72	91.46
	Precision	83.81	89.64	89.72	90.71	91.46
Random forest[a]	Recall	86.52	93.74	94.18	94.04	94.55
	Precision	86.49	93.71	94.28	94.05	94.58

[a]. Best performing classification model

The results show that the random forest has the maximum accuracy at distinguishing the different diseases. This model was also used to plot the decision surface in Fig. 3.

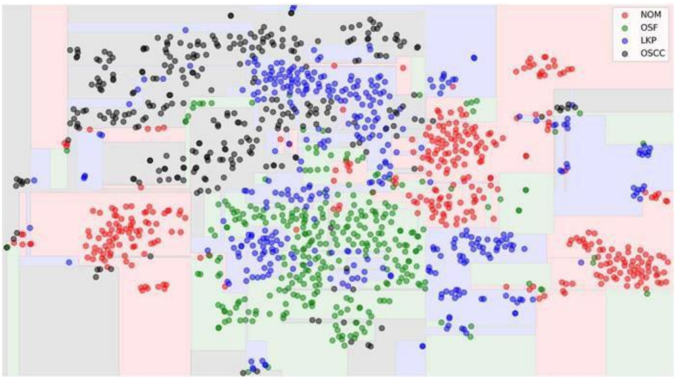

Fig. 3: Scatter plot of dimension reduced data color labeled according to disease classes. Circles on the plot denote the data points and the background color denotes the decision surface.

IV. Conclusion

Addressing the ambiguity present in oral cytology in medical diagnosis, this work shows that use of machine learning disease prediction can help reduce it. Through the findings in this paper we have observed that the augmentation of statistical features with cytomorphometric features helps predictive classifiers to discriminate between disease and control groups. Additionally, with the use of powerful classifiers like random forest, a robust computer aided diagnostic system can be developed to diagnose oral cancer.

Acknowledgment

The authors are grateful for financial support from the MHRD, Government of India, New Delhi.

References

[1] J. Ferlay, I. Soerjomataram, R. Dikshit, S. Eser, C. Mathers, M. Rebelo, D. M. Parkin, D. Forman, and F. Bray, "Cancer incidence and mortality worldwide: sources, methods and major patterns in globocan 2012," *International journal of cancer*, vol. 136, no. 5, 2015.

[2] E. A. Omar, "The outline of prognosis and new advances in diagnosis of oral squamous cell carcinoma (oscc): Review of the literature," *Journal of Oral Oncology*, vol. 2013, 2013.

[3] G. Yardimci, Z. Kutlubay, B. Engin, and Y. Tuzun, "Wjcc," *World*, vol. 2, no. 12, pp. 866–872, 2014.

[4] L. Feller and J. Lemmer, "Cell transformation and the evolution of a field of precancerization as it relates to oral leukoplakia," *International journal of dentistry*, vol. 2011, 2011.

[5] S. Vellappally, Z. Fiala, J. Smejkalová, V. Jacob, and R. Somanathan, "Smoking related systemic and oral diseases," *ACTA MEDICA-HRADEC KRALOVE-*, vol. 50, no. 3, p. 161, 2007.

[6] P. Gupta, P. Sinor, R. Bhonsle, V. Pawar, and H. Mehta, "Oral submucous fibrosis in india: a new epidemic?," *National Medical Journal of India*, vol. 11, no. 3, 1998.

[7] G. Arakeri and P. A. Brennan, "Oral submucous fibrosis: an overview of the aetiology, pathogenesis, classification, and principles of management," *British Journal of Oral and Maxillofacial Surgery*, vol. 51, no. 7, pp. 587– 593, 2013.

[8] L. L. Patton, J. B. Epstein, and A. R. Kerr, "Adjunctive techniques for oral cancer examination and lesion diagnosis: a systematic review of the literature," *The Journal of the American Dental Association*, vol. 139, no. 7, pp. 896–905, 2008.

[9] S. Fedele, "Diagnostic aids in the screening of oral cancer," *Head & neck oncology*, vol. 1, no. 1, p. 5, 2009.

[10] D. V. Rajput and J. V. Tupkari, "Early detection of oral cancer: Pap and agnor staining in brush biopsies," *Journal of oral and maxillofacial pathology: JOMFP*, vol. 14, no. 2, p. 52, 2010.

[11] T. Ramaesh, B. Mendis, N. Ratnatunga, and R. Thattil, "Cytomorphometric analysis of squames obtained from normal oral mucosa and lesions of oral leukoplakia and squamous cell carcinoma," *Journal of oral pathology & medicine*, vol. 27, no. 2, pp. 83–86, 1998.

[12] Z. Ö. Pektas, A. Keskin, Ö. Günhan, and Y. Karslioglu, "Evaluation of nuclear morphometry and dna ploidy status for detection of malignant and premalignant oral lesions: quantitative cytologic assessment and review of methods for cytomorphometric measurements," *Journal of oral and maxillofacial surgery*, vol. 64, no. 4, pp. 628–635, 2006.

[13] P. Perona and J. Malik, "Scale-space and edge detection using anisotropic diffusion," *IEEE Transactions on pattern analysis and machine intelligence*, vol. 12, no. 7, pp. 629–639, 1990.

[14] A. C. Ruifrok, D. A. Johnston, *et al.*, "Quantification of histochemical staining by color deconvolution," *Analytical and quantitative cytology and histology*, vol. 23, no. 4, pp. 291–299, 2001.

[15] R. M. Haralick, K. Shanmugam, *et al.*, "Textural features for image classification," *IEEE Transactions on systems, man, and cybernetics*, no. 6, pp. 610–621, 1973.

ISBN 978-1-5386-4473-7
IEEE sponsored 4th International Conference on Biosignals, Images and Instrumentation, SSNCE, Chennai. ICBSII 2018 – 22nd-24thMar'18

Examination of Glioblastoma Images by Thresholding using Heuristic Approach

A. Ruby Catharin, A. Sadeesh Kumar, M. Rakshiga, Sahana Kumaresan*, N.Sri Madhava Raja
Department of Electronics and Instrumentation Engineering,
St. Joseph's College of Engineering,
OMR, Chennai 600119, Tamilnadu, India.
*e-mail:sahana13997@gmail.com

***Abstract*— Brain tumor is a deadliest sickness in human community. It affects most of the humans despite of their age, gender and race. Medical imaging procedure is widely adopted to detect and evaluate the brain tumor. In this paper, a semi-automated approach is proposed to examine the high grade brain tumor called the Glioblastoma. During this study, the RGB slices of the brain views, like axial, coronal and sagittal are considered. The integration of the thresholding based on the Otsu and segmentation with the active contour is implemented to extract the tumor section. Initially the thresholding procedure monitored by the Social Group Optimization (SGO) acts as the pre- processing approach to enhance the tumor section and the segmentation procedure act as the post-processing section to extract the tumor. Finally, Haralick texture features are considered to compute the tumor characteristic. The experimental result confirms that, proposed approach helps to achieve better segmentation result on the RGB brain MRI pictures.**

Keywords*— Glioblastoma; RGB MRI; Otsu; active contour; Texture features.

I. INTRODUCTION

Computer based illness appraisal is generally used in medical field to realize the anatomical and pathological divisions with clinical images. Medical imaging procedures will support the premature detection and examination of a collection of diseases and also helps to reduce the morbidity and death rates. In literature, considerable actions are discussed and executed by the researchers to mine significant information from medical images [1-4].

The heuristic algorithm guided image processing is broadly considered in recent years, due to its simplicity and easiness in implementation [5-9]. Otsu is one of the procedures, largely adopted by most of the researchers because of its supremacy and flexibility [10,11]. From the image processing literature, it can be noted that, Otsu based multi-level thresholding was largely adopted by the researchers to extract the important information from the RGB / gray scale test images [12-14] and medical images [15]. The work by Despotovic et al. [16] suggest the segmentation challenges and the available procedures in brain image processing. This work also notifies that, combination of several techniques is essential to reach improved segmentation result.

In the literature, a number of automated and semi-automated approaches are existing to examine brain MRI recorded with a chosen modality. All the existing methods are modality specific approaches and the method works well with a chosen modality sometimes may fail to offer better outcome with other modalities. Moreover, the soft-computing assisted approaches will enhance the outcome of the disease examination procedure. Hence, in this paper an approach based on the SGO assisted thresholding is implemented to examine the brain MRI registered with the Flair modality.

This work proposes a computer supported semi- automated practice to segment and analyze the tumor from the Radiopedia database [17]. Firstly, tri-level thresholding based on the SGO+Otsu is implemented to improve the cancerous division in brain image. Later, the Active Contour (AC) based segmentation is implemented to extract the suspicious/enhanced region of RGB brain MRI.

The capability of proposed segmentation task is then confirmed by means of a texture features. The outcome of the proposed technique confirms that, the implemented section offers better result on the RGB brain MRI with various views, such as axial, coronal and sagittal.

II. METHODOLOGY

This section of the paper presents the methodology implemented to process the considered brain MRI image. The pre-processing and the post-processing procedures are outlined in this section and the considered texture feature extraction is also outlined.

A. Social Group Optimization

SGO is a recently proposed heuristic approach by Satapathy and Naik [18]. It is based on the group resolve capability of the human being during complicated circumstances. It is identical to the Teaching Learning based Optimization existing in the literature [19]. In SGO, each person in the group is the candidate having capacity to offer the solution for the assigned task based on the fitness value. In this algorithm, the knowledge among the group members is used to find the solution for the given task.

This algorithm has two stages as follows;

i. Improving phase

Let X is the persons in the chosen social group with i = 1, 2,…, N and D is the dimension of the optimization problem with j = 1, 2, …, D.

ISBN 978-1-5386-4473-7
IEEE sponsored 4th International Conference on Biosignals, Images and Instrumentation, SSNCE, Chennai. ICBSII 2018 – 22nd-24thMar'18

$$Xnew_{i,j} = C * Xold_{i,j} + r* (gbest_j - Xold_{i,j}) \quad (1)$$

ii. Acquiring phase

$$Xnew_{i,j} = Xold_{i,j} + r_1 * (X_{i,j} - X_{r,j}) + r_2 * (gbest_j - X_{i,j}) \quad (2)$$

$$Xnew_{i,:} = Xold_{i,:} + r_1 * (X_{r,:} - X_{i,:}) + r_2 * (gbest_j - X_{i,j}) \quad (3)$$

where, i = 1to N; j = 1 to D, r = r_1=r_2= random number ~ U (0,1)

In this work, initial algorithm parameters are assigned based on the paper [19]. Other parameters are assigned as follows; the group size is assigned as thirty, the dimension of the search is chosen as three, the number of run is fixed as 1200 and the stopping criteria is considered as the maximal value of Otsu's function.

B. Otsu's Function

Otsu's between-class variance based approach was proposed in 1979 to segment gray scale images. Otsu's tri-level thresholding is adopted in this paper to threshold the image. Let us consider that there are thresholds , such as t_1, t_2, and t_3, which partition the input picture into three separate sections, such as C_0 (gray levels of range 0 to t_1-1), C_1 (gray levels of range t_1 to t_2-1) and, C_2 (gray levels of range t_2 to L-1). Where L = 256.

Objective value for this three-level thresholding can be expressed as;

$$Jmax = \sigma_0 + \sigma_1 + \sigma_2 \quad (4)$$

More feature regarding the Otsu is existing in the literature [10-12]. Eqn.4 is known as the Otsu's between class variance function which supports the exploration process of heuristic search.

C. Active Contour Segmentation

AC is a well accepted segmentation practice used to mine crucial area from pre-processed image [7]. In ACS, a variable snake is selected to chase matching pixel groups obtainable in the image with reverence to minimal energy scheme.

Snake's energy value is expressed as;

$$\min_{C} \left\{ E_{GAC}(C) = \int_0^{L(C)} g(|\nabla I^0 C(s))| ds \right\} \quad (5)$$

where *ds* - the Euclidean element of length and *L(C)* - the span of curve *C* which assures $L(C) = \int_0^{L(C)} ds$. The constraint *g* is an border pointer, it may vanish based on the object frontier shown below;

$$g(|\nabla I_0|) = \frac{1}{1 + \beta|\nabla I_0|^2} \quad (6)$$

where I_0 denotes base picture & β is a random numeral. The energy function quickly diminishes based on boundary.

D. Texture feature extraction

If an image classifier scheme is employed along with the image processing practice, the k features are usually considered to extract the essential section features of the tumor [1,6]. Later, these features are used to train and to test the classifier system. The accuracy of the classifier unit mainly depends on the accuracy of the feature extraction system. In this paper, texture features are extracted using the well known Haralick feature.

E. Execution

The execution procedure followed in this paper is depicted in Fig 1. Initially, the collected 2D brain MRI image is collected from the Radiopedia database [17]. This MRI is in RGB form; initially a pre-processing based on the SGO+Otsu is implemented to enhance the tumor section. Later a post-processing based on the AC segmentation is implemented to extract the tumor. In this work, the RGB image is considered as it is in this work. The extracted tumor is then considered to examine the texture features. In order to confirm the superiority of the proposed method, the various views of the brain MRI, such as the axial, coronal and sagittal views are considered in this paper. The experimental outcome confirms that, proposed approach is efficient in extracting the tumor from the considered RGB brain MRI.

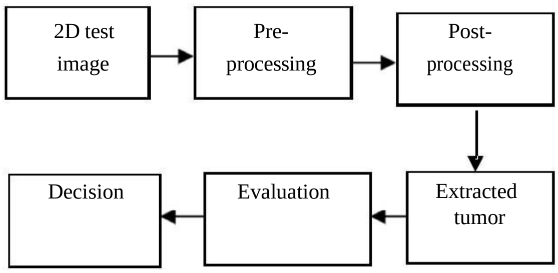

Fig 1. Methodology implemented to examine tumor

III. RESULTS AND DISCUSSIONS

The experimental implementation and the corresponding results are presented and discussed in this section. Initially, the RGB scaled brain MRI of size 630 x 630 pixels with various orientations, such as axial, coronal and sagittal are initially collected from the Radiopaedia image database. These RGB images are considered for the tumor extraction process without implementing the skull stripping procedure [7,8]. Skull stripping is normally considered to examine the brain tumor evaluation in order to eliminate the skull region from the brain section. If the skull is eliminated, it is easy to implement the chosen image processing procedure to examine the soft tissue of the brain.

Initially, the RGB thresholding procedure is implemented using the Otsu+SGO on the axial brain MRI image depicted in Fig 2. During this procedure, the optimization search is allowed to search the optimal threshold values, until the J_{max} is reached. In this work, the search offers the three layer optimal thresholds, such as R = 57, 183, 207, G = 28, 194, 236, and B = 61, 128, 184 with an average J_{max} of 2217.2874. Fig 2 (a) presents the considered test picture and Fig 2 (b) depicts the tri-level thresholded image. This picture confirms that, proposed thresholding approach enhances the tumor region by eliminating the soft tissue of the brain region. Next, the AC segmentation is implemented on the pre-processed image, in order to extract the tumor section. Fig 2 (c) and (d) presents the initial and final contour of the AC approach. This is a semi-automated procedure; hence initially the bounding box value is to be assigned by the operator at the initiation of segmentation.

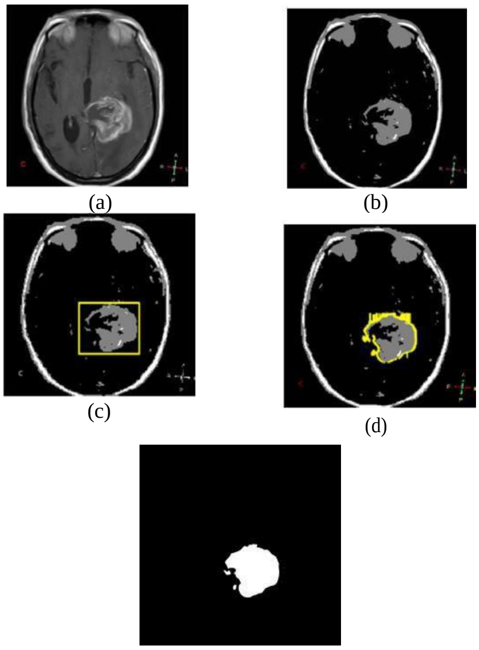

Fig 2. Result of the proposed approach. a. Test image, b. Thresholded picture, c. Initial contour, d. Final contour, e. Segmented tumor

TABLE I. VARIOUS TEST IMAGES AND ITS OUTCOME

	Test picture	Thresholded picture	Extracted tumor
Axial	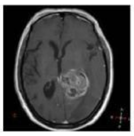	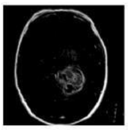	
Coronal	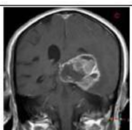	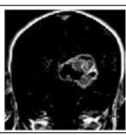	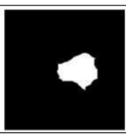
	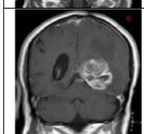		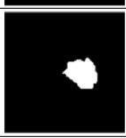
Sagittal	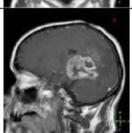	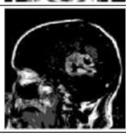	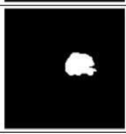
	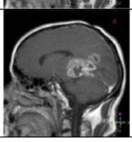		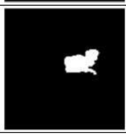

The bounding box is initiated with X- axis value of [250, 450] and the Y-axis values of [300, 475] and the box is allowed to shrink towards the tumor as in Fig 2 (c). When iteration increases, the box will move towards the tumor as depicted in Fig 2 (d) and finally at the end of the segmentation iteration, the result shown in Fig 2 (e) is obtained. Similar procedure is implemented for the other test images considered in the paper and the corresponding results are presented in Table I. From Fig 2 and Table I, it can be noted that, proposed approach is efficient in extracting the tumor section from the considered brain MRI.

In order to evaluate the tumor size and also to classify the tumor as the benign and malignant, the texture values are extracted using the Haralick features existing in the literature. Table II presents the values of these features and this table confirms that, based on the orientation, the tumor size varies [20].

TABLE II. GEOMETRIC FEATURE OF TUMOR

Test image	Area	Major axis length	Minor axis length	Equiv diameter	Solidity	Extent
Axial	1116	38.1416	22.1974	34.2984	0.8475	0.6315
	1083	38.0271	22.0646	34.1828	0.8339	0.6622
Coronal	1372	44.0037	28.1639	36.1173	0.8154	0.6517
	984	34.2745	23.1937	32.2874	0.8264	0.6028
Sagittal	895	30.7184	21.0083	31.9277	0.8331	0.6225
	926	32.1954	21.1783	30.8362	0.8592	0.6162

Further, the superiority of the proposed technique is confirmed by considering the brain MRI of BRATS 2015 database depicted in Table III and the results in Table IV. The main advantage of BRATS is as follows; the test images are recorded with a variety of modalities and it is free from the skull section. This work considered the Flair modality based brain MRI to test the performance the proposed tool.

TABLE III. SAMPLE TEST IMAGES (FLAIR)

Slice	Test image	GT	Tumor
$Slice_{100}$	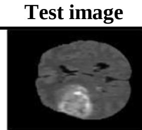		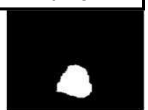
$Slice_{120}$	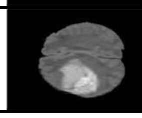	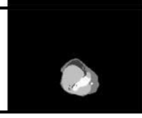	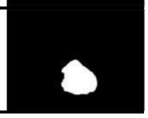

TABLE IV. IMAGE SIMILARITY VALUES OF FLAIR IMAGES

Slice	Jaccard	Dice	False Positive Rate	False Negative Rate
$Slice_{100}$	0.8926	0.9174	0.1347	0.0475
$Slice_{120}$	0.8857	0.9083	0.1749	0.0384

This dataset is associated with the Ground Truth (GT) picture. Hence, after extracting the tumor section, the image similarity measures can be computed with a comparative study between the tumor and GT. This work computes the image metrics, such as Jaccard, Dice, FPR and FNR [7,8]. The results of Table IV confirms that, proposed approach offers better values of these parameters, hence, in future, it can be considered to examine clinical brain MRI images.

IV. CONCLUSION

In this paper, a semi-automated image processing procedure is proposed to examine the RGB brain MRI recorded with various orientations, such as axial, coronal and sagittal. A technique based on the integration of Otsu and SGO assisted pre-processing and the AC based post-processing is implemented to extract the tumor section from the RGB scaled brain MRI recorded with Flair modality. The texture features of these tumors are extracted using the Haralick procedure and it can be considered to design a classifier system in future. Finally, proposed approach is also implemented on the Brats 2015 dataset in order to confirm its efficiency. The results of this paper confirm that, proposed approach is efficient in offering the better values of Jaccard and Dice, hence the developed tool is efficient to examine the brain MRI recorded with the flair.

REFERENCE

[1] K. Manickavasagam, S. Sutha and K, Kamalanand, An automated system based on 2D empirical mode decomposition and k-means clustering for classification of Plasmodium species in thin blood smear images, BMC Infectious Diseases, vol.14, no.3, pp.1, 2014.

[2] C.W. Wang, Y.C. Lee, H. Pradana, Z. Zhou and H. Peng, "Ensemble Neuron Tracer for 3D Neuron Reconstruction," Neuroinformatics, vol.15, no.2, pp.185-198, 2017.

[3] C. Lindner, C.W. Wang, C. Huang, C. Li, S. Chang and T. Cootes, "Fully automatic system for accurate localisation and analysis of cephalometric landmarks in lateral cephalograms," Nature-Scientific Reports, vol. 6, Article number .33581, 2016. DOI:10.1038/srep33581.

[4] R. Vishnupriya, N.S.M. Raja, and V.Rajinikanth, "An efficient clustering technique and analysis of infrared thermograms," Third International Conference onBiosignals, Images and Instrumentation (ICBSII), IEEE, pp.1-5, 2017. DOI: 10.1109/ICBSII.2017.8082275.

[5] N.S.M.Raja, V. Rajinikanth, S.L. Fernandes and S.C. Satapathy, "Segmentation of Breast Thermal Images Using Kapur's Entropy and Hidden Markov Random Field," Journal of Medical Imaging and Health Informatics, vol.7, no.8, pp. 1825-1829, 2017.

[6] K. Manickavasagam, S. Sutha and K. Kamalanand, Development of systems for classification of different plasmodium species in thin blood smear microscopic images, Journal of Advanced Microscopy Research, vol.9, no.2, pp. 86-92, 2014.

[7] V. Rajinikanth, S.C. Satapathy, S.L. Fernandes and S. Nachiappan, "Entropy based Segmentation of Tumor from Brain MR Images–A study with Teaching Learning Based Optimization," Pattern Recognition Letters, vol.94, pp.87-95, 2017. DOI: 10.1016/j.patrec.2017.05.028.

[8] V. Rajinikanth, N.S.M. Raja and K. Kamalanand, "Firefly Algorithm Assisted Segmentation of Tumor from Brain MRI using Tsallis Function and Markov Random Field," Journal of Control Engineering and Applied Informatics, vol.19, no.3, pp. 97-106, 2017.

[9] V. S. Lakshmi, S.G. Tebby, D. Shriranjani, and V. Rajinikanth, "Chaotic cuckoo search and Kapur/Tsallis approach in segmentation of t.cruzi from blood smear images," International Journal of Computer Science and Information Security (IJCSIS), vol.14, CIC 2016, pp. 51-56, 2016.

[10] T.K. Palani, B. Parvathavarthini and K. Chitra, "Segmentation of brain regions by integrating meta heuristic multilevel threshold with Markov random field," Current Medical Imaging Reviews, vol.12, no.1,pp. 4-12, 2016.

[11] N.S.M. Raja, V. Rajinikanth and K. Latha, "Otsu Based Optimal Multilevel Image Thresholding Using Firefly Algorithm," Modelling and Simulation in Engineering, vol.2014, paper id.794574, 2014.

[12] V. Rajinikanth, and M.S. Couceiro, "Optimal multilevel image threshold selection using a novel objective function", Advances in Intelligent Systems and Computing, vol. 340, pp 177-186, 2015.

[13] K. Kamalanand, and S. Ramakrishnan, "Effect of gadolinium concentration on segmentation of vasculature in cardiopulmonary magnetic resonance angiograms," Journal of Medical Imaging and Health Informatics, vol. 5, pp.1–5, 2015.

[14] V. Rajinikanth, and M.S. Couceiro, "RGB histogram based color image segmentation using firefly algorithm", Procedia Computer Science, vol.46, pp. 1449-1457, 2015.

[15] V. Rajinikanth, N.S.M.Raja, S.C. Satapathy and S.L. Fernandes, "Otsu's Multi-Thresholding and Active Contour Snake Model to Segment Dermoscopy Images," Journal of Medical Imaging and Health Informatics, vol.7, no.8, pp. 1837-1840, 2017.

[16] Despotovic, B. Goossens, and W. Philips, "MRI Segmentation of the human brain: Challenges, Methods, and Applications," Comput. Math. Method M., vol. 2015, Article ID 450341, 23 pages, 2015.

[17] Radiopaedia.org (Case courtesy of Dr Ahmed Abd Rabou, Radiopaedia.org, rID: 22779)

[18] S.Satapathy, and A. Naik, "Social group optimization (SGO): a new population evolutionary optimization technique," Complex & Intelligent Systems, vol.2, no.3, pp. 173-203, 2016.

[19] A.Naik, S.C. Satapathy, A.S. Ashour, and N. Dey, N, " Social group optimization for global optimization of multimodal functions and data clustering problems," Neural Computing and Applications ,2016. DOI:10.1007/s00521-016-2686-9.

[20] G. K.Vaishnavi, K. Jeevananthan, S. R. Begum, and K. Kamalanand, "Geometrical Analysis of Schistosome Egg Images Using Distance Regularized Level Set Method for Automated Species Identification," Journal of Bioinformatics and Intelligent Control, vol.3, no.2, pp. 147-152, 2014.

DEXSIT: A Benchmark Database for BMD Measurement and Analysis

[#1]S.M.Nazia Fathima, [*2]R.Tamilselvi, and [*3]M.Parisa Beham
[#]Department of CSE, [*]Department of ECE, [#*]Sethu Institute of Technology, Tamilnadu-626 115. [1]naziafathima@sethu.ac.in, [2]tamilselvi@sethu.ac.in, [3]parisabeham@sethu.ac.in

Abstract – In the medical field, a bone mineral density (BMD) test is presented as a picture of your bone health. The test determines the risk for bone fractures of a human. From the test report one can identify the symptoms of osteopenia or osteoporosis disease which is the most common type of bone disease. The most extensively renowned BMD test is called a Dual-Energy X-ray absorptiometry, or DEXA test. The test can measure bone mineral density at spine, left and right femur bones. Superior properties of DEXA compared to conventional methods unveil the potential for new medical applications among the researchers. Thus it is mandatory to have a standard DEXA database for the researchers so as to take the treatments to the advance level by properly analyzing the clinical results of the scan images. The proposed DEXA database, named as DEXSIT, represents an initial attempt to provide a set of DEXA scan images of Anteroposterior (AP) spine, dual left and right femur bones. The database interprets all the clinical details such as age, weight, height, BMD level, T-score, Z-score and area of the bone part. In addition to describing the details of the database, some specific performance evaluation measures have also been done as an effort to make research achieved with the database as consistent and comparable as possible.

Keywords: DEXA scan database, DEXSIT, BMD test, Femur bone images, T-score and Z-score.

1. Introduction

Biomedical engineering (BME) is the application of engineering principles and design concepts to medicine and biology for healthcare purposes. The recent biomedical engineering field is bridging the gap between engineering and medicine. In that, the researchers are combining the design and problem solving ability of engineering with biological sciences to progress health care treatments such as diagnosis, monitoring, prevention of diseases and therapy.

Early challenge of the measurement of bone mineral density used conventional x-rays with a step wedge made from an aluminum or ivory phantom. The next development in the field of measurement of bone density was the discovery of single-photon absorptiometry (SPA) by Cameron and Sorenson in 1963. This technique established a good place in medical field in terms of bone quantification, but it was limited to a peripheral site. As an advancement, Dual energy problem is engaged in Dual-photon absorptiometry (DPA), facilitating the concurrent transmission of gamma rays with photon energies [1]. Algebraic derivations are used for the estimation of bone and soft tissue. In late 1980s, superior and expensive radioactive sources have been outdated by single x-ray absorptiometry (SXA) and Dual Energy X-ray absorptiometry (DEXA). A Dual Energy X -ray absorptiometry can produce a whole body image and discriminate dissimilar body structures.

In the recent biomedical applications, DEXA scans are being used extensively. Their success rate is also very high compared to other conventional scanning methods used for BMD [2]. The main usage of BMD measurement is to help the health care provider to detect osteoporosis and predict the risk of bone fractures. Thus osteoporosis is a diverse syndrome that influences different regions of the skeleton with different severity. This disease occurs commonly in women; in particular those who are older than 50 years, men also commonly affected by osteoporosis.

The primary obstacle of osteoporosis is fractures happening after minimum trauma. Hip fractures are related with increased short term mortality and high morbidity. Hip, vertebral, and radius fractures increase the threat of future fractures. Osteoporosis causes your bone tissue to become thin and frail over time and leads to risk of bone fractures [3]. Thus it is a mandatory effort for biomedical researcher community, to take appropriate prevention techniques or suitable treatment processes for the patients.

ISBN 978-1-5386-4473-7
IEEE sponsored 4th International Conference on Biosignals, Images and Instrumentation, SSNCE, Chennai. ICBSII 2018 – 22nd-24thMar'18

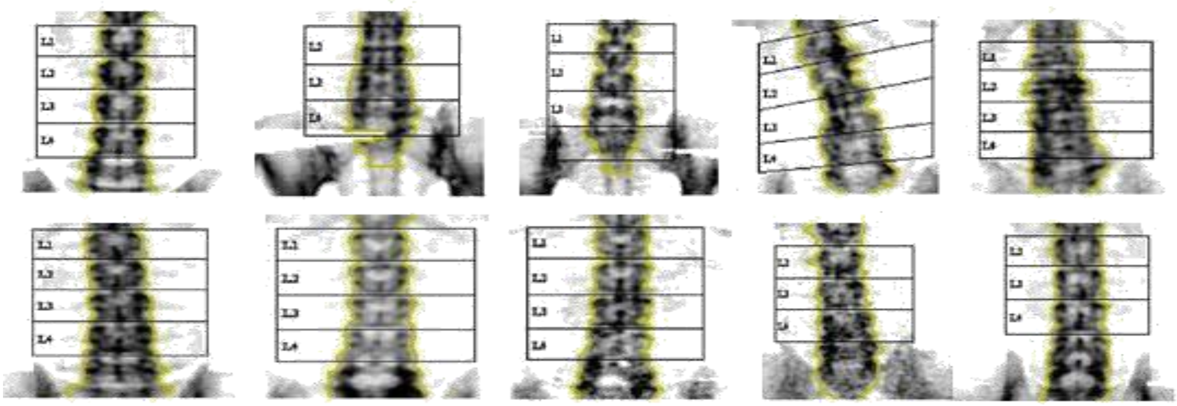

(a)

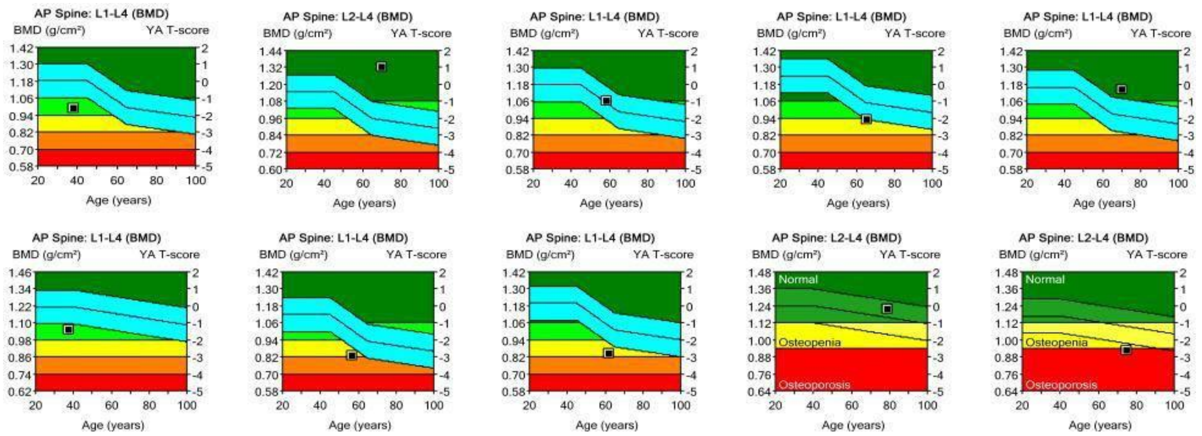

(b)

Fig.1. (a) DEXA scan images of AP spine of 10 selected subjects from the DEXSIT
(b) BMD plots of corresponding AP spine Dexa images

A bone mineral density (BMD) test measures how much calcium and other types of minerals are in an area of the bone [4].

Base on these facts, in this work we proposed to build a database of Dexa scan images which we named it as 'DEXSIT Database', for the benefit of biomedical engineering research community. The important pitfall in the research and development of this community is that, unavailability of suitable medical databases. Even though some related papers have discussed the issues of SPA, SXA and DEXA, they didn't provide any such databases publically available for the researchers.

Thus motivated by these factors, our main contributions in this work are:

- Create a new DEXSIT database, involves 42 Antero-Posterior (AP) spine, 42 dual left femur and 42 dual right femur bone Dexa scan images.
- Provide 122 BMD plots for all the Dexa scan images.
- Present the annotation of all the 126 (42 3) subject's biological data, BMD levels, T-score, Z-score and area.
- Provide clinical report as per WHO standard with suggestions of the health care provider for all the subjects.

2. DEXIT Database

In the biomedical field and in healthcare applications, unavailability of suitable database for further research and development motivated us to create a new and rare database, what we called is DEXSIT database. We designed this DEXSIT database primarily as a benchmark for the BMD measurements. DEXSIT is built from the DEXA bone images collected from a popular and standard scan centre in Tamilnadu. This database consists of 126 dexa scan images collected from 42 subjects. Among the 42 subjects the DEXSIT consist of 38 female and 4 male subjects. Each subject comprises of one AnteroPosterior (AP) spine image, one left femur bone (LF) image and one right femur bone (RF) image. All the images are also provided with their respective BMD measurement plots. The sample DEXA AP spine scan images of 10 subjects and their respective BMD plots are shown in Fig.1 (a) and Fig. 1(b) respectively. Similarly, the sample DEXA left femur scan images of 10 subjects and their respective BMD plots are shown in Fig.2 (a) and Fig.2 (b) respectively. The sample DEXA right femur scan images of 10 subjects and their respective BMD plots are shown in Fig.3 (a) and Fig.3 (b) respectively.

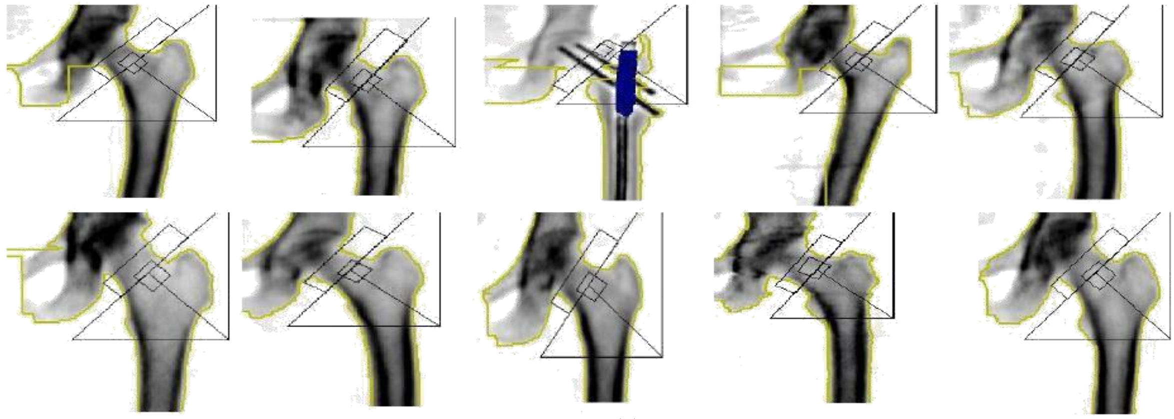

(a)

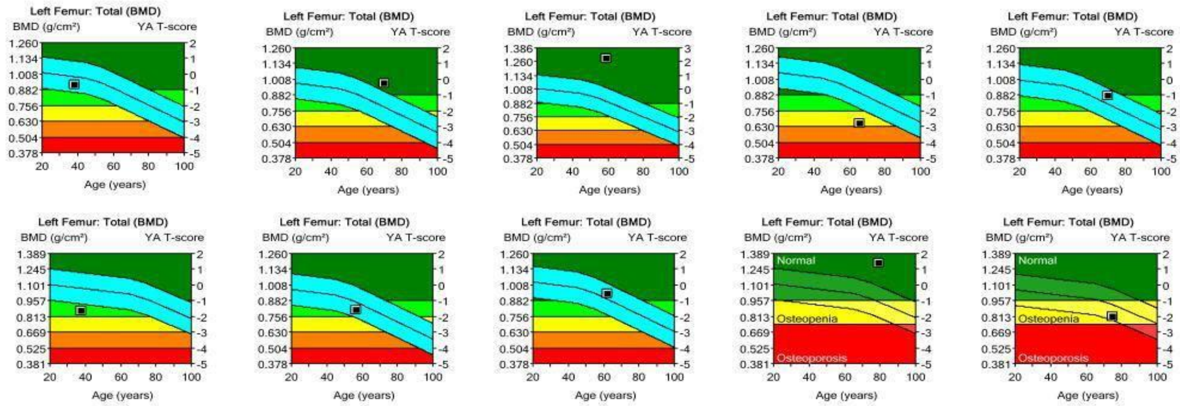

(b)

Fig.2. (a) DEXA scan images of Left femur bone of 10 selected subjects from the DEXSIT database
(b) BMD plots of corresponding left femur bone dexa images

The DEXSIT database is designed through following steps:

1) Construction and composition
2) Labeling the DEXSIT images
3) Annotation
4) Clinical Interpretation
5) Performance measure

Each and every step is described in detail in the following subsections.

2.1. Construction and Composition Details

The DEXSIT database is constructed from the dexa scan images of Indian people. From the 42 Indian subjects, totally 126 dexa bone images have been collected. All the images are cropped manually and saved as separate images in 'png' (portable network graphics) format.

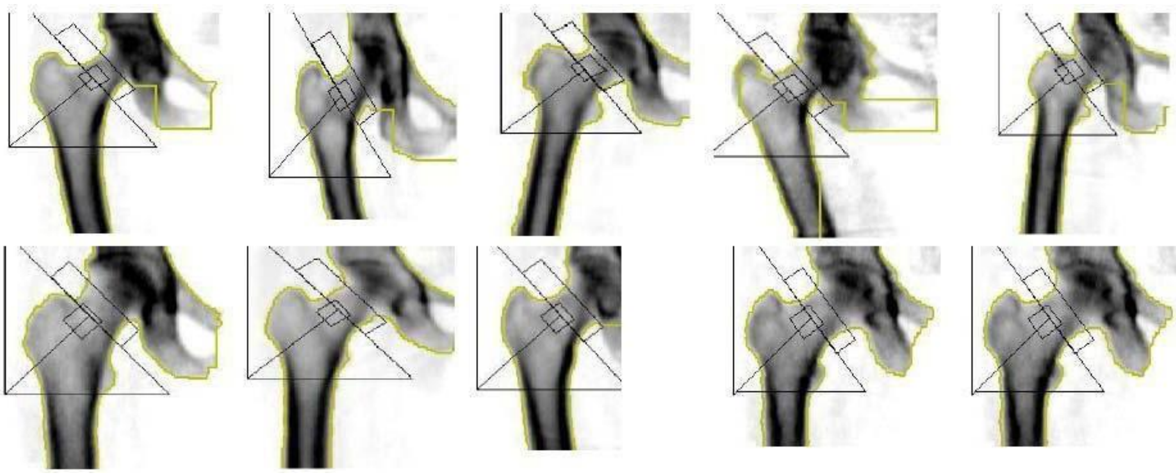

Fig.3. (a) DEXA scan images of right femur bone of 10 selected subjects from the DEXSIT database

ISBN 978-1-5386-4473-7

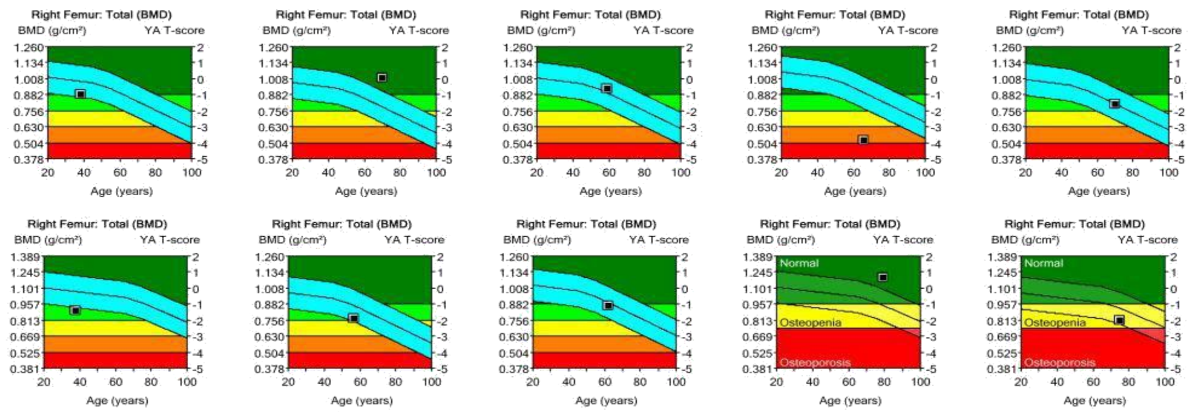

Fig.3. (b) BMD plots of corresponding left femur bone dexa images

Table1. Interpretation of clinical values of AP spine dexa images and their respective fracture risk

Subject Id	Gender	Age	Height (Cm)	Weight (Kg)	AP Spine (L1-L4)				Fracture Risk
					T-Score	Z-Score	BMD (g/cm^2)	Area cm^2	
Dexa_APF_001	F	37	162	66	-1.6	-1.6	0.99	48.07	Moderate
Dexa_APF_003	F	70	142	52	1	3.1	1.325	42.41	Low
Dexa_APF_006	F	58	155	64	-1	0.1	1.06	51.72	Moderate
Dexa_APF_009	**F**	**65**	**150**	**80**	**-2.1**	**-1**	**0.929**	**51.04**	**High**
Dexa_APF_010	F	69	142	60	-0.3	1.5	1.141	47.45	Low
Dexa_APM_011	M	37	171	76	-1.4	-1.4	1.048	55.22	Moderate
Dexa_APF_012	**F**	**56**	**154**	**50**	**-2.9**	**-1.5**	**0.829**	**44.88**	**High**
Dexa_APF_013	**F**	**61**	**152**	**70**	**-2.8**	**-1.6**	**0.846**	**47.52**	**High**
Dexa_APM_022	M	78	166	78	-0.2	0.5	1.216	44	Low
Dexa_APM_036	**M**	**74**	**161**	**60**	**-2.6**	**-1.4**	**0.922**	**38.79**	**High**

For all the dexa scan images of each subject, their respective BMD measurement plots have also been provided in the same png format. The whole database is split into four groups such as DEXSIT-DB, DEXSIT-APS, DEXSIT-LF and DEXSIT-RF. The DEXSIT-DB is the main database which consist all the scan images and BMD plots of 42 subjects with 126 scan images and 122 BMD plots. The DEXSIT-APS comprises only the dexa images of 42 AP spine bone images and their respective plots. Similarly DEXSIT-LF and DEXSIT-RF consists of 42 left femur, 42 right femur bone images and their BMD plots respectively. The categorization of the database, based on the bone images, motivate the researchers to interpret and analyze the performance of the spine, left and right femur bones separately.

2.2. Labeling the DEXSIT Images

In the DEXSIT database all the images are labeled perfectly for the ease of researchers. From the label itself one can easily identify the subject ID, Dexa or BMD, bone part and gender of the subject. For each subject, two images are obtained viz., Dexa scan image and BMD plot image. For example, the label for a Dexa scan image and the BMD plot of a subject is given as: *DEXA_APF_032.png* and *BMD_APF_032.png*. Here, in the first case DEXA refers to dexa scan image, APF refers to the spine image of female subject and 032 is the subject ID. In the later case, BMD refers to BMD plot, APF refers to the spine image of female subject and 032 is the subject ID. Similarly *DEXA_LFM_011.png* and *BMD_RFF_001.png* refer to dexa scan left femur image of a male subject with a subject ID of 011 and BMD plot of the right femur image of a female subject with a subject ID of 001 respectively.

2.3. Annotation

DEXSIT provides a detailed annotation through a careful analysis of each and every dexa scan image. We manually annotated the following attributes for each bone image.

- Unique ID of the subject
- Gender
- Age
- Height (cm)
- Weight (kg)
- AP Spine (L1-L4): *T-score, Z-score, BMD(g/cm^2), Area (cm^2)*
- Dual Left Femur: *T-score, Z-score, BMD(g/cm^2), Area (cm^2)*
- Dual Right Femur: *T-score, Z-score, BMD(g/cm^2), Area (cm^2)*
- Fracture risk: *Status of fracture risk for each AP spine, left and right femur bones.*

Table 2. Interpretation of clinical values of dual left femur dexa images and their respective fracture risk

Subject Id	Gender	Age	Height (Cm)	Weight (Kg)	Dual Left Femur				Fracture Risk
					T-Score	Z-Score	BMD (g/cm^2)	Area cm^2	
Dexa_LFF_001	F	37	162	66	-0.7	-0.5	0.923	26.84	Low
Dexa_LFF_003	F	70	142	52	-0.2	1.6	0.976	24.26	Low
Dexa_LFF_006	F	58	155	64	2.2	3.1	1.287	9.33	Low
Dexa_LFF_009	**F**	**65**	**150**	**80**	**-2.8**	**-1.9**	**0.654**	**25.85**	**High**
Dexa_LFF_010	F	69	142	60	-1	0.6	0.879	24.08	Moderate
Dexa_LFM_011	M	37	171	76	-1.7	-1.5	0.862	31.99	Moderate
Dexa_LFF_012	F	56	154	50	-1.6	-0.5	0.808	28.59	Moderate
Dexa_LFF_013	F	61	152	70	-0.5	0.4	0.939	27.93	Low
Dexa_LFM_022	M	78	166	78	1.4	2.5	1.296	30.08	Low
Dexa_LFM_036	**M**	**74**	**161**	**60**	**-2**	**-0.8**	**0.809**	**31.52**	**High**

These attributes and annotations are motivated by the large variety of problems related to orthopedic biomedical applications. Here we attempted to provide all clinical report values for the spine, left and right femur bone images which might have useful in the advancement of orthopedic research. Fig. 4 shows the example of annotation detail of the sample subject from the DEXSIT database.

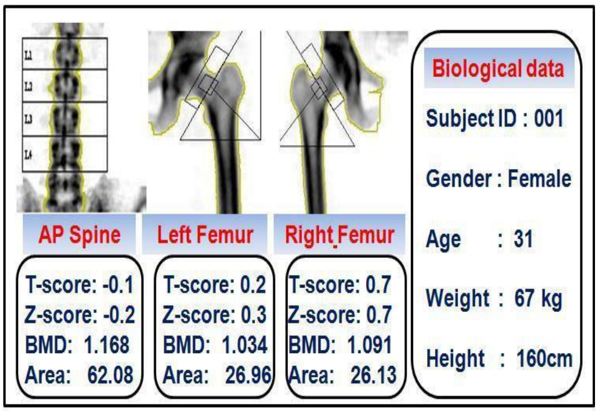

Fig.4. Annotation of spine, left and right femur bone images of a subject

3. Clinical Interpretation

Osteoporosis, an illness generally associated with human beings, is characterized by loss of both bone mass and micro architectural integrity [5]. One crucial determinate in the development of osteoporosis is the acquisition of appropriate peak mass in adolescence and early adulthood [6]. A failure to achieve adolescent peak bone mass may be associated with premature osteoporosis and increased risk of fracture [7]. The aim of the proposed database was to inspire the research community to identify risk factors associated with osteoporosis in this patient population. According to world health organization (WHO), for human beings, in the BMD plot T-score values are defined as:

Normal: T-score at or above -1 SD (Standard Deviation)
Osteopenia: T-score between -1 and -2.5 SD
Osteoporosis: T-score at or below -2.5 SD

Table 1 shows the clinical result of LF spine images for the 10 selected subjects and their respective fracture risk status. Table 2 and Table 3 shows the clinical results of left femur and right femur bone images for the same subjects and their corresponding fracture risk status respectively. From the tables, for the subject ID 001, it is observed that, the BMD measured at LF Spine L1-L4 is 0.990 g/cm² with a T-score of -1.6 is considered moderately low. Thus it is reported that the fracture risk is moderate in the spine part. The BMD measured at femur total left is 0.923 g/cm² with a T-score of -0.7 is normal and thus the fracture risk is low. The BMD measured at femur total right is 0.887 g/cm² with a T-score of -1.0 is considered moderately low, thus the fracture risk is moderate. With a Z-score of -1.6, this subject's BMD is low for someone of this age. With a Z-score of -0.5, the BMD is within normal limits for the subject's age and sex. Similarly, with a Z-score of -0.8, the BMD is within normal limits as per the WHO standard [8].

Table 4 shows the clinical report of the sample subjects in the DEXSIT database based on their fracture risk presented in the clinical report. For example, if the fracture risk in LF spine, left femur and right femur bones are low then it is reported as normal. Such that, if the fracture risk in LF spine, left femur and right femur bones are moderate then it is reported as the subject is affected by Osteopenia. For all the dexa scanned part, if the fracture risk is high then it is suggested to take treatment for Osteoporosis.

Thus according to the BMD levels, T-score and Z-score, mild to aggressive therapies are available in the form of Hormone replacement therapy (HRT), Bisphosphonates, Calcitonin and SERMs. Additionally, all patients should ensure an adequate intake of dietary calcium (1200 mg/d) and vitamin D (400-800 IU daily). Through proper analysis of the dexa scan bone images and their clinical results, we can prevent the people from the osteoporosis disease.

Table 3. Interpretation of clinical values of dual right femur Dexa images and their respective fracture risk

Subject Id	Gender	Age	Height (Cm)	Weight (Kg)	Dual Right Femur				Fracture Risk
					T-Score	Z-Score	BMD (g/cm^2)	Area cm^2	
Dexa_RFF_001	F	37	162	66	-1	-0.8	0.887	26.7	Moderate
Dexa_RFF_003	F	70	142	52	0.1	1.8	1.015	24.59	Low
Dexa_RFF_006	F	58	155	64	-0.6	0.3	0.933	27.62	Low
Dexa_RFF_009	**F**	**65**	**150**	**80**	**-3.8**	**-3**	**0.524**	**25.83**	**High**
Dexa_RFF_010	F	69	142	60	-1.6	0	0.808	23.8	Moderate
Dexa_RFM_011	M	37	171	76	-1.4	-1.2	0.902	30.6	Moderate
Dexa_RFF_012	F	56	154	50	-1.9	-0.8	0.771	27.56	Moderate
Dexa_RFF_013	F	61	152	70	-1.1	-0.2	0.872	27.28	Moderate
Dexa_RFM_022	M	78	166	78	0.7	1.8	1.198	32.02	Low
Dexa_RFM_036	**M**	**74**	**161**	**60**	**-2**	**-0.8**	**0.813**	**30.79**	**High**

Table 4. Clinical reports of the subjects based on their fracture risk

Subject ID	Gender	Age	Clinical Report - Fracture Risk			Sugges-tions
			AP Spine	Dual LF bone	Dual RF bone	
001	F	37	Mod	Low	Mod	*SCI
003	**F**	**70**	**Low**	**Low**	**Low**	**Normal**
006	F	58	Mod	Low	Low	*SCI
009	F	65	High	High	High	*SCI
010	F	69	Low	Mod	Mod	*SCI
011	**M**	**37**	**Mod**	**Mod**	**Mod**	**Osteopenia**
012	F	56	High	Mod	Mod	*SCI
013	F	61	High	Low	Mod	*SCI
022	M	78	Low	Low	Low	*SCI
036	**M**	**74**	**High**	**High**	**High**	**Osteoporosis**

**SCI – Suggestion for Calcium intake , Mod-Moderate*

This database can also pave the way for new research and analysis in the measurement of BMD, T-score and Z-score. Thus one can verify the accuracy of the reports provided by the radiologist using the novel biomedical engineering sciences.

4. Conclusion

In this paper, we have introduced a new medical image database called DEXSIT, a collection of dexa scan images for biomedical and healthcare application research. It is developed with the intention of providing a common benchmark for orthopedic research and related development. The main characteristics of this DEXSIT database are: a) 42 AP spine dexa images, 42 dual left femur and right femur bone dexa images each. b) 122 BMD plots for the dexa scan images c) Annotation of the entire subject's biological data, BMD levels, T-score, Z-score and area. d) Clinical report with suggestions for all the subjects. By providing this database available to the biomedical research community, we hope to promote the analysis of many uncertain problems. DEXSIT database along with all clinical measures will be publically made available for research. The database can be viewed and downloaded at the following web address:**http://www.sethu.ac.in/ DEXSIT/.**

Acknowledgement

The authors thank to Dr. Rajkumar, Radiologist, Government Hospital, Ramnad, India for his help and suggestions in building this database. The authors also immensely thank Dr. Ilayaraja Venkatachalam, Radiologist, Pixel Scans, Trichirappalli, India for providing Dexa scan images with all clinical interpretation to create this DEXSIT database.

References

[1] Nicola J. Crabtree, Mary B. Leonard, Babette S. Zemel, "Dual-Energy X-Ray Absorptiometry" Current Clinical Practice: Bone Densitometry in Growing Patients: Guidelines for Clinical Practice, pp.41-57, 2004.

[2] Robert H. Choplin , Leon Lenchik "A Practical Approach to Interpretation of Dual-Energy X-ray Absorptiometry (DXA) for Assessment of Bone Density", Curr Radiol Report 2:48, 2014.

[3] Rosa Lorente-Ramos Javier Azpeitia-Armán Araceli Muñoz-Hernández José Manuel arcía- Gómez Patricia Díez-Martínez Miguel rande- Bárez Dual-Energy X-Ray absorptiometry in the Diagnosis of Osteoporosis: A Practical Guide, AJR ; 196:897–904 0361–803X/11/1964–897, 2011.

[4] M. K. Garg and Sandeep Kharb ,"Dual energy X-ray absorptiometry: Pitfalls in measurement and interpretation of bone mineral density" Indian Journal of Endrocrinology and metabolism,2013.

[5] Roth J, Palm C, Scheunemann I, Ranke MB, Schweizer R, Dannecker GE. "Musculoskeletal abnormalities of the forearm in patients with juvenile idiopathic arthritis relate mainly to bone geometry", Arthritis Rheum, 50:12, pp.77–85, 2004.

[6] Rabinovich CE. "Bone mineral status in juvenile rheumatoid arthritis", J Rheumatol Suppl , 58:34–7, 2000.

[7] S C Lacassagne, P N. Tyrrell, E Atenafu, A S. Doria, D Stephens, D Gilday, and E D. Silverman "Prevalence and Etiology of Low Bone Mineral Density in Juvenile Systemic Lupus Erythematosus", Arthritis & Rheumatism, vol. 56, No. 6, June 2007, pp 1966–1973.

[8] R.M. Lorente Ramos, J. Azpeitia Armán, N. Arévalo Galeano, A. Mu˜noz Hernández, J.M. García Gómez, J. Gredilla Molinero "Dual energy X-ray absorptimetry: Fundamentals, methodology, and clinical applications" Radiología.;54(5):410-423, 2012.

A Proposed Design of an Universal Electrochemical Reader based on a collated Medical Device Innovation Framework and Systems Thinking

Nair Siddharth Shivakumar[i]
Centre for Product Design and Manufacturing,
Indian Institute of Science
Bengaluru, India
siddharthnair@iisc.ac.in[i]

Manish Arora[ii]
Centre for Product Design and Manufacturing,
Indian Institute of Science
Bengaluru, India
marora@iisc.ac.in[ii]

Monto Mani[iii]
Centre for Sustainable Technologies,
Indian Institute of Science
Bengaluru, India
monto@iisc.ac.in[iii]

***Abstract*—Glucometers are the most common electrochemical readers that people are using frequently, but, similar readers can be used for analyzing many other tests like HbA1c, Hemoglobin, Serum Albumin, Urine ACR, etc. However, at this moment most of the tests are conducted using proprietary readers, which add on to a lot of energy being consumed (with sustainability in focus, we consider energy consumed in form of all resources that is utilized for development, manufacturing, handling and disposal of the product) and also leads to increase in cost of tests and thereby raises the question on cost effectiveness of these tests. There are multiple other parameters which probably at the moment are not even considered while design of these products, thus, directly raising questions on sustainability of these products.**

In this paper we propose a design of a universal electrochemical reader which is generic in nature and can be adapted to any tests which can be measured or analyzed using an electrochemical measurement process and requires a small quantity of liquid samples like blood or urine. The proposed design is the result of following a Medical Device Innovation framework that was collated by the authors through reviews of existing frameworks and interviews. Systems Thinking was also used as a tool to understand the problem at a systems level with the help of cross-impact simulation models in the current solutions available across the market.

The aim of this study was to optimize the design of electrochemical reader, especially considering the case of glucometers with the focus being on study of Sustainability. With the help of the Medical Device Innovation framework model an optimized design for electrochemical readers was conceived.

Keywords*—Electrochemical reader, glucometers, systems thinking, medical device innovation framework, design framework, Internet of Things, Pervasive Computing, e-Health, Telemedicine.

I. INTRODUCTION

The most common electro-chemical reader in the market is the home blood glucometer, which is used for monitoring of blood glucose levels especially for people suffering with Diabetes. Diabetes is a chronic metabolic disease and if the blood sugar level remains above 150 mg/dl leads to various complications like neuropathy, blindness and also affects the heart and kidney. The TABLE I. shows a brief history of how blood glucometers evolved over a period of time [1,2,3].

TABLE I.: Evolution of Blood Glucometers

YEAR	DESCRIPTION
1552 BC	Earliest known record of Diabetes
250 BC	Apollonius of Memphis is credited with coining the term "diabetes"
1897 AD	Avg. life expectancy of newly diagnosed |10 Years Kid – 1year|30Years Adult - ~4Years|50 Years Old – 8 Years
Late 1940's	Helen Free develops the "dip-and-read" urine test (Clinistix), for instant glucose monitoring
1960's	Home testing for glucose levels in urine increases level of control for people with Diabetes
1970	First Glucose meter (Ames) introduced for Doctor's office and priced around US$500
1983	"Reflolux", later known as "Accu-Chek", is introduced for easy and accurate check
1990's	Continuous Glucose Monitoring Systems
Then On	Incremental Developments

The main reason for the growth in blood glucometer market is due to frequent test of blood glucose levels for a diabetic patient as uncontrolled sugar levels may be fatal for a diabetic patient. Similar to test of blood glucose levels these days, it's common in hospitals to have systems which could test multiple various platforms like HbA1c, Hemoglobin, Serum Albumin etc., but the problem majorly is that the equipment's in hospitals which can do multiple analysis are bulky and expensive thereby increasing the cost of tests as compared to the manual and generally time-consuming testing methods that is in practice. Apart from these issues we also see that these equipment's do not talk to each other hence needs manual updates in Electronic Health Records. Though integration with Laboratory Information Management System is supposed to handle this such practices are not fully implemented in resource limited countries like India and records are maintained manually thereby digital records are not accessible over a period of time.

Now we have two scenarios which can use similar solutions, but has different product requirements so we need to come up with a solution which is cost effective and has a simple design but caters to home based markets as well as hospitals. A systematic design approach could help to solve such a problem and come up with a cost-effective system.

II. Background

A. Medical Device Innovation Framework

A typical Medical device innovation consists of product planning, product design, product development, production, sales activities and post market surveillance. However, there is no common innovation framework that has been used across all the medical device industry, institutes or academics, which covers all the specific requirements and support for various medical devices irrespective of the device category and risks associated with the category. To formalize the process and make an innovation framework which would cover all the aspects of medical device innovation, we reviewed various design models, innovation models and industry practices for about 14 months and have collated a Medical Device Innovation Framework which would cover all the aspects of a medical devices including regulatory requirements. The collated Medical Device Innovation Framework is shown in Fig. 1.

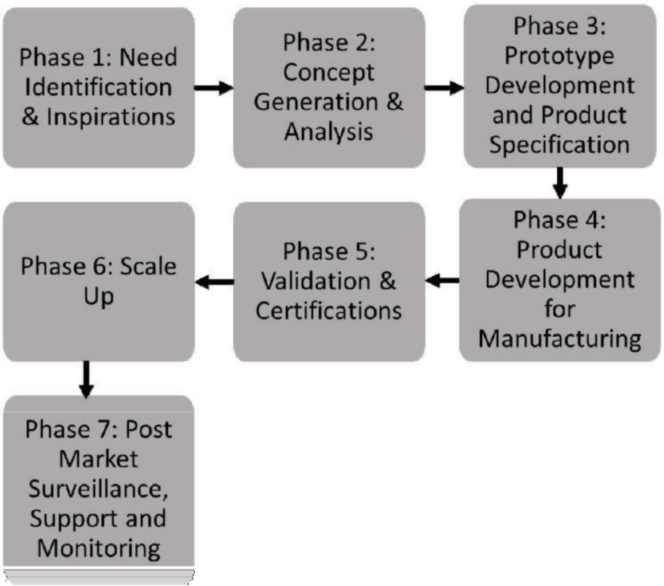

Fig. 1: The Medical Device Innovation Framework

The collated Medical Device Innovation Framework consists of seven critical phases which is further divided into multiple sub-phases. Each phase gets completed when the criteria that is set during the product planning phase is fulfilled satisfactorily before we start the next phase. We expect that when such a framework is used for medical device development, the probability of errors reduces thereby saving critical time and resources in development of a medical device.

B. Systems Thinking

The systems thinking approach helps us in the analysis of any solution or context with a macro as well as micro view. A systems perspective involves identifying the entities (players or stakeholders) involved and their attributes (variable characteristics) that define or capture interactions involved associated with a product (in this context). Thus, we can traceback or feedforward the product or object to its manufacturing processes followed, product design, source of raw materials to waste created, recycling and disposal methods as well. The overall approach helps us in understanding the gaps of the current solution. This method was first defined by Barry Richmond in 1987 and subsequently many others have redefined it [8].

The systems thinking approach helps us to think about an innovation in terms of sustainability of the product be it economic, social and environmental. Here we can define our scope of sustainability based on the short or long-term vision of the innovator or the organization.

C. Blood Glucose Meter

A Blood Glucose meter is the most common type of electrochemical reader, which helps in measuring the glucose level of Blood. A functional block diagram of a Blood Glucometer adapted from application note of Cypress Semiconductor [4] is shown in Fig. 2.

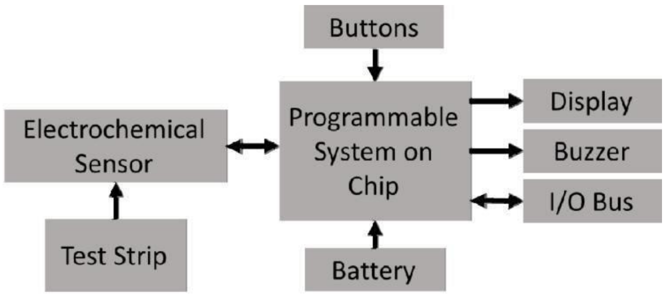

Fig. 2: Functional Block Diagram of a Blood Glucometer

There are multiple Programmable System on Chip (PSoC) these day, which can directly be used for such applications. First the sample in order of 0.3 to 3uL is collected on the test strip, which reacts to the bio-marker present on the test strip and inserted into an electrochemical sensor. A small voltage is passed onto the test strip and based on the reaction of the sample and the bio-marker a proportional current is sensed by a trans-impedance amplifier present in the PSoC which is then read by an analog to digital converter for further processing in a microcontroller of the PSoC. Based on the value readout blood sugar level is presented onto the display and/or buzzer beeps. The Blood Glucometer has an inbuilt battery and certain systems has a memory and an I/O bus for data transfer. Working of a Blood Glucometer is shown in Fig. 3.

ISBN 978-1-5386-4473-7
IEEE sponsored 4th International Conference on Biosignals, Images and Instrumentation, SSNCE, Chennai. ICBSII 2018 – 22nd-24thMar'18

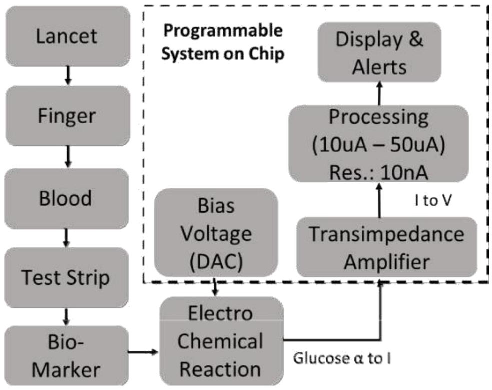

Fig. 3: Working of a Blood Glucometer

An entire package of a Glucometer when sold consists of a device, Lancing device, Lancet, Lancet package, Electrochemical Test Strip (ETS), ETS – Sterile outer pack, ETS – Box, Outer package, User manual and inner shelf. A small device like glucometer has so many sub components that go together into a market. If we understand what goes inside the device, it can be fragmented into: Plastic Enclosure, Printed Circuit Board (PCB), Passive Electronic Components, Display, Buzzer, Battery, Electrochemical sensor, Programmable System on Chip, battery management IC and labels. Thus, a glucometer which looks a small and simple device requires a large amount of energy to be built and all this gets together majorly for the advent of making the glucose measurement unit a standalone embedded system. The contents of a glucometer which needs to be manufactured [10] is shown in Fig. 4.

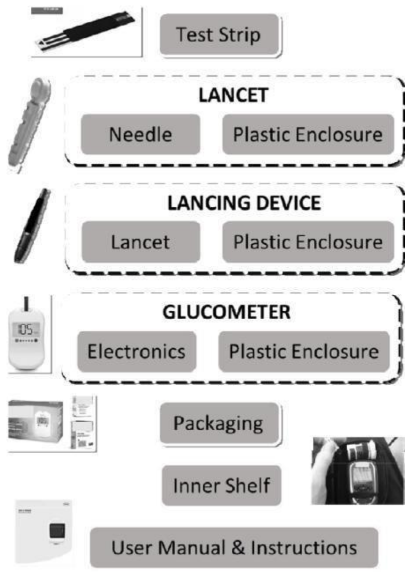

Fig. 4: Contents of an entire Glucometer package to be manufactured

III. Process

The first step in the design process as part of the Medical Device Innovation Framework is Need Identification followed by generation of concepts analyzing and validation of the design conceived as shown in Fig. 1. The scope of this paper is limited to, proposed concept, but we have plans to keep the design as an open source project so that other innovators can contribute towards the further development and possibly take the same forward for manufacturing and market.

A. Identifying the Problem and Understanding the Need

Initially, Glucometer as a case was chosen and an in-depth study was carried out to understand its making, uses and various problems attached in the current state. Based on the study a morphology of the product was generated which would give a fair idea of where the product currently stands and what are the alternative options available.

With better understanding of the product, we went ahead with systems thinking approach and as part of it, the tool used for understanding the entire scenario of glucometer and its trends in the market is Cross Impact Analysis or KSIM which was proposed by Julius Kane in his work described in "Technological Forecasting and Social Change" [9]. KSIM primarily captures systems level activities as binary-interactions amongst attributes of entities that define the various sub-systems involved. It further progresses to forecast various scenarios based on the nature and intensity of the binary interactions. Sustainability indicators are identified from the systemic variable set, and generally classified as environmental, societal and economic variables. Every variable is scaled from 0~1 corresponding to its characteristic upper and lower bound occurring naturally.

In the analysis, we started to categorize various activities involved in the entire life cycle of Glucometers based on the activities we identified various entities in the system and started mapping their interactions with each other. Which led to generations of various variables and we mapped the interactions of the variables with different entities and activities. Overall, we came up with 93 variables in the process. The next step was to perform a cross-impact analysis based on the interactions mapped and thus a 93 * 93 matrix for created which means we had 8649 values that generates a trend analysis, forecasting the gaps in the system. The major trends obtained are as follows:

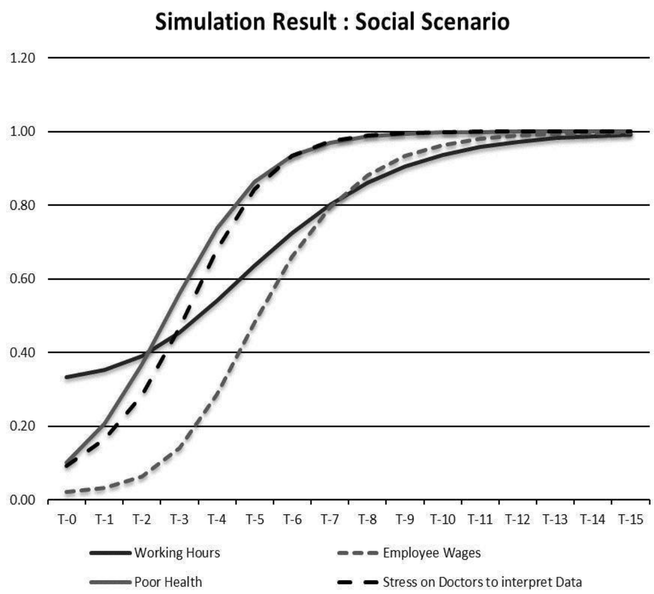

Fig. 5: Forecast Trends based on Social Variables of the system

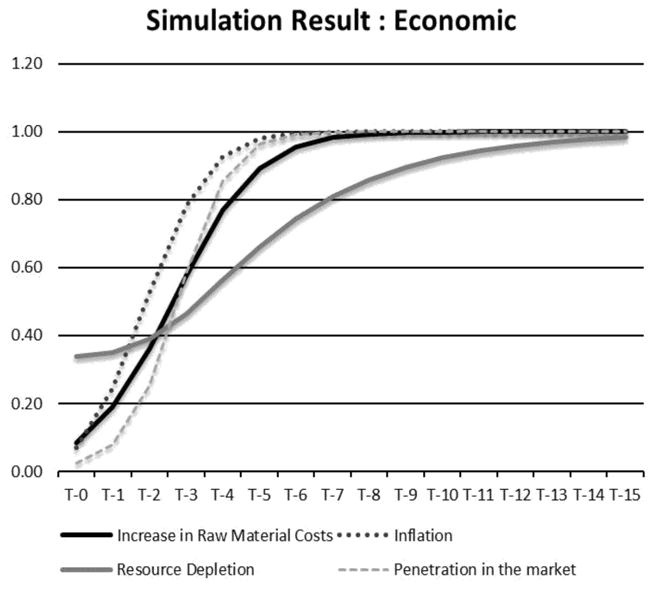

Fig. 6: Forecast Trends based on Economic Variables of the system

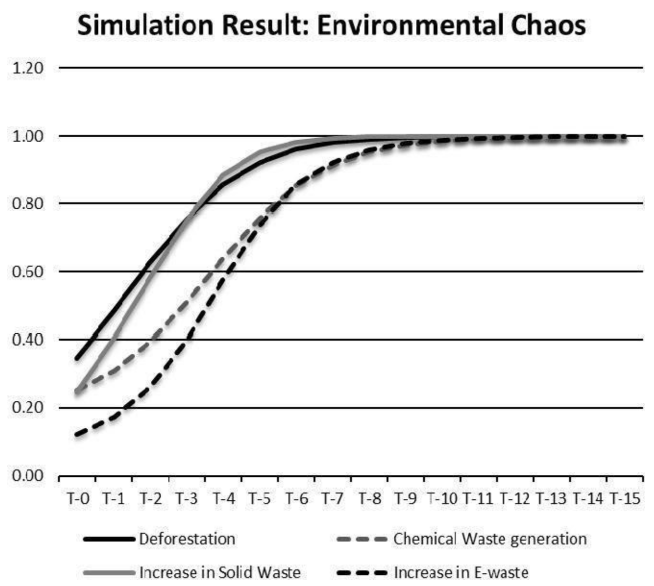

Fig. 7: Forecast Trends based on Environmental Variables of the system

Fig. 5 shows the forecast trends based on the selected social variables identified in the system, and as we can observe the ill effects on health can be observed with increased wages and working hours which also leads to increase in stress for the doctors. In about 12 interaction periods from T-0 the system will reach its peak and socially the current system will not be able to sustain.

Fig. 6 shows the forecast trends based on the selected economic variables identified. The trends look positive and in the next few interaction periods the system would be economically sustainable but would lead to inflation, issues in logistics and resources being depleted.

Fig. 7 shows the forecast trends based on selected economical variables identified. And the results indicate environmentally the current system will add on a lot to pollution and waste creation, hence, environmentally the current state of the system is not sustainable.

The Interaction matrix along with the 93 variables used to generate the simulation results can be accessed through our website [13]. The simulation forecast has been partially validated through an expert review, particularly for the directionality of the trends more than their change-rate. In the current study, the simulation results have been relied on for capturing the sytemicity of interaction and the direction of trends, which is generally accepted in similar forecasting studies [14].

The current system shows the characteristics of a week system which may be profitable economically, but would create chaos in the society and the environment and hence there is a need to look at the system from its design perspective to create a sustainable ecosystem.

Some of the major questions that come up by following the systems thinking approach are:

- Is increased use of semiconductors needed?
- Should we use batteries for small applications?
- Do we always need a stand-alone system?
- How frequently should we test our glucose levels?
- Do we ever consider Social and Economical Sustainability during designs?
- What is Affordable Healthcare?

B. *Defining the Requirements*

Based on the understanding of the current solution and in-depth study of the entire system with the help of systems thinking approach the following requirements are highlighted apart from the functional, aesthetics, safety and usability requirements followed in a typical industry scenario:

- The universal electrochemical reader should be able to measure glucose as well other tests which could use the similar measuring technique and the sample quantity to be limited to 1-3uL of a fluid like blood, urine etc.
- The system could be adapted to be used in Home as well as Hospitals
- The consumable cost, especially the cost of test strip should be low
- The system should follow all the regulatory guidelines and should give comparable results to the gold standard test.
- The system should be modular such that the devices used in the hospital be able to communicate with the Electronic Health Records (EHR) and have seamless data exchange with required security and data integrity. Whereas, the home-based modules collect data in the device and only when the clinician needs the data be synchronized with the EHR.

- The system design should focus on overall sustainability where the social and environmental aspects are considered along with the usual economic aspects.

C. *Understanding the Ecosystem*

A medical device is always a collaborative effort and thus it is very important to consider the entire eco-system and all stakeholders in the design phase itself as it helps not only in validation of the entire product from design to market phase, but also help in decrypting certain critical element of the product which may not have been considered in a usual scenario.

IV. Proposed Concept Design

The proposed concept needs to satisfy all the requirements stated above and will follow the principle of minimal design with very low amount of waste that would be generated in the process. The block-diagram of a proposed concept is shown in Fig. 8.

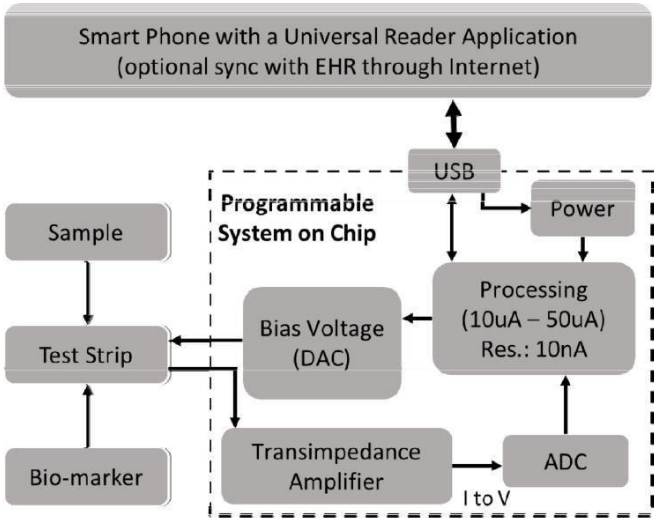

Fig. 8: Block-Diagram of the Proposed Universal Electrochemical Reader

The above concept as shown in Fig. 8 uses the principle of minimalist design and as compared to the current solutions multiple components like display and alert systems can get completely replaced. Use of a smart phone with a reader application reduces signal processing capability needed to a large extent and the proposed device could be used in a slave mode. Further, since there is no requirement of an inbuilt battery for the proposed design. The overall footprint of the device also reduces as we eliminate the space consuming components and hence the resources required to build the proposed device further reduces. Fig. 9 shows the X-ray view of the preliminary 3D CAD Model of the proposed concept.

However, since we now introduce a software component in the system the regulatory requirements would slightly increase with the design controls being similar to the code on a microcontroller. This gives us the freedom to adapt our system to any kind of electrochemical measurements for any tests that can be analyzed using electrochemical measurement principle with low sample volumes. Having the analysis in mobile phone means we have memory available for storage and with the existing communication medium the data can be exchanged as needed.

The test strip will still remain a small challenge for the innovators. Though the manufacturing process of a test strip has been quite standardized, the selection of the right type of membrane and bio-markers becomes a critical element for accurate analysis and scale-up.

The proposed design satisfies all the requirements discussed above. We solve the challenges related to sustainability to a large extent, but its quantitative assessment would require a lot more data and further detailed design of the proposed solution.

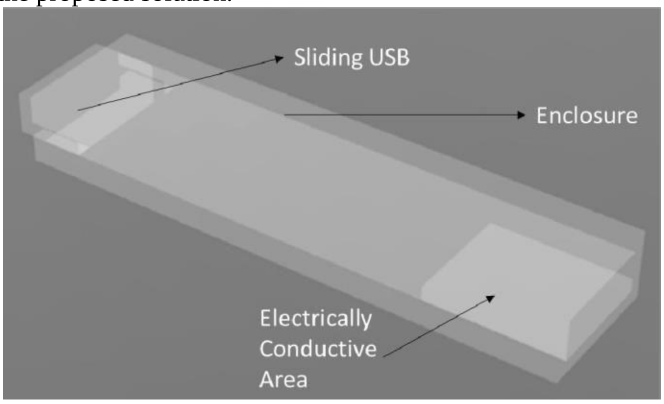

Fig. 9 X-Ray view of 3D CAD Model of the proposed concept

V. Discussion

The need identification and concept generation phases of the proposed conceptual design were discussed in this paper based on which following recommendations are made.

In the current approach there are multiple components like display, alarms, batteries and processing unit which were repeated for each realization of product. Following the current design trend of IoT based systems, we would further replicate more components which are already available in basic smart phones used by users. For optimal sustainable design, use of resources already available to the users during the activity should be considered while designing a system.

Currently, most of the design activities are carried out independently instead of in collaboration with all stakeholders thereby a systemic view is not considered whilst designing a product. With stringent regulation in medical device sector being implemented globally, if a designer does not have a holistic view, then the product instead of solving a problem may create a new problem on its own.

With the advent of IoT we are able to gather a lot of patient specific data, although the general trend now is to present the data to the doctors, but the actual question to answer is, if the doctors need that data or have capability to process the data available? Data analytics is one of the major areas of work in the future, which could help in better disease management, especially in chronic conditions like diabetes, hypertension, arthritis, *etc*.. Healthcare is currently moving towards product as a service model and more structured data could help in improving the quality of care provided.

In the current form domestic glucometer follows a weak sustainability model which focuses on economic sustainability alone. Currently products like glucometers are quick build product, thus it would be better if the products are designed with a holistic view rather than a narrow economic view alone.

Minimal design methods should be followed on products to optimize the use of resources including raw materials, computational power, packaging, aesthetics, etc. but, it does not mean that we can reduce the quality of outcome or have a system with poor performance. The design of medical devices needs to ensure high safety, low risks and optimum performance at affordable costs.

References

[1] Zajac J., Shrestha A., Patel P., Poretsky L., The Main Events in the History of Diabetes Mellitus. In: Poretsky L. (eds) Principles of Diabetes Mellitus. Springer, Boston, MA, 2010

[2] The Diabetes Council, https://www.thediabetescouncil.com/the-history-of-diabetes/ , Reviewed: May 30, 2016, Last Updated: September 25, 2017

[3] The Diabetes.org,http://www.diabetes.org/research-and-practice/student-resources/history-of-diabetes.html, Reviewed: November 11, 2013, Last Updated: May 9, 2014

[4] Cypress Semiconductor: Application Notes – Blood Glucometer http://www.cypress.com/applications/blood-glucose-meter

[5] Hagedorn, Thomas J. and Grosse, Ian R. and Krishnamurty, Sundar," A concept ideation framework for medical device design.," Journal of biomedical informatics, 2015, vol 55, pp 218-230

[6] Dexter Matt, Atkinson Paul and Dearden Andrew, "Open design and medical products: irreconcilable differences, or natural bedfellows?," Proceedings of the 10th European Academy of Design Conference, Gothenburg.,2013

[7] Bitterman, Noemi," Design of medical devices--a home perspective.," European journal of internal medicine, 2011, Vol 22, pp 39-42

[8] Ross D. Arnold, Jon P. Wade, "A Definition of Systems Thinking: A Systems Approach," Conference on Systems Engineering Research, 2015, pp 669-678

[9] Hubert Lipinski, John Tydeman, "Cross-impact analysis: Extended KSIM", in Futures, Volume 11, Issue 2, 1979, Pages 151-154, ISSN 0016-3287, https://doi.org/10.1016/0016-3287(79)90035-1

[10] Adapted from images of Accu-check http://www.flipkart.com

[11] S. F. Clarke and J. R. Foster, "A history of blood glucose meters and their role in self-monitoring of diabetes mellitus", British Journal of Biomedical Science, 2012 69 (2), pp 83-93

[12] Self - Monitoring Blood Glucose Test Systems for Over-the-Counter Use, Guidance for Industry and Food and Drug Administration Staff, issued on Oct 11, 2016

[13] The data used to generate the simulation results can be accessed here: http://cst.iisc.ac.in/sudesi/wp-content/uploads/2018/03/Simulation_Glucometer.xlsx

[14] Mani M., Ganesh L. S. and Varghese K., "Enhanced Futures System: Integrated Cross-Impact Analysis and Geographic Information Systems.", Futures Research Quarterly, 2005, 21(3), pp. 19−45

ISBN 978-1-5386-4473-7
IEEE sponsored 4th International Conference on Biosignals, Images and Instrumentation, SSNCE, Chennai. ICBSII 2018 – 22nd-24thMar'18

A review of present and futuristic development of Near Infrared Spectroscopy system in the assessment of diabetic foot risk

1Resham Raj Shivwanshi, 2N P Guhan Seshadri, 3R Periyasamy*

Abstract—**Diabetic foot is a common, immobilizing and often engender to the amputation of the lower limb. The utmost originating facet to the upshot of diabetic foot ulcers are neuropathy (i.e. peripheral nerve dysfunction), arterial occlusive diseases, PVD (i.e. peripheral vascular disease), malformation and disorder. It has been widely studied that the one fourth of overall number of diabetic mellitus patients will suffer from foot ulcers. These types of patients are at menace of amputation and can soon turn towards mortality. To dwindle the rates of mortality and morbidity, prudent detection of the menace foot areas is indispensable. This article mainly focused on vascular disease at lower limbs, which is one of the main factors causing diabetic foot ulcers. This review article aims at providing brief overview in development of near infrared spectroscopy (NIRS) in assessing the vascular parameters in lower extremities of the patients. The parameters obtained from the NIRS method shows high clinical significance and it well correlated with the existing methods.**

I. Introduction

The huge network of interconnecting veins, arteries, nerves and several other small capillary tubes is responsible for the nourishment of different parts of human body. Continuous and uninterrupted blood flow is required to run metabolic system of different cells. It contains required amount of oxygen for the functioning of ligaments and cells. In a healthy human adult male, the appropriate amount (i.e. 14gm/100gm) of hemoglobin exists in the blood which is also a media for the transportation of oxygen. Some part of hemoglobin is oxygenated (HbO_2) and the rest is deoxygenated (dHB). The Near infrared spectroscopy (NIRS) manages to analyse HbO_2 and dHb in the blood. One the cause of impairment of tissues and part of the body is improper flow of blood and oxygen. Oxygen perfusion gets weak in diabetic patients, due to high glucose level. This tends to increasing risk of foot ulcers. NIRS can be used to early detection of diabetic foot ulcers.

Research funded by DST-SERB India(ECR/2015/000161) and the authors detail are as follows:

Resham Raj Shivwanshi, Department of Biomedical Engineering, National Institute of Technology, Raipur 492001, Chattisgarh, India, *email:resham.electronics@gmail.com*

N P Guhan Seshadri, Department of Bimedical Engineering, National Institute of Technology, Raipur 492001, Chattisgarh, India. *email: guhan131192@gmail.com.*

R Periyasamy, AssistantProfessor, Department of Biomedical Engineering, National Institute of Technology, Raipur 492001, Chattisgarh, India. *email: rperiya.bm@nitrr.ac.in.*

*Corresponding Author (and IEEE member)

Increasing rate of incidence of diabetes across the world is the emerging problem for the cause of Diabetic foot ulcers [1]. The another fact which is evaluated in several studies is that the prevalence of foot ulcers among diabetic group 15% which may get hike up to 25 % and certainly become more dangerous for them[2,3,4,5]. Diabetic patients with foot ulcers often increased the menace of limb amputation and higher the rate of mortality. Detection of menace of the foot areas in early stages is important, and consequently appropriate treatment can improve the patient's life quality. Factors which are highly responsible for the development of foot ulcers are peripheral nerve dysfunction (neuropathy), Peripheral arterial disease (PAD), deformity, and disorder [2]. Timely detection of the high-risk foot areas is essential to decrease the rates of mortality and morbidity. Diabetic patient become imprudent because of impaired ability to feel the pain which is due to the peripheral nerve dysfunction. This means that minor injuries may remain undiscovered for a long while. In diabetes, peripheral nerve dysfunction can be combined with PAD is a narrowing of blood vessels due to the accumulation of plaque in the vascular walls, which results in poor circulation of blood to the vital organs mainly in the lower extremity of the body (diabetic angiopathy). This disease often occurred after the age of sixties and people suffered with several other related disorders such as peripheral artery disease and diabetic foot ulcers [3]. In this case, any kind of wound cannot heal easily and takes longer time than usual consequently infestations may spread and it tends to further amputation of limbs. The people suffering from diabetes some time have non traumatic amputation. The menace of peripheral vascular disease (PVD) gets higher in people who are subjected to diabetes and sometime they caught by immense pain and utmost disorder [6]. The increased rate of menace of PAD is also related limb impairment which soon turns into amputation. Because of the PAD and diabetes, people sometime suffer from long term disability [7]. To get proper remedy for this disease, people generally expends lots of time and money for their tests, diagnosis, therapeutic procedures and sometimes they end up with hospitalization[8, 7]. It has been studied that there are no any authentic and precise methodology available to trace out the diabetic foot ulcers and till date, health-care research planning and clinical practice is solely build more on opinion than scientific fact [9]. Early identification of the foot areas under risk and suitable treatment will improve the quality of patient's life [1, 10, 11]. There are several techniques currently being used by clinicians to assess and diagnose the severity of vascular diseases in lower extremities. Most commonly used method is Ankle-brachial pressure index (ABI/ ABPI) but the measures has no information about the blood flow and the oxygen perfusion to the tissues. Other methods are Laser Doppler flowmeter (LDF), transcutaneous oximetry ($TcpO_2$), magnetic resonance spectroscopy and venous plethysmography.

NIRS is a non-invasive diagnostic technique which is widely used to quantify the changes in the concentrations of tissue oxygenation in clinical levels and in research laboratories [12,13,14]. NIRS uses the near infrared region (700 nm -1100 nm) in the electromagnetic spectrum where the tissue is relatively transparent in this region and hence allows the light to penetrate deep structures [15]. NIRS method measures the changes in the light absorption spectra of HbO_2 and dHb at different wavelengths (in near-infrared region) to assess the tissue oxygenation. NIRS is being widely used in the evaluation of cerebral circulation [13]. NIRS offers continuous, real-time together measurement of cellular respiration and blood volume in skin tissue and it offers more direct indication of tissue nutritional condition than is feasible using laser Doppler or transcutaneous oxygen measurements [6]. When the study has been done on the optical attenuation in brain tissue, it is observed that Near Infrared Spectroscopy is useful to detect level of metabolites, for example hemoglobin, cytochrome, c oxidase and deoxyhemoglobin, this gives the idea for further development of NIRS system. NIRS measures oxygenation at both capillary bed and post-capillary venule [17] [18]. The NIRS system was combined with vascular occlusion technique in order to assess the response for the standard ischemic stimulus. NIRS is equipped with an optical probe in which detection has been done with the help of optical transducers. Generally the detector has been placed around 2 to 4 cm far from the source thus attenuation factor can be measured to the intensity of the source. The transmitted optical signal attenuated due to several obstacles such as tissue chromophores and scattering loss. This phenomenon responsible for the variation of optical path, which is traveled by photon, and it increase the percentage of absorb optical signal. By analyzing the spectrum of absorption, Beer-Lambartz law implied to study the relation between concentration of dHb and HbO_2. This review article reviewed the recent developments in clinical applications of NIRS in the assessment of vascular diseased state in the lower extremity which is one of the main causes in diabetic foot ulcers.

Concerning the limitations of NIRS in assessing vascular parameters includes the i) influence of subcutaneous fat tissues at the site of assessment area, ii) role of myoglobin on tissue oxygenation evaluation because both hemoglobin and myoglobin shares identical absorption spectra, and some experimental studies found that myoglobin concentration corresponds to only 10% of absorbed light and the majority of signal accounts to hemoglobin concentration [19, 20]. In the severely obese, subcutaneous fat considered to be a limiting factor, however, the distance from skin to fascia was never more than 2.5 cm, despite of the existence of swelling, edema, or high body mass index and also use of spatially resolved NIRS methods may reduce the effect of subcutaneous layer [20]. Despite limitations, NIRS has the potential to offer a continuous, non-invasive monitoring system in real time that more accurately estimates tissue oxygenation parameters.

II. .METHODS

Potential clinical studies were selected in which NIRS was used as a diagnostic tool to evaluate the severity of PVD. We searched Pubmed and SCOPUS (until 2016) with the following strategy, 'Near infrared spectroscopy' or 'NIRS' or 'Tissue oxygenation' or 'Peripheral vascular disease' or 'Peripheral arterial disease' or 'Intermittent claudication (IC)' or 'microcirculation' or 'muscle oxygen consumption' or 'muscle hypoxia' or 'leg ischemia' or 'PVD and diabetes' or 'foot ulcers'. We further included some studies which are identified from the references of relevant trails.

III. CLINICAL APPLICATIONS OF NIRS

A. *Assessing muscle oxygenation in PAD patients*

Anna Maria Malagoni [21] studied the feasibility of NIRS in the assessment of clinical parameters in patients with PAD. Authors analyzed the resting muscle VO_2 consumption ($rmVO_2$) in 119 PAD patients and 30 healthy controls along with the measure of ABI ratio and thickness of adipose tissue. Muscle oxygen consumption during arterial occlusion ($rmVO_2art$) and venous occlusion ($rmVO_2ven$) were compared. The study result shows that reduced pain in $rmVO_2$ with elevated values and it could be appropriate for the clinical analysis of PAD non-invasively.

B. *Assessing Tissue oxygenation parameters in patients with claudication*

Takashi Komiyama [22] investigated the alterations in tissue oxygenation in the calf during tredmill test for 62 intermittent claudicants. Authors measured the oxygenated and deoxygenated hemoglobin with three distinct patterns. Investigators found that mean maximal walking distance of type 1 is significantly high than type 2 and there were no significant difference found in the mean ABI between type1 and type 2. Authors concluded through their results that NIRS can be used to analyze the progression or severity of IC accurately. Toshiaki watanable [23] managed to assess exercise-induced ischemia in IC patient's calf using NIRS and observed the similarity between the obtained results with those acquired by ABI test. The experiments were done on 62 patients who reported with IC due to atherosclerotic occlusive disease. Patients are allowed to exercise on treadmill until they are attaining the utmost endurance walking distance. Investigators measured ABI during rest and past exercise till it reach the baseline value. Similarly, NIRS parameters such as oxygen saturation (StO_2), dHb and HbO_2 before and after exercise. Authors found that when performing exercise, the StO_2 and HbO_2 decreased and dHb increased and the recovery time for ABI (i.e., the time taken for every measurement to reach the baseline) is well correlated with StO_2, HbO_2 and dHb.

C. *NIRS in assessing post occlusive reactive hyperemia in patients with PVD*

Rudi Kragelj [24] assessed post occlusive hyperemia parameters from the oxyhemoglobin signal obtain through NIRS. 24 patients with PVD and 18 healthy volunteer were recruited for this study and NIRS was employed over foot dorsal and lateral surfaces while oxygenation parameters were measured during arterial occlusion. It is observed by the investigator that different parameters for reactive hyperemia rate, reactive hyperemia and maximum variation in hyperemia are notably lesser in the group of patient as compared to the group of controlled patient. They further analyzed the correlation of obtained values with ABI and $TcpO_2$ and the results showed decent correlation.

D. NIRS in assessing the oxygen saturation recovery time rate:

Kevin K. Mccully [25] observed similarities in recovery time constant of oxygen saturation during and after the mild plantar flexion exercise in patients with PVD and healthy controls in addition with old people using NIRS in lateral soleus. Authors found that the rate of oxygen saturation is in near maximal throughout the test in PVD patients related to healthy controls and also found that recovery time constant and ABI were significantly correlated (r_2=0.63, p<0.01). Cheatle T R [26] employed NIRS on calf muscles of 28 normal healthy controls and 17 patients with PVD in order to measure the oxygen consumption using NIRS. HbO_2 to dHb conversion rate when the time of induced ischemia defines oxygen consumption and investigators found that oxygen consumption in diminished in patients with PVD.

E. Measuring oxygen saturation and NIRS parameters in patients with IC during exercise test

Andrew W Gardner [27] analyzed the relationship between the exercise performance and characteristics of StO_2 in patients with IC. Oxygen saturation for 39 patients evaluated during, before and after a treadmill test along with the ABI, ischemic window, and initial claudication window (ICD), demographic and cardiovascular risk factors and absolute claudication distance (ACD). The authors found that the decrease in value of StO_2 as soon as the exercise start is correlated with the shorter ICD and ACD values and the recovery time is delayed after the exercise. Seifalian A M [28] studied the alterations of NIRS parameter in 14 IC patients and 10 controls before and after the treadmill test. The author found that the rate of deoxygenation is significantly high in patient with claudication than to controls. Similarly, the degree of HbO_2 is significantly different between patients and controls. Authors also noted that the recovery time of HbO_2 is significantly low in patients compared to controls. Stephen F Figoni [29] analyzed the effect of treadmill exercise on the calf muscle tissue oxygenation in patients (n=15 males) with PAD and Intermittent calf claudication. Authors observed greater improvement in treadmill walking was assisted by the higher calf tissue deoxygenation after exercise intervention. Miriam kooijman [30] conducted experiments on 11 claudicants and 15 non-claudicants in order to learn more about the application of NIRS on assessing peripheral arterial occlusive disease. Authors investigated the oxygen consumption, O_2 saturation, and recovery times constantly during and post walking exercise. The results showed that significant difference in VO_2 between claudicants and non-claudicants after walking exercise and claudicants showed significantly diminished post arterial occlusion oxygen resaturation and walking exercise and the recovery times and resaturation rates were highly correlated with ABI parameters.

F. Assessment of Tissue oxygenation parameters in PAD patients with diabetes

Manfredini [31] reported the consistency of vascular claudication in diabetic patients with PAD with the use of NIRS. Authors recruited 152 claudicants including 74 PAD with diabetes and 78 were PAD without diabetes. NIRS measurements were carried out to quantify the muscle oxygenation at symptom beginning and maximal speed (Smax) during treadmill test and also measured the area under the curve of oxyheamoglobin (AUC-HbO) and area under the curve of differential hemoglobin (AUC-Hb). The authors found that the similar exercise capacities in both groups which is inversely proportional to the muscle oxygenation and in addition to that the values of AUC-HbO and AUC-Hb at symptom onset and Smax was significantly lower in DM-PAD group. It shows that in diabetes shows delayed response in claudication than patients with PAD. Khalil M A [32] observed the hemodynamic response within the foot of healthy volunteer, PAD patients and patients with both PAD and DM. Investigators used NIRS optical tomography technique to image the foot hemodynamics parameter by applying cuff occlusion technique. The finding shows differences in total hemoglobin between all the groups during thigh cuff occlusion. Komiyama [22] evaluated the sternness of the IC in 153 patients with diabetes using NIRS merged with treadmill walking test. The investigators found that NIRS measurements has differentiated three distinct types of IC, similarly ABPI has major difference between all three groups of non-diabetic patients but it failed rate the severity of the intermittent claudication in diabetic patients. Authors compared the recovery time of oxygen saturation with the ABPI and found that there was significant correlation between non-diabetic patients and patients with diabetes more than 10 years. Therefore they concluded that recovery time of oxygen saturation helps in identifying the progression of the IC in diabetic patients than ABPI. Mohler ER [33] investigated the hemodynamic responses in diabetic patients with PAD on the calf muscles while performing plantar flexion and treadmill walking exercise. Authors found that the NIRS measurement of dHb and HbO_2 recovery times significantly correlates with the presence of PAD.

G. NIRS in assessing hemodynamic parameters at diabetic wound

Micheal Neidrauer [1] studied the usefulness of NIRS in quantifying the hemoglobin concentration at the wound site of 16 diabetic patients concerning prediction of wound healing. It is also observed by the authors that, continuous demeaning of quantity of hemoglobin concentration several weeks before of termination and total hemoglobin concentration reaching the value at control site. The final outcome which was concluded by the author is that, the evaluation of diabetic foot ulcers using NIRS is an effective and more complete as well as suitable measurement

ISBN 978-1-5386-4473-7
IEEE sponsored 4th International Conference on Biosignals, Images and Instrumentation, SSNCE, Chennai. ICBSII 2018 – 22nd-24thMar'18

comparing present clinical methods. Elizabeth papazoglou [34] conducted a pilot study on seven diabetic patients with wounds using diffuse NIRS method to analyze the tissue oxygenation at wound site to interpret wound healing process over time. Results indicate that, with NIRS, the dissimilarity in optical properties can be seen among wounds with diverse healing behaviors. Chen ML [7] investigated the peripheral circulation on diabetic patients with foot ulcer using wireless NIRS while doing Buerger's exercise. Authors divided the patients group into diabetes with PAD and diabetes without PAD and analyzed the peripheral circulation on patient's dorsal foot while doing Buerger's exercise. Authors found significant difference between diabetic patients and healthy participants in both pre- and post-exercise stages. Authors also found significant differences among diabetic group in pre-exercise status but not in post-exercise. Authors concluded that NIRS could be used to monitor real-time peripheral circulation in postural changes continuously and quantitatively.

H. NIRS on assessing the severity of PAD

Manfredini [36] conducted experiments on 67 patients and 28 healthy subjects in order to evaluate the PVD using NIRS. The investigators analyzed in addition to echo color Doppler and ABI were also calculated. NIRS was employed on the gastrocnemius when the patients performing treadmill test. Parameters such as variation in HbO_2, dHb, total hemoglobin (HHb) and differential hemoglobin (diffHb) and the quantified area under the curve (AUC) was analyzed. In addition to this they monitored the heart rate of the patients. The investigators found that significant difference between the HbO(AUC), HHb(AUC), Hb(AUC) diseased and non-diseased legs and showed different patterns associated with PAD severity. Authors also observed simultaneous increase in heart rate in PAD patients during exercise.

I. NIRS Reproducibility in PVD evaluation

Mccully [37] analyzed the usefulness of NIRS measurements in distinguishing the PVD by accounting the frequency of a successfully test and comparing it with existing standards. Authors investigated half time recovery of O_2 saturation on subjects (n=117) in the soleus muscles. The investigators finding shows that the half time recovery of O_2 saturation was significantly longer in subjects with claudication. Sensitivity and specificity was analyzed in order to assess the effectiveness of NIRS in diagnosing PVD. Furthermore, it is used to analyze different diseased condition in medical field. From the past two decades, use of NIRS has been discussed by several author in their studies, which is given in the Table.1.

TABLE I. CHRONOLOGICAL DEVELOPMENT IN NIRS AND ITS APPLICATIONS

S. no.	Application Of NIRS Technology	Parameter	Author	Year
1	NIRS in accessing the rate of recovery time of oxygen saturation	Time constant of recovery of oxygen saturation (HbO_2T_c)	Kevin K Mccully	1994
2	for noninvasive assessment of claudication	relative O_2 saturation of hemoglobin	Macully	1997
3	NIRS in accessing post occlusive reactive hyperemia in patients with PVD	Oxygen Consumption (VO_2) and oxygen partial pressure, recovery time	Rudi Krageli	2001
4	NIRS with other technique on evaluation of PVD	VO_2, recovery time	Tomaz Jarm	2003
5	Measuring oxygen saturation and NIRS parameter I patients with IC during exercise test	oxygen saturation (StO_2)	Andrew W Gardner	2008
6	Assessment of tissue oxygenation parameter in PAD patients with diabetes	HbO_2, dHb	F. Manfredini	2009
7	NIRS in accessing hemodynamic parameter at diabetic wound	HbO_2, dHb	MicheaINeidrauer	2010
8	Skeletal muscle oxygen saturation (StO_2) measured by near-infrared spectroscopy in the critically ill patients.	StO_2	Mesquida J	2013
9	Near infrared spectroscopy (NIRS) derived tissue oxygenation in critical illness.	StO_2	RS Samraj	2015
10	NIRS for assessing tissue oxygenation and microvascular reactivity in critically ill patients	StO_2 and vascular occlusion test (VOT)	Abele Donati	2016

IV. DISCUSSION

The utmost facets, which are responsible for the genesis of foot ulcers in diabetic patients, are lower limb vascular disease, neuropathy, and local infectious disorders [43, 38, and 39]. It has been studied that arterial occlusive disease becomes more common problem when the people completes their fifty years of life. It is vascular abnormalities, which obstruct the vascular system either on the macro-circulatory or micro-circulatory level, which further reduces the oxygen availability to the tissues [40, 41]. This suppresses the transporting of oxygen to the body tissues and cells and thereby it ends in reduced supply of oxygen and reduced blood circulation to the cells later it ends in cell necrosis due to ischemia. Poor long-term glycemic control is the main reason for the disease progression in diabetic patients with lower extremity difficulties, which leads to arteriosclerosis and coagulation inside the blood vessel walls, and consequently reduced oxygen perfusion [42]. Therefore, rise in stiffening of blood walls and less oxygen permeability responsible to hike the chances of blood clot. It creates the favorable condition for the growth of thrombus, stenosis, vascular or arterial occlusion and ischemic situation of the lower leg. Therefore it is necessary to diagnose the vascular abnormalities in lower extremities at early stage in order to prevent it from the formation of arteriosclerosis, ulceration and finally from amputation.

There are many well-established methods like Ankle-brachial pressure index, magnetic resonance spectroscopy, Doppler fluximetry, $TcpO_2$ and venous fiber oximetry to identify and estimate the intensity of PVD in clinical levels [43]. In that, most common method is ABPI but this is the unsuitable technique, which is not able to estimate the blood flow. Laser Doppler flowmetry helps in analyzing the relative values of blood perfusion in but constraints its clinical use because of its unknown origin of the signal [42, 43]. $TcpO_2$ is widely used for evaluation micro-circulatory evaluation and $TcpO_2$ measurement is employed to specify the skin perfusion additionally, while it is unclear that whether the $TcpO_2$ measurements shows the latent tissue oxygen partial pressure or not [44]. On the other hand, NIRS helps in monitoring the tissue oxygenation parameters non-invasively and it offers the evaluation of tissue oxygenation at specific area level. NIRS offers uninterrupted as well as live estimation of cellular respiration and amount of blood in skin tissue. It also renders highly specific estimation of tissue nourishment state as compared to the other technique such as Laser Doppler or Transcutaneous oxygen measurement [45]. NIRS gives estimation of oxygenation at both capillary bed and post-capillary venule [9]. Therefore, in lower extremities, the tissue oxygenation parameters derived using NIRS can be helpful in diagnosing the vascular diseases, which will reduce further complication of lower extremity amputation. In this technology, there are two wavelengths (760nm and 850nm) has been used by all the previous researchers. If we introduce the probe with multi wavelength source (more than two) and variable source-detector distance, may improve the accuracy in the quantification of tissue oxygenation and provides better penetration depth to assess micro vascular circulation in capillary beds.

Recent time NIRS technology employed probe, which make contact with patients in order to analyze hemodynamic parameters. In future, with the help of high precision software and hardware, non-contact NIRS data acquisition is possible which will improve the ease of recording with patient's serenity. Further NIRS imaging canbe used to monitor oxygen concentration and other relevant parameter. This system can alsoemployed to detect thrombosis and ischemic condition non-invasively. The overall system is connected thorough wires and cables, which can be replaced by wireless technology. It will help to access the patient's data remotely on the computer screen and reduce the time for diagnosis.

V. CONCLUSION

NIRS helps in monitoring the tissue oxygenation parameters non-invasively and it offers the evaluation of tissue oxygenation at specific area level. It helps in diagnosing the PVD and the changes in tissue oxygenation level at the micro and macro circulatory level because the NIRS parameters represent the oxygen delivery to tissues themselves. It give the impression from the above results, NIRS is a promising technique to evaluate the tissue hemodynamics and the many parameters obtained from NIRS helps in assessing the severity of the PVD. There is no statement about the efficiency issues and the cost regard NIRS in the work reviewed. Therefore, NIRS is a simple, non-invasive technique to assess the tissue hemodynamics with safety to the patients.

ACKNOWLEDGMENT

Authors are grateful to Science and Engineering Research Board (SERB), Ministry of Science and Technology, Govt. of India, New Delhi for providing financial support (ECR/2015/000161).

REFERENCES

[1] M. Neidrauer, L. Zubkov, M.S. Weingarten, K. Pourrezaei, et al., Near infrared wound monitor helps clinical assessment of diabetic foot ulcers, (2010).
[2] A. Alavi, R.G. Sibbald, D. Mayer, L. Goodman, M. Botros, D.G. Armstrong, et al., Diabetic foot ulcers: Part I. Pathophysiology and prevention., J Am AcadDermatol. 70 (2014) 1.e1-18; quiz 19.
[3] R.J. Hinchliffe, J.R.W. Brownrigg, J. Apelqvist, E.J. Boyko, R. Fitridge, J.L. Mills, et al., IWGDF guidance on the diagnosis, prognosis and management of peripheral artery disease in patients with foot ulcers in diabetes., Diabetes Metab Res Rev. 32 Suppl 1 (2016) 37–44
[4] B.A. Lipsky, A.R. Berendt, H.G. Deery, J.M. Embil, W.S. Joseph, A.W. Karchmer, et al., Diagnosis and treatment of diabetic foot infections., Clin Infect Dis. 39 (2004) 885–910.
[5] N. Singh, D.G. Armstrong, B.A. Lipsky, Preventing foot ulcersin patients with diabetes., JAMA. 293 (2005) 217–228.
[6] F. Huysman, C. Mathieu, Diabetes and peripheral vasculardisease, ActaChirurgicaBelgica. (2009).
[7] T. Thiruvoipati, C.E. Kielhorn, E.J. Armstrong, Peripheral artery disease in patients with diabetes: Epidemiology, mechanisms, and outcomes., World J Diabetes. 6 (2015) 961–969.
[8] A.T. Hirsch, L. Hartman, R.J. Town, et al., National health care costs of peripheral arterial disease in the Medicare population, Vascular …. (2008).

[9] W.J. Jeffcoate, K.G. Harding, Diabetic foot ulcers., Lancet. 361 (2003) 1545–1551.
[10] N. Wells, C. Pasero, M. McCaffery, Improving the Quality of Care Through Pain Assessment and Management, in: R.G. Hughes, R.G. Hughes (Eds.), Patient Safety and Quality: An Evidence-Based Handbook for Nurses, Agency for Healthcare Research and Quality (US), Rockville (MD), 2008.
[11] McCulloch, D. K., Munshi, M., Nathan, D. M., Schmader, K. E., & Mulder, J. E. (2014). Treatment of type 2 diabetes mellitus in the older patient. UpTodate. October 2014.
[12] C.O. Olopade, E. Mensah, R. Gupta, D. Huo, D.L. Picchietti, E. Gratton, et al., Noninvasive determination of brain tissue oxygenation during sleep in obstructive sleep apnea: a near-infrared spectroscopic approach., Sleep. 30 (2007) 1747–1755.
[13] T.W.L. Scheeren, P. Schober, L.A. Schwarte, Monitoring tissue oxygenation by near infrared spectroscopy (NIRS): background and current applications., J ClinMonitComput. 26 (2012) 279–287.13
[14] Noninvasive Monitoring of Gas Exchange - Assisted Ventilation of the Neonate (Sixth Edition) - 11, (n.d.).
[15] J. Cobb, D. Claremont, Noninvasive measurement techniques for monitoring of microvascular function in the diabetic foot.,Int J Low Extrem Wounds. 1 (2002) 161–169.
[16] F.F. Jöbsis, Noninvasive, infrared monitoring of cerebral and myocardial oxygen sufficiency and circulatory parameters., Science. 198 (1977) 1264–1267.
[17] A.N. Gay, D.A. Lazar, B. Stoll, B. Naik-Mathuria, O.P. Mushin, M.A. Rodriguez, et al., Near-infrared spectroscopy measurement of abdominal tissue oxygenation is a useful indicator of intestinal blood flow and necrotizing enterocolitis in premature piglets., J Pediatr Surg. 46 (2011) 1034–1040.
[18] J. Mesquida, G. Gruartmoner, C. Espinal, Skeletal muscle oxygen saturation (StO_2) measured by near-infrared spectroscopy in the critically ill patients., Biomed Res Int. 2013 (2013) 502194.
[19] R. Boushel, C.A. Piantadosi, Near-infrared spectroscopy for monitoring muscle oxygenation., ActaPhysiol Scand. 168 (2000) 615–622
[20] A. Lima, J. Bakker, Espectroscopia no infravermelhopróximo para a monitorização da perfusãotecidual, Rev Bras TerIntensiva. 23 (2011) 341–351
[21] A.M. Malagoni, M. Felisatti, S. Mandini, F. Mascoli, et al., Resting muscle oxygen consumption by near-infrared spectroscopy in peripheral arterial disease: a parameter to be considered in a clinical setting?, …. (2010).
[22] T. Komiyama, H. Shigematsu, H. Yasuhara, T. Muto, Near-infrared pectroscopy grades the severity of intermittent claudication in diabetics more accurately than ankle pressure measurement., Br J Surg. 87 (2000) 459–466.
[23] T. Watanabe, M. Matsushita, N. Nishikimi, T. Sakurai, et al., Near-infrared spectroscopy with treadmill exercise to assess lower limb ischemia in patients with atherosclerotic occlusive disease, Surgery Today. (2004).
[24] R. Kragelj, T. Jarm, T. Erjavec, M. Presern-Strukelj, D. Miklavcic, Parameters of postocclusive reactive hyperemia measured by near infrared spectroscopy in patients with peripheral vascular disease and in healthy volunteers., Ann Biomed Eng. 29 (2001) 311–320.
[25] K.K. McCully, C. Halber, J.D. Posner, Exercise-induced changes in oxygen saturation in the calf muscles of elderly subjects with peripheral vascular disease, Journal of Gerontology. (1994).
[26] T.R. Cheatle, L.A. Potter, M. Cope, D.T. Delpy, P.D. Coleridge Smith, J.H. Scurr, Near-infrared spectroscopy in peripheral vascular disease., Br J Surg. 78 (1991) 405–408.
[27] A.W. Gardner, D.E. Parker, N. Webb, P.S. Montgomery, K.J. Scott, S.M. Blevins, Calf muscle hemoglobin oxygen saturation characteristics and exercise performance in patients with intermittent claudication., J Vasc Surg. 48 (2008) 644–649.
[28] A.M. Seifalian, A. Atwal, S. White, et al., A role for near infrared spectoscopy in the assessment of intermittent claudication, International …. (2001).
[29] S.F. Figoni, C.F. Kunkel, A.M.E. Scremin, A. Asher, et al., Effects of exercise training on calf tissue oxygenation in men with intermittent claudication, PM&R. (2009).
[30] H.M. Kooijman, M.T. Hopman, W.N. Colier, J.A. van der Vliet, B. Oeseburg, Near infrared spectroscopy for noninvasive assessment of claudication., J Surg Res. 72 ,1-7,(1997).
[31] F. Manfredini, N. Lamberti, A.M. Malagoni, et al., Reliability of the vascular claudication reporting in diabetic patients with peripheral arterial disease: a study with near-infrared spectroscopy, …. (2015).
[32] M.A. Khalil, Development of a Vascular Optical Tomographic Imaging System for the Diagnosis and Monitoring of Peripheral Arterial Disease, search.proquest.com, 2014.
[33] E.R. Mohler, G. Lech, G.E. Supple, H. Wang, B. Chance, Impaired exercise-induced blood volume in type 2 diabetes with or without peripheral arterial disease measured by continuous-wave near-infrared spectroscopy., Diabetes Care. 29 (2006) 1856–1859.
[34] E.S. Papazoglou, M. Neidrauer, L. Zubkov, M.S. Weingarten, K. Pourrezaei, Noninvasive assessment of diabetic foot ulcers with diffuse photon density wave methodology: pilot human study., J Biomed Opt. 14 (2009) 064032.
[35] M.-L. Chen, B.-S. Lin, C.-W. Su, Y.-B. Lin, M.-Y. Chen, J.-H. Shen, et al., The application of wireless near infrared spectroscopy on detecting peripheral circulation in patients with diabetes foot ulcer when doing Buerger'sexercise., Lasers Surg Med. 49 (2017) 652–657.
[36] F. Manfredini, A.M. Malagoni, M. Felisatti, S. Mandini, F. Mascoli, R. Manfredini, et al., A dynamic objective evaluation of peripheral arterial disease by near-infrared spectroscopy., Eur J VascEndovasc Surg. 38 (2009) 441–448.
[37] K.K. McCully, L. Landsberg, M. Suarez, M. Hofmann, J.D. Posner, Identification of peripheral vascular disease in elderly subjects using optical spectroscopy., J Gerontol A BiolSci Med Sci. 52 B159-65. (1997)
[38] M. Volmer-Thole, R. Lobmann, Neuropathy and diabetic foot syndrome.,Int J Mol Sci. 17 (2016).
[39] S.C. Wu, V.R. Driver, J.S. Wrobel, D.G. Armstrong, Foot ulcers in the diabetic patient, prevention and treatment., Vasc Health Risk Manag. 3 (2007) 65–76.
[40] W.T. Cade, Diabetes-related microvascular and macrovascular diseases in the physical therapy setting.,PhysTher. 88 (2008) 1322–1335.
[41] D.E. Strandness, J.F. Eidt, Peripheral vascular disease.,Circulation. 102 (2000) IV46-51
[42] O.-H. Lin, J.-Y. Lai, H.-Y. Tsai, O.-H. Lin, J.-Y. Lai, H.-Y. Tsai, Preventing Diabetes Extremity Vascular Disease with Blood Oxygen Saturation Images, International Journal of Instrumentation Science. (n.d.).
[43] M. Vardi, A. Nini, Near-infrared spectroscopy for evaluation of peripheral vascular disease. A systematic review of literature.,Eur J VascEndovasc Surg. 35 (2008) 68–74.
[44] D.T. Ubbink, M. Jacobs, D.W. Slaaf, Can transcutaneous oximetry detect nutritive perfusion disturbances in patients with lower limb ischemia?, Microvascular Research. (1995).
[45] K.B. Hobizal, D.K. Wukich, Diabetic foot infections: current concept review.,Diabet Foot Ankle. 3 (2012).

ISBN 978-1-5386-4473-7
IEEE sponsored 4th International Conference on Biosignals, Images and Instrumentation, SSNCE, Chennai. ICBSII 2018 – 22nd-24thMar'18

Robustness of Single ended measurement to electrode errors in Electrical Impedance Tomography: An experimental study

Mukta Verma, Dr. D C Gharpure, Dr. V G Wagh

Abstract— **Detachment of electrodes is the most common problem in EIT while monitoring due to patient's movement or sweat etc. which results in significant image artifacts. Though several compensation strategies had been proposed to manage these errors, however it also degrades the quality of actual image especially if the target is closer to the electrodes. The degradation effect not only depends on the compensation strategy but also on the measurement methodology used. It has already been reported earlier that for the adjacent method (differential measurement) the actual images are not significantly affected if the target is at a distance greater than 15% of the diameter from the affected electrode. Recently single ended measurements with internal electrode have gained more popularity because of its greater sensitivity. This paper reports on the robustness of single ended measurement towards electrode errors. In vitro studies are carried out for single ended measurement(common ground method) and differential measurement(adjacent method) to find how the actual images are affected after compensating for electrode errors as the target moves closer to the affected electrode and as the number of failed electrodes increases. Adjacent electrodes are removed to have the maximum effect on the target as the target is placed closer to the affected electrodes.**

Different algorithms had been suggested earlier to detect these faulty electrodes in case of differential measurements. In this paper we have also discussed the applicability of current voltage reciprocity principle to automatically detect faulty electrodes in case of single ended measurement. Maximum number of adjacent and non-adjacent faulty electrodes that can be detected for both methods using the algorithm is reported. It is observed that for single ended measurement up to four adjacent faulty electrodes are detected however, in case of adjacent method only up to two faulty electrodes are detected. Bayesian imaging model, where electrode errors are fed as a priori large measurement noise on all measurements using affected electrode is used to account for the erroneous data. In case of single ended measurement there isn't any significant change in resolution and position error of the reconstructed image for 1 faulty electrode if the target is at a distance greater than or equal to 10% of the diameter from the electrodes. Also for single ended measurement the images are not significantly affected even for 3 adjacent faulty electrodes after compensation. Overall, results indicate that single ended measurement is more robust and gives better images than differential measurement after compensating for electrode errors.

*Research supported by UGC NET JRF Scheme.

Mukta Verma is with Department of Electronic Science, Savitribai Phule Pune University, Pune, India (e-mail: muktavrm@gmail.com).

Dr. D C Gharpure is a Professor in Department of Electronic Science, Savitribai Phule Pune University,Pune, India (e-mail: dcg@electronics.unipune.ac.in)

Dr. V G Wagh is with V N Naik College, Nashik, Pune,India, (email-vgwaghale@gmail.com)

I INTRODUCTION

Electrical Impedance Tomography is a non-invasive technique which produces images of the changes in conductivity within the body by injecting currents or voltages through the electrodes attached to the surface of the body[1]. It has many advantages over other imaging techniques like it is non-invasive, non-expensive, portable and has high temporal resolution. Due to its ill-posed nature, small measurement errors may affect the reconstruction significantly.

Measurement error due to electrode detachment is the most common problem in biomedical EIT applications which occurs due to patient's movement, sweat etc. [2]. This results in significant image artifacts. To avoid these artifacts, the electrode errors should be managed by detecting the detached electrodes and fixing them. To detect faulty electrodes, Adler[3] proposed an algorithm based on measuring the consistency of data. This method required large number of calculations, another method was proposed by Alzbeta and Adler [3] based on the principle of voltage current reciprocity. Principle of voltage current reciprocity states that data acquired with an excitation and measurement pair of electrodes is equivalent. Faulty electrodes can be detected as they will not follow the principal of reciprocity. So far reciprocity principal had been applied to different current injection patterns based on differential measurement to calculate reciprocity error for automatic detection of faulty electrodes, however its applicability to single ended measurement hasn't been explored yet[2,3].

The most common differential measurement methodologies used in EIT are : the adjacent method, the opposite method, the cross method and the trigonometric method. Out of these adjacent method is most popular because of its highest selectivity [4]. In EIT systems based on adjacent method, the sensitivity towards the center is very low. Recently single ended measurements with internal electrode have gained more popularity because of its greater sensitivity towards the center. Also placing an internal electrode increases the sensitivity towards the center thus yielding good quality images. In clinical applications internal electrode is placed in the esophagus to improve the sensitivity towards the center [6]. Single ended measurement is gaining popularity because of reasons discussed earlier and it becomes important to study its response to electrode errors. This paper reports on the robustness of single ended measurement towards electrode errors by :

(1) Finding the number of faulty electrodes that can be detected using the algorithm based on reciprocity principle for both single ended and differential method

(2) Comparing how the actual images are affected after completely detaching electrodes, without and with compensation(discussed later in the section) in case of both single ended and differential measurement

Normalized total reciprocity error (TREn) in terms of percentage was calculated for each electrode to automatically detect faulty electrodes as proposed by Adler[3]. Maximum number of faulty electrodes that can be detected in case of single ended and differential measurement is reported. Two scenarios are taken : one where adjacent electrodes are faulty and other with random faulty electrodes. These faulty electrodes can either be fixed while acquiring the data or these errors can be eliminated during reconstruction [2].Different compensation strategies had been proposed earlier to manage these errors like setting all the measurements related to faulty electrodes as zero during reconstruction and second method is based on Bayesian imaging model where electrode errors are fed as a priori large measurement noise on all measurements using affected electrode as proposed by Adler[2] It is reported that second method gives better images and works for targets kept at a distance greater than 15% diameter from the electrodes[2,3]. Any of the above methods are employed to manage the invalid data, however it also degrades the quality of reconstructed image especially if the target is closer to the affected electrode. The degradation effect not only depends on the compensation strategy but also on the current injection and measurement pattern.

This paper reports on how the reconstructed images for two different current injection methods are affected by removing the erroneous data as the number of faulty electrodes are increased. So far only current injection patterns based on pair-wise measurement methodology(differential measurement) are analyzed for this [2,3]. In this paper we have compared the degradation effect of removing erroneous electrode data on the actual images for adjacent(differential) and single ended measurement (with internal electrode at the center) as the target moves closer to the affected electrodes. Second method proposed by Adler based on Bayesian imaging model is used to compensate for electrode errors. Electrodes closer to the target contain maximum information about the target and hence if these electrodes fail, it degrades the quality of image considerably. For the worst-case scenario, maximum of three adjacent electrodes are removed and the reconstructed images for both the methods are analyzed after compensating for these electrode errors as the target moves closer to these affected electrodes. We have taken the scenario till 3 detached electrodes as more than 3 detached electrodes will result in large portion of invalid data which is also very unlikely situation in clinical applications while real time monitoring [3].We have also found the maximum number of adjacent faulty electrodes for which the methods give reasonably fair images after compensation at the shortest distance from the affected electrodes.

II Materials and Methods

A Measurement Protocols

Two different measurement protocols mentioned in the paper are: adjacent method(differential measurement), single ended measurement (will be called common ground method hereafter).Most EIT systems are based on adjacent method where adjacent pair of electrodes are used for current injection and voltages are measured between other remaining pairs[5]. Fig. 1(a) shows current density is highest near the electrodes and lowest towards the center for adjacent method and hence this method is less sensitive to anomalies towards center.

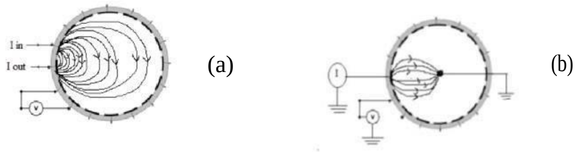

Fig. 1. (a) adjacent method (b) common ground method

It has been reported earlier that placing an internal electrode in the center improves the sensitivity of the EIT system towards the center[6].In common ground method(single ended measurement) the current is injected through one electrode with center electrode as ground reference and voltage is measured at each electrode with respect to the ground as shown in Fig. 1(b)[7].

B Hardware and Phantom Design

A vessel of diameter 20cm is taken and 16 stainless steel electrodes of 1.5cm each are attached to its inner surface. It is filled with the saline solution(electrolyte) of conductivity 0.06S/m and circular plastic cylinder of radius 1.0cm is introduced at different positions. Ratio of target to vessel radius is 0.1. Howland current source with grounded load is designed to inject constant current. Multiplexers are used to switch between the electrodes. Data is acquired using NimyDaQ whose sampling frequency was set at 200KS/s. The acquired data is further processed using instrumentation amplifier. For common ground method, a stainless steel rod of 1.5cm radius is placed in the center of the circular vessel which acts as a reference electrode. Fig 2 shows Phantom images for adjacent and common ground method as the target moves closer to the electrodes.

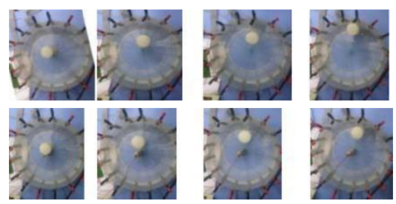

Figure2 Phantom images for adjacent and common ground method as the target moves closer to the boundary

C Research Approach :

1. Practical phantom experiments are carried out. Data is acquired using an EIT system by intentionally detaching the electrodes for both the methods.
2. Normalized total reciprocity error (TREn) is calculated to detect faulty electrodes
3. Maximum number of faulty electrodes that can be detected for both methods is reported.
4. These faulty electrodes data are eliminated during reconstruction based on Bayesian imaging model
5. Reconstructed images for both methods are then compared with and without compensation

D Methodology for detection of faulty electrode

Algorithm based on the principle of voltage-current reciprocity was used for detecting faulty electrodes as proposed by Adler[3]. Total Reciprocity error (TRE) for each electrode is calculated as :

= ([ ] − [ ]())^2 (1)

Where [ ] is the average of all the measurements on other electrodes when current is injected through electrode *i* and [ ]() is the average of all measurements taken on electrode

i when current is injected on other electrodes. All the measurements are normalized by the maximum value. TRE for each electrode is then normalized with its maximum value to obtain TRE_n in percentageas:

TREn(i) = (TRE(i)/maxTRE(i)) *100 (2)

For faulty electrodes TREn will be closer to 100% and for other electrodes it will be closer to zero.

E Compensation method:

For small changes in conductivity measured data can be linearized as [8]:

$$\mathbf{z = Hx + n}$$

Where z is the change in measurement, x is the change in conductivity, H is the sensitivity matrix which relates a small change in conductivity to a change in difference measurements and n is the random noise.
Using the maximum *a posteriori* (MAP) regularization the estimated conductivity change x^* is calculated as [9]:

* = (+)

R_n is the diagonal element which represents noise variance values. It is inverted to get which is equal to 1/ .

A completely detached electrode is modeled as infinite noise thus yielding equal to 1/∞which is zero [9].
Using this compensation methodology for any electrode errors, images are reconstructed.

III Results And Discussions

This section is divided into two parts: First parts deals with the detection of faulty electrodes for both the methods, and second part shows the effect of compensating electrode errors on the reconstructed images in case of both adjacent and common ground method.

A Detection of faulty electrodes:

In Vitro sudies are carried out using practical phantom. To detect faulty electrodes, initially EIT data is acquired without detaching any electrode. Normalized Total reciprocity error for each electrode is calculated as per equation (2) in case of both adjacent and common ground method when no electrode is faulty.Fig.3 shows plots showing correspondingTREn values for each electrode

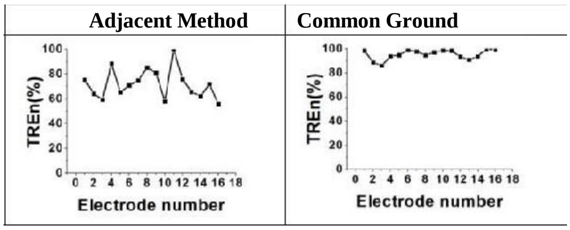

Figure 3. TREn plots for both methods when no electrode is faulty

When there is no faulty electrode, the reciprocity error for all electrodes are very small which gives similar TRE and hence normalized TREn for each electrode is in the range of60-100% in case of adjacent method and 80-100% in case of common ground method. Fauly Electrodes are realized by detaching them complelety from the system so that they are no longer in contact with the electrolyte.Two cases are analyzed : one where adjacent electrodes are detached and another by detaching randomelectrodes.
To detect faulty electrodes TREn values for each electrode is calculated for both methods in case of adjacent and non adjacent faulty electrodes.

Case1: Adjacent faulty electrodes
Fig.4 shows normalized TREn plots for both methodswhen adjacent electrodes are faulty.For common ground method when electrode 5 is faulty TREn value for 5th electrode is 100% whereas for all the other electrodes it is closer to zero. The plots show that TREn values for faulty electrodes are higher than 75% up to 3 faulty electrodes.In case of common ground method up to four faulty electrodes are detected accurately as shown in Fig 4(d). In case of 5 faulty electrodes

only three electrodes(4,5,6) are detected accurately with TREn values higher than 75% , the other two electrodes(7,8) shows TREn values closer to 40% which is also shown by electrodes 15 & 16. We can say that the algorithm based on reciprocity principle as proposed by Adler also holds good for single ended measurement. It detects up to 4 faulty electrodes with 100% accuracy.

In case of Adjacent method though up to two faulty electrodes are detected accurately, electrode 3 and 6 also shows higher TREn values. For three and more faulty electrodes, only one electrode is detected in case of adjacent method. The TREn plot for adjacent method in Fig 4(b) shows there are four faulty electrodes whereas only two electrodes are detached.

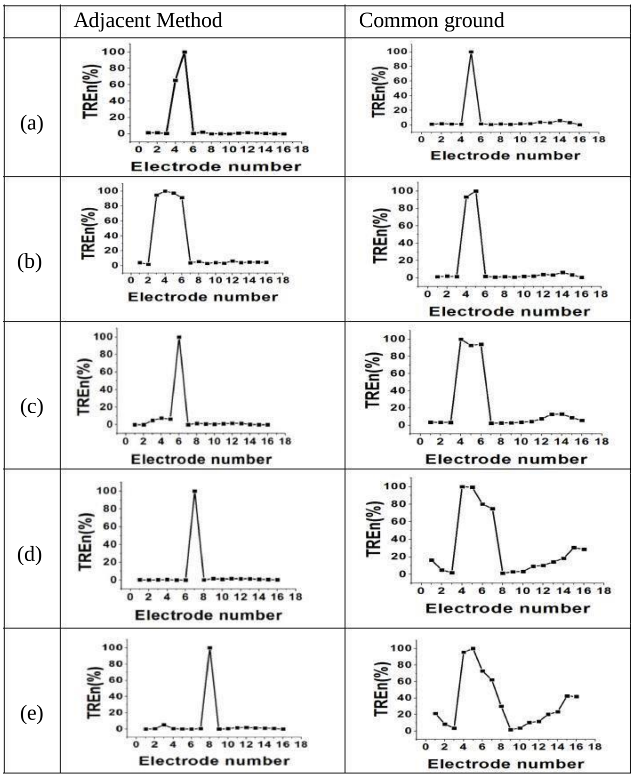

Figure 4. Normalized TREn when (a)electrode 5 is detached, (b) electrode 4,5 is detached , (c) electrode 4,5,6 are detached, (d)electrode 4,5,6,7 detached, (e)electrodes 4,5,6,7,8 detached

Case 2: Non-adjacent faulty electrodes

Fig. 5shows TREn plots for both methods when random electrodes are faulty. It shows that in adjacent method we can detect up to three non-adjacent faulty electrodes whereas in common ground method up to four random faulty electrodes can be detected.

Considering both the cases where adjacent and non adjacent electrodes are faulty it can be generalized that for adjacent method up to two faulty electrodes can be detected and for common ground method we can detect up to 4 faulty electrodes.

Overall, we can say that more number of faulty electrodes can be automatically detected in case of common ground method than in adjacent method making single ended measurement more robust to faulty electrode detection.

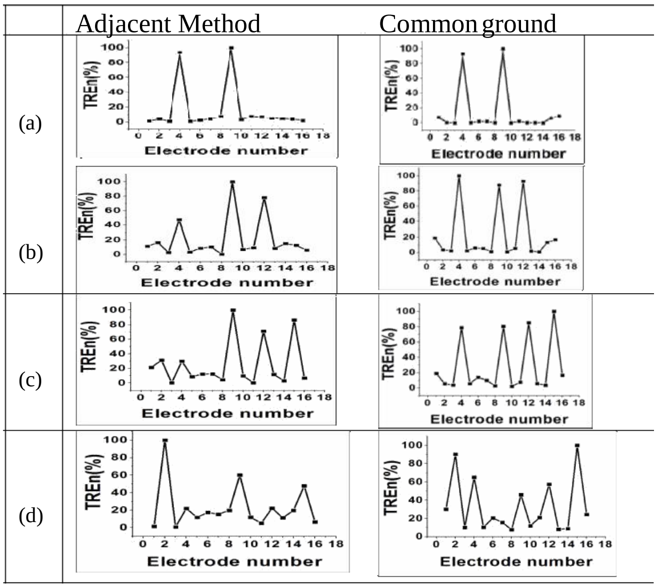

Figure5. Normalized total Reciprocity error (TREn) when: (a) electrode 4,9 detached, (b) electrode 4,9,12 , (c) electrodes 4,9,12,15 are detached, (d) electrode 4,9,12,15,2 are detached

B Effect of Compensation on reconstruction

After the faulty electrodes are detected, erroneous data corresponding to the faulty electrodes are replaced using Bayesian imaging model where electrode errors are modeled as a priori large measurement noise on all measurements using affected electrode. Due to this, the actual image also gets affected especially when the target is closer to the detached electrode. Effect of compensation on the reconstruction for both methods is analyzed using in vitro studies. To have maximum effect on the reconstruction especially when the target is closer to the affected electrodes, adjacent electrodes are detached. A non conducting cylindrical rod of radius 1cm is introduced at different positions and the data is acquired with and without detaching electrodes for both methods.

Position of the target is defined in terms of radial position(d') as the ratio of the distance of circular anomaly from the center to that of the radius of the circular vessel.

Experiments are carried out as follow:

First electrode number 5 is detached, target is keptdiametrically opposite to the affected electrode (d'=-0.8)and images are reconstructed as the target moves closer to the affected electrode(d' = -0.8,-0.7,-0.6,-0.5,-04,-0.3, -0.2,0.2, 0.3, 0.4, 0.5, 0.6, 0.7, 0.8). Then for each position erroneous data is compensated during reconstruction based

ISBN 978-1-5386-4473-7
IEEE sponsored 4th International Conference on Biosignals, Images and Instrumentation, SSNCE, Chennai. ICBSII 2018 – 22nd-24thMar'18

on Bayesian imaging model. The process is repeated for maximum of three electrodes (4 th, 5th and 6 th) detached as shown in Fig.6(1st column) for both the methods.

To compare the reconstructed images quantitatively parameters like *Resolution, Position Error* are calculated [8]. We have defined a new paramter, *Detectability limit (DL)* as the minimum distance from the faulty electrodes in terms of the diameter of the circular body surrounded by the electrodes for which the target is detectable after compensation with no significant change in the RES and PE.Fig.6shows the reconstructed images for both the methods with and without compensation for electrode errors.Target is kept at a position diametrically opposite to the affected electrode and images are reconstructed as it is gradually moved closer to the affected electrode.

First row for both Fig. 6(a) and (b) shows reconstruted images without any electrode errors.Fig. 6(a)shows the reconstructed images for common ground method . It is observed that for 1, 2 and 3 detached electrodes, target kept at radial positions from -0.8 to -0.2 is detectable with artefacts without even compensating for the electrode error (2nd row, 4 th row, 6th row). Reconstructed images after compensation for 1 failed electrode show good results even for the target kept closer (radial position = 0.8) to the affected electrode (3rd row).Reconstruction after compensating for 2 and 3 failed electrodes gives fairly acceptable images even for the target kept closer to the affected electrodes.

Fig 6(b)shows the reconstructed images for adjacent method. In this case target is not detectable at all without compensating for electrode errors even if the target is at a position diametrically opposite to the affected electrodes.

For 1 failed electrode after compensation, target isdetectable after compensation if it is kept at a radial position 0.8, but with artefacts and its shape is also deformed. For 2 failed electrodes target is detectable after compensation only if it is kept at a radial position less than 0.6.For 3 failed electrodes target gets detected only if itis kept towards the center or to the other sideof the central electrode as shown in the last row in Fig. 6(b).

To quantitatively compare the above reconstructed images parameters like *resolution, position error and Detectability limit* are calculated. Fig 7 shows the corresponding plots for both methods.

From Fig 7(a) it is observed that there isn't any significant change in the resolution for common ground method after compensating for 1 and 2 failed electrodes. For 3 failed electrodes resolution increases which is depicted by the spread out images as shown in Fig6(a) last row. There is no significant change in the position erroreven for 3 failed electrodes.

For adjacent method till 1 failed electrode there isn't much change in the resolution but for 2 and 3 failed electrodes RES drops to minimum as the target itself is not detected at all.PE goes maximum for 2 and 3 failed electrodes as the target moves closer to the affected electrode.

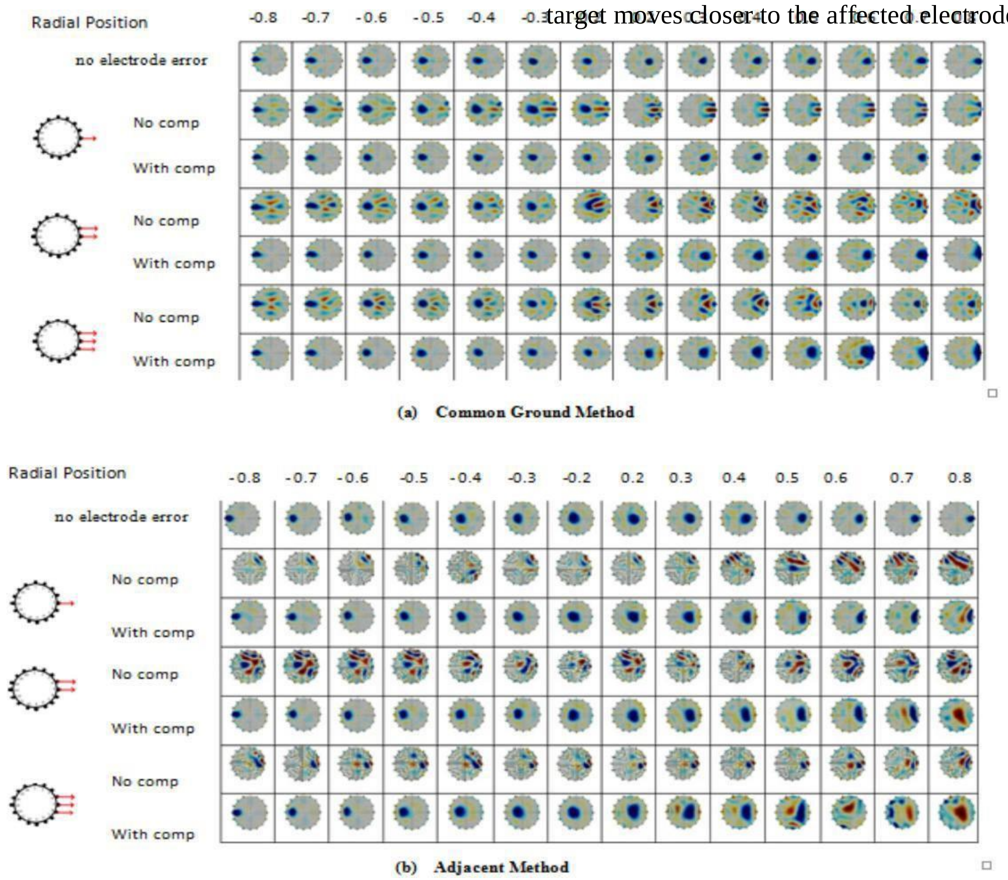

Figure 6. Reconstructed images for (a) common ground method, (b) Adjacent Method without and with compensation as the target moves closer to the affected electrodes for 1 , 2 and 3 adjacent faulty electrodes

ISBN 978-1-5386-4473-7
IEEE sponsored 4th International Conference on Biosignals, Images and Instrumentation, SSNCE, Chennai. ICBSII 2018 – 22nd-24thMar'18

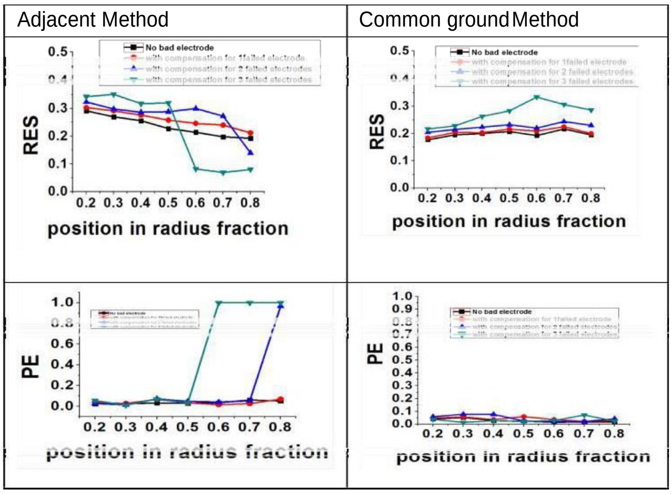

(a)

No. of faulty electrodes	Common ground detectability limit	Adjacent Method detectability limit
1	DL = 10% of the diameter	DL = 15% of the diameter (b)
2	DL = 15% of the diameter	DL = 25% of the diameter
3	DL = 20% of the diameter	DL = 40% of the diameter

(b)

No. of faulty electrodes	0	1	2	3
Common Grnd Max PE	0.06	0.07	0.08	0.08
Adjacent Max PE	0.06	0.07	1.0	1.0

(c) (c)

Figure . (a) RES, PE for both the methods with regard to number of failed electrodes as the target moves closer to the affected electrode/electrodes, (b) Table showing Detectability limit for both the methods after compensating for the faulty electrodes, (c) Table showing maximum PE for both the methods as the number of failed electrodes increases,

Table in Fig. 7(c) shows maximum PE for both the methods as the number of failed electrodes are increased. Common ground method shows maximum PE of 0.08 for 3 failed electrodes whereas adjacent method shows maximum PE of 1.0 for 2 and 3 failed electrodes.
The detectability limit for the two methods was observed to be as shown in Table in Fig. 7(b). The results clearly indicate that the detection limit for common ground method is better as compared to Adjacent method.

IV CONCLUSION

The gaining popularity of single ended measurement with internal electrode (common ground method) led us to study and anayze its response to electrode errors which is the most common problem in medical applications. Results indicate that common ground method is more robust in terms of automatic detection of faulty electrodes as we could detect up to 4 faulty electrodes whereas for adjacent method up to 2 faulty electrodes were detected and also gives better images than adjacent method after compensating for electrode errors. Upto 2 faultyelectrodes common ground method doesn't show any significant change in the resolution of the image if the target is kept at a distance greater than or equal to 10% of the diameter from the affected electrode. There isn't any significant change in the position error even for 3 faulty electrodes in case of single ended measurement. Detectability limit after compensation is calculated as the distance from the affected electrode in terms of diameter of the circular body. For 1,2 and 3 faulty electrodes detectability limit for the common ground method is 10%, 15% and 20% of the diameter as against 15%, 20%, 40% of the diameter for adjacent method.Overall we can conclude that single ended measurement (common ground method) is more robust towards the electrode errors.

VREFERENCES

[1] Barber, David C., and Brian H. Brown. "Electrical impedance tomography." U.S. Patent No. 5,626,146. 6 May 1997.
[2] Asfaw, Yednek, and Andy Adler. "Automatic detection of detached and erroneous electrodes in electrical impedance tomography." *Physiological measurement* 26.2 (2005): S175.
[3] Hartinger, Alzbeta E., et al. "Real-time management of faulty electrodes in electrical impedance tomography." *IEEE Transactions on Biomedical Engineering* 56.2 (2009): 369-377.
[4] Kauppinen, P., Hyttinen, J. and Malmivuo, J., 2006. Sensitivity distribution visualizations of impedance tomography measurement strategies. *International Journal of Bioelectromagnetism*, *8*(1), pp.1-9.
[5] Brown, Brian H., and Andrew D. Seagar. "The Sheffield data collection system." *Clinical Physics and Physiological Measurement* 8.4A (1987): 91
[6] Tehrani, J.N., Jin, C. and McEwan, A.L., 2012. Modelling of an oesophageal electrode for cardiac function tomography. *Computational and mathematical methods in medicine*, *2012*.
[7] Bera, T.K. and Nagaraju, J., 2012. Common ground method of current injection in electrical impedance tomography. In *Global Trends in Information Systems and Software Applications* (pp. 574-587). Springer, Berlin, Heidelberg.
[8] Yasin, M., Böhm, S., Gaggero, P.O. and Adler, A., 2011. Evaluation of EIT system performance. *Physiological measurement*, *32*(7), p.851.

ISBN 978-1-5386-4473-7
IEEE sponsored 4th International Conference on Biosignals, Images and Instrumentation, SSNCE, Chennai. ICBSII 2018 – 22nd-24thMar'18

TREMOMARKER

Tremor detection for diagnosis in a non-clinical approach using IoT

[1]Vijay Anand K [2]Sangeetha K [3]Shibani Akshara A [4]Pranitha M
[1]kva.eie@rmkec.ac.in [2]sang15215.ei@rmkec.ac.in [3]shib15216.ei@rmkec.ac.in [4]pran15209.ei@rmkec.ac.in
Department of Electronics and Instrumentation Engineering
RMK Engineering College
Chennai, India

***Abstract*—Tremomarker is a wearable, hand tremor quantification device and it is made up of accelerometer and gyroscope used for the detection of tremor. For many neurological diseases tremor is marked as a major symptom, by knowing its intensity, different types of diseases can be identified and treated correspondingly. Parkinson's disease is taken for case study because its pathological tremor is one of the major visible symptom and by knowing its intensity, other diseases can also be treated. The data of the detected tremor is transferred to the diagnosis system using IoT gateway, from which the intensity and severity of the disease is determined. The device is small, light weight, easily portable and low cost. Because of the above features it is easily accessible and user friendly to all category of people.**

Keywords— hand tremor motion, intensity, Parkinson's disease, approach, observance, applications

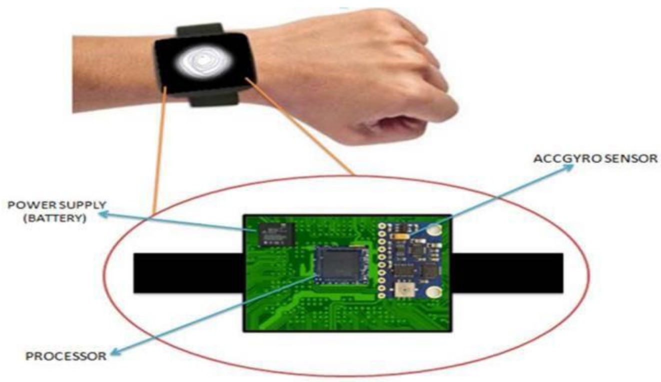

Figure1.1 Prototype Model

I. Introduction

Tremor exists in humans both physiologically and pathologically. While physiological tremor is a normal tremor observed in the body that helps to maintain tone and steadiness of the extremities to perform complex tasks, pathological tremors are the most commonly observed neurological illness. Assessment of tremor can be based on clinical or biomechanical evaluations. Clinical evaluation involves the use of clinical tremor rating scales for ranking the severity of the observed tremor after performing specific actions. There is no such device for the identification of bio marker in a non-clinical approach. In this proposed paper, the amount of hardware used for the construction of device(Fig 1.1) is reduced which makes it less complex and can be easily accessed by all people.

A tremor involves shuddering movements of body parts. It is an involuntary action due to muscle contraction and relaxation. One of the symptoms for neurological diseases is tremor(Fig 1.2)such as multiple sclerosis, stroke, traumatic brain injury, chronic kidney disease and a number of neurodegenerative diseases. These diseases damages or destroys the certain parts of the brainstem or the cerebellum. Here pParkinson's disease is taken as case study.

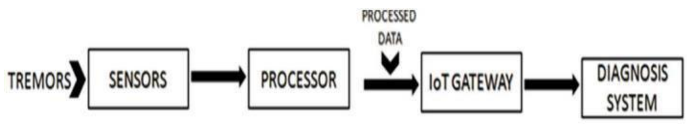

Figure 1.2 Block diagram

II. Case Study

A. *Parkinson's disease*

Parkinson's disease is a deteriorating, neurological sickness which usually occurs in later, rarely affects people of age 30. Pathologically, Parkinson's is characterized by the deterioration of the nuclear masses in the extra pyramidal system. Parkinson's disease is by no means the only source of pathological tremor, but it is a major one.

B. Diagnosis

Occurrence of tremor is determined by the doctors through a physical examination.The doctor checks for the symmetry, sensory losses, muscle weakening or atrophy of the patient. The tremor caused due to drug interaction or chronic alcoholism can be determined from blood and urine tests taken for the detection of thyroid malfunctioning and abnormal levels of chemicals causing tremor. Neurological examinations are conducted for the assessment of nerve function and

ISBN 978-1-5386-4473-7

sensory skills and the functional limitations are determined. For example inability to write and hold things.The electromyogram is used for the diagnosis of muscle or nerve problems and measures the stimulation of nerves along with the involuntary muscle activity.

C. Symptoms

The symptoms(Fig 2.1) and stages of Parkinson's diseases(PD) are,

i. EARLY PD: The patient suffers from tremor in one hand, rigidity in muscles and abnormalities in speech. He may experience decrease in blinking rate and one side of the face may be affected impacting the expressions. As it results in loss of facial expressions.

ii. MID PD: Inability to make rapid, automatic and involuntary movements, thus balance is compromised. The patient is unable to walk and stand unassisted. Therefore the affected person is unable to lead an independent life without assistance.

iii. ADVANCED PD: Patients fall when standing or turning. The patient undergoes hallucinations or illusions. All other symptoms of PD are present.

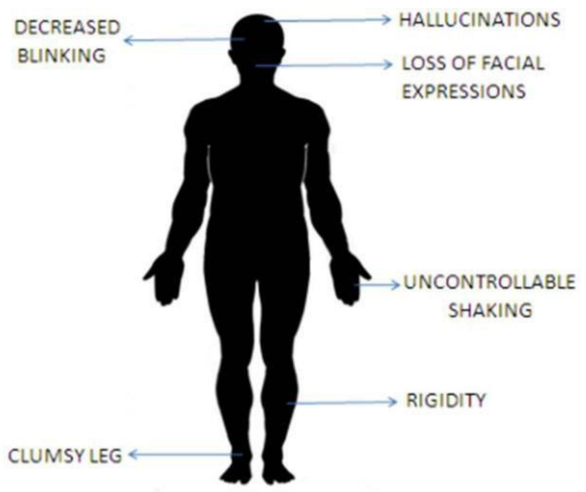

Figure 2.1 Symptoms of PD disease

The symptoms also include 4 types of tremors,

- Resting tremor (4-7 Hz)
- Postural tremor (6- 8 Hz)
- Intention tremor (2- 5 Hz)
- Cogwheel tremor (4-9 Hz)

D. Treatment

The treatment of tremor depends on accurate diagnosis of the cause as there is no proper cure for most tremor. Either by using certain medications the symptoms can be relieved temporarily or L-DOPA drug treatment is used which may be dangerous as it involves drugs like bromocriptine , ropinirole and pergolide that results in other symptoms such as akathisia ,tardive dyskinesia,clonus and in case of tardive psychosis. In some cases, amantadine and anticholinergic drugs like benztropine are used to lessen parkinsonian tremor.

III. TREMOMARKER

Tremomarker is a wearable device designed for the measurement of tremors in a non-clinical method (Fig 1.1). Using this device intensity of the tremor is found with which severity of the neurological diseases is found and the efficacy of the treatment is improved. Here a hand tremor quantification device was designed as a diagnosis option for Parkinson's disease. Hand tremor is the visible symptom of Parkinson's disease.

A. Construction

Tremomarker consist of,

i. SENSORS: As shown in the figure 2.1 accelerometer works on the principle Newton's second law of motion (F = m * a) with which the linear movement in 3 axes is calculated. Gyroscope works on the principle of precession with which the angular movement in 3 axes is calculated.

ii. PROCESSOR: myRIO by National Instruments is used as a processor, which is interfaced with the IoT module. It consists of the Xilinx chip and the communication between the host and myRIO can be done either by using serial USB or by WIFI module.

iii. IoT MODULE: The sensors installed in the device are connected to the internet via the gateway. The sensors can be controlled through IoT using graphical programming done in LabVIEW. The processor and LabVIEW are interfaced.

iv. DIAGNOSIS SYSTEM: The required data collected is passed to the investigator through the diagnosis system which can either be an application or computer. From which the identification and concerned treatment is done.

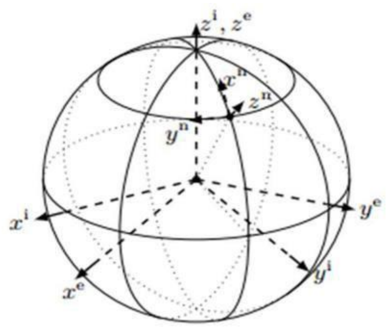

Figure 2.2 Illustration of angle of measurement

ISBN 978-1-5386-4473-7

B. Working principle

Primarily, the device collectively combines the action of two sensing elements namely, accelerometer and gyroscope. The orientations caused due to the tremor are detected by the sensor board and the output is given to the processor. myRIO acts as the processor, which categorizes the data received based on their frequency and the resultant is given to the receiver. Considering the case study (Parkinson's disease), the frequency must lie in the range of 4 Hz to 5 Hz or can also be in the range of 5.5 Hz to 7.5 Hz, the behavioral characteristics for the above range can either be at rest or can be postural/kinetic. The myRIO is interfaced with LabVIEW software ,where the corresponding graphical programming is done for the determination of the intensity of the tremor , for displaying the result that can be taken into consideration for the diagnosis of the disease.

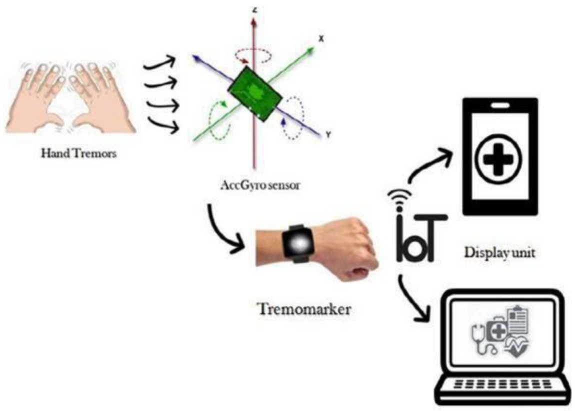

Figure 3.1 Process involved

C. Post processing

The main purpose of this approach is to provide an adequate and proper medical hardware for the diagnosis of various diseases in a non-clinical manner, tremor is considered as the main parameter for measurement (Fig3.1).By knowing the intensity of the tremor, physicians can easily diagnose the type of disease the patient is suffering from and the corresponding treatment can be provided at the earliest. Apart from Parkinson's syndrome, diseases such as hyperthyroidism, strokes, multiple sclerosis , chronic kidney failure and Huntington diseases can also be found based on the severity of the tremor.

FREQUENCY(Hz)	DISEASE PROCESS
2.5-3.5	•Cerebellar/Brainstem •Multiple sclerosis •Alcoholic degeneration •Post-Traumatic
4-5	•Parkinson's disease •Cerebellar disease •Rubral •Drug induced
5.5-7.5	•Essential tremor •Clonus •Parkinson's disease •Drug induced
8-12	•Enhanced-physiological tremor •Drug intoxications •Cerebrocortical

D. Equations

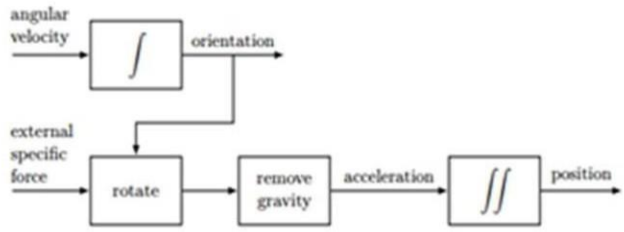

Figure 3.2 Schematic representation of accelerometer and gyroscopic measurement

Mathematical model of accelerometer

The force f_t^b for each instance at t is measured using accelerometer(2). Thus the accelerometer measurements are assumed to be biased $\delta_{a,t}$ and affected by noise $e_{a,t}$ (1),it is expressed by the following equation,

$$y_{a,t} = f_t^b + e_{a,t} + e^b_{a,t} \quad \textbf{(1)}$$

$$\text{Force, } f^b = R^{bn}(a^n_{ii} - g^n). \quad \textbf{(2)}$$

Hence the mathematical model is given by ,

$$y_{a,t} = R^{bn}_t (a^n_{nn} - g^n) + \delta^b_{a,t} + e^b_{a,t} \quad \textbf{(3)}$$

In order to determine the positional and inclination change accelerometer is used which measures the gravity vector and the linear acceleration..

The accelerometer measurements depends on the gravity vector, assume the linear acceleration to be zero, because for the orientation estimation, only the inclination is concerned.

$$y_{a,t} = -R^{bn}_t g^n + \delta^b_{a,t} + e^b_{a,t} \quad \textbf{(4)}$$

The model is never absolutely true but can be used for approximation of reality.

Mathematical model of gyroscope

The angular velocity ω^b_{ib} at t is measured using gyroscope.A slowly time-varying bias $\delta\omega,t$ and noise $e_{\omega,t.}$ affects the readings. The expression for measurement model is given by,

$$y_{\omega,t} = \omega^b_{ib,t} + \delta^b_{\omega,t} + e^b_{\omega,t.} \quad \textbf{(5)}$$

the three gyroscope axes are independent. The gyroscope bias $\delta^b_{\omega,t}$ is slowly time-varying. There are two conceptually different ways to treat this slowly time-varying bias where in first case the bias is treated as a constant parameter, as it typically changes over a longer time period than the time of the experiment. And the other way is to either pre-calibrate the bias or is considered as a unknown parameter θ alternatively, and is assumed to be slowly time-varying.

Further $\delta^b_{\omega,t}$ is considered as part of the state vector x_t and the model is given by,

$$\delta^b_{\omega,t+1} = \delta^b_{\omega,t} + e^b_{\delta\omega,t} \quad \textbf{(6)}$$

where $e^b_{\delta\omega,t} \sim N(0, \Sigma_{\delta\omega,t})$ is the representation of constant the gyroscope bias. Modeling the sensor noise and bias is related

ISBN 978-1-5386-4473-7

to the sensor properties and other choices can also be made relatively.

The angular velocity is defined as

$$\omega^{b}_{ib,t}=R^{bn}_{t}\,(\omega^{n}_{ie,t}+\omega^{n}_{en,t})+\omega^{b}_{nb,t} \quad \textbf{(7)}$$

Thus the simplified mathematical model is expressed as

$$y_{\omega,t} = \omega^{b}_{nb,t} + \delta^{b}_{\omega,t} + e^{b}_{\omega,t}. \quad \textbf{(8)}$$

E. Correlation with clinical study

The motion of the hand caused due to tremor is collected as data using the sensor are displayed in graphical form mentioned below. The dominant frequency for motion in each axis is estimated by the frequency component with the largest peak.

Figure 3.3 Graphical representation of a normal person

Figure 3.4 Graphical representation of patient with early stage of Parkinson's disease.

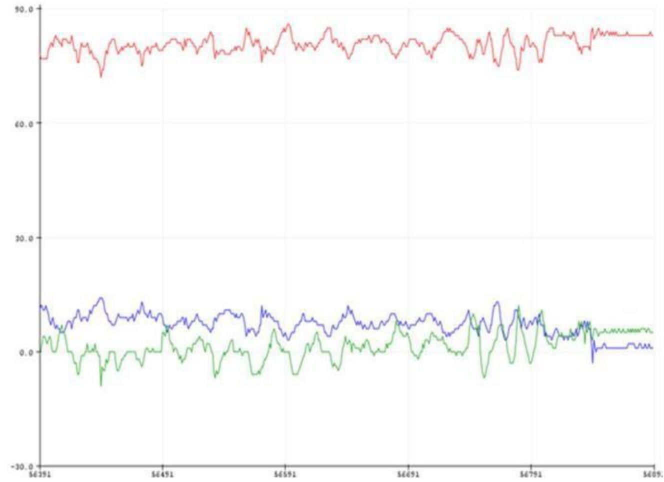

Figure 3.5 Graphical representation of patient with mid stage of Parkinson's disease

Figure 3.6 Graphical representation of patient with advanced stage of Parkinson's disease

The intensity ratings are given below in the tabulation,

INTENSITY RATING	STAGES OF PD
0	NORMAL
0-3	EARLY STAGE
3-6	MID STAGE
7-10	ADVANCED STAGE

Future development

In future, the proposed device is developed into a product constructed using ARM processor in which the gyroscope and accelerometer are inbuilt into the system, this makes the data acquisition easy and the transmission is made more efficient. For example, Person having tremors due to PD , after a range of intensity the device starts detecting and if the range goes beyond the specified limits, the device generates an alert signal along with which the data is transmitted using IoT gateway to the diagnosis system.

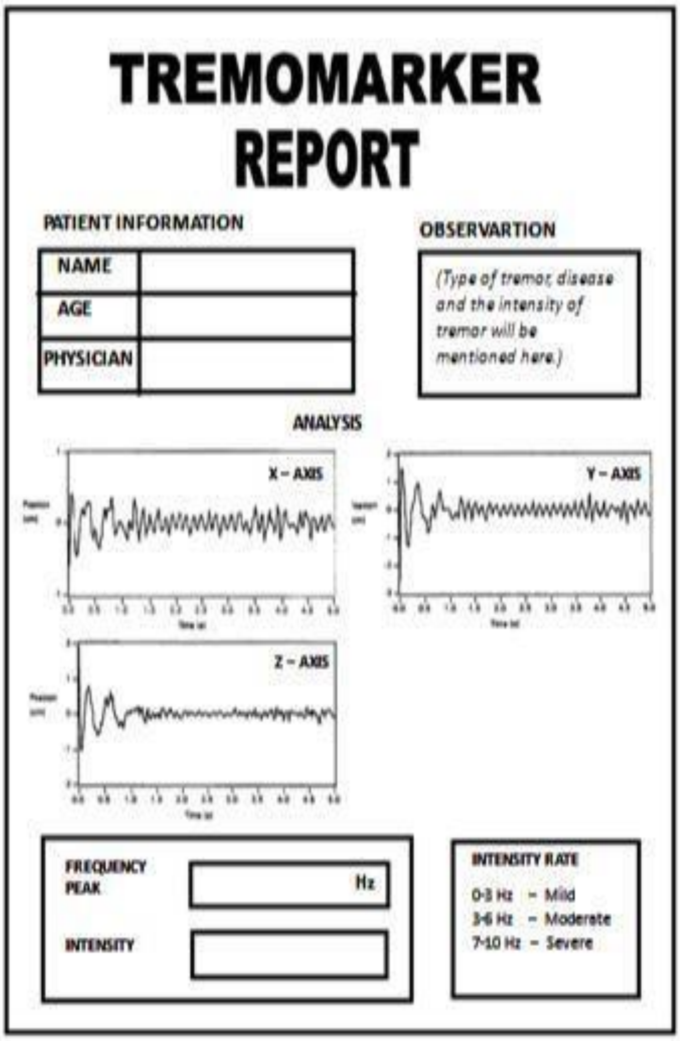

Figure 3.7 An illustration of the final report

F. Advantages

The proposed device is small, uses light-weight sensors, which makes portability easy. Minimal amount of hardware is used, because of which there is a reduction in the production cost making it readily available for people in both rural and urban areas. The sensors used are both environment friendly and non-radioactive in nature. The software used here is Lab View ,due to its drag and drop option it is easy to make changes in the software for customization and the result obtained is highly accurate. Thus, the device can determine all parameters with positional data information which makes the device more efficient.

G. Limitations

According to the changes in the external environment, the process of acquiring the data through sensors and the transmission through IoT gateway is delayed. Therefore, there is variation in the efficiency. As the device is constructed using MEMS device, well trained person can only design the circuit with high precision and so there is a difficulty in circuit layout. Fabrication of circuit elements becomes complex because we need to incorporate all the circuit elements on to a single chip.

IV. CONCLUSION

The targeted area of implementation is for people in remote and suburban areas where adequate medical facilities is not readily available, in such cases the Tremomarker can be used as a non-clinical approach for improvising the efficacy of both the diagnosis and treatment of the disease that is been identified based on the severity of the tremor levels. Since IMU devices are used the sensor errors are minimized and the cost is reduced so that the design is less complex and can be easily worn on the person's wrist with which the tremor levels are recorded, stored and the corresponding treatment is carried out on account to the beneficiary of the person's health.

REFERENCES

[1] "Development of a hand tremor quantification device for the measurement of a pathological tremor",Sonja Markez.
[2] "An In-Laboratory validity and realabilty tested sytem for quantifying hand on tremor in motions",Ping Yi Chan,Zaidi Mohd Ripin,Gaik Bee Eow,Linda Then,Ahmad Shukiri Yahya,Mustapha Muzaimi.
[3] "Using Inertial sensors for position and orientation estimation",Manon Kok ,Jeroen D Hol,Thomas B Schon.
[4] "A system for measuring tremor intensity in rats",Markku S.Lehtinen,Patrick R.Gothoni.
[5] "Essential tremor measuringdevice",Kailash Bohra,Ingrid Menegazzo, Jonathan Cayce,Eric DuBois.
[6] Deuschi G, Krack P, "Tremor: Differential Diagnosis, Neurophysiology, and Pharmacology." Parkinson's Disease and Movement Disorders.
[7] Cohen O, Pullman S, Jurewicz E, Watner D, Louis E.D, "Rest Tremor in Patients with Essential Tremor." Arch Neurol 2003, 60: 405-410.
[8] Ghika J,Wiegner A.W,Fang J.J,Davies L,Young R.R,Growdon,"Portable system for quantifying motor abnormalities in Parkinson 's disease".

IEEE Transactions on Biomedical Engineering Volume 40, No. 3, Mar.1993:276-283

[9] McAlister H.G , McCullagh P.J , Kelly, Quantification of body tremor. IEEE Engineering in Medicine & Biology Society – in Annual International Conference Volume 6.1985 .

[10] J. Jankovic, "Parkinson's disease: Clinical features and diagnosis," J. Neurol., Neurosurg. Psychiatry, vol. 79, no. 4, pp. 368–376, 2008.

[11] J. Volkmann, E. Moro, and R. Pahwa, "Basic algorithms for the programming of deep brain stimulation in Parkinson's disease," Movement Disorders, volume 21, no. S14, pp. S284–S289, Jun. 2006

[12] M. Hallett, "Tremor: Pathophysiology," Parkinsonism Rel. Disorders, volume 20, pp. S118–S122, Jan. 2014.

[13] N. D. Darnall, "Detecting dyskinesia and tremor in people with Parkinson's disease or essential tremor during activities of daily living using body worn accelerometers and machine learning algorithms," .

[14] H. Dai, P. Zhang, and T. C. Lueth, "Quantitative assessment of parkinsonian tremor based on an inertial measurement unit," Sensors, volume15,no.10,pp.25055–25071,2015.

Wireless Emergency Patient Monitoring System

Shweta Yadav[1], Tanvi V. Pulekar[2]
[1,2]Department of Electrical Engineering
VJTI, Mumbai, India-400019
[1]yadavshweta666@gmail.com
[2]tanvipulekar@gmail.com

A.N.Cheeran
Department of Electrical Engineering
VJTI, Mumbai, India-400019
ancheeran@vjti.org.in

Vaibhav D. Awandekar
A3 RMT Pvt. Ltd.
Vikhroli, Mumbai, India-400079
vaibhav.awandekar@gmail.com

Abstract*— A real time system is proposed in which an Android application is developed to monitor the patient's vital signs like SpO2, ECG, NIBP, Heart Rate, Temperature and Respiration Rate and send them to the doctor wirelessly. The patient monitoring device is interfaced with the application via Bluetooth Low Energy. The parameters are acquired, processed and displayed in the application and then sent to the server in real time using high level of compression and advanced file transfer protocol. SQLite database is maintained in the phone to store multiple patients' information. The doctor can access the data remotely. In case of abnormal values a notification pops up in the application. Also, the doctor and relatives can be notified via Email and SMS in emergency situations. The tested results showed that there is only a few seconds delay between data acquisition and their upload over the server.

***Keywords*— Android application; Bluetooth Low Energy; advanced file transfer protocol; SQLite database**

I. INTRODUCTION

Currently the focus of health policy has moved away from the provision of reactive acute care, towards preventive care outside hospital [1]. Technology plays a very significant role in health monitoring nowadays. Patient's quality of life is improved by remote monitoring at reduced cost. Wearable sensors like peripheral capillary oxygen saturation (SpO2) sensor, Heart rate monitor and Blood Pressure monitor with wireless communication allow immediate data transfer and significantly increased patient's comfort during measurements. Remote communication is crucial in telemedicine. It provides health care assistance of individuals remotely by means of telecommunication [2]. The reconciliation of wearable sensors with mobile communications has simplified the shift of healthcare services from clinic-centric to patient-centric and is named as "Telemedicine" [3]. It is advantageous for people living in remote regions. Telemedicine is one of the most developing technological applications applied to medical field because of its cost reduction and full monitoring capability [4] [5]. There are a few weaknesses present in existing systems for patient monitoring. The patient is examined in Intensive Care Unit (ICU) and the information exchanged to the Personal Computer (PC) is wired. Such systems get challenging when the system and PC is placed at larger distance from each other. The accessible systems are bulky and costly. Customary examining of patients is unrealistic once he/she is away from doctor's facilities. These systems cannot be utilized at individual level. The other issue is that it is not fit for transmitting information continuously.

A Context Aware quick subordinate healthcare architecture is utilized and remote live checking of a patient is given by healthcare professionals [6]. To monitor SpO2, Electrocardiograph (ECG) and blood pressure wireless Body Area Network sensors are used. At the point when patients are stuck in an unfortunate situation, Global System for Mobile Communication (GSM) and Global Positioning System (GPS) based framework is utilized to find them and alert is activated. The alarm message is received by the doctor or their family and action can be taken immediately [7]. Remote patient monitoring is another common practice of telemedicine that has generated a lot of curiosity in the networking community [8]. It enables an improved quality of life for the patient by permitting remote measurements and hence decreases routine trips to the clinic [9]. It assures further advances by providing patient mobility, continuous monitoring and improving patient compliance with frequent and better quality estimations. Bluetooth Low Energy (BLE) based system is ideal for battery-driven medical devices compared to low-cost Bluetooth modules as it consumes low power [10]. A prototype of physiological parameter monitoring system based on Arduino and Raspberry Pi (Rpi) is implemented [11]. The various vital parameters are measured and processed in Arduino and sent to Rpi based web server for displaying. Zigbee is used for communication between Arduino and Rpi. The updated parameters can be viewed from anywhere using an internet enabled device. Wireless ECG monitoring system based on BLE technology transmits the ECG data to a smartphone for further processing and graphical representation. The proposed system can function for a longer period of time due to BLE [12].

Section 2 introduces the hardware and software of patient monitoring system. The results are shown in section 3. Finally, section 4 concludes the entire work.

II. PATIENT MONITORING SYSTEM

In this section, the block diagram of the proposed system along with its hardware and software specifications is described. Also, the parameters considered for measurement are briefly explained.

A. Block Diagram

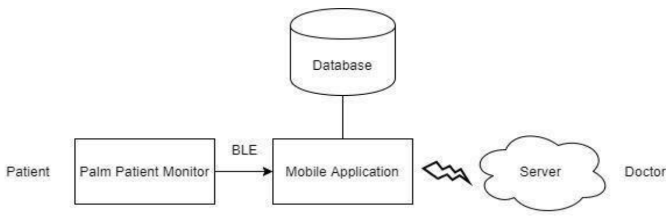

Fig. 1. Proposed System Block diagram

Fig. 1 shows the block diagram of the wireless patient monitoring system. The system comprises of three steps namely PM6100 Palm Patient Monitoring, Android application and a web interface for doctors. In the first step, light weight and compact wearable sensing devices (PM6100) for measuring six vital signs are connected to the patient's body which continuously reads the parameters. Android smartphone extracts patient readings from sensors in the second step. The sensors transmit real time data to the mobile application that is integrated with the device through BLE. The data are displayed on the Android application of patient's phone and transmitted to the doctor via server. The readings are stored in SQLite database of the phone. Android smartphone communicates with the server via 3G, Wi-Fi, General Packet Radio Service (GPRS) or other networks. In the third step, the patient information and his medical history stored on the server can be retrieved anytime and anywhere by the doctor. This information is used to create reports, abnormality detection, notification or alarm generation for doctors and patients if necessary. The following sub-sections details the hardware and software involved.

B. Hardware

Fig. 2. Palm Patient Monitor [13]

PM6100 Palm Patient Monitor can be used for waveform monitoring and parameter measurement. It is an easy-to-use system due to its One-Button-Design and can be associated with the smart terminals such as Android phones, IPhone and PC. The monitor is compact in size, portable and lightweight and hence is easy-to-carry. It has a built-in battery and it allows measuring body temperature, SpO2, ECG, Heart Rate, Pulse Rate and Non Invasive Blood Pressure (NIBP).

C. Software

The software specifications include the following:

1) Android Studio: Android Studio Integrated Development Environment (IDE) has been used for developing the application. It is the official IDE for Google's Android Operating System (OS). It is now the prime IDE for Android application development thus replacing Eclipse Android Development Tools (ADT). It is specifically designed for Android development and is available for download on macOS, Windows and Linux based OS.

2) Bluetooth Low Energy: The high power consumption of classic Bluetooth makes the technology inappropriate for continuous medical monitoring applications. However, this problem is overcome by BLE, a lower power consumption form of Bluetooth technology. It consumes only 10% of the power of classic Bluetooth. BLE also operates in the 2.4 GHz band and features a bandwidth of 1 Mbps (four times that of ZigBee) with a range of 15 to 30 m. Generic attribute profile (GATT) is a general description for transfer of short pieces of data known as attributes over a low energy link; this forms the basis for all low energy application profiles.

3) Database: SQLite is an open source Structured Query Language (SQL) database implementation available in Android that supports all the relational database features.

4) File Transfer Protocol (FTP): It is a standard network protocol used for exchanging files from one host to another over a Transmission Control Protocol (TCP) based network such as web. It is client-server architecture and uses separate data and control connections. FTP users may authenticate themselves using a sign-in protocol.

D. Vital Parameters

Following vital parameters are considered in this work.

1) Heart Rate: Heart rate is based on the number of contractions of the ventricles and gives the number of heart beats per minute.

2) Respiration rate: It is the number of breaths per minute. In practice, it is usually determined by counting the number of times the chest falls or rises per minute.

3) Electrocardiography: It is the process of recording the electrical activity of the heart using electrodes placed on the skin over a period of time.

4) SpO2: It gives a gauge of the measure of oxygen in the blood i.e. oxygenated hemoglobin.

ISBN 978-1-5386-4473-7

5) NIBP: It's a feature common in a lot of patient monitors in the hospital where the patient's blood pressure can be checked either by a cuff on the arm, or the leg. It is unique in relation to the regular blood pressure where the cuff is pumped up by a small bulb. This is done by electric driven motor which pumps up the cuff, and then deflates it.

Fig. 3 shows the flow of the proposed system. When the application is started for the first time, basic information like patient's name, age, gender, height, weight and doctor's name is to be filled. There is also a provision to mention comments regarding patient's medical history and capture multiple photos. If any specific information is to be conveyed it can be written in the comment section. The application is continuously linked to the database and hence while entering names, suggestions are provided. Once the details are entered, the mobile's Bluetooth is automatically turned on. On pressing the connect button, the phone search for nearby device for 12 seconds duration. If device is found the parameters are acquired, processed and displayed. The sampling frequency of SpO2, Temperature, Heart Rate and Respiration Rate is 1 sample/sec while for NIBP it is 2 samples/sec. The device doesn't provide the parameter values directly. The incoming data are available in packages of hexadecimal bytes that are specific for each sensor. It is then formatted using Palm Monitor Communication protocol and values of each sensor are extracted. Bidirectional communication is possible between the device and the application wherein the user can enable or disable any specific sensor. The user can also start the cuff from application itself for NIBP measurement.

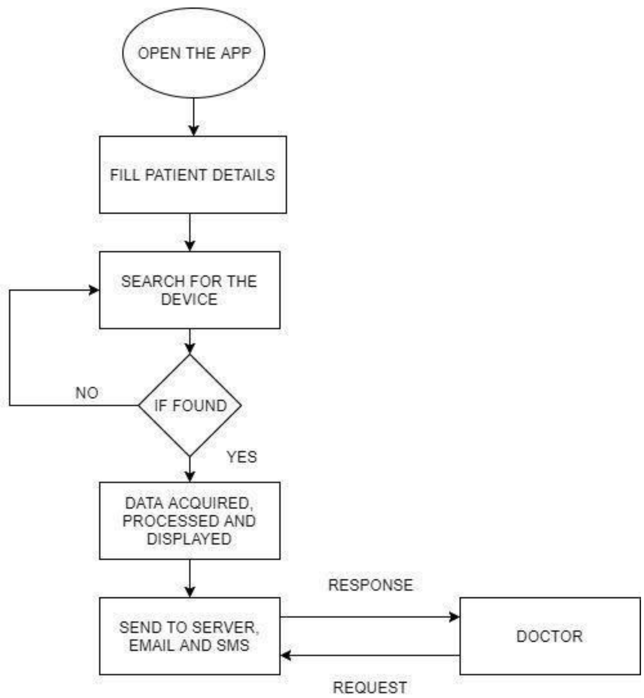

Fig. 3. System Flowchart

The ECG signal obtained at a sampling frequency of 250 samples/sec is contaminated with different kinds of noise like power line interference, false signals from nearby electrodes and electromagnetic noise that results in baseline wander and motion artifacts. The noises are removed using different digital filtering algorithms embedded in mobile application. High pass filter is used to remove the baseline wander whereas low pass and Savitzky Golay filters are used to remove the motion artifacts. Pan Tompkins algorithm is used for detection of QRS complexes of ECG signal. The QRS complexes have frequency of 5-15 Hertz. Thus a digital Band pass filter is applied to extract them from ECG signal. The filtered signal is then differentiated to get slope information. The differentiated signal is squared and appropriate threshold is used for finding the R peaks. Once the R peaks are detected, other peaks are obtained with reference to each R peak by using a windowing technique. The various diagnostic parameters like R amplitude, PR interval, QRS complex etc. are then extracted.

Every reading is stored in the database which is maintained in the phone memory and is not directly accessible to the user. Database serves two purposes; firstly it helps in maintaining patient history in the application and secondly it helps in generating patient records which can be directly emailed or can be sent through SMS in case of emergency. While sending the record on the server, the file and images is first compressed, zipped and is sent using FTP that is a standard protocol for file transfer. The application is designed in such a way that if internet connection is lost, the files will be queued in the outbox folder and will be send and shifted to sent folder once link is established. Every process runs in background so that users' time is utilized efficiently and need not wait every time for the process to get completed.

Standard files are generated when every patient takes the readings. The server-side is coded in such a way that it reads these files and automatically updates the server database. For making the proposed system more efficient, sending graphs and reports to the server is avoided because transmitting images takes lots of bandwidth. Hence only readings are sent from the client side and the reports are generated on the server side. Timestamp is included in every record to avoid ambiguity. The patient can also generate trend reports available in tabular as well as graphical format. This can be helpful for early detection of any trend in parameters.

III. RESULTS AND DISCUSSION

The designed application's user interface is presented in this section. Fig. 4(a) shows the snapshot of screen where the basic details of patient need to be entered for the first time. The camera icon allows the patient to capture multiple pictures which are useful for electronic medical records. The Portable Document Format (PDF) icon generates the patient care form which has details of past medical history and it is similar to Patient Admission Form filled prior to patients' admission to the hospital.

The next button redirects the user to the screen shown in Fig. 4(b). Here the Palm Monitor device is connected with mobile application via BLE and the readings are displayed.

There is a delay of approximately 2 seconds between searching for device and display of reading on the application. Blinking text alerts and beep sound is generated if the readings are out of normal range. Also the patient can send the readings to the doctor i.e. the files will be sent to the server via FTP which can be accessed by the doctor via his login credentials. Also in case of emergency the patient can either email or message the doctor. The patient can email and SMS the report to any other doctor for further diagnosis.

The patient can view the trend in his readings in a tabular or graphical format as shown in Fig. 5(a). For trend analysis, the sensor values are stored for a particular user and for a particular session in a SQLite database at an interval of 5 seconds. A same timeline is maintained for all the sensor values. Trend analysis is useful in early detection of deterioration of health, thus decreasing the number of emergency visits to hospital.

ECG signal holds important physiological information. Since raw ECG signal is contaminated with noise, it is first processed using digital filters. After preprocessing, QRS complexes are obtained using Pan-Tompkins algorithm. P and T peaks are detected using windowing technique with reference to R peak. The parameters like QRS interval, PR interval, QT interval, R peak amplitude are averaged over an interval of 10 seconds. The different peaks obtained are highlighted with different colors as shown in Fig. 5(b). To ensure that the app does not crash, various cases of error are handled. The application prompts the user in case of any exception. For example, during NIBP measurement if the cuff is unattached or is loose, the application displays relevant message on the screen. This is one of the cases of error handling.

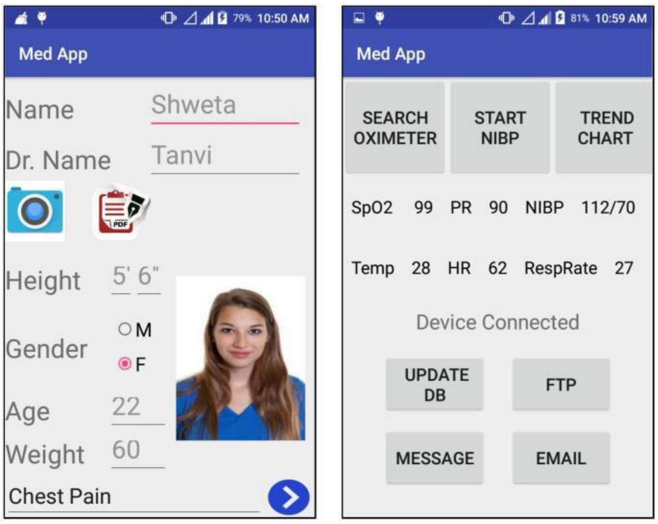

(a) (b)

Fig. 4. Android Application Screenshots

(a) (b)

Fig. 5. Trend Analysis and ECG

IV. CONCLUSION

A serious concern nowadays is rapidly growing rate of prolonged diseases due to very high cost and shortage of sufficient amenities. The situation worsens for the people located in unreachable areas. Our study and assessment clearly exhibits that currently available systems for monitoring physiological signals suffer from technical confinements. The proposed system offers low complexity, high power efficiency and is highly portable for health care monitoring. Our innovative approach brings down the cost required for monitoring patients and increases the efficient exploitation of physiological data. Accordingly, patients will approach the most astounding quality therapeutic care in their own home, and in this way keep away from the pain and interruption caused by an extensive inpatient stay.

ACKNOWLEDGMENT

The authors would like to express their gratitude to all those people whose support and cooperation has been an invaluable asset during the work. The authors would also like to thank all the teaching and non-teaching staff members of the Electrical Engineering Department, VJTI, Mumbai, India and the team of A3 RMT Pvt. Ltd., Vikhroli, Mumbai, India for their support and motivation.

REFERENCES

[1] Ettelt, Stefanie, Ellen Nolte, Nicholas Mays, Sarah Thomson, Martin McKee, and World Health Organization. "Health Care Outside Hospital: Accessing generalist and specialist care in eight countries." (2006).

[2] Cerny, M. and Penhaker, M., “Wireless body sensor network in Health Maintenance systems”, ElektronikairElektrotechnika, (9), pp. 113-116, 2011.

[3] Kakria, Priyanka, N. K. Tripathi, and Peerapong Kitipawang."A real-time health monitoring system for remote cardiac patients using smartphone and wearable sensors." International journal of telemedicine and applications 2015 (2015): 8.

[4] V. Garshnek and F. J. Burkle, "Telemedicine applied to disaster medicine and humanitarian response: history and future," in 32nd Annual International Conference on Systems Sciences, Hawaii, 1999

[5] A. Martinez, V. Villarroel, J. Seoane and F. Pozo, "Rural telemedicine for primary healthcare in developing countries," IEEE Technology and Society Magazine, vol. 23, no. 2, pp. 13-22, 2004.

[6] Bingchuan Yuan and John Herbert "Web based real time remote monitoring for pervasive healthcare" IEEE International Conference on Pervasive Computing and Communications Workshops, pp. 625-629, march 2011.

[7] Yuanyuan Du,YuChen,DanWang,Jinzhao Liu and Yongqiang "An Android based emergency alarm and healthcare management system" IT in Medicine and Education (ITME), vo1.1, pp. 375-379, Dec.2011.

[8] E. Jovanov,"Wireless Technology and System Integration in Body Area Networks for m-Health Applications," IEEE Engineering in Medicine and Biology 27th Annual Conference, 2005.

[9] Atack, L., and D. Duff. "East York Telehome care Project-Final Report." 2009 年 11 (2004).

[10] Babusiak, Branko, and Stefan Borik. "Low energy wireless communication for medical devices." In Telecommunications and Signal Processing (TSP), 2015 38th International Conference on, pp. 444-447. IEEE, 2015.

[11] Sunehra, Dhiraj, and Pini Ramakrishna. "Web based patient health monitoring system using Raspberry Pi." In Contemporary Computing and Informatics (IC3I), 2016 2nd International Conference on, pp. 568-574. IEEE, 2016.

[12] Bin Yu ; LishengXu ; Yongxu Li(2012) "Bluetooth Low Energy (BLE) based mobile electrocardiogram monitoring system", In the proceedings of International Conference on Information and Automation, June 6-8, 2012, Shenyang, pp. 763-767

[13] http://www.shberrymed.com/patient-monitor-pm6100-p00020p1.html last accessed on 19th January,2018

Designing an Intelligent Elderly Behavior Detection System

Erlito M. Albina, Alexander A. Hernandez, *College of Information Technology Education, Technological Institute of the Philippines, Manila, Philippines*

***Abstract*— This is a research-in-progress of developing an intelligent system of elderly abnormal behavior detection with real-time notifications on a mobile platform. This study involves surveillance of elderly participants in the Philippines using image processing and machine learning to detect abnormal behavior. A real-time mobile notification of abnormal behavior is provided for the elderly's immediate family members and emergency care personnel. The initial testing for abnormal detection achieved an average of ninety percent. Thus, this study contributes to the need for elderly care information systems.**

Keywords – elderly, machine learning, artificial intelligence processing, pattern detection, image processing, MHoEI algorithm

I. INTRODUCTION

There is a growing awareness of the necessity to proactively respond to the aging population worldwide due to changing the lifestyle of individuals and families, demand for productivity at work, and culture. The challenge of responding to the aging population issues has changed many aspects of elderly care at home, more specifically, actively monitoring the elderly while family members are away from home. Thus, this global phenomenon poses the need for Information Technology (IT) as a significant contributor to active elderly monitoring and improve their quality of life.

From the global demographic change, it is evident with the rapid aging of the population indicating a 2.6% annual growth in the population of the elderly as estimated by the United Nations. It explains that the tremendous increase in the costs of elderly care [1]. In the Philippines, there is faster growth in the population of the people annually and still continually increasing the number of elderly people [2]. Since the age of 60 and above, there is 6.9% total population for the year 2000, and it was compromised up to 4. 6 million senior citizens. According to the National Statistics Office, in 2030, the older people will make up around 11.5% of the total population. It is expected that 11.5% of the total population will be the elderly. In a decade, it will grow to 6.5 up to 6.9 million of the total population of elderly. [3].

The demand for health services increases in an aging population [4]. With the aging of the immune system of the body, degenerative and communicable diseases in the elderly. In the Philippine Health Statistics report, infections are the causes of morbidity with common health-related problems of impairment in vision, difficulties in walking, chewing, hearing, osteoporosis, arthritis, and continence [5].

It was from the Department of Social Welfare that is 31.4% of the elderly living in the state of poverty [6]. Moreover, presently, it is approximately 1.3 million older people [4]. Active at work in 2000 was more than half of these older people, registering 57.1%, with more employed males at 63.6% and employed females at 37.4%.

Given the above developments, this study aims to develop an elderly abnormal behavior detection using image processing and machine learning. Also, this study contributes to developing a Philippine database for elderly behavior patterns. Primarily, the study could be used to efficiently and effectively assist family members and nursing assistants to actively monitor their elderly family members at home while they are at a distance at work.

II. RELATED WORKS

A. Machine Learning

It is a field of computer science that provides the system's ability to learn automatically and to develop from the experience without being explicitly programmed [7]. Also focuses on prediction, making the development of computer programs or software applications to become accurate to access the data and use for personal or individual learning. The primary aim of machine learning is to allow the computers to learn without human intervention or any assistance to perform actions accordingly. It also explores and studies of computational learning theory and pattern recognition in the application of artificial intelligence. It begins with the observation of data from the examples like, instructions and direct experience to look for the patterns that make better decisions in the future based examples [8].

From the set of training examples, there are supervised learning techniques, and one of this is the medical image analysis. It learns how to map the data into an input and output data. It has many studies for the pattern classification which characterize to detect the abnormalities for the mammograms and nodules of the given chest radiographs. It was based on the appearance of the local image [9].

Also, in the computer hardware developments, the sets of training data and complex model became more feasible for the last the few years. There is accelerated learning for the image segmentation, registration, and recognition for the supervised learning. The accomplished models were replacing intensity, breakdown systems are for the incline models, and numerical variations were described in the set training shape models. These models have been replaced Freeform deformable models in many cases. Using the multivariate regression or classification, these are new methods used to diagnose and to detect the diseases from the data-driven as well as the imaging data [10]. The studies are

Erlito M. Albina is with College of Information Technology Education, Technological Institute of the Philippines, Manila, Philippines (e-mail: erlito.albina@lpu.edu.ph).

Alexander A. Hernandez is with College of Information Technology Education, Technological Institute of the Philippines, Manila, Philippines (email: alexander.hernandez@tip.edu.ph)

ISBN 978-1-5386-4473-7
IEEE sponsored 4th International Conference on Biosignals, Images and Instrumentation, SSNCE, Chennai. ICBSII 2018 – 22nd-24thMar'18

not limited to the present knowledge regarding the disease-related, radial higher analytical accuracy is his more traditional quantitative analysis additional quantitative analysis based on simple volume or density measures. The machine learning methods can be taken over the field and are gradually successful in prognosis, risk assessment, and image-based diagnosis. To interpret the clinical practice, there are many factors to be resolved on how to train the models from the little data, access data and expand data. To come up with the best image structure, it must depend on the design models on how did you interpret and apply in the clinical practice.

B. Image Processing

The study argues that the image classification and related imaging tasks performed using machine learning tools may be accelerated by using one or more of such tools to associate an image with a cluster of such labels or categories, and then to select one of the labels or categories of the cluster as associated with the image. The clusters of labels or categories may comprise labels that are mutually confused for one another, e.g., two or more labels or categories that have been identified as associated with a single image. By defining clusters of labels or categories, and configuring a machine learning tool to associate an image with one of the clusters, processes for identifying labels or categories associated with images may be accelerated because computations associated with labels or categories not included in the cluster may be omitted [11].

Pattern recognition is a branch of machine learning that emphasizes the data patterns, which also known as data regularities. The large database can be integrated for the abstraction and preparation of a classifier that can be potential and recognize of inbound data sample. One of the constraints encountered from the different claims is the required tremendous storage size. This constraint has motivated thesearch to find storage reduction solutions that have no or small effect on the pattern recognition process [12].

C. Posture Detection

Human posture detection is now widely explored in many application contexts and study. The real-time challenge of posture and cognition is called “dual task.” It may isolate components of postural control or predict falls [12]. For the first part, it was compared from the poorer postural performance of older-healthy adults and the younger-healthy adults. These summarize the main important models that capable to explain the cross-domain, task, prioritization model and the competition model [13]. Secondly, one of the significant limitations of the traditional-posturographic analyses is to use the dual-task exploration and dialogue with, on how can these accounts for some differences found in the literature. Another approach will be based on the wavelet transforms and stabilogram-diffusion analysis for better understanding of posture control. One of the advantages of these systems were demonstrated in young adults and elderly people in executing postural tasks with a mental or spatial task.

Nikou’s investigative study in 2015 stresses that it must be in the early stages to use of technology tools for the elderly people [14]. It highlights many actors for the modernization and adaptation of the processes. The specialist usually disregards the essential roles of the actor to another actor [15]. Thus, the issues may delay, and dispersion of elders’ advanced technology tools acceptance is essential [16].

It was mentioned that to track the indoor movement of the subject automatically, you must analyze the human behavior. camshift algorithm, meanshift algorithm, Feature matching algorithm, and shape and sized-based algorithm are the standard examples of human subject tracking algorithms and most of the common problems of these algorithms are, they are all very computationally intensive [16]. Thus, it is suitable to implement this in real time monitoring applications. The (MHoEI), a Motion History or Energy Image-based technique was developed because the researcher believed that this is fast, efficient, and effective [17].

Another study for the elderly fall detection is the use of a computer vision-based application. It extracts the foreground of the human body and post-processing for the better results. To distinguish the varied human postures, the projection histogram along the axis of the ellipses must be obtained, and all the information is coming from fitting ellipse. Eventually, these features are nourished directed from acyclic graph support vector machine to categorize the posture, which fall detection might affect from the information and then fused or merged within the derived floor. From the fifteen (15) participants, the study reveals that the high fall detection rate of 97.8% can be achieved from the system, while is recorded a shallow fall detection of (0.8%) from the simulated home environment [18].

An intelligent surveillance system is used in the analyzing behavior. This system can provide an operable for a series of sequential images under surveillance of serial time points. The approach comprises the steps of each image and to set of points defining at least one moving silhouette on an image and comprising of the following: predefined trajectories corresponding to behavior database, set of points for the tracing of consecutive images to generate trajectories of points, generated and compared trajectories of points. From these, it responds all output records and information regarding the typed of predefined behavior from the moving silhouette correspondence [19].

The study suggests that the elderly can easily detect their abnormal behaviors in the indoor places, there is much equipment installed from the different places like a living room, bathroom, bedroom, kitchen, and other similar places. In this case, it can improve the monitoring cost, as well as the fall detection of an elderly due to fall detection algorithm and their relatively complex. Although there is much equipment installed in the indoor places, the detection will not be worked out if the elderly fall outside [20].

III. METHODOLOGY

A. System Design

The goal of this project is to present an intelligent system capable of detecting abnormal behavior in elderly. The system should be able to provide real-time notifications to immediate family members during emergency situations. Furthermore, the family members' must be able to observe and check the daily task of the elderly people under their consent. A notification to the family members should include time, images of posture or action, and physical environment.

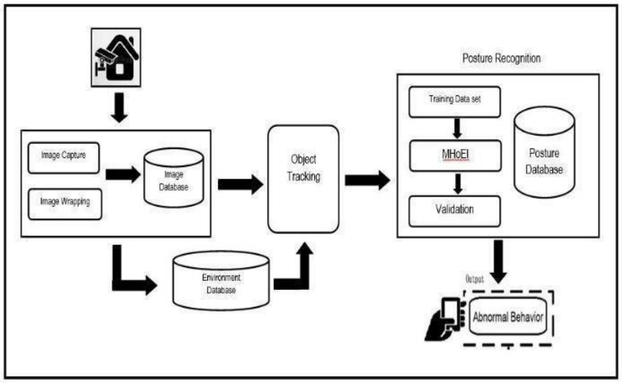

Figure 1: System Design

Figure 1 presents the system design of an intelligent abnormal behavior detection system. First, the actual images of the elderly person are derived from high definition video and image capturing device. Second, the images of the elderly are pre-processed and from the database. Moreover, the recorded videos were also used in object-tracking and pattern recognition solutions. Third, by joining the posture data and physical environment data, the system can detect the abnormal behavior and notify the family member during emergency situations.

A.1 Video Acquisition

One of the challenges of the device is that it can only capture one direction space of the environment. Thus, multiple devices were set up in different directions (north-south, east -west) to ensure real-time capturing of videos of the elderly participants. The devices were also installed and adjusted regarding the height of the elderly participant, the distance of device with each other considering the house dimension and camera focus to minimize the error during the real-time surveillance for all elderly participants.

In Figure 2, shows an image extraction from captured from the closed observation of the elderly participants. Second, background extraction takes place to identify objects available in the scenes initially. Third, the identified objects in motion are presented through the computed information properties of each object to be used for early analysis.

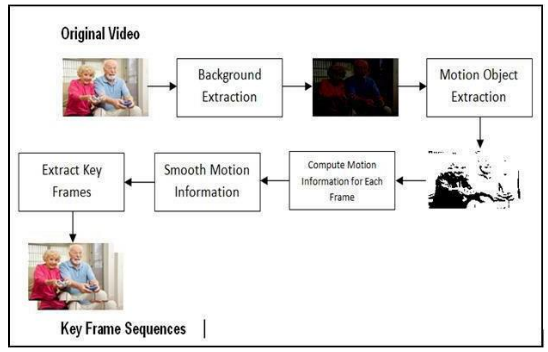

Figure 2: Image Segmentation

A.2 Human Object Tracking

This study used the Motion History or Energy Image (MHoEI) technique, an algorithm that used for the real-time monitoring system which is firm, proficient and effective applications. The goal of this procedure is to solve the indoor movement of subjects. This algorithm is defined by the given equation:

$$H_\tau(x,y,t) = \begin{cases} \tau \cdots (D(x,y,t)=1) \\ max(0, H_\tau(x,y,t-1)) \cdots (S \leq \delta) \\ max(0, H_\tau(x,y,t-1)-1) \cdots otherwise, \end{cases}$$

To implement an elderly monitoring application, there is a proposed trajectory and the lowest value of the bounding rectangle information of the elderly people. This method must be used to test the posture detection, motion object tracking, detection of the moving object, and behavior examination. The study also considers the aspect of relationships by the different distance between the object and to obtain the following: behavioral abnormality, activity rhythm, and detection method using time, space, action, and environment [20].

A.3 Posture Recognition

Table 1.0 presents the threshold used as a reference in abnormal activity detection, including standing, sitting, bending, lying, kneeling, and squatting. At this phase, this study only covers these postures to test the performance of the algorithm used initially.

Table 1: Human Posture for Threshold Detection

Posture	Threshold (t)
Standing	t > = 1.8
Sitting	1.8 > t >= 0.7
Bending	t < 0.7
Lying	t <= 1.8
Kneeling	t <= 1.7
Squatting	t<= 1.8

Using human posture ratio, the human posture can be analyzed. The human posture formula was written as t = H /

W, where H is the height of the bounding rectangle and W is the width.

IV. RESULTS AND DISCUSSION

This study involves three major phases in abnormal activity or behavior detection in elderly living without a companion or family members due to work conditions, life style, and other related factors. First, videos should be captured from the four (4) elderly participants to capture relevant motion or activity, a resulting object in the image sequences is identified through extraction procedure. Second, the key motion object is used to create a classifier model of normal activity or behavior of the elderly. Lastly, the expected to provide key features of normal pattern or activity of elderly, and hence, providing a threshold matrix of each pattern or activity recognized.

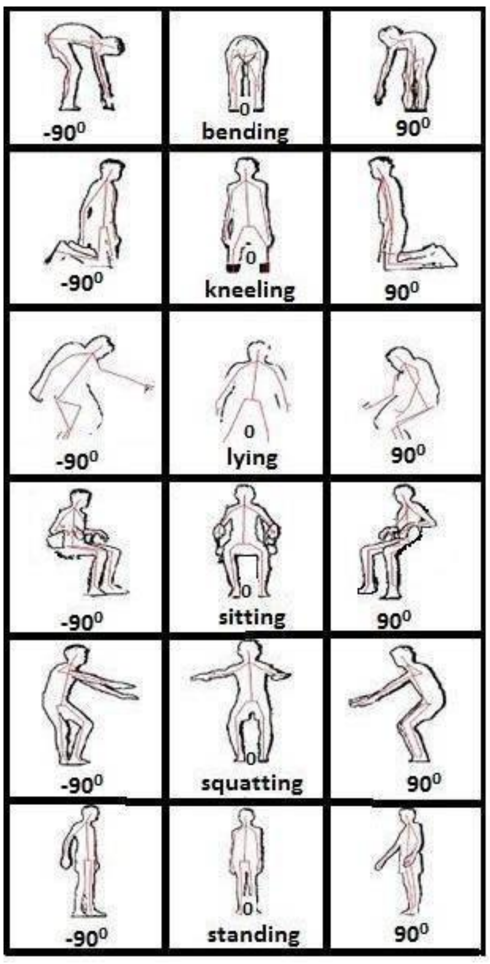

Figure 3. Elderly Postures

Figure 3 shows the different postures of the elderly of the actual segmented images with the different angles or views. In the first column, it shows the angle position in -900, while the second column shows the position in 00, and the third column shows the 900. From the different angles and views, the different postures were recognized whether it is bending, kneeling, lying, sitting, squatting, and standing.

For the dataset, there are two males and two females elderly, captured in the different postures: 60 images for the bending and standing, and 70 images for the kneeling, lying, sitting and squatting.

Table 2: Initial Recognition Accuracy

	Bending	Kneeling	Lying	Sitting	Squatting	Standing
M1	57/60	68/70	68/70	61/70	70/70	58/60
F1	56/60	68/70	67/70	62/70	68/70	57/60
M2	58/60	65/70	65/70	65/70	69/70	56/60
F2	58/60	67/70	68/70	64/70	70/70	58/60

Table 2. shows the result of recognized images from the given data set. First, for bending position, 58 out of 60 images were recognized with the average of 97%. Second, for the kneeling position, 67 out of 70 images were recognized with the average of 96%. Third, for the lying position, 67 out of 70 images were recognized with the average of 96%. Fourth, for the sitting position, 63 out of 70 images were recognized with the average of 90%. Fifth, for the squatting position, 69 out of 70 images were recognized with an average of 99%. Lastly, for the standing position, 57 out of 60 images were recognized with the average of 95%.

V. CONCLUSION

This paper presents a research-in-progress of designing an intelligent abnormal activity detection using Kinect devices. This device was used to capture the movements of an elderly person in a variety of positions and gestures.

First, this study presents an initial result of elderly abnormal behavior detection. Second, this paper presents the geometrical vector features of postures including standing, sitting, bending, lying, kneeling and squatting in different views. Third, the results also include a training data gathered from the actual surveillance of elderly participants in the study as well as initial recognition accuracy and performance. Thus, this paper contributes to the development of a database for Philippine elderly abnormal behaviors.

However, this study is not yet complete, and aims to progress by (a) adding more training data set from at least four elderly participants, (b) conducting tests of the intelligent model to verify accuracy, reliability, and performance of the intelligent abnormal behaviour detection system, and (c) perform an end-user software evaluation.

References

[1] mondiale de la Santé, O. (2017). Health situation and trend assessment.

[2] Qu, Y. (2014). The Comparative Study of Household Elderly Care in China, the Philippines, and Japan. *Home Health Care Management & Practice*, *26*(3), 175-181.

[3] Cabral, E. I. (2016). The Philippine health agenda for 2016 to 2022. *Phil Journal of Internal Medicine*, *54*(2).

[4] World Health Organization. (2015). Health in 2015: from MDGs, millennium development goals to SDGs, sustainable development goals.

[5] Hoffmann, R., & Lutz, S. U. (2018). The health knowledge mechanism: evidence on the link between education and health lifestyle in the Philippines. *The European Journal of Health Economics*, 1-17.

[6] Okamuro, M., & Someya, M. Social Protection in the Philippines. *Chiba keizai ronso*, (50), 1-25.

[7] Jordan, M. I., & Mitchell, T. M. (2015). Machine learning: Trends, perspectives, and prospects. *Science*, *349*(6245), 255-260.

[8] Deo, R. C. (2015). Machine learning in medicine. *Circulation*, *132*(20), 1920-1930.

[9] Milletari, F., Navab, N., & Ahmadi, S. A. (2016, October). V-net: Fully convolutional neural networks for volumetric medical image segmentation. In *3D Vision (3DV), 2016 Fourth International Conference on* (pp. 565-571). IEEE.

[10] de Bruijne, M. (2016). Machine learning approaches in medical image analysis: From detection to diagnosis. *Medical image analysis*, *33*, 94-97.

[11] Ojha, S., & Sakhare, S. (2015, January). Image processing techniques for object tracking in video surveillance-Asurvey. In *Pervasive Computing (ICPC), 2015 International Conference on* (pp. 1-6). IEEE.

[12] Sharma, P., & Suji, J. (2016). A review on image segmentation with its clustering techniques. *International Journal of Signal Processing, Image Processing and Pattern Recognition*, *9*(5), 209-218.

[13] Liu, Z., Song, Y., Shang, Y., & Wang, J. (2015, May). Posture recognition algorithm for the elderly based on BP neural networks. In *Control and Decision Conference (CCDC), 2015 27th Chinese* (pp. 1446-1449). IEEE.

[14] Mostaghel, R. (2016). Innovation and technology for the elderly: Systematic literature review. *Journal of Business Research*, *69*(11), 4896-4900.

[15] Siegel, C., & Dorner, T. E. (2017). Information technologies for active and assisted living—Influences to the quality of life of an ageing society. *International journal of medical informatics*, *100*, 32-45.

[16] Samuel, O. W., Asogbon, G. M., Sangaiah, A. K., & Li, G. (2017). Multi-technique object tracking approach-A reinforcement paradigm. *Computers & Electrical Engineering*.

[17] Xiang, Y., Tang, Y. P., Ma, B. Q., Yan, H. C., Jiang, J., & Tian, X. Y. (2015). Remote safety monitoring for elderly persons based on omni-vision analysis. *PloS one*, *10*(5), e0124068.

[18] Peetoom, K. K., Lexis, M. A., Joore, M., Dirksen, C. D., & De Witte, L. P. (2015). Literature review on monitoring technologies and their outcomes in independently living elderly people. *Disability and Rehabilitation: Assistive Technology*, *10*(4), 271-294.

[19] Ojha, S., & Sakhare, S. (2015, January). Image processing techniques for object tracking in video surveillance-Asurvey. In *Pervasive Computing (ICPC), 2015 International Conference on* (pp. 1-6). IEEE.

[20] Dias, P. V. G., Costa, E. D. M., Tcheou, M. P., & Lovisolo, L. (2016, November). Fall detection monitoring system with position detection for elderly at indoor environments under supervision. In *Communications (LATINCOM), 2016 8th IEEE Latin-American Conference on* (pp. 1-6). IEEE.

ISBN 978-1-5386-4473-7
IEEE sponsored 4th International Conference on Biosignals, Images and Instrumentation, SSNCE, Chennai. ICBSII 2018 – 22nd-24thMar'18

Smart Wearable Systems for Personal care with Internet of Things

V. M. Karthicraja
Department of Instrumentation Engineering
MIT Campus, Anna University, Chennai, India.
karthikmunisamy@gmail.com

V.L. Krishna Prasad
Cognizant Technology Solutions
Chennai, India.
vlkrishna247@gmail.com

U. Kruthika
Department of Instrumentation Engineering
MIT Campus, Anna University
Chennai, India.
kruthika41095@gmail.com

R. Sivakumar
Deaprtemnt of Electronics and Instrumentation Engineering
St Joseph's College of Engineering
Chennai, India.
rsivakumar1@gmail.com*

***Abstract*—Modern technological advances in miniaturization of sensors, micro- and nanotechnologies, smart gadgets, and smart fabric, and the unremitting advances in smart wearable systems have gradually changed the landscape of personal care, by permitting personality supervision and unremitting supervision of an individual's fitness grade by the trending Internet of Things technology. Consequently, Internet-Of-Things (IoT) is competent to connect a great amount of secluded devices among the internet in an apparent and flawless manner. The proposed work focuses on Wearable Smart System using IoT, which emulates the concept of personal care primarily concentrating on health and safety services. An open source operating system, Contiki 3.0, is used to realize the personal safety and security system using Cooja simulator. Furthermore, this paper provides a comprehensive study of the various topologies, which are used to realize the smart body area network concepts with minimum power consumption and end-to-end delay**

Keywords—*Constrained application protocol (CoAP); Cooja; Ipv6; Sensors.*

I. Introduction

IoT is a latest exemplar, which growing swiftly with the development of wireless communication. IoT can help improve the people's standard of living in a plethora of domains. This concept finds application in health care, personal safety, home automation, industrial automation, automotive and traffic management, etc. Using this technology, a huge value of information can be composed from secluded devices which could be used for providing services to people, industries and public management. The Internet of Things adds elegance to normal devices by making the Internet ubiquitous to enhance human life. The prediction is, quantity of devices linked with internet will gather from 100.4million (2011) to 2.1billion (2021). The cost related with M2M over mobile networks are generally cheaper than fixed networks [1,6].

Recently, everybody from various locality can be connected together using the smart networks and advanced dynamic network of IoTs [2,5-6].

Far-reaching efforts are implemented by the researchers on elegant wearable structure for individual security and fitness state observation. Largely prejudiced by escalating monitoring expenses plus alarmingly increasing harassment against women, children, and elderly people, the explication for these problems is addressed by many IoT applications as wearable devices and smart fabric concepts. But the problems faced in realization of these monitoring devices and security systems are numerous and that to when the system acts as a wireless networks [3].

Though Internet of Things is an emerging concept, there are various glitches regarding the practical application of these applications. Which includes issues such as the amount of power consumed and the rate at which the information transmission are made. The social and economic aspect of our country may be escalated by the elevating the advancements through technologies of public healthcare and protection. On the positive side, it increases the safety and security of the denizens [4,7,8].

This paper has two objectives. The first one is to discuss the various topologies available in Contiki OS such that the topology, which results in minimum power consumption and reduced end-to-end delay, is implemented for the required application. The second objective is to design a wireless smart system for personal health monitoring and security system constrains using Constrained Application Protocol (CoAP). For this purpose, Contiki OS is used which a light-weight is operating structure through maintain for active loading and unloading, and substitute of personality curriculums and services [9-11]. Recently, IoT plays a major role in medical domain in the exchange of medical signals and images between the server and the client. The doctor will develop an analyzing tool which may be available in the client level or universal server called cloud. By this way, the IoT system offers efficient data transmission between various levels.

II. Methodology

A. Contiki

First, Contiki is an operating system (OS) for implementing Internet of Things (IoT), since its origin in the year 2002 []. It allows swift prototyping and easy shift between diverse hardware platforms. This OS is desired mainly because the developer need not design the basic operating system for the internet connected devices. The designer of Contiki has managed to fit an entire operating system, including a networking software, graphical user interface (GUI), and web browser [12].

ISBN 978-1-5386-4473-7

IEEE sponsored 4th International Conference on Biosignals, Images and Instrumentation, SSNCE, Chennai. ICBSII 2018 – 22nd-24thMar'18

Contiki facilitate IPv6 protocol for networking the relaying datagrams across network boundaries. It comprises the Routing Protocol for Low-power-networks (RPL), and an Internet Protocol (IP) optimized for WSN. Contiki is affected in the C language and can be ported to a number of micro controllers such as, CC2430, Arduino Atmel AVR, MSP430, etc. The applications implementation is achived using Constrained Application Protocol (CoAP) which hels low radio duty cycling mechanism provides power efficient operation. CoAP adopts patterns from HTTP but unlike the latter, CoAP uses User Datagram Protocol [13].

B. Comparison of topologies

The remote sensors (motes) can be organized in a number of topologies according to the required application. The mote type has the capability to determine the type of sensor hardware and which Contiki applications are to be simulated. In the case of smart wearable system concept, the major concern would be power consumption and the transmission-reception delay. The three major topologies are linear, ellipse and random. In this example, IPv6 routing with RPL is considered. Therefore, arpl-border -router with three clients and servers are simulated using Cooja simulator. Fig. 1 (a), (b), and (c) shows the various topologies.

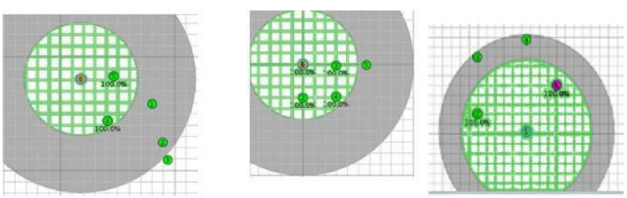

(a) Linear (b) Random (c) Sky mote

Fig. 1 Topologies

To estimate the power consumption, Tmote Sky mote was used in different topologies. From Fig. 2, it is inferred that power consumed during transmission and reception between motes is less in random topology.

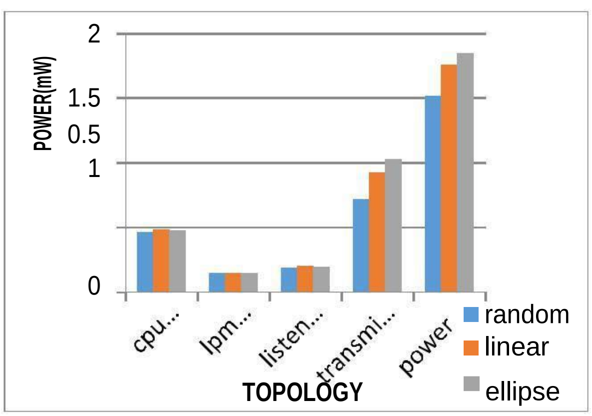

Fig 2. Power for various topologies

Transmission range of the various motes also affects the extent of power consumed. From Fig 3; it can be perceived that for various transmission ranges, the motes in random topology has consumed less power over its counterparts [14].

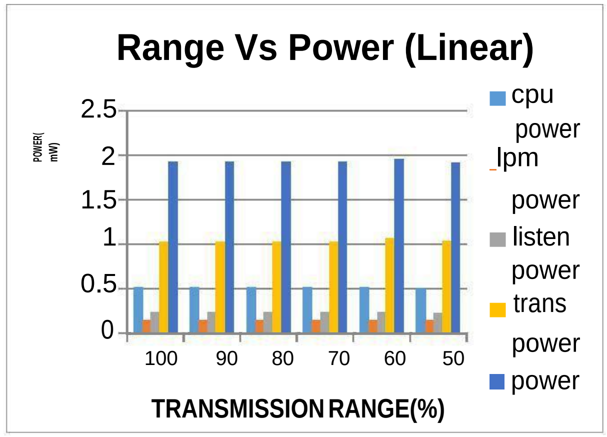

Fig 3. Liner's Range Vs Power

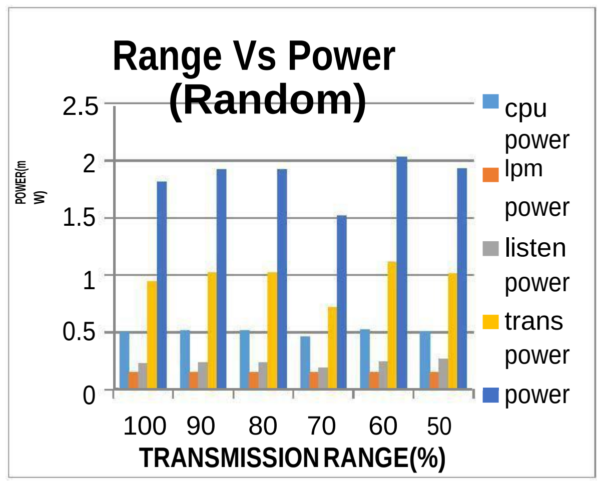

Fig 4. Random's Range Vs Power

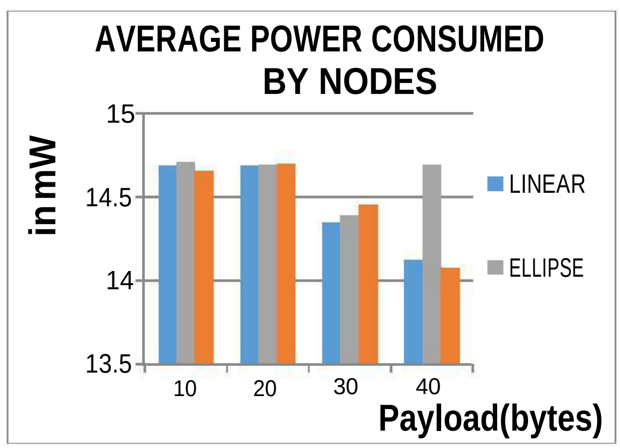

Fig 5. Payload variation

The next concern is the amount of data, i.e., payload, sent by the servers during transmission of signals. The Figure 5. Plots the power consumed by the nodes with increasing payload. It can be seen that for random topology, the power consumed decreases drastically with increase in payload. Therefore, random topology can be used even when large amount of server data has to be transmitted. The payload also affects the end-to-end delay of the nodes. Hence, an experiment is steered by increasing the payload and determining the corresponding power changes. From figure 6, it can be inferred that as the payload increases, transmission-reception delay also increases. When the topologies are compared, linear topology has been found to have lesser delay.

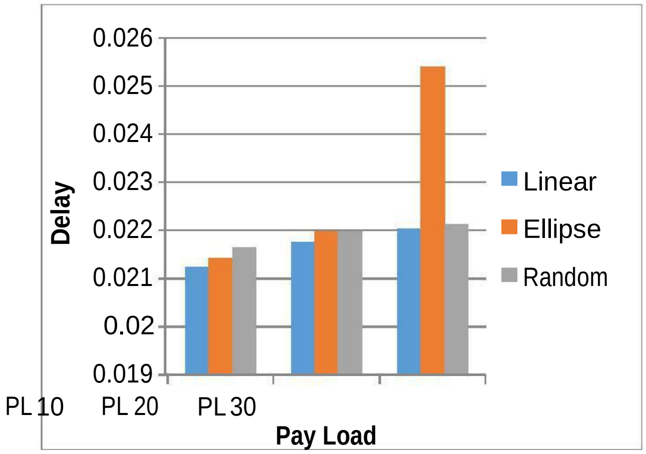

Fig. 6 Payload Vs Delay

From all the above comparisons, it can be observed that random topology can be used for practical applications.

C. Wearable Sensor Network Using IoT

Due to advancement in arrangement transportation, wireless arrangement has overthrow earlier methods, while previous sensors were straightly associated to a wearable CPU by wires. Researchers created WSN to implant sensors in garments or permit sensors to be worn as accessories. Normally, a wireless body region arrangement was set up on the patient’s body. This scheme comprises all the wearable sensors and a hand held wearable processor.

In next setup called personal-area-network, various signal recording sensors, like video, audio, smartphone and environmental devices are considered to monitor a person. These devices will transfer the information to the client or server through the wire -based or wireless basis. After receiving these information, the server or the PC will take the necessary action based on the predefined tasks listed in program, which includes, alerting the nearby person, alarm, secret message, text/voice message, etc.

D. Personalized Health and Safety Systems

For monitoring heath condition, a wearable sensor system comprise a widespread class of wearing or embedded gadgets, which comprise transducers, actuators, amplifiers, WSN with IoT, battery, software’s and algorithms for data spasm, pre and post handing, and conclusion creation systems. For human interface, it has multimedia devices, Graphical User Interfaces (GUI) as separate entities.

These systems are designed to acquire and measure vital signs, which include pulse-rate, respiratory-rate, blood-pressure, body-temperature, oxygen saturation level, ECG, EEG, and Electro Dermal Activity (EDA) of the skin. This information is broadcasted via WSN to their central or sub nodes. For example, let, the sensor is a digital camera which captures the person’s information with a gray scale [15-18] or RGB scale picture. Later these information may be pre-processed or the raw picture can be sent to the doctor through WSN, wire or cloud in order to support the decision making process [19-22]. This doctor can supervise these data with a PC or a mobile phone, which is connected in the network as a sub node or the server node. An optimal therapeutic supervision is possible to provide real-time processing and feedback to doctors, patients, sports persons, and strong persons.

Similar measurements are used and they can be dictated to serve for the purpose of safety and security of individuals mainly children, woman, and elderly people. The wearable security gadgets powered by IoT works the same way as of the health monitoring devices it has the same hardware and software specification but with little enhancements in the predictive algorithms. So, there is a rising attention in discovering novel safety and security answers to supply care and security to woman, children and elderly anywhere at any time.

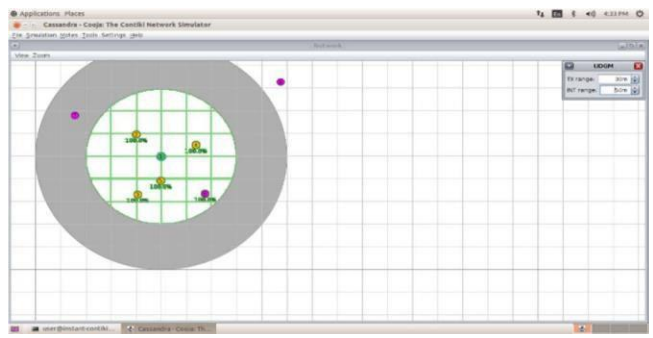

Fig. 7. Cooja simulator

Smart wearable security systems have the ability to monitor individuals 24/7 in their own homeland out -of-doors, according to precautionary security procedures. The checking scheme is connected with cloud-server using IoT, to monitor and measure signals coming out from the sensors/nodes. The cloud-server can also supply assist whenever required. The vital signs of women and children such as pulse rate, heart rate, temperature and EDA are continuously monitored and used for assessing the emotion and situation of the wearer and provided needed help at right time. The actions or movement of senior people can be supervised and lifestyles abruptly alter, like the propensity to stay at house or drop of mobility, starvation, and communal behavior, can be foreknown based on psychiatry of the behavior of everyday livelihood, which is essential, as these are dangerous circumstances.

An individual as an accessory can wear the discussed sensing systems: which can be piece of jewelry, wristwatch, wristband, or ring, measuring pulse, body temperature, galvanic skin response (GSR), and EMG data. These can also be a brooch, earring, belt buckle, pinor necklace.

III. RESULTS AND DISCUSSION

In this section discuss, the practical implementation issues of Wearable Smart health monitoring and safety System. This application is extremely important as they have the ability to save one from threat and even death. However, concerns mentioned earlier and few new issues such as the range of transmission and remote client communication influences causes degradation in novel capabilities these system.

However, similar framework has been already executed but the use of Contiki for programming reduces the power consumption and the programming is easier. The target application in simulation consists of a mote based body area network using the Contiki Cooja simulator in CoAP environment. A sensor network platform for monitoring the vital signs of an individual is architected using sky motes placed in random topology with border router. The main constituents of the simulated sensor network are server sensor nodes, border router and client. Figure 7.Gives the simulation illustrating the arrangement of the CoAP server and client system with border router.

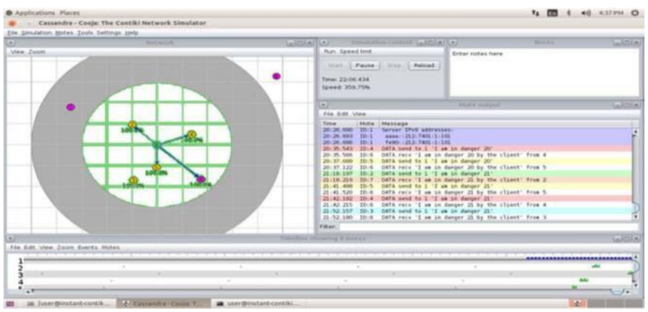

Fig. 8a. Initial transmission range

The outcomes of the simulations summarizes the following that when the communication is enabled the data from the servers are continuously transmitted to the border router from there they are sent to the client. The client response also tracks back the same path. One of the outcomes shows that it is possible to increase the range of the transmission. By the increase of transmission range, even in rare cases there will be communication between the sensor node and the border router. Figure 8a, b. gives the validation of the outcome stated above.

For instance, let us investigate this property with a scenario that in smart safety wearable which has two main parts the sensor network and the processer. The communication between the latter and the sensor network is wireless communication, during crime if a perpetuator separates the processor and the sensor network, which is implanted in the victim's body. These sensors has a particular range of transmission and this range can be increased by making steering changes in the network layer and transportation layer of the sensor network in Contiki, by which the range of transmission can be increased up to 100 meters from the specified transmission range of the mote.

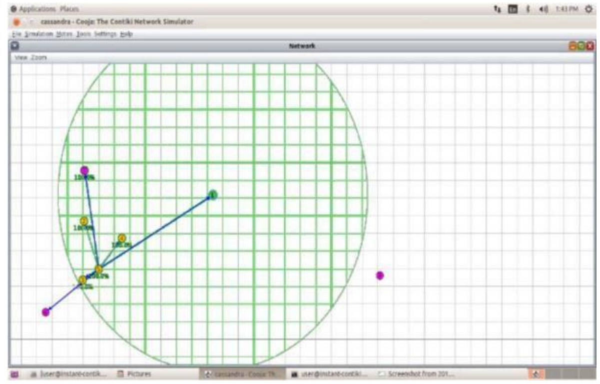

Fig. 8b. Extended transmission range

Next notable result is that ability of the client to communicate with the remote client system when the corresponding is located out of the transmission range, which is showcased by Figure 9, explaining the remote client communication. Thus, this makes it as prominent outcome, making data transmission feasible between two remote client systems, which is not in the transmission range. This can be further explained by the illustration of alert signals that are sent from the cloud to the remote user interface in any health monitoring or personal safety service. All the transmissions take place with less power consumption and through put.

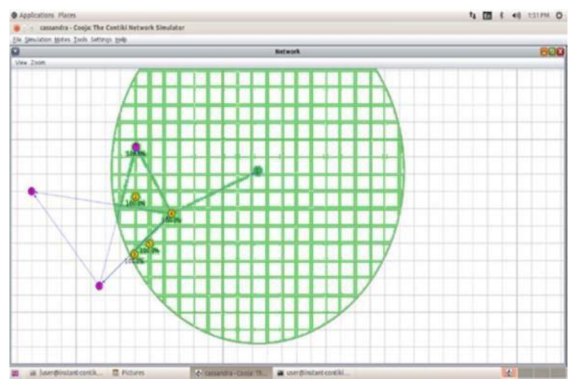

Fig.9. Remote client communication

IV. CONCLUSION

In this paper, we analysed the different topologies for the smart wearable devices and concluded that random topology is best suited for practical application because it is power efficient in respect to transmission range and payload variations. Even though linear topology has lesser delay, it is not always feasible to have remote sensor devices arranged in a linear fashion. Then the application of Internet of Things to health monitoring and personal safety was also discussed. The use of Contiki can minimize power consumption and enable real-time implementation of personal health and safety services enabling extension of transmission ranges and remote client system communication.

REFERENCES

[1] Shobha Tyagi, Subhranil Som, Qamar Parvez Rana, Trust based dynamic multicast group routing ensuring reliability for ubiquitous environment in MANETs, International Journal of Ambient Computing and Intelligence (IJACI), vol.8, no.1, pp.70-97, 2017. DOI: 10.4018/IJACI.2017010104.

[2] Mohammad Yamin , Adnan Ahmed Abi Sen , Improving privacy and security of user data in location based services, International Journal of Ambient Computing andIntelligence (IJACI) 9(1), pp.19-42, 2018. DOI: 10.4018/IJACI.2018010102

[3] Mohammed Chennoufi, Fatima Bendella, Maroua Bouzid, Multi-agent simulation collision avoidance of complex system: application to evacuation crowd behavior, International Journal of Ambient Computing and Intelligence (IJACI), vol.9, no.1, pp. 43-59, 2018. DOI: 10.4018/IJACI.2018010103.

[4] Wenli Yang, Xiaojing Wang, Xianghui Song, Yun Yang, Srikanta Patnaik, Design of intelligent transportation system supported by new generation wireless communication technology, International Journal of Ambient Computing and Intelligence (IJACI), vol.9, no.1, pp. 78-94, 2018. DOI: 10.4018/IJACI.2018010105.

[5] L. Atzori, A. Iera, and G. Morabito, "The internet of things: A survey," Comput. Netw., vol. 54, no. 15, pp. 2787–2805, 2010.

[6] A.Dunkels, B. Gronvall, and T. Voigt, "Contiki – a Lightweight and Flexible Operating Sytem for Tiny Networked Sensors," IEEE International Conference, Local Computer Networks,2004.

[7] F. Osterlind, A. Dunkels, J. Eriksson, N. Finne, and T. Voigt, "Cross-Level Sensor Network Simulation with COOJA," Proceedings-Conference on Local Computer Networks, LCN, pp: 641-648, 2006.

[8] Y.M. Yusoff, R. Rosli, M.U. Kamaluddin, and M. Samad, "Towards Smart Street Lighting System in Malaysia," IEEE Symposium on Wireless Technology and Applications, ISWTA, pp: 301-305, 2013.

[9] M. Shankar, J.B. Burchett, Q. Hao, B.D. Guenther, and D.J. Brady, "Human Tracking Sytems using Pyroelectric Infrared Detectors," Optical Engineering, vol: 45(10) pp: 106401, 2006.

[10] G. Ren, H. Guo, Y. Yang, and Z. Yang, " Ultrasonic sensor based material level and liquid level measurement technology," Lecture Notes in Electrical Engineering, vol: 132 LNEE (VOL. 1) pp: 25-30, 2011.

[11] N. Tsiftes, J. Erikkson, A. Dunkels, "Poster Abstract: Low-Power Wireless IPv6 Routing with ContikiRPL," North, vol: 3(3.5) pp: 4-5, 2010.

[12] Doukas C, Metsis V, Becker E, Le Z, Makedon F, Magliogiannis I. Digital cities of the future: extending @home assistive technologies for the elderly and the disabled. Telematics and Informatics 2011;28:176–90.

[13] M. Kovatsch, S. Duquennoy, A. Dunkels, "A low-power CoAP for Contiki," Proceedings- 8th IEEE International Conference on Mobile Ad-hoc and Sensor Systems, MAS, pp: 855-860, 2011.

[14] Kluge EHW. Ethical and legal challenges for health telematics in a global world: telehealth and the technological imperative. International Journal of Medical Informatics 2011;80(2):1–5.

[15] V. Rajinikanth, S.L. Fernandes, B. Bhushan, N.R.Sunder, "Segmentation and analysis of brain tumor using Tsallis entropy and regularised level set," Lecture Notes in Electrical Engineering, vol.434, pp. 313-321, 2018.

[16] V. Rajinikanth and S.C. Satapathy, Segmentation of ischemic stroke lesion in brain MRI based on social group optimization and Fuzzy-Tsallis entropy, Arabian Journal for Science and Engineering, pp.1-14, 2018. doi: 10.1007/s13369-017-3053-6.

[17] T.D.V. Shree, K. Revanth, N.S.M. Raja and V.Rajinikanth, A Hybrid Image Processing Approach to Examine Abnormality in Retinal Optic Disc, Procedia Computer Science, vol.125, pp. 157-164, 2018.

[18] V. Rajinikanth, S.C. Satapathy, S.L. Fernandes, S. Nachiappan, "Entropy based Segmentation of Tumor from Brain MR Images–A study with Teaching Learning Based Optimization," Pattern Recognition Letters, vol.94, pp.87-95, 2017. DOI: 10.1016/j.patrec.2017.05.028.

[19] V. Rajinikanth, N.S.M. Raja, K. Kamalanand, "Firefly Algorithm Assisted Segmentation of Tumor from Brain MRI using Tsallis Function and Markov Random Field," Journal of Control Engineering and Applied Informatics, vol.19, no.3, pp. 97-106, 2017.

[20] V. Rajinikanth, N.S.M. Raja, S.C. Satapathy, S.L. Fernandes, "Otsu's multi-thresholding and active contour snake model to segment dermoscopy images," Journal of Medical Imaging and Health Informatics, vol.7, no.8, pp.1837–1840, 2017.

[21] R. Vishnupriya, N.S.M. Raja, V. Rajinikanth, "An efficient clustering technique and analysis of infrared thermograms," Third International Conference on Biosignals, Images and Instrumentation (ICBSII), IEEE, pp.1-5, 2017. DOI: 10.1109/ICBSII.2017.8082275.

[22] N. Dey, V. Rajinikanth, A.S. Ashour and J.M.R.S. Tavares, Social group optimization supported segmentation and evaluation of skin melanoma images, Symmetry, vol.10, no.2, pp. 51, 2018. doi:10.3390/sym10020051.

Classification and Prediction of Human Cognitive Skills using EEG Signals

Malak Shah* and Ruma Ghosh
Department of Electrical and Electronics Engineering, BITS Pilani, K. K. Birla Goa Campus, Goa-403726
*malakshah96@gmail.com

Abstract—In this paper, a novel method to perform binary classification of human cognitive skill using electroencephalography (EEG) signals was developed. The classification was done by assessing activity in the brain, at different frequencies while the subjects were solving a series of arithmetic questions of varying complexity. Recording of brain activity was done through EEG signals with the aid of the EMOTIV EPOC+ neural headset. The acquired data was analyzed and the classifications were accomplished with the help of supervised learning classifiers, namely K Nearest Neighbors (KNN), Support Vector Machine (SVM), Regression, Discriminant, Tree and Ensemble classifiers. The mental skill of the test subject was classified in binary terms of a state of solving/not solving in a manner similar to emotional classification using the valence/arousal model. The results are presented and discussed in detail in this paper. It is believed that this work would lead to the development of accurate methods to predict cognitive skills of human beings for a better understanding of their learning capabilities.

Index Terms—feature extraction, feature selection, machine learning classifiers, electroencephalography

I. Introduction

There are two fundamental approaches to classify human emotions- (1)Emotions are assumed to be discrete and fundamentally unrelated. (2)Emotions can be described on a dimensional basis. The two-dimensional approach using valence and arousal as the dimensions for classification of emotion is popular and is utilized in various models like circumplex model [1], vector model [2], [3], and positive activation-negative activation model [4]. There is evidence to show that valence-arousal dimensions behave interactively and not distinctly [5]–[7]. Valence-arousal based classification models' assumption of distinct behavior, prompted the necessity to develop a new method for cognitive predictions, because accurate prediction of cognitive skills could potentially lead to advances in teaching and help better understand certain learning disabilities.

The electroencephalography (EEG) signal provides an objective mode of recording brain stimulation and thus has far-reaching applications in brain computer interfacing, medical diagnosis and research. EEG signals are produced by synchro-nized electrical pulses from masses of neurons communicating with each other. These signals have characteristic frequencies that are divided into bandwidths to describe their functions. These bandwidths are: delta waves (.5 to 3 Hz), theta waves (3 to 8 Hz), alpha waves (8 to 12 Hz), beta waves (12 to 38 Hz) and gamma waves (38 to 42 Hz).

In systems that do not necessitate whole brain coverage, the effective number of channels can be reduced by selecting a region of interest to increase accuracy or to achieve equal accuracy with less data [8]. This can be selected beforehand based on pre-existing knowledge about brain activity related to the task [9]. Existing works establish a link between cognitive control/skills and the prefrontal cortex of the brain [10], [11]. Features can also be selected efficiently by eliminating features irrelevant to emotional classification [12].

Existing works showed that it was possible to classify EEG signals with an accuracy above 98% for a complex cognitive task vs no task baseline [13], [14]. For brain-computer interface applications, the EEG signal classification accuracy was shown to be as high as 73% [15]. This paper expanded upon the existing EEG studies of the brain by: (1) Carrying out classification of EEG signals by assigning cog-nitive tasks of varying complexity. (2) Developing a method for real time prediction of cognitive skill. (3) Testing different classification algorithms to find out the most efficient one with high accuracy.

II. Experimental Methods

A. Data Recording

Emotiv EPOC+ Premium Model 1.1 (Serial Number: 3B9AD53F) was used to record the brain activity of subjects under test. It is a 14 channel wireless EEG headset with a sampling rate of 128Hz and an effective bandwidth of 0.2-43 Hz. The electrodes are located at the following standard international 10-20 reference positions: AF3, F7, F3, FC5, T7, P7, O1, O2, P8, T8, FC6, F4, F8, AF4. In addition, 2 reference electrodes in the CMS/DRL noise cancellation configuration are present at P3/P4 locations. The electrode signals were passed through a 0.16 Hz cut-off frequency high-pass filter, pre-amplifier and 83 Hz cut-off low-pass filter. The analogue signals were then digitized at 2048 Hz, filtered using a digital 5th-order sinc filter (50-60 Hz), low-pass filtered and down-sampled to 128 Hz. These signals were then Fourier Transformed (Hamming Window) and split into the five frequency bands, providing average power in each frequency band.

The data used for predicting parameters and training the machine learning algorithm was collected from 8 volunteers (4 male, 4 female) after receiving informed consent. The volunteers were given 3 sets of 5 arithmetic questions to solve with 60 second cool down periods in between two arithmetic problems. The Emotiv Headset's Application Programming Interface provided the recorded information in terms of EMOstates which could be obtained by connecting to the EMOengine. Using the guidelines and examples provided by the Emotiv Epoc+ Community Software Development Kit, C++ code was written in Microsoft Visual Studio Community Edition 2017 to acquire EEG data from the EMOengine. The code displayed the questions, logged subject responses and the EMOstate readings of average band powers. Additionally it used the CPU clock to create highly accurate (ms) timestamps of time taken for the subject to solve the questions.

B. Data Classification

MatLab R2016a™ and the classification learner application in the MatLab Statistics and Machine Learning Toolbox were used to analyze the acquired data and determine the best possi-ble algorithm for developing a real time prediction system. K-Nearest Neighbors Classification (KNN) is a commonly used supervised machine learning algorithm. In its simplest form (without k-d tree space partitioning) KNN simply involves reading all the training data points from a log file, then calculating the distance of each training point from every new test point received and sorting the training points by order of distance from test point, selecting the K closest points for consideration in classification. A flowchart of the real time predictor using KNN that was used to develop the present method is shown in Fig. 1. The parameters of the same were naive search KNN with euclidean distance metric, equal distance weights and K=1.

III. Results

As the Emotiv EPOC+ EEG headset uses saline based wet sensors, the contact impedance varied depending on amount of solution applied to the sensors in a particular recording session. To enable homogeneous classification of data from multiple sessions/subjects, an L2-norm of the Fourier Trans-formed signals was taken and therefore Normalized Spectral Intensity was used for classification.

As mentioned in the introduction, we attempted to reduce the effective number of channels. To this end, the Correlation Coefficients of the normalized spectral intensities in a band and the solving state of the subject were calculated and are displayed in Table I. As can be seen from Table I the AF4 electrode showed relatively higher levels of correlation with the solving state in a majority of the bands, hence the data from AF4 was used to make classifications. Fig. 2 and Fig. 3 show the normalized data from this electrode for two users. The figures also display the solving state (solving/not solving) of the subject. As the figures show, the normalized spectral intensity displayed peaks while the subjects were in a state of solving and and absence of peaks while the subjects were in a rest/cool-down period.

For the machine learning analysis, values of spectral intensity in the Theta, Alpha, Low beta, High beta and Gamma bands were used as predictor variables. The response variable took two values (or classes), 0 and 1. 0 corresponded to a

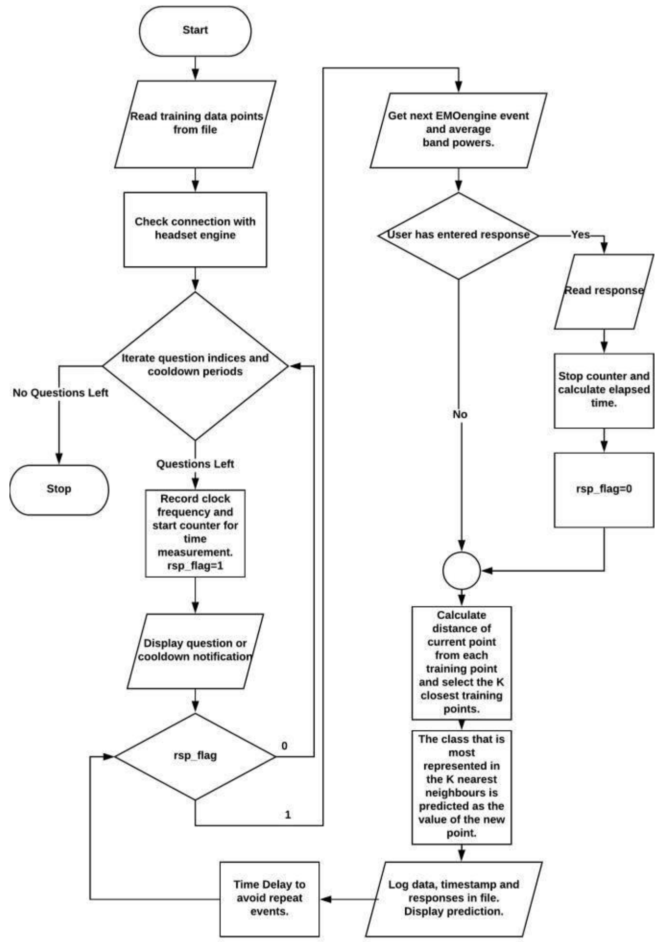

Fig. 1. Overview flowchart of real time predictor with K- Nearest Neighbors

TABLE I
Correlation Coefficients of Normalized Spectral Intensity in each Band and Solving State for each Electrode

Electrode	Theta	Alpha	Low Beta	High Beta	Gamma
AF3	0.0883	0.1161	0.1421	0.2062	0.2139
F7	0.0783	0.1188	0.1482	0.2096	0.1730
F3	0.0657	0.0855	0.0928	0.1349	0.1191
FC5	0.0760	0.0911	0.1017	0.1456	0.1238
T7	0.0819	0.1205	0.1453	0.2039	0.1937
P7	0.0800	0.1138	0.1390	0.2175	0.2085
O1	0.0695	0.0880	0.0982	0.1435	0.1189
O2	0.0643	0.0766	0.0862	0.1401	0.1196
P8	0.0774	0.1199	0.1285	0.2044	0.1595
T8	0.0316	0.0688	0.0744	0.0471	0.0930
FC6	0.0645	0.0857	0.0959	0.1416	0.1075
F4	0.0671	0.0858	0.0892	0.1037	0.1268
F8	0.0818	0.1137	0.1397	0.1927	0.2140
AF4	0.0860	0.1197	0.1453	0.2234	0.2320

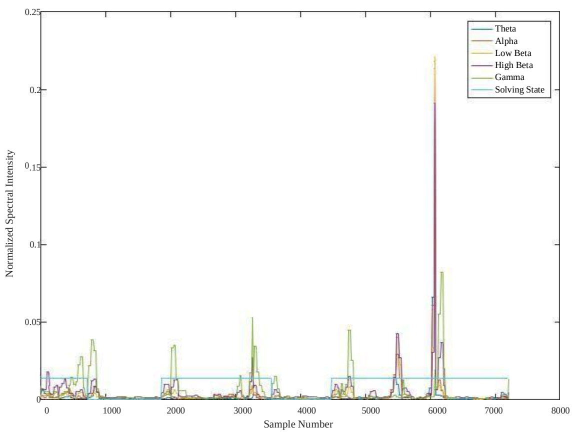

Fig. 2. Normalized Spectral Intensity of frequency bands vs Sample Number for user A's AF4 electrode. Figure also shows whether subject was solving/not solving at any particular time.

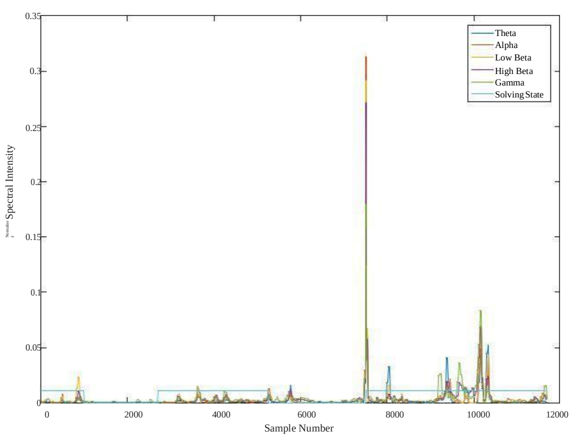

Fig. 3. Normalized Spectral Intensity of frequency bands vs Sample Number for user B's AF4 electrode. Figure also shows whether subject was solving/not solving at any particular time.

mental state of not solving while 1 corresponded to a mental state of solving a particular arithmetic problem. Principal Component Analysis (PCA) was used to reduce the dimensionality of the data set. The PCA was aimed at retaining at least 95% explained variance in the dataset post exclusion of the excess components. It could be seen from Fig. 4 that more than 95% variance was explained by a single component and hence only a single component was retained after training. The data set was cross validated using 5 folds.

We compare of the performance of several machine learning algorithms in Table II. The table shows validation accuracy, the number of observations that the algorithm predicted in a second and the time taken to train the classifier. As our aim was to develop a real time application, the prediction speed played an important role in the performance analysis. It can be seen from the table that Ensemble and KNN classifiers

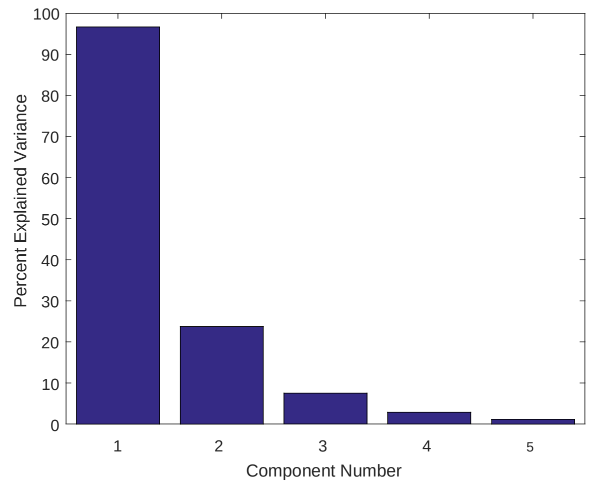

Fig. 4. Percent explained variance versus component in Principal Component Analysis.

outperform Tree, Discriminant, Regression and SVM classifiers in terms of validation accuracy. Furthermore, from the high accuracy achieving classifiers the Fine KNN had the fastest prediction speed and lowest training time and hence was selected as the predictor for the real time system with the parameters mentioned in the experimental methods section.

After developing the system shown in Fig.1 using the Fine KNN parameters, the experiment was conducted on an additional subject and it was found that the system was providing an accuracy of 70.6% on the predictions of solving state being displayed in real time. For classification of the stored data, Fine KNN, Medium KNN, Cubic KNN, Weighted KNN, Bagged Tree Ensemble, and Subspace KNN Ensemble displayed the best performance with accuracies above 99%. The results indicate that the proposed method yields high classification accuracy for stored data and is accurate and fast enough to perform real time prediction. Faster data acquisition is obtained by reducing the number of scanned electrodes and dimensionality reduction leads to better classification speeds. This, coupled with the high performance of a simple algorithm like KNN enabled the real time aspect. Another significance is that the algorithm performs well despite varying complexity of the arithmetic task.

IV. Conclusions

This paper presented a method to classify and predict the cognitive skill of solving or not solving an arithmetic problem by an individual with a high degree of accuracy using simple machine learning algorithms. The algorithm was employed to make predictions based on real time EEG signals and the prediction accuracy with KNN classification algorithm was found out to be as high as 70.6%. It is believed that this algorithm can be integrated into applications for cognitive re-search, like identifying classroom teaching techniques that can help students better engage with cognitive tasks or detection of

TABLE II
PERFORMANCE COMPARISON OF VARIOUS CLASSIFICATION ALGORITHMS.

Algorithm	Accuracy	Prediction Speed	Training Time
Complex Tree	67.7%	430000 obs/sec	2.4866 secs
Medium Tree	63.3%	480000 obs/sec	2.1011 secs
Simple Tree	61.3%	480000 obs/sec	1.9679 secs
Linear Discriminant	61.3%	410000 obs/sec	2.1025 secs
Quadratic Discriminant	41.0%	410000 obs/sec	2.0192 secs
Logistic Regression	61.3%	400000 obs/sec	3.9651 secs
Linear SVM	43.9%	79000 obs/sec	13031 secs
Quadratic SVM	61.3%	500000 obs/sec	8394.1 secs
Cubic SVM	61.3%	400000 obs/sec	2568.7 secs
Fine Gaussian SVM	61.3%	960 obs/sec	1765 secs
Medium Gaussian SVM	61.3%	980 obs/sec	1079.6 secs
Coarse Gaussian SVM	61.3%	1000 obs/sec	1047.5 secs
Fine KNN	100%	91000 obs/sec	3.5856 secs
Medium KNN	99.9%	69000 obs/sec	4.0504 secs
Coarse KNN	76.0%	36000 obs/sec	6.1258 secs
Cosine KNN	61.3%	1400 obs/sec	115.05 secs
Cubic KNN	99.9%	63000 obs/sec	4.2279 secs
Weighted KNN	100%	68000 obs/sec	4.0634 secs
Boosted Trees Ensemble	62.5%	68000 obs/sec	25.699 secs
Bagged Trees Ensemble	100%	35000 obs/sec	42.467 secs
Subspace Discriminant Ensemble	61.3%	71000 obs/sec	13.008 secs
Subspace KNN Ensemble	100%	2500 obs/sec	87.864 secs
RUSBoosted Trees Ensemble	58.0%	75000 obs/sec	29.593 secs

certain learning disabilities from patterns of EEG signal while engaged in tasks.

ACKNOWLEDGMENT

The authors thank the Head of Department, Department of Electrical and Electronics Engineering, BITS Pilani, KK Birla Goa Campus for providing us with the lab facility to perform the experiments. The authors also acknowledge Mr. Pushparaj M Paradkar, Senior Technical Assistant, for extending his help and support to accomplish this work.

REFERENCES

[1] R. J. Larsen and E. Diener, ser. Review of personality and social psychology, No. 13. Thousand Oaks, CA, US: Sage Publications, Inc, 1992, ch. Promises and problems with the circumplex model of emotion., pp. 25–59.

[2] R. Xia and Y. Liu, "Using i-vector space model for emotion recognition," in INTERSPEECH, 2012.

[3] T. Danisman and A. Alpkocak, "Feeler: Emotion classification of text using vector space model," in Proceedings of the ASIB 2008 Symposium on Affective Language in Human and Machine, Vol. 2, 2008.

[4] D. C. Rubin and J. M. Talarico, "A comparison of dimensional models of emotion: Evidence from emotions, prototypical events, autobiographical memories, and words," Memory, vol. 17, no. 8, pp. 802–808, Nov 2009, 19691001[pmid]. [Online]. Available: http://www.ncbi.nlm.nih.gov/pmc/articles/PMC2784275/

[5] F. M. Citron, M. A. Gray, H. D. Critchley, B. S. Weekes, and E. C. Ferstl, "Emotional valence and arousal affect reading in an interactive way: Neuroimaging evidence for an approach-withdrawal framework," Neuropsychologia, vol. 56, no. 100, pp. 79–89, Apr 2014, s0028-3932(14)00006-2[PII]. [Online]. Available: http://www.ncbi.nlm.nih.gov/pmc/articles/PMC4098114/

[6] A. B. Eder and K. Rothermund, "Automatic influence of arousal information on evaluative processing: Valence-arousal interactions in an affective simon task," Cognition and Emotion, vol. 24, no. 6, pp. 1053–1061, 2010. [Online]. Available: https://doi.org/10.1080/02699930903056836

[7] M. D. Robinson, J. Storbeck, B. P. Meier, and B. S. Kirkeby, "Watch out! that could be dangerous: Valence-arousal interactions in evaluative processing," Personality and Social Psychology Bulletin, vol. 30, no. 11, pp. 1472–1484, 2004, pMID: 15448310. [Online]. Available: https://doi.org/10.1177/0146167204266647

[8] A. Oswal, V. Litvak, P. Brown, M. Woolrich, and G. Barnes, "Optimising beamformer regions of interest analysis," NeuroImage, vol. 102, no. Part 2, pp. 945 – 954, 2014. [Online]. Available: http://www.sciencedirect.com/science/article/pii/S1053811914006806

[9] A. Rodriguez-Rivera, B. V. Baryshnikov, B. D. V. Veen, and R. T. Wakai, "Meg and eeg source localization in beamspace," IEEE Transactions on Biomedical Engineering, vol. 53, no. 3, pp. 430–441, March 2006.

[10] E. K. Miller, "The prefontral cortex and cognitive control," Nature Reviews Neuroscience, vol. 1, pp. 59 EP –, Oct 2000, review Article. [Online]. Available: http://dx.doi.org/10.1038/35036228

[11] T. Mondejar,´ R. Hervas,´ E. Johnson, C. Gutierrez,´ and J. M. Latorre, "Correlation between videogame mechanics and executive functions through eeg analysis," Journal of biomedical informatics, vol. 63, pp. 131–140, 2016.

[12] Y.-P. Lin, S.-H. Hsu, and T.-P. Jung, Exploring Day-to-Day Variability in the Relations Between Emotion and EEG Signals. Cham: Springer International Publishing, 2015, pp. 461–469.

[13] H. U. Amin, W. Mumtaz, A. R. Subhani, M. N. M. Saad, and A. S. Malik, "Classification of eeg signals based on pattern recognition approach," Frontiers in Computational Neuroscience, vol. 11, p. 103, 2017. [Online]. Available: https://www.frontiersin.org/article/10.3389/fncom.2017.00103

[14] H. U. Amin, A. S. Malik, R. F. Ahmad, N. Badruddin, N. Kamel, M. Hussain, and W.-T. Chooi, "Feature extraction and classification for eeg signals using wavelet transform and machine learning techniques," Australasian Physical & Engineering Sciences in Medicine, vol. 38, no. 1, pp. 139–149, Mar 2015. [Online]. Available: https://doi.org/10.1007/s13246-015-0333-x

[15] M. Z. Ilyas, P. Saad, M. I. Ahmad, and A. R. I. Ghani, "Classification of eeg signals for brain-computer interface applications: Performance comparison," in 2016 International Conference on Robotics, Automation and Sciences (ICORAS), Nov 2016, pp. 1–4.

[16] A. S. Al-Fahoum and A. A. Al-Fraihat, "Methods of eeg signal features extraction using linear analysis in frequency and time-frequency domains," ISRN Neurosci, vol. 2014, p. 730218, Feb 2014, 24967316[pmid]. [Online]. Available: http://www.ncbi.nlm.nih.gov/pmc/articles/PMC4045570/

ISBN 978-1-5386-4473-7
IEEE sponsored 4th International Conference on Biosignals, Images and Instrumentation, SSNCE, Chennai. ICBSII 2018 – 22nd-24thMar'18

Comparison of envelope detection and signal normalization methods for foetal heart rate extraction from foetal heart sound

Amrutha B
Centre for Product Design and Manufacturing
Indian Institute of Science
Bangalore, India
amruthab@iisc.ac.in

Manish Arora
Centre for Product Design and Manufacturing
Indian Institute of Science
Bangalore, India
marora@iisc.ac.in

***Abstract*— Foetal heart rate is an important indicator of foetal well-being which indicates fetal distress during antepartum and intrapartum period. This paper provides systematic comparison of four different methods envelope detection and four different methods of signal normalization to determine the fetal heart rate from fetal heart sound. To obtain the ground truth, each heart beat was manually identified by visualizing the sound recording on a computer screen. Four different measure of error are used compare various combinations of envelop detection and normalization methods. It is found that the homomorphic filtering gave highest accuracy. Choice of normalization methods did not affect accuracy measurement in most cases.**

Keywords—fetal heart sound;envelope;

I. Introduction

Though the first observation of foetal heart sound was reported during the 17th, it was Lejumeau Kergaradec who reported the usefulness of the auscultation in diagnosis of twins, foetal lie and presentation during the pregnancy [1]. Foetal heart rate is an important parameter in the assessment of foetal wellbeing both intrapartum and antepartum, Kilian was the first to propose that changes in heart rate can be used to diagnose foetal distress and to indicate the time for clinical intervention [1]. The normal range of foetal heart rate(FHR) is 120-160bpm.The foetal heart rate helps in assessing various conditions: hypoxia, asphyxia, foetal bradycardia(<110bpm) and foetal tachycardia (>160 bpm). Apart from directly listening to the foetal heart sounds using stethoscope or pinard cone, various devices are currently in use for monitoring foetal heart rate: foetal Doppler, foetal electrocardiography(fECG), foetal magnetocardiography(fMC) and foetal phonocardiography(fPCG) [2].The foetal cardiotocography(CTG) which is used in Non-Stress Test includes two transducers: one for measuring the foetal heart rate and the other one for uterine activity. In CTG machine, the foetal heart rate is measured using Doppler ultrasound. It is the most widely used method to monitor the foetal heart rate. Foetal Doppler probe exposes foetus to Ultrasound waves and shift in frequency of the reflected signal is used to detect the heart motion. The fECG obtained due to electrical activity of the heart is of two types namely: Direct and Indirect. The direct method uses fetal scalp electrode to obtain the signal whereas indirect methods uses electrode placed on maternal abdomen to obtain the signal and can be done from the 16th week of pregnancy but the signal may contain various artifacts along with maternal electrocardiogram, therefore various advanced signal processing techniques must be applied to obtain fECG [3]. The amplitude of the fECG also decreases in 28-32 week of pregnancy due to vernix caseosa surrounding the foetus [4]. Foetal Magenetocardiogram is the recording of the magnetic field produced by the electrical activity of the heart. It is recorded by squid array placed over maternal abdomen and measuring foetal and maternal magentocadiographic signals [5]. The fMCG is extracted and the heart rate is calculated. The major disadvantage of this method includes: cost, trained staff required, no long term monitoring. In fPCG, natural acoustic signals from the maternal abdomen are acquired using electronic stethoscope to assess the foetal wellbeing. Though this approach is non-invasive and requires simpler instrumentation, the foetal heart rate measurement in this approach has two problems: firstly, the intensity of the foetal heart sound is low compared to the interference signals such as digestive sounds or the signals from the environment. Secondly, the intensity and the frequency varies depending on the position of the foetus (occiput anterior position/occiput posterior position) [6].

A preliminary evaluation foetal heart sounds is reported in [7] to determine the foetal heart sound characteristics between intrauterine growth retarded foetus and normal foetus and gave a pathway to use the heart sound to determine the foetal wellbeing. Various signal processing techniques reported in the literature for extraction of fetal heart rate include: autocorrelation method, S1 heart sound positions, repetition frequency determination and blind source separation. In autocorrelation based method, the signal is passed through a bandpass filter followed by envelope detection and autocorrelation of the signal [6]. Matched filtering or other de-noising techniques can be used before the envelope

ISBN 978-1-5386-4473-7
IEEE sponsored 4th International Conference on Biosignals, Images and Instrumentation, SSNCE, Chennai. ICBSII 2018 – 22nd-24thMar'18

detection and autocorrelation step to improve the accuracy of FHR measurement. Methods using S1 heart sound positions determines the FHR by locating the S1 heart sound in the signal [9,10,11,12]. The heart sounds are repetitive in nature, therefore a method which describes tracking these frequency repetition to determine the heart rate and tested in the noisy environment using the simulated data from the physionet is proposed by Tang. *et.al* [13] Single channel blind source separation uses empirical mode decomposition and Nonnegative matrix factorization to extract the fPCG and the FHR is determined [14]. Though more advanced techniques are being proposed requiring additional computational resources, there is no comparison available in literature on adequacy of these approaches using real clinical data.

Though various signal processing techniques are proposed in literatures, there is no insight whether the techniques can be used in resource limited settings. This paper systematically compares various methods suitable for implementation on low cost electronics formed by combination of various envelope detection approaches named: Shannon Energy envelope, Hilbert Envelope, Full wave rectification and low pass filter (FWR-LPF) and Homomorphic envelope along with four common normalization techniques to determine the best performing foetal heart rate extraction method for resource limited settings.

II. METHODOLOGY

The heart sound contains two major heart sounds S1 (due to atrioventricular valve closure) and S2 (due to closure of semilunar valve) occurring at different time intervals. The time interval between first heart sound and second heart sound is shorter compared to adults. Therefore, during auscultation typically only one dominant sound is heard in the case of foetal [14]. The various methods to extract heart rate is tested on randomly selected 15 datasets from 26 datasets made available by Ruffo *et al.* on physionet [10, 15]. To determine the accuracy of various methods, a benchmark is needed against which the heart rate readings can be compared. The benchmark used in this case is the reference HR measurements determined by manually annotated heart sound positions similar to method used by Springer *et al.* [16].

A. Reference Heart Rate Measurement

The reference HR measurements were computed by manually detecting heart sound positions in every 4s window of one-minute-long data resulting in 15 HR measurements for a subject. In each of the 4s window, the median time interval between detected peaks is calculated to determine the HR[16]. The process is repeated for remaining datasets to obtain the reference HR resulting in total of 210 measurements. An example of the manually detected S1 positions is shown in Fig 1.

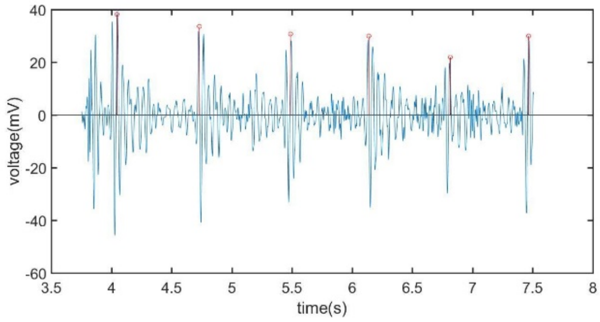

Fig.1 Manually Annotated S1 positions

III. ANALYSIS OF FOETAL HEART SOUND

The automated heart rate estimation is done using a total of 16 methods (combination of 4 envelope detection methods and 4 normalization methods).

A. Pre-processing

Prior to envelop detection, filtering of foetal heart sound is done using band pass butterworth filter with the passband of 30-150 Hz and filter order of 3.

B. Envelope Detection

(i) FWR-LPF

The FWR-LPF is type of envelope detection method where the signal is full wave rectified followed by low pass butterworth filter of order 3 at 50 Hz to remove unwanted frequencies.

(ii) Hilbert Envelope:

The Hilbert envelope is obtained by determining the absolute value of the analytic signal, the analytic signal is nothing but the addition of the original signal with the hilbert transform of the original signal to form a complex signal given by:

$$z(n) = x(n) + j\acute{x}(n) \tag{2}$$

Where,
Z(n) is the analytic signal
x(n) is the original signal
$\acute{x}$(n) is the Hilbert transform of x(n)

The Hilbert transform of the signal is determined by:

$$\acute{x}(n) = \frac{1}{\pi}\int_{-\infty}^{\infty}\frac{x(u)}{\pi-u}du \tag{3}$$

(iii) Homomorphic Filter:
Homomorphic filtering is mostly used in image processing for image enhancement. It transforms the original signal into another domain, where the linear filter is applied to remove unwanted components, then transformed to the original signal. The homomorphic filtering process is explained below:

ISBN 978-1-5386-4473-7

A signal can be considered to have a slow varying component and a fast varying component [18] shown in the equation below:

$$x(t) = m(t) * f(t) \quad (4)$$

where,
m(t) - slow varying part in the signal.
f(t) - fast varying part in the signal.

Applying logarithm to the above equation, we get

$$\ln(x(t)) = \ln(m(t) * f(t)) \quad (5)$$

The envelope of the signal is extracted by low pass filtering (LPF)the signal at 50 Hz after log transformations to remove high frequency f(t)

$$LPF(ln(x(t))) = LPF(ln(m(t)) + ln(f(t))) \quad (6)$$

$$(ln(x(t))) = (ln(m(t)) \quad (7)$$

Finally, the envelope is obtained by taking exponential of the above term.

(iv) Shannon Envelope:
The Shannon envelope is based on the Shannon energy given by the formula:

$$Z_{Es} = \frac{1}{N}\sum_{n=1}^{N} x(n)^2 * \log(x(n))^2 \quad (8)$$

where,
x(n) is the original signal.

The envelope is determined by taking a window of length of 0.02s and overlapping segment of 0.01s [18,19]. The Shannon envelope has the property of accentuating medium intensity signals, while attenuating the low and high intensity signals.

C. Normalization Methods

After the envelope detection, normalization of the signal is done to limit variation between the signal obtained from various subjects, four normalization methods were investigated: Maximum amplitude in the signal, Subtracting the mean and dividing by the percentile value in the signal [18], dividing by root mean square of the signal and lastly subtracting the mean and dividing by the standard deviation. All the four normalization methods were applied to above explained envelope detection methods.

D. Autocorrelation

The autocorrelation of the signal is taken after normalizing the Envelope signal. It is defined as:

$$R_x(m) = \frac{1}{N-|m|}\sum_{m=1}^{N-1-m} z(n) * z(n+m) \quad (9)$$

Where,
z(n) is the signal after envelope.
z(n+m) is the shifted version of the signal s(n)

As seen from the equation above, autocorrelation measures the similarity between the original signal and its shifted version for a series of time interval. It gives lag versus correlation graph. The autocorrelation graph is Fig. 2

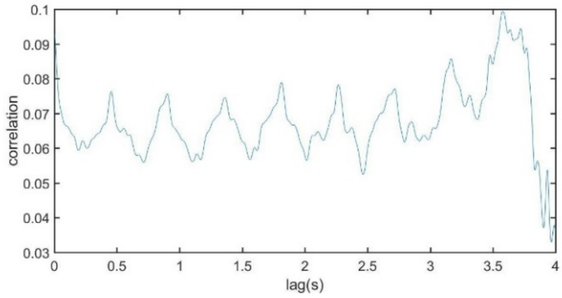

Fig. 2: Autocorrelation of the signal after normalization

E. Heart Rate Estimation Method

The Peaks are detected in the auto correlation waveform using the equation:

$$R_x(m)-R_x(m-1)>0 \quad (10)$$

$$R_x(m)-R_x(m+1) <0 \quad (11)$$

This method computes the maximum peak in the permissible range 0.3s -0.75s [12] in the auto-correlation waveform which corresponds to 80 to 200 bpm. The heart rate is calculated as:

HR=60/lag (maximum peak) bpm (12)

IV. RESULT

The difference between the reference HR measurements and the measurements obtained after the automated HR estimation algorithms is computed to compare the accuracy of these methods. (i) Fraction of results within 5% of reference measurement (5% tolerance), (ii) 10% tolerance, (iii) Mean Absolute Error (MAE) (iv) Root Mean Squared Error (RMSE)

A. 5% and 10% tolerance:

Absolute difference between automated HR measurements and reference measurements is obtained and the fraction of measurements that are not within the 5% or 10% of reference HR measurements are calculated and shown in in Fig.3 &4 respectively. Results show minor variation between various normalization and HR estimations methods. 70-75% of the measurements are within 5% of the reference values and 82-88% are within 10% of the reference value.

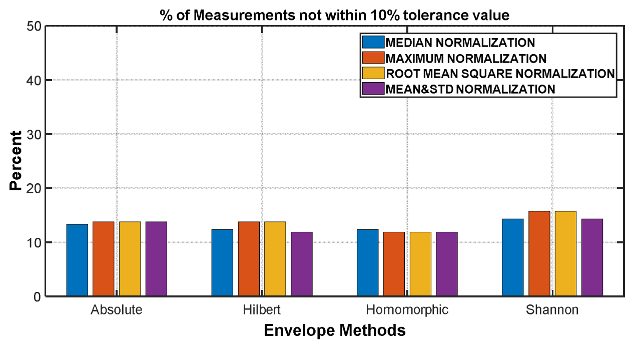

Fig.3. Fraction of measurements not within 10% of HR reference measurements

ISBN 978-1-5386-4473-7

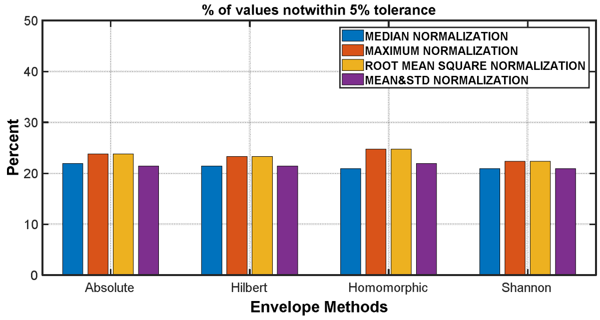

Fig.4. Fraction of measurements not within 5% of HR reference measurements

B.Mean absolute and Root mean square error

Mean absolute error and root mean square error measures how far the estimated value is from the actual value. The estimated value here is the automated HR and the actual value is the manual measurement. The RMSE and MAE is calculated by using the formula in eq. 13 and 14 respectively:

$$MAE = \frac{1}{n}\sum(absolute(Xa - Xe)) \qquad (13)$$

$$RMSE = \sqrt{\frac{1}{n}\sum(Xa - Xe)^2} \qquad (14)$$

Where,
n= total number of values
Xa = Reference Value from manual measurement
Xe=Estimated Value from automated HR algorithm

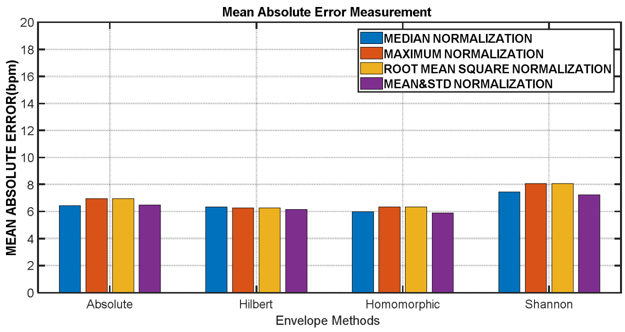

Fig.5: Mean Absolute Error

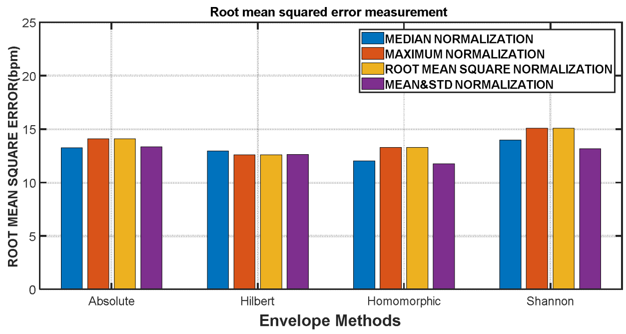

Fig.6: Root mean squared error

The comparison of various envelope techniques and normalization method is done to determine which combination gives better heart rate estimates when used with auto-correlation technique. It is seen from the above results that the heart rate determination accuracy at 10% shows homomorphic envelope gives better results and at 5% hilbert envelope gives better results even though the variation of accuracy among the envelope methods is only 1-2%. Similarly, the MAE and RMSE also shows only 1-3bpm difference among the envelope methods. Thus, no significant difference is seen among the various methods used in this paper. In order to see how well the automated methods, agree with the manual measurements over the range of heart rate values a Bland-Altman difference plot is shown in Fig.7

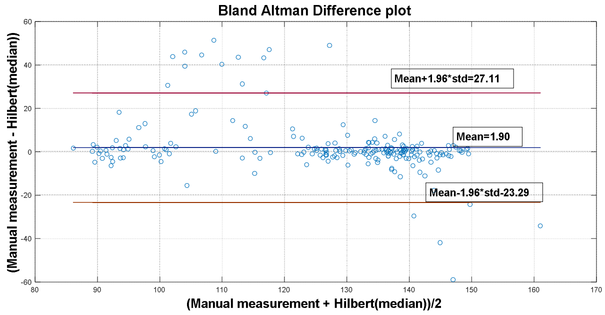

Fig.7: Bland-Altman difference Plot of hilbert(Median) and difference between hilbert(Median) and Gold standard

The plot shows a good agreement between the manual measurement and hilbert(median) except in the range of 110-120bpm, this trend is seen in all the Bland-Altman plot of for other normalizations envelope detection technique. This may be due autocorrelation peak being wrongly identified for this range HR values. Autocorrelation plots show multiple peaks with similar amplitude (figures not shown). The wrong peak detection in the autocorrelation plots can be avoided by either validating the detected peaks or by using advanced signal processing techniques such as Wavelet denoising, cyclostationary analysis [13] or single channel blind source separation [14] to effectively remove the noise and erroneous peaks.

CONCLUSION & DISCUSSION

This paper, compares of 16 combinations of envelope detection methods and normalization technique to manually extracted fetal heart rate measurements. These techniques are tested on the clinical data from the Physionet and a total of 210 measurements and accuracy measurements are obtained for each of the combination of envelop detection method and normalization technique. The accuracy of heart rate detection is about 79% for 5% tolerance and 85% for 10% tolerance respectively but no significant difference are obtained between various combination envelop detection methods and normalizations techniques; Further improvement to the algorithm can be done by applying advanced signal processing techniques namely: wavelet denoising, single channel blind source separation, and cyclostationary signal processing, therefore the future work includes implementing the above processing techniques and comparing them with methods explored for and manual measurement being used as gold standard.

REFERENCE

[1] Freeman, Roger K., et al. *Fetal heart rate monitoring*. Lippincott Williams & Wilkins, 2012.

[2] Chourasia, V., and A. Mittra. "Passive acoustic signal acquisition system for non-invasive fetal heart sound monitoring applications." *Internet J. Med. Technol* 5.1 (2009): 1-7.

[3] Kupka, T., et al. "Timing events in Doppler ultrasound signal of fetal heart activity." *Engineering in Medicine and Biology Society, 2004. IEMBS'04. 26th Annual International Conference of the IEEE*. Vol. 1. IEEE, 2004.

[4] Oostendorp, T. F., A. Van Oosterom, and H. W. Jongsma. "Electrical properties of tissues involved in the conduction of foetal ECG." *Medical and Biological Engineering and Computing* 27.3 (1989): 322-324.

[5] Gutiérrez, D., et al. "On-line fetal heart rate monitoring using SQUID sensor arrays." *Proc. 14th Biennial BIOMAG Conf*. 2004

[6] Zahorian, Stephen A., Allan J. Zuckerwar, and Montri Karnjanadecha. "Dual transmission model and related spectral content of the fetal heart sounds." *Computer methods and programs in biomedicine* 108.1 (2012): 20-27.

[7] Baskaran, A., and N. Sivalingam. "Fetal heart sound analysis: a preliminary evaluation." *The Medical journal of Malaysia* 51.1 (1996): 64-67

[8] Kovacs, F., et al. "Long-term phonocardiographic fetal home monitoring for telemedicine systems." *Engineering in Medicine and Biology Society, 2005. IEEE-EMBS 2005. 27th Annual International Conference of the*. IEEE, 2006

[9] Chourasia, Vijay S., Anil Kumar Tiwari, and Ranjan Gangopadhyay. "A novel approach for phonocardiographic signals processing to make possible fetal heart rate evaluations." *Digital Signal Processing* 30 (2014): 165-183.

[10] Ruffo, Mariano, et al. "An algorithm for FHR estimation from foetal phonocardiographic signals." *Biomedical Signal Processing and Control* 5.2 (2010): 131-141.

[11] Vargas, C. G., and G. Valencia. "Comparison of abdominal ECG and phonocardiography for instantaneous fetal heart rate detection." *Engineering in Medicine and Biology Society, 1995., IEEE 17th Annual Conference*. Vol. 1. IEEE, 1995.

[12]Varady, Peter, et al. "An advanced method in fetal phonocardiography." *Computer Methods and programs in Biomedicine* 71.3 (2003): 283-296.

[13] Tang, Hong, et al. "Fetal Heart Rate Monitoring from Phonocardiograph Signal Using Repetition Frequency of Heart Sounds." *Journal of Electrical and Computer Engineering* 2016 (2016).

[14]Samieinasab, Maryam, and Reza Sameni. "Fetal phonocardiogram extraction using single channel blind source separation." *Electrical Engineering (ICEE), 2015 23rd Iranian Conference on*. IEEE, 2015.

[15]Goldberger, Ary L., et al. "Physiobank, physiotoolkit, and physionet." *Circulation* 101.23 (2000): e215-e220.

[16] Springer, David B., et al. "Robust heart rate estimation from noisy phonocardiograms." *Computing in Cardiology Conference (CinC), 2014*. IEEE, 2014.

[17] Goovaerts, H. G., et al. "Recording and processing of fetal movements and sounds obtained with the Inpho inductive transducer." *Medical and Biological Engineering and Computing*29.6 (1991): NS20

[18] Gupta, Cota Navin, et al. "Neural network classification of homomorphic segmented heart sounds." *Applied Soft Computing*7.1 (2007): 286-297

[19] Choi, Samjin, and Zhongwei Jiang. "Comparison of envelope extraction algorithms for cardiac sound signal segmentation." *Expert Systems with Applications* 34.2 (2008): 1056-1069..

[20] Liang, H., S. Lukkarinen, and I. Hartimo. "Heart sound segmentation algorithm based on heart sound envelogram." *Computers in Cardiology 1997*. IEEE, 1997.

[21] Schmidt, S. E., et al. "Segmentation of heart sound recordings by a duration-dependent hidden Markov model." *Physiological measurement* 31.4 (2010): 513.

[22] Hassani, K., et al. "Heart sound segmentation based on homomorphic filtering." *Perfusion* 29.4 (2014): 351-359.

ISBN 978-1-5386-4473-7
IEEE sponsored 4th International Conference on Biosignals, Images and Instrumentation, SSNCE, Chennai. ICBSII 2018 – 22nd-24thMar'18

Epileptic Seizure Detection using wavelets and EMD

Shaik. Jakeer Hussain
Professor, Departmet of Electronics and Communication Engineering
Vignan's Foundation for Science, Technology & Research
Vadlamudi Guntur Dist-522213 A.P, India
Jk.shaik@gmail.com

Abstract **— Complex information about the brain dynamics is given by Electroencephalography (EEG). For identifying epileptic seizures, skilled interpreters are required and it is difficult. Unexpected occurrence of seizure disturbs the quality of life and causes physical damage. This paper uses methods such as Discrete Wavelet Transform and Empirical Mode Decomposition for extraction of features from EEG and detection of epilepsy. This paper describes what wavelet is chosen for analysis and why is it suitable for this study. It also talks about the number of levels of decomposition of the wavelet and why. EMD is another tool used for signal decomposition. The Detection of epileptic seizures using wavelets and EMD gave results of good accuracy of over 92% for single and multiple subjects. It can be used as a clinical application for the diagnosis and effective epilepsy management.**

Keywords— Electroencephalogram (EEG) signals, Epileptic Seizures, Discrete wavelet transform (DWT), Empirical Mode Decomposition (EMD).

I. INTRODUCTION

Out of many neurological disorders epilepsy is the one which is most common which is seen in 0.6–0.8% of the world's population. While the patients who achieve sufficient seizure control are nearly two-thirds, they do it from anticonvulsive medication, while the other 8–10% could benefit from respective surgery. For the rest of the significant 25% of patients, no sufficient treatment is currently available. The epilepsy is characterized by a sudden and recurrent malfunction of the brain, which is termed "seizure." Epileptic seizures reflect the clinical signs of an excessive and hyper synchronous activity of neurons in the brain. Visual examination of recordings of EEG for inter-ictal and ictal activities by an experienced neurophysiologist is used for epilepsy detection. There are serious shortcomings if visual review of the vast amount of EEG data is done.

If seizures are long and unstoppable, they may cause irrevocable harm to the brain. The mainstay of treatment of epilepsy, today, is primarily pharmacological. Anticonvulsant drugs are taken daily, in fixed doses, titrated to get a steady state blood concentration. There are multiple frequency domain techniques available for epileptic seizure detection. Frequency Domain methods are. The Welch method for instance, computes the power spectrum by dividing the data into segments of successive blocks. The mean of the periodograms computed from each of the blocks is taken as an estimate for the Power Spectral Density. A notable example for the use of the Welch method is system of two-class epilepsy detection proposed by Polat and Gunes [2].

Frequency methods are rather inadequate in providing information pertaining to both time and frequency domains simultaneously. In cases dealing with event related potentials, events are localized in both time and frequency domains [1] [3]. Wavelets were introduced to bridge this gap and to provide additional information pertaining to signal's instability and randomness. Of late, methods utilizing wavelet techniques have become increasingly pervasive. Wavelet analysis can be used as a tool for analyzing the signal at different frequency bands [4].

A wavelet can be considered as a small function which is correlated with the original signal at each level of signal decomposition and at each time instance. This function is referred to as the "mother wavelet". Wavelets are advantageous over Fourier based methods as they give precise time information at high frequencies and vice-versa. This implies that EEG signals can be separated into their bands along with noise, artifacts and seizure related spikes [5]. The Continuous Wavelet Transform (CWT) and the Discrete Wavelet Transform (DWT) are two techniques employed in this regard.

The DWT employs "cascading low-pass and high-pass filters and the signal is down-sampled at each stage in a process called as multi resolution decomposition. Subasi [6], leveraged DWT in their work pertaining to automated detection of epilepsy [7][8]".

The Hilbert-Huang Transform (HHT) is a technique that employs the Hilbert spectral analysis in conjunction with Empirical Mode Decomposition (EMD) to split the signal into its characteristic oscillatory components. These oscillatory parts are dubbed as Intrinsic Mode Functions (IMFs). This property of segregation of IMF`s was put into use to separate seizure and non seizure data [9] and Pachori et al[10] [11] [12] has shown very good results for extracting features from the EEG signals [9]. The HHT is adaptive in nature [13][14]and is non-linear in its approach.

ISBN 978-1-5386-4473-7

II. Materials and Methods

2.1 Experimental Data

The CHB-MIT scalp EEG database [16] is being used for Seizure localization and prediction. This database collected at Boston hospital for children has EEG recordings from paediatric subjects with obstinate seizures. Monitoring of patients for several days following abandonment of anti-seizure drugs in order to characterize the seizures and gauge their candidature for surgical intercession was performed. Recordings that were heaped into 23 cases were taken from 22 subjects (five males aged between 3 to 22; and 17 females aged between one and a half to nineteen), (Case chb21 and case chb01 belong to the same female patient but at different ages having a gap of 1.5 years). Sampling rate with 16-bit resolution was 256 samples per second.

2.2 Wavelets

Wavelet transform is a powerful mathematical tool for characterization of non stationary signals. It is adaptive and has multi resolution capability, thus making it suitable for decomposing EEG signals of varying time and frequency resolutions [17].

The concept of Wavelets is briefed below:

The family of wavelets is generated by scaling (s) and translating (τ) a mother wavelet. The condition to qualify as a mother wavelet is that it should satisfy the admissibility condition [18]

$$\int_{-\infty}^{\infty} \frac{|\Psi(f)|^2}{(f)} df < \infty \quad \text{->} \quad (1)$$

where $\Psi(f)$ is the frequency domain expression of the time domain wavelet function $\psi(t)$. The implication of the admissibility condition is that the Fourier transform of the wavelet function $\psi(t)$ becomes zero at zero frequency i.e.

$$\left|\Psi(f)^2\right|_{f=0} = 0 \quad \text{->} \quad (2)$$

From the equation 2, it can be seen that the wavelet has a band-pass spectrum which also means that the average value of the wavelet $\psi(t)$ in the time domain is zero.

$$\int_{-\infty}^{\infty} \psi(t)dt = 0 \quad \text{->} \quad (3)$$

The process of stretching or squeezing the mother wavelet function by 1/s is called as scaling, shifting along the time axis by τ called as translation. These operations result in a wavelet function defined as

$$\psi_{\tau,s} = \frac{1}{\sqrt{s}} \psi\left(\frac{t-\tau}{s}\right) \qquad \tau, s \in R \;\; s > 0 \qquad (4)$$

The continuous wavelet transform [CWT] of a signal x(t) is defined as the inner product of the signal with the wavelet functions and is represented as:

$$wt(s,\tau) = \frac{1}{\sqrt{s}} \int_{-\infty}^{\infty} x(t)\psi^*\left(\frac{t-\tau}{s}\right)dt \quad \text{->} \quad (5)$$

The CWT provides highly redundant information because the parameters s and τ are varied continuously. This repetitive information requires a large amount of resources and time for computation [17]. In order to reduce the redundancy of the information, discrete values of scale and translation parameters are used.

The discrete wavelet transform [DWT] is not an exact discrete transform though it mimics as one in the computer. In strict terms, the discrete wavelet series is merely a sampled version of the continuous wavelet series. In this work, DWT has been used for the time–frequency analysis (a key feature of DWT) on EEG signals whose basis is a wavelet. In Discrete wavelet Transform (DWT) the scale and translation parameters are discretized as represented in equation 6. [18]

$$\left.\begin{aligned} & s = s_0^j \\ & \tau = k\tau_0 s_0^j \\ & s_0 > 1 \\ & \tau_0 \neq 0 \\ & k \in z \end{aligned}\right\} \quad \text{->}(6)$$

Thus, from equations 4 and 6, the discrete wavelet can be represented as:

$$\psi_{s,\tau}(t) = \frac{1}{\sqrt{s_0^j}} \psi\left(\frac{t - k\tau_0 s_0^j}{s_0^j}\right) \quad \text{->} \quad (7\text{ a})$$

The DWT provides sufficient information both for analysis and synthesis of the original signal, with a significant reduction in the computation time compared to CWT. The decomposition of the signal (scaling and shifting process in time is nothing but performing high pass and low pass filtering and can be denoted as filter banks) generates a set of wavelet coefficients. Thus, there is a possibility to reconstruct the original signal as a linear combination of the wavelet coefficients multiplied by the corresponding wavelet functions.

To reconstruct the original signal from wavelet coefficients s_0=2 and $s_0 = 2$ are chosen which satisfies the wavelet tight frame condition then the DWT in equation 7a becomes equation 7b[18],

$$\psi_{j,k}(t) = \frac{1}{\sqrt{2^j}} \psi\left(\frac{t - k2^j}{2^j}\right) \quad \text{->} \quad (7b)$$

The above tight frame condition allows to select the base wavelet constituting an orthogonal basis. The Multi Resolution Analysis [MRA] forms the foundation in constructing a base wavelet satisfying orthogonality.

A Multi Resolution Analysis (MRA) of the space $L^2(R)$ consists of successive approximation sub spaces

ISBN 978-1-5386-4473-7
IEEE sponsored 4th International Conference on Biosignals, Images and Instrumentation, SSNCE, Chennai. ICBSII 2018 – 22nd-24thMar'18

$\{V_{j}, j \in z\}$ satisfying monotonicity as represented in equation (3.8).

$$--V_{m+2} \subset V_{m+1} \subset V_m \subset V_{m-1} \subset --- \quad -> \quad (8)$$

Where V_m is the m^{th} sub space.

It must also satisfy completeness. Let W_j represent an orthogonal component in between V_j and V_{j-1} then the direct summation of V_j with W_j gives V_{j-1}.

$$V_{j-1} = V_j \oplus W_j \quad -> \quad (9)$$

From the definition of the MRA, the zero scale sub space can be represented as in equation 10 [18].

$$V_0 = V_1 \oplus W_1 = V_2 \oplus W_2 \oplus W_1 = ... -> \quad (10)$$

The equation 10 tells that a zero scale space can decompose into two parts W_1 and V_1 where the detailed information is W_1 and the approximate information is V_1. The process of decomposition is repeated on the approximate information V_1 i.e. at another resolution of space giving another set of approximate and detailed information V_2 and W_2 respectively. The process can be repeated further giving a successive set of approximate and detailed information.

According to Mallat algorithm the detailed information ($d_{j,k}$) is expressed as in equation 11 [18].

$$d_{j,k} = \langle x(t), \psi_{j,k}(t) \rangle = \sum_k x(t) 2^{j/2} \psi^*\left(2^j t - k\right) \quad -> \quad (11)$$

Similarly the approximate coefficients ($a_{j,k}$) are represented as per the equation 12,

$$a_{j,k} = \langle x(t), \phi_{j,k}(t) \rangle = \sum_k x(t) 2^{j/2} \phi^*\left(2^j t - k\right) \quad -> \quad (12)$$

The signal x(t) can be decomposed as

$$x(t) = \sum_k a_{j,k} 2^{j/2} \phi\left(2^j t - k\right) + \sum_k d_{j,k} 2^{j/2} \psi\left(2^j t - k\right) -> (13)$$

In equations 11 and 12, $\phi(t)$ is the scale function and $\psi(t)$ is wavelet function.

There is an inherent relationship between scale function, wavelet function and filter coefficients which can be expressed as a dual-scale. They are represented in equations 14 and 15.

$$\phi(t) = \sqrt{2} \sum_m h(m) \phi(2t - m) \quad -> (14)$$

$$\psi(t) = \sqrt{2} \sum_m g(m) \phi(2t - m) \quad -> (15)$$

In the equations 14 and 15, h(n) and g(n) are a pair of low-pass and high-pass filter coefficients [18]. The recursive relations of approximations and the details are obtained from the dual – scale equations 14 and 15 as shown in equation 16.

$$\left. \begin{aligned} a_{j,k} &= \sum_m h(m - 2k) a_{j-1,m} \\ d_{j,k} &= \sum_m g(m - 2k) a_{j-1,m} \end{aligned} \right\} -> (16)$$

In order to analyze a signal using DWT, two important parameters need to be selected. The first parameter is the selection of wavelet. After the wavelet is selected, the filter coefficients h(n) and g(n) are calculated. The second parameter is the number of levels of decomposition.

2.2 a) *Choosing wavelet family:*

It was now the task of selecting the effective wavelet to fit the case of epileptic seizure studies. The db4 wavelet was selected over the other range of wavelets available. It is observed that the natural signal in the form of a neuronal potential has a shape similar in comparison with Daubechies 4 wavelet. This increases the chance of greater correlation with the original signal than any other wavelet.

2.2 b) Calculation of filter coefficients for db4:

Daubeschies wavelets have 2p non-zero filter coefficients where p is the number of vanishing moments. Daubeschies 4 (db4) wavelet has 4 vanishing moments, thus has 8 non-zero filter coefficients [18][17].

The wavelet coefficients of the db4 wavelet are generated by using the relations as mentioned below: [18]

a) The low pass filter characteristics

$$\sum_{n=0}^{N-1} h(n) = \sqrt{2} \quad -> \quad (17)$$

Substituting N=8 in the above equation 17, it is expanded as

$$\left. \begin{aligned} & h(0)+h(1)+h(2)+h(3)+ \\ & h(4)+h(5)+h(6)+h(7)=\sqrt{2} \end{aligned} \right\} \rightarrow (18)$$

b) Ortho normality of scaling function

$$\sum_{n=0}^{N-1} h(n)\,\mathrm{h(n+2\,k)} = \delta(k) ....k = N/2 \quad -> \quad (19)$$

In this case, N=8 so the equation reduces to the form,

$$\sum_{n=0}^{7} h(n)h(n+2k) = \delta(k) \quad -> \quad (20)$$

$$k = 0,1,2,3$$

$$\left. \begin{aligned} & k=0 \Rightarrow h^2(0)+h^2(1)+h^2(2)+h^2(3) \\ & +h^2(4)+h^2(5)+h^2(6)+h^2(7)=1 \end{aligned} \right\} -> (21)$$

$$\left. \begin{aligned} & k=1 \Rightarrow h(0)h(2)+h(1)h(3)+h(2)h(4) \\ & +h(3)h(5)+h(4)h(6)+h(5)h(7)=0 \end{aligned} \right\} -> (22)$$

$$\left.\begin{array}{l} k=2 \Rightarrow h(0)h(4)+h(1)h(5)+ \\ h(2)h(6)+h(3)h(7)=0 \end{array}\right\} \quad -> \quad (23)$$

$$k=3 \Rightarrow h(0)h(6)+h(1)h(7)=0 \quad -> \quad (24)$$

c) Vanishing moments

$$\sum_{n=0}^{N-1}(-1)^n n^k h(n)=0 \quad -> (25)$$

$$\left.\begin{array}{l} k=0 \Rightarrow h(0)-h(1)+h(2)-h(3)+ \\ h(4)-h(5)+h(6)-h(7)=0 \end{array}\right\} \quad -> \quad (26)$$

$$\left.\begin{array}{l} k=1 \Rightarrow -h(1)+2h(2)-3h(3)+4h(4) \\ -5h(5)+6h(6)-7h(7)=0 \end{array}\right\} \quad -> (27)$$

$$\left.\begin{array}{l} k=2 \Rightarrow -h(1)+4h(2)-9h(3)+16h(4) \\ -25h(5)+36h(6)-49h(7)=0 \end{array}\right\} \quad -> \quad (28)$$

$$\left.\begin{array}{l} k=3 \Rightarrow -h(1)+8h(2)-27h(3)+64h(4)- \\ 125h(5)+216h(6)-343h(7)=0 \end{array}\right\} \quad -> (29)$$

Thus the above three filter constraints a), b) and c) give 9 (i.e. N+1) linearly dependent equations for 8 (N) unknowns. Since 8 equations are sufficient enough to solve for 8 unknowns, any one of the equation can be omitted and the rest can be solved to get the low pass filter coefficients h(0) to h(7). The high pass filter coefficients can be obtained by using the relation

$$g(n)=(-1)^{1-n}h(1-n) \quad -> \quad (30)$$

2.2 C) *Selection of decomposition levels:*

The second important parameter for using the DWT is the selection of number of decomposition levels. Using the data from University of Bonn, energy of each level is evaluated. The decomposition levels are considered as per the ratio between energy in each sub band and total energy. It can be observed that after five levels, the ratio is not significant. Thus, only five levels of decomposition are required.

III. RESULTS AND DISCUSSIONS

3.1 *FEATURE EXTRACTION USING WAVELETS AND CLASSIFICATION USING NEURAL NETWORKS:*

Using the CHBMIT database, channel selection has been made. CHBMIT database has 23 channels. Out of the 23, there are 6 subjects taken into consideration. Data selection is done as shown in the table 1 below

Table 1: Data selection using CHBMIT database

subjects	CHBMIT database label	Number of seizures	Seizure label to each Seizures	Seizure free data labels
1	chb01	3	s1,s2,s3	N1
2	chb02	2	s4,s5	N2
3	chb03	3	s6,s7,s8	N3
4	chb05	4	s9,s10,s11,s12	N4
5	chb08	2	s13,s14	N5
6	chb24	15	s15,s16,s17,s18,s19,s20,s21,s22,s23,s24s25,s26,s27,s28,s29	N6

The data considered has an epoch length 2s which has sampling frequency is 256 epoch length 512 samples. The seizure and seizure free data is decomposed with discrete wavelet transform using db4 wavelet as the mother wavelet. The reason is discussed earlier in the above sections with Bonn database. The number of levels of decomposition is restricted to five as the energy is efficiently consumed within these levels of decomposition.

From the decomposed wavelet coefficients, features are extracted from wavelet bands A5, D5, D3 and D2. From each band four features Inter Quartile Range (IQR), Median absolute deviation (MAD), coefficient of variation(C) and energy changes are taken. Though five levels of decomposition is done in each channel, only four levels of decompositions are considered and from each sub band 4 features are extracted.

Thus, 16 features in each channel and a grand total of 23X16 feature`s from each epoch. Since the number of features is huge, a reduction in the number of features is necessary. The best considered technique to lower the no. of features is that the average of the 23 channels be considered which would result in (23x16)/23=16 features from each epoch. The features extracted from 28 seizures and seizure free data of 6 patients are classified using Feed forward back propagation neural network with 2 layers.

The input and the hidden layers have sixteen neurons respectively and the output has only one neuron. For the purpose of training, seizures s2, s4, s6, s8, s10, s12, s14, s16, s18, s20, s22, s24, s26 and s28 are used. The remaining seizures used for testing.

a) The testing results obtained for Seizure free data testing have Number of epochs 2000 with false positive value being 114.

b) In comparison the testing the data with Seizure had the following results and tabulated in table 2.

Table 2: Testing of data with seizure for 6 subjects.

Seizure	NUMBER of epochs	False Negative
s1	14	0
s3	25	1
s5	40	8
s7	34	34
s9	57	1
s11	47	1
s13	66	6
s15	12	2
s17	14	2
s19	15	3
s21	09	1
s23	10	2
s25	34	25
s27	13	4
s29	33	0
TOTAL	423	90

From the table 2, it can be seen that the number of false negatives whose value is equal to zero was '2'. Thus, out of the total 15 seizures considered 13 seizures were classified correctly. On a comparative note the classification technique was applied on single subject chb24 which had 15 seizures.

The Seizures s15, s17, s19, s21, s23, s25, s27, s29 were used for testing. It`s performance was as follows:

a. The Seizure free data had 150 epochs and the number of false positive obtained were '8'.
b. When data with seizure is used for testing the results are tabulated as in the table 2.

Table 3: Testing for data with seizure for multiple and single subjects using the wavelet technique.

Subjects	Sensitivity (%)	Specificity (%)	Over all accuracy (%)
Multiple(6)	78.72	94.6	91.58
Single(chb24)	93.24	95.3	94.64

3.2) Epileptic Seizure Detection using Empirical Mode Decomposition:

Table 4: Testing of data with seizures using EMD technique for detection.

Seizure	Number of epochs	False Negative
s1	14	0
s3	25	3
s5	40	4
s7	34	11
s9	57	0
s11	47	0
s13	66	05
s15	12	03
s17	14	2
s19	15	3
s21	09	1
s23	10	1
s25	34	05
s27	13	2
s29	33	0
TOTAL	423	40

Each channel is decomposed into the following Intrinsic Mode Functions imf1, imf2, imf3 and imf4. From these IMF`s the following four features are extracted:

a) IQR
b) MAD
c) Co efficient variation
d) Energy

The data was tested the following results were obtained:

a) The data free from seizures had 825 epochs and the false positive number obtained was 57.

The data with seizures had the testing results as tabulated in table 4.

If only one subject chb24 was considered the following was the result as shown in table 5.

Table 5: Testing for data with seizure for multiple and single subjects using the EMD technique

Subjects	Sensitivity (%)	Specificity (%)	Over all accuracy (%)
Multiple(6)	90.54	93.07	92.27
Single(chb24)	96.8	97.33	97.18

The testing for data with seizure for multiple and single subjects using the EMD technique generated good results. With multiple subjects, the accuracy was 92.27% whereas with single subject, the accuracy was 97.18%.

IV. CONCLUSIONS

EEG signal is non-stationary and nonlinear in nature. This work uses the Discrete Wavelet Transform and EMD as signal decomposition methods. Two parameters necessary to work with DWT are the wavelet selection and the number of levels of decomposition. The wavelet suitable for EEG analysis is the 'db4' wavelet and the reason behind its selection was because of its close resemblance with the neural action potential. Five levels of decomposition were carried out. From the decomposed signal using DWT, features such as mean, coefficient of variance, IQR, MAD were extracted. These features were classified using neural network.

Using neural network, if the features are normalized independently, the best result achieved was 94.64% classification accuracy. This result was again validated using 10-fold cross validation technique. The consistency accuracy was above 96.25%. Using EMD, the signal was decomposed into corresponding IMF`s and features were extracted based upon mean weighted frequency. The variation in frequency was observed in the seizure period. The classification accuracy was 97.18%.

V. REFERENCES

[1] Tzallas, Alexandros T., Markos G. Tsipouras, and Dimitrios I. Fotiadis. "Epileptic seizure detection in EEGs using time–frequency analysis." Information Technology in Biomedicine, IEEE Transactions on, 13(5), 2009, pp. 703-710

[2] Polat, Kemal, and Salih Güneş. "Classification of epileptiform EEG using a hybrid system based on decision tree classifier and fast Fourier transform."Applied Mathematics and Computation, 187(2), 2007, pp. 1017-1026..

[3] Zandi, Ali Shahidi, Manouchehr Javidan, Guy A. Dumont, and Reza Tafreshi. "Automated real-time epileptic seizure detection in scalp EEG recordings using an algorithm based on wavelet packet transform." Biomedical Engineering, IEEE Transactions, 57(7), 2010, pp. 1639-1651.

[4] Omerhodzic, Ibrahim, Samir Avdakovic, Amir Nuhanovic, and Kemal Dizdarevic. "Energy distribution of EEG signals: EEG signal wavelet-neural network classifier." arXiv preprint arXiv:1307.7897, 2013.

[5] Najumnissa, D., and S. ShenbagaDevi. "Intelligent identification and classification of epileptic seizures using wavelet transform." International Journal of Biomedical Engineering and Technology, Vol. No. 3, 2008, pp. 293-314.

[6] Subasi, Abdulhamit, and M. Ismail Gursoy. "EEG signal classification using PCA, ICA, LDA and support vector machines." Expert Systems with Applications, 37(12), 2010, pp. 8659-8666.

[7] Omidvarnia, Amir, Boualem Boashash, Ghasem Azemi, Paul B. Colditz, and Sampsa Vanhatalo. "Generalised phase synchrony within multivariate signals: An emerging concept in time-frequency analysis." ICASSP, 2012, pp. 3417-3420.

[8] Dominguez, Luis Garcia, Richard A. Wennberg, William Gaetz, Douglas Cheyne, O. Carter Snead, and Jose Luis Perez Velazquez. "Enhanced synchrony in epileptiform activity? Local versus distant phase synchronization in generalized seizures." The Journal of neuroscience, 25(35), 2005, pp. 8077-8084..

[9] Oweis, Rami J., and Enas W. Abdulhay. "Seizure classification in EEG signals utilizing Hilbert-Huang transform." Biomed. Eng. Online 10, 2011, pp. 38

[10] Sharma, Rajeev, and Ram Bilas Pachori. "Classification of epileptic seizures in EEG signals based on phase space representation of intrinsic mode functions."Expert Systems with Applications, 42(3), 2015, pp. 1106-1117.

[11] Bajaj, Varun, and Ram Bilas Pachori. "Epileptic seizure detection based on the instantaneous area of analytic intrinsic mode functions of EEG signals."Biomedical Engineering Letters, 3(1), 2013, pp. 17-21.

[12] Pachori, Ram Bilas, and Shivnarayan Patidar. "Epileptic seizure classification in EEG signals using second-order difference plot of intrinsic mode functions." Computer methods and programs in biomedicine, 113(2), 2014, pp. 494-502.

[13] Tafreshi, Azadeh Kamali, Ali M. Nasrabadi, and Amir H. Omidvarnia. "Epileptic seizure detection using empirical mode decomposition." Signal Processing and Information Technology, IEEE International Symposium, 2008, pp. 238-242.

[14] Orosco, Lorena, Eric Laciar, A. Garcés Correa, Abel Torres, and Juan P. Graffigna. "An epileptic seizures detection algorithm based on the empirical mode decomposition of EEG." Engineering in Medicine and Biology Society (EMBC), Annual International Conference of the IEEE, 2009, pp. 2651-2654.

[15] Chua, K. C., Vinod Chandran, U. Rajendra Acharya, and C. M. Lim. "Analysis of epileptic EEG signals using higher order spectra." Journal of medical engineering & technology, 33(1), 2009, pp. 42-50.

[16] Najumnissa, D., and S. ShenbagaDevi. "Intelligent identification and classification of epileptic seizures using wavelet transform." International Journal of Biomedical Engineering and Technology, Vol. No. 3, 2008, pp. 293-314.

[17] Gao, Robert X., and Ruqiang Yan. Wavelets: Theory and applications for manufacturing. Springer Science & Business Media, 2010.

ISBN 978-1-5386-4473-7
IEEE sponsored 4th International Conference on Biosignals, Images and Instrumentation, SSNCE, Chennai. ICBSII 2018 – 22nd-24th Mar'18

Epileptic Seizure Prediction based on localization

Shaik. Jakeer Hussain, *Member, IEEE*
Department of Electronics and Communication Engineering,
Vignan's Foundation for Science, Technology and Research, Guntur,
Andhra Pradesh, India.
E-Mail: JK.shaik@gmail.com

***Abstract*— Electroencephalography (EEG) gives complex information about the brain dynamics. Visual Inspection of EEG signal is difficult and requires skilled interpreters in identifying epileptic seizures. One third of the people having epilepsy are drug resistant and the latest anti-epileptic drugs cannot stop the seizures completely. Unexpected occurrence of seizure disturbs the quality of life and causes physical damage. The Prediction based on localization of Epileptic Zone using EMD and neural network has resulted excellent prediction accuracy. A seizure prediction time of 30.4 minutes was achieved. It can be used as a clinical application for the diagnosis and effective epilepsy management.**

Index Terms*— Electroencephalogram (EEG) signals, Epileptic Seizures, Discrete wavelet transform (DWT), Artificial Neural Network (ANN) component

I. Introduction

Epilepsy is one of the most common neurological disorders with a prevalence of 0.6–0.8% of the world's population.

Two-thirds of the patients achieve sufficient seizure control from anticonvulsive medication, and another 8–10% could benefit from respective surgery. For the remaining 25% of patients, no sufficient treatment is currently available. The epilepsy is characterized by a sudden and recurrent malfunction of the brain, which is termed "seizure."[12] Epileptic seizures reflect the clinical signs of an excessive and hyper synchronous activity of neurons in the brain. The epilepsy detection can be done by visual examination of EEG recordings for inter-ictal and ictal activities by an experienced neurophysiologist. There are serious shortcomings if visual review of the vast amount of EEG data is done.

Different neurophysiologists can have different opinion on the same EEG recording due to the narrowness in the analysis and the variation of morphology pertaining to inter-ictal spikes. In addition, some artifacts such as blinking of eyes and background noise inherent in the data sometimes make the pattern indistinguishable with the seizure pattern in the EEG signal [13]. Thus the computationally efficient methods would be useful to overcome the above hurdles. When seizures are not kept under check, the patient experiences trouble in handling vocational and trivial activities of his/her life. It is also to be noted that if seizures are long and unstoppable, they may cause irrevocable harm to the brain. The mainstay of treatment of epilepsy, today, is primarily pharmacological. Anticonvulsant drugs are taken daily, in fixed doses, titrated to get a steady state blood concentration.

The specific concentration is chosen for least degree of side effects and effective control. Medical treatment can control seizures in approximately 67% of the patients [1]. Seizure prediction is necessary in these cases for better treatment. Seizures are sporadic and do not occur regularly, however the patients diagnosed with epilepsy experience some anxious moments for the possibility of falling prey to one. For these patients, seizure forecasting systems have become a boon in order to lead a more conventional life. An effective forecasting system needs computational algorithms which must and should pinpoint the span of the seizure attack with good probability. Manufacturing of devices to warn patients of a looming seizure would be possible if these states are identified. This would help the patients to avoid hazardous activities like driving, swimming etc and receive medication to prevent imminent seizures also reducing the overall side effects. The occurrence of seizure will not start suddenly, its precursor's start few minutes before it occurs. Using the precursor`s, it is possible to identify pre-seizure state of several minutes which can in turn predict an epileptic seizure.

Source localization means identifying the area of the brain where a seizure can occur. In general, source localization is necessary for patients with a special condition in epilepsy, i.e. when their disease is resistant to drugs. In the prediction of epilepsy, continuous monitoring of EEG is employed. This involves observing data from more number of channels, resulting in computational complexity. To cut the costs involved with more channels, epileptic zone can be identified. In this work, epileptic zone was localized by evaluating the phase synchrony of scalp EEG. The observed fluctuations in phase synchrony are reflected in inter-ictal, pre-ictal, ictal and post-ictal EEG. Among these, the channels exhibiting the higher phase synchrony are associated with epilepsy. In drug-resistant epilepsy patients, pre-surgical evaluation is needed to localize the epileptic zone in the brain, for which noninvasive techniques are more preferable. In such cases, synchronization between the brain regions fluctuates between seizure and non-seizure periods. Localization can be achieved by the concept of phase synchronization. Phase synchrony essentially conveys the correlation of two signals, with respect to their instantaneous phases.

It takes values between 0 and 1. The value of zero represents that the two signals are at different frequencies and the value of one represents a constant difference in the instantaneous phase i.e. the signal is compared with a time shifted version of itself. The essential requirement is pre filtering at a frequency of own choice. The phase synchrony has two brilliant properties. While one is that it is not dependent upon the amplitudes of the signal, the other is that the nature of the signals is irrelevant. This paper proposes a method for calculating phase synchronization of EEG signals between brain regions utilizing modified Multivariate Empirical Mode Decomposition.

II. MATERIALS AND METHODS

A. *Experimental Data*

The CHB-MIT scalp EEG database [2] is being used for seizure localization and prediction. This database collected at Boston hospital for children has EEG recordings from paediatric subjects with obstinate seizures. Monitoring of patients for several days following abandonment of anti seizure drugs in order to characterize the seizures and gauge their candidature for surgical intercession was performed. Recordings that were heaped into 23 cases were taken from 22 subjects (five males aged between 3 to 22; and 17 females aged between one and a half to nineteen), (Case chb21 and case chb01 belong to the same female patient but at different ages having a gap of 1.5 years). Sampling rate with 16-bit resolution was 256 samples per second.

B. *Empirical Mode Decomposition*

EMD is the fundamental part of the HHT method. EMD is similar to other methods of analysis such as Fourier transform and Wavelet transform when it decomposes the signals portraying a filter function. Any intricate data set can be chopped into a finite and often small number of components using EMD. The above components form a complete and almost orthogonal basis for the original signal known as intrinsic mode functions (IMF).

An IMF is a function that satisfying the following conditions [3]:

1. The mean value of the envelope at any point defined by the local minima and the envelope defined by the local maxima is zero.
2. The number of extrema and the number of Zero crossings must either be equal or differ at most by one at any given point.

In order to perform EMD on a signal, there are some steps that need to be followed and they constitute a process known as sifting [3]. The sifting process is explained as below:

1) Evaluation of all the local maxima and minima of the signal $s(t)$ is to be done first.
2) Upon interpolating all the local maxima points an envelope $e_m(t)$ is formed. Similarly by interpolating all the local minima points another envelope $e_l(t)$ is formed.
3) Average of these two envelope`s are computed as

$$m(t)=\frac{e_m(t)+e_l(t)}{2} \quad \text{-> (1)}$$

4) The detail of the original signal $s(t)$ is evaluated as

$$c(t)=s(t)-m(t) \quad \text{-> (2)}$$

5) Check whether the detail, $c(t)$ satisfies the above stated two conditions.
6) If the detail fails to satisfy any of the above two conditions then repeat steps 1 to 5 upon the evaluated detail signal $c(t)$ until it satisfies the IMF conditions.

Once the first IMF $C_1(t)$ has been extracted, the residue is evaluated as:

$$R_1(t)=s(t)-C_1(t) \quad \text{-> (3)}$$

The steps 1-5 are again applied upon this residue to obtain other IMF`s.

The total number of IMF`s to be evaluated is determined by four kinds stopping criteria. One such stopping criterion determined by the standard deviation given as [4]:

$$SD_k=\frac{\sum_{t=0}^{T}\left|c_{k-1}(t)-c_k(t)\right|^2}{\sum_{t=0}^{T}c_{k-1}^2(t)} \quad \text{-> (4)}$$

If the value of the SD is smaller than an initially given value, then the sifting process is stopped.

C. *Multivariate Empirical Mode Decomposition*

The multivariate signals can be decomposed by Multivariate Empirical Mode Decomposition.

Algorithm for MEMD [5]:

1. In a $(n-1)$ sphere, a point set is to be chosen.
2. Projections denoted as $\left\{P^{\theta_k}(t)\right\}_{t=1}^{T}$ of the input $\left\{V(t)\right\}_{t=1}^{T}$ are calculated which are along the direction vector X^{θ_k}, $\forall k$ (the whole set of direction vectors), resulting in the set of projections as $\left\{P^{\theta_k}(t)\right\}_{k=1}^{K}$.

3. Find the time instants $\left\{ t_i^{\theta_k} \right\}$ corresponding to the maxima of the set of projected signals $\left\{ P^{\theta_k}(t) \right\}_{k=1}^{K}$
4. Interpolate $\left[t_i^{\theta_k}, V(t_i^{\theta_k}) \right]$ to obtain multivariate envelope curves $\left\{ e^{\theta_k}(t) \right\}_{k=1}^{K}$.
5. For a set of k direction vectors, the mean m (t) of the envelope curves is calculated as $m(t) = \frac{1}{K} \sum_{k=1}^{K} e^{\theta_k}(t)$ -> (5).

The 'detail' $d(t)$ is extracted by the relation $d(t) = x(t) - m(t)$ -> (6).

If the detail ' $d(t)$ ' satisfies the criterion necessary for stoppage for a multivariate IMF, apply the above procedure to $v(t) - m(t)$, else apply it to $d(t)$.

The knowledge of MEMD and phase synchrony feature will help in performing the experiment of epileptic seizure localization.

D. Hilbert Transform

In order to get the Phase component, the Hilbert spectrum of the IMF's of EEG data is calculated by evaluating Hilbert transform [14]. The phase component thus evaluated gives the feature phase synchrony.

E. Neural Network

Artificial neural networks are computing systems made up of large number of simple, highly interconnected processing elements (called nodes or artificial neurons) that abstractly emulate the structure and operation of the biological nervous system [15]. Learning in ANNs is accomplished through special training algorithms developed based on learning rules presumed to mimic the learning mechanisms of biological systems. There are many different types and architectures of neural networks varying fundamentally in the way they learn. In this paper, 12-12 -1 feed forward back propagation neural network considered [3 features, 4 channels] to classify regions.

III. RESULTS AND DISCUSSIONS

Source localization means identifying the area of the brain where a seizure can occur. MEMD technique is applied to all the pairs of a EEG channels of post-ictal, ictal, pre-ictal, and inter-ictal. This technique is applied on all the channels of 6 patients: 1, 2, 3, 5, 8 and 24. From MEMD IMF's calculated the phase synchronous values for post -ictal , preictal , and ictal, inter-ictal periods. Based on phase value a few channels were found, which have more phase variations in each patient and those channels were selected.

Table 1: Results of source localization

Patient	Selected Channels
1	1, 5, 9, 13, 14, 15 and 21
2	1,12,15 and 9
3	1,4,6,8,14,20 and 21
5	2,3,9,15,19 and 23
8	6,8,20 and 21
24	5,6,20 and 21

From the above table 1, it can be noted that Patient 1 has 1, 5, 9, 13, 14, 15 and 21 as the most significant channels. Patient 2 has 1, 12, 15 and 9 as the most significant channels. Patient 3 has 1, 4, 6, 8, 14, 20 and 21 as the most significant channels. Patient 5 has 2, 3, 9, 15, 19 and 23 as the most significant channels. Patient 8 has 6, 8, 20 and 21 as the most significant channels. Patient 24 has 5, 6, 20 and 21 as the most significant channels.

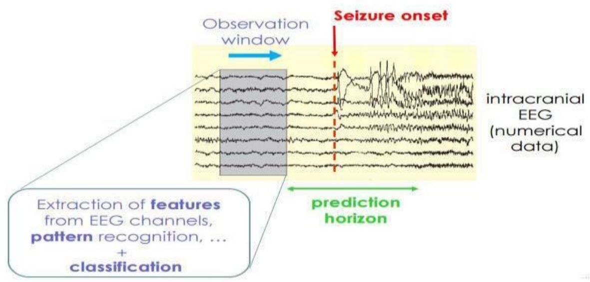

Figure 1: Seizure prediction methodology.

The main objective in the seizure prediction is detecting the precursor for seizure as shown in the Figure 1.Using the results obtained for source localization, prediction can be performed with few channels.

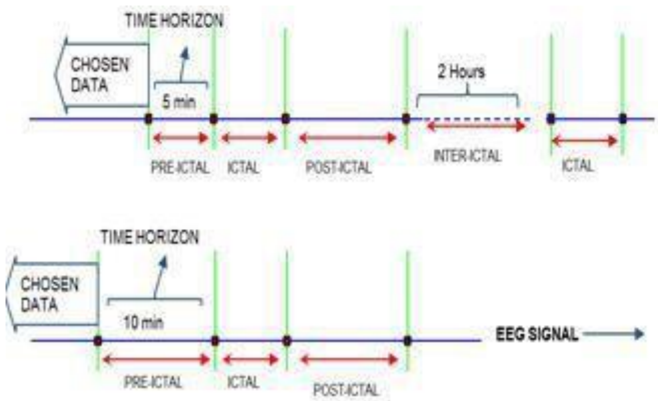

Figure 2 : Two types of data is chosen. First data has a time horizon of around 5 minutes for the pre-ictal period while the second has the time horizon for 10 minutes. The inter-ictal period is considered to be around 2 hours in order to nullify the post-ictal or seizure effects.

The selection is choosen such that to reduce the effects of the post seizure by taking a minimum gap of 2 hours in the inter-ictal period. The markings of a pre-ictal data is shown in Figure 2. Care has been taken to reduce the effects of post seizure

Using the EEG data as per the Fig.2, IMF`s are extracted using the EMD technique. Using these IMF`s, features such as Kurtosis, Inter-quartile range and Median Absolute Deviation

ISBN 978-1-5386-4473-7
IEEE sponsored 4th International Conference on Biosignals, Images and Instrumentation, SSNCE, Chennai. ICBSII 2018 – 22nd-24thMar'18

are extracted. The following figure 3 shows the steps involved in the seizure prediction. The extracted features are used for training the Neural network and the results are tabulated.

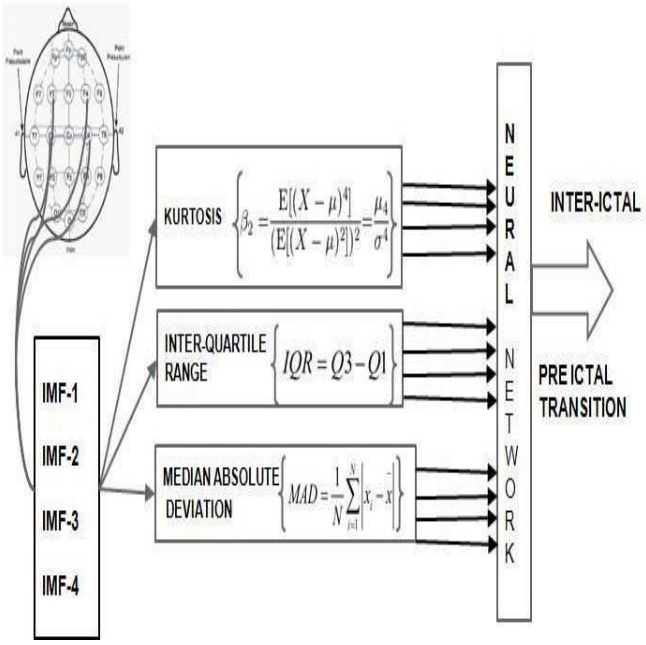

Figure 3: Steps involved in Epileptic seizure prediction using epileptic zone. It is divided into three parts. 1) The first part extracted the IMF`s while in the second part 2) features are extracted from these IMF`s. These features are given as 3) input to the neural network in the third part

For patient 8, source has been localized as discussed in the table 1. It has been observed that 4 channels 6,8,20 and 21 have been the most significant channels. These channels are decomposed into 4 IMF`s out of which 3 significant features are extracted thus a total of 4x4x3=48 features are extracted. 600 pre-ictal and inter-ictal epochs of 2 second duration are considered respectively, which means 1200 epochs (600+600=1200) with 48 features add up to a total input vector of 1200x48 to the neural network. This is tabulated as shown below in table 2.

Table2: An overview of the input vector to neural network

FEATURE	VECTOR LENGTH
CHANNELS	4 (6,8,20 and 21)
INTRINSIC MODE FUNCTIONS	4 levels
FEATURES	3 (MAD, IQR, Kurtosis)
TOTAL FEATURE VECTOR	4 X 4 X 3 = 48
PRE-ICTAL EPOCHS [2 SECOND]	600
INTER-ICTAL EPOCHS [2 SECOND]	600
TOTAL INPUT VECTOR TO NN	(1200) X 48

Table 3: Sensitivity, Specificity and Classification accuracy using epileptic zone for prediction where TP=True Positive, FN= False Negative, TN=True Negative and FP= False Positive

	TP	FN	Sensitivity (%)	TN	FP	Specificity (%)	Over all Accuracy
[5 Min]	289	11	96.33	290	10	96.67	96.5
[10 Min]	300	--	100	295	5	98.33	99.16

The concept is extended to all the patients whose source has been localized earlier in table 1.The prediction method is run on the entire channels localized from the source as derived from table 1.

Table 4: Sensitivity, Specificity and Classification accuracy using epileptic zone for prediction for all patients from source localization in table 2 SE= Sensitivity and SP= Specificity

	TP	FN	SE (%)	TN	FP	SP (%)	Over all accuracy
chb01	290	10	96.66	277	33	89	92.8
Chb02	282	18	94	290	10	96.66	95.3
Chb03	284	16	94.66	288	12	96	95.3
Chb05	270	30	90	264	36	88	89
Chb24	288	12	96	286	14	95.33	95.6

The results are as shown in the table 4. The above results are obtained for data of short intervals. A testing has been run for continues data whose results are as shown in the figures below:

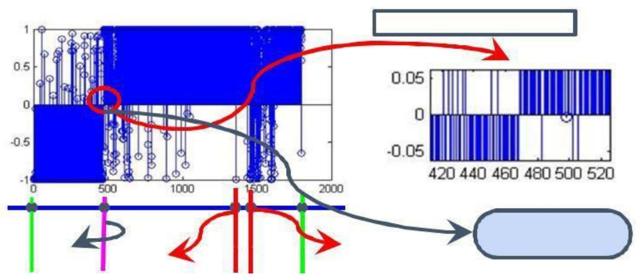

Figure 4: The testing for continuous seizure data.

In the above Figure 4, the seizure is predicted 30.4 minutes before the onset. When a seizure free data is considered, there is a chance for false alarm. Consider the figure 5 where the result of testing of continuous seizure free data is shown.

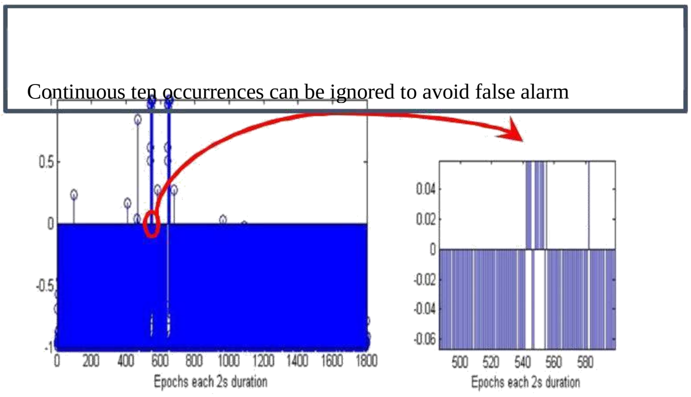

Figure 5: A continuous seizure free data is used for testing. Since it is seizure free no transition should occur. There can be some spikes observed from the above zoomed in the figure.

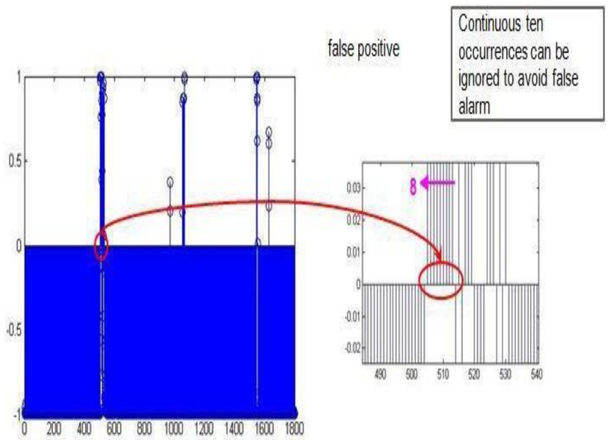

Figure 6: Continuous seizure data with false positive values.

A continuous occurrence of around 10 can be ignored so that no false alarm is triggered. In the above figure 5, 6 continuous occurrences happen. Thus, it can be ignored.

IV. CONCLUSION

Localization is identifying the source of the seizure in the brain region. The method used for localization was Multivariate Empirical Mode Decomposition. Most significant channels were identified as tabulated in table 1. The main principle behind prediction is observing the differences from inter-ictal to pre ictal period. Based upon the results from source localization, minimum number of channels was selected and Empirical Mode Decomposition was applied to extract features. The extracted features classification results were 98.33% specificity and a sensitivity of 100% with over all prediction accuracy of 99.16%.

This concept was tested on continuous data. It`s testing had achieved prediction time of 30.4 minutes. For continuous testing of seizure free data, nominal false positives are observed. By close observation, these false positives were not more than 10 (Refer figure 5 and 6). Thus false alarm can be raised after 10 continuous false positives.

The epileptic seizure prediction is more challenging than detection. The difficulty in prediction is the variation of data from time to time. The duration of pre-ictal state may change from seizure to seizure. This variation may be caused due to factors such as medication, which cured the state to an extent etc. The variation issue can be addressed by retraining the neural network by accumulating data. To implement the prediction algorithms in reality, the specificity and sensitivity should be monitored until a safe margin is achieved. The algorithm can be implemented on a portable device. The prediction time should also be improved so that more time is available to take medical interventions. This work opened up the concept of generalization of seizure epileptic seizure detection and prediction which can act as a semi-automatic screening technique.

V. REFERENCES

[1] Mormann, Florian, Ralph G. Andrzejak, Christian E. Elger, and Klaus Lehnertz. "Seizure prediction: the long and winding road." Brain, Vol. No. 2, 2007, pp. 314-333.

[2] Goldberger, Ary L., Luis AN Amaral, Leon Glass, Jeffrey M. Hausdorff, Plamen Ch Ivanov, Roger G. Mark, Joseph E. Mietus, George B. Moody, Chung-Kang Peng, and H. Eugene Stanley. "Physiobank, physiotoolkit, and physionet components of a new research resource for complex physiologic signals." Circulation 101, No. 23, 2000, e215-e220.

[3] Huang, Norden E., Zheng Shen, Steven R. Long, Manli C. Wu, Hsing H. Shih, Quanan Zheng, Nai-Chyuan Yen, Chi Chao Tung, and Henry H. Liu. "The empirical mode decomposition and the Hilbert spectrum for nonlinear and non-stationary time series analysis." Proceedings of the Royal Society of London. Series A: Mathematical, Physical and Engineering Sciences, Vol. 454, No. 1971, 1998, pp. 903-995.

[4] Rehman, Naveed, and Danilo P. Mandic. "Multivariate empirical mode decomposition." Proceedings of the Royal Society A: Mathematical, Physical and Engineering Science (2009): rspa 20090502.

[5] Oweis, Rami J., and Enas W. Abdulhay. "Seizure classification in EEG signals utilizing Hilbert-Huang transform." Biomed. Eng. Online Vol. No. 10, 2011, pp. 38.

[6] Oweis, Rami J., and Enas W. Abdulhay. "Seizure classification in EEG signals utilizing Hilbert-Huang transform." Biomed. Eng. Online 10, 2011, pp. 38.

[7] Sharma, Rajeev, and Ram Bilas Pachori. "Classification of epileptic seizures in EEG signals based on phase space representation of intrinsic mode functions."Expert Systems with Applications, 42(3), 2015, pp. 1106-1117.

[8] Bajaj, Varun, and Ram Bilas Pachori. "Epileptic seizure detection based on the instantaneous area of analytic intrinsic mode functions of EEG signals."Biomedical Engineering Letters, 3(1), 2013, pp. 17-21.

[9] Pachori, Ram Bilas, and Shivnarayan Patidar. "Epileptic seizure classification in EEG signals using second-order difference plot of intrinsic mode functions." Computer methods and programs in biomedicine, 113(2), 2014, pp. 494-502.

[10] Tafreshi, Azadeh Kamali, Ali M. Nasrabadi, and Amir H. Omidvarnia. "Epileptic seizure detection using empirical mode decomposition." Signal Processing and Information Technology, IEEE International Symposium, 2008, pp. 238-242.

[11] Orosco, Lorena, Eric Laciar, A. Garcés Correa, Abel Torres, and Juan P. Graffigna. "An epileptic seizures detection algorithm based on the empirical mode decomposition of EEG." Engineering in Medicine and Biology Society (EMBC), Annual International Conference of the IEEE, 2009, pp. 2651-2654.

[12] Berg, Anne T., Samuel F. Berkovic, Martin J. Brodie, Jeffrey Buchhalter, J. Helen Cross, Walter van Emde Boas, Jerome Engel et

al. "Revised terminology and concepts for organization of seizures and epilepsies: report of the ILAE Commission on Classification and Terminology, 2005–2009." Epilepsia 51, no. 4 (2010): 676-685.

[13] Joyce, Carrie A., Irina F. Gorodnitsky, and Marta Kutas. "Automatic removal of eye movement and blink artifacts from EEG data using blind component separation." Psychophysiology 41, no. 2 (2004): 313-325.

[14] Huang, Norden E., Zheng Shen, Steven R. Long, Manli C. Wu, Hsing H. Shih, Quanan Zheng, Nai-Chyuan Yen, Chi Chao Tung, and Henry H. Liu. "The empirical mode decomposition and the Hilbert spectrum for nonlinear and non-stationary time series analysis." Proceedings of the Royal Society of London. Series A: Mathematical, Physical and Engineering Sciences, Vol. 454, No. 1971, 1998, pp. 903-995.

[15] Srinivasan, Vairavan, Chikkannan Eswaran, and Natarajan Sriraam. "Approximate entropy-based epileptic EEG detection using artificial neural networks." Information Technology in Biomedicine, IEEE Transactions, 11.3, 2007, pp. 288-295.

ISBN 978-1-5386-4473-7
IEEE sponsored 4th International Conference on Biosignals, Images and Instrumentation, SSNCE, Chennai. ICBSII 2018 – 22nd-24th Mar'18

Myoelectric Control System based on Wavelet Features

Supriya Mary Sunil, K.I.Ramachandran
Amrita School of Engineering, Coimbatore, Amrita Vishwa Vidyapeetham
Amrita University, India-641112
Email Id: supriyamsunil@gmail.com, ki_ram@cb.amrita.edu

***Abstract*— Electromyography (EMG) finds enormous applications in clinical/biomedical, prosthesis and rehabilitation devices. The main objective of this paper is to develop a cost-effective implementation of a prosthetic control system based on EMG signals. Non-invasive surface electrodes are used to acquire the signal for various actions. Since the signal is highly contaminated with noise, they are not used in its raw form to handle any sort of device. Amplification and filtering are therefore inevitable and becomes the foremost task prior to further processing so as to obtain a high-quality signal. After the conditioning of the signal, multi-level decomposition based on wavelet transform is performed and features are extracted from all the levels. They are then reduced to find the optimal performance. Finally, the selected features are able to distinguish between various hand movements and therefore helps in the recognition of the intended motion of the amputee.**

Keywords—Electromyography; Wavelet transform; Daubechies wavelet; Feature extraction

I. Introduction

The human body is a wonder of nature. The role of the hand in human life is not just limited to functional movements, but, rather is essential in communication, sensation and any other area that can be imagined. About 23,500 amputees are born in India annually, among which 30% cases are those with the upper limb amputations [1]. Researchers are on their way to develop a prosthetic arm/device that almost replicates the functioning of a natural limb. According to recent literature, there are various prosthetic options available for upper extremity amputees ranging from passive cosmetic hand to the highly operational electrically powered prosthetic hands. Functional arm prosthetics offer high dexterity, but they are often difficult to use and are of high cost [2]. So there originates the need to develop a natural means of a control system for the prosthetic arm. Poor accuracy in terms of motion recognition limits the utilization of EMG signals beyond the laboratory experiments [3]. This paper puts an effort to develop a low-cost control system based on the acquired signals that can identify the motion intention of the user in a better accuracy rate.

Electromyography gives a correlation about the skeletal muscle activity. EMG signals are considered to be one of the most useful biological signals in both medical and engineering fields [4]. EMG signal finds its area not only in the prosthesis, but also in rehabilitation, human machine interfaces, robotics and clinical diagnosis [4], [5]. A non-invasive technique is preferred for signal measurement. Surface detected signal tends to provide quantitative information about the muscle action [4]. The signal amplitude lies in the order of microvolts and is contaminated by a high level of noise during recording. As a result, signal conditioning is necessary to amplify and filter the signal before processing it. The signal passes through various stages of amplification and filtering to obtain a high-quality signal. Multi-level decomposition using wavelet transform is done to extract the features from the conditioned signal. The reduced features are then able to classify between the intended motions of the subject. Fig.1 shows the proposed methodology.

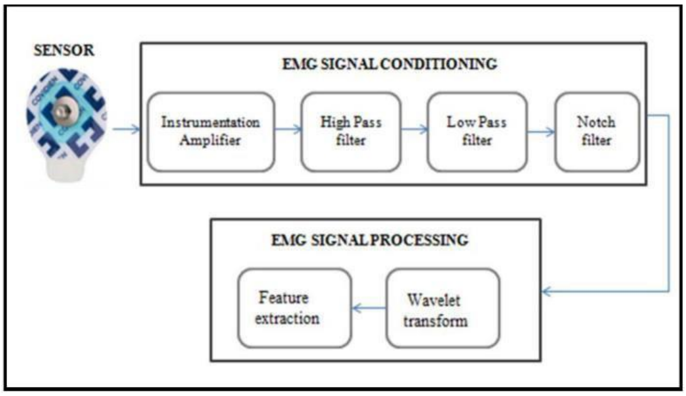

Figure 1. Block diagram of the proposed system.

The paper is organized as follows. Section 2 explains the set-up for EMG signal conditioning. Section 3 describes the various steps under EMG signal processing. Section 4 shows the experimental results and Section 5 gives the conclusion and future scope.

II. EMG Signal Conditioning

Whenever a person intends to move his/her hand, an electrical impulse travels down from the axon of the motor nerve to all the motor cells that it innervates, thus resulting in contraction of the muscle. Measurement of those developed electrical potentials is called Electromyography and the recorded signal is known as electromyogram. Forearm surface electromyography is a technique by which the potentials generated by the activation of the muscles are picked up by electrodes placed on the subject's forearm over a targeted group of muscles. The EMG signals acquired from this group of muscles can provide relevant information with regard to the hand movement.

ISBN 978-1-5386-4473-7

During the process of recording, the electric fields linked with the electrode and their cables superimpose with the original signal resulting in interference. Ambient noise introduced to the system due to the electromagnetic fields associated with components such as televisions, mobile phones, computer monitors, electrical power lines can also affect the signal characteristics. The motion artifacts at the skin-electrode interface may alter the system performance [4]. A circuit with a good connection and a stable contact between the skin and electrode eliminates the above-mentioned difficulties in the EMG signal acquisition.

The signal amplitude range from 50µV to 5mV and the usable energy is limited to the 10 -500Hz frequency [6]. The EMG signals are measured with the help of non-invasive surface electrodes. The signal so recorded will be composed of all the action potentials from the muscles underlying the electrode. Hence, they have to be electronically amplified, conditioned and processed using analog components. Fig.2 shows the set-up of the signal conditioning circuit. A bipolar electrode arrangement is used to serve the two inputs of the pre-amplifier and a reference electrode is connected to the ground.

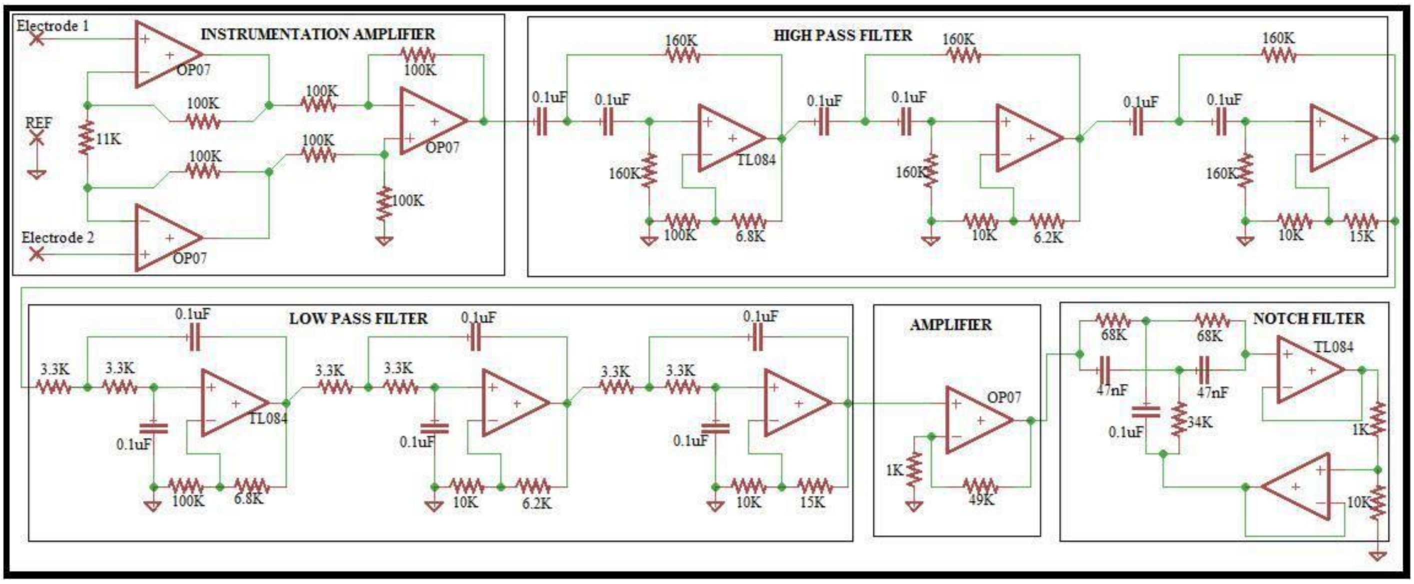

Figure 2. Signal conditioning circuit

To eliminate the noise common to both the inputs, an instrumentation amplifier (IA) of gain 20 is used as pre-amplifier. The IA used is a three op-amp configuration using OP07 to achieve high CMRR so that it accurately amplifies a weak signal in the presence of large noise [7]. The frequency range lies between 10-500Hz [8]. Hence a 6th order active high pass filter of cutoff frequency 10Hz followed by an active low pass filter of the same order with cutoff 500Hz is used. A second stage amplifier of gain 50 is needed to further amplify the signal to a reliable range. A notch filter of 50Hz cut-off is added finally to reject the power line interference. Fig.3 shows the signal obtained from the above circuit.

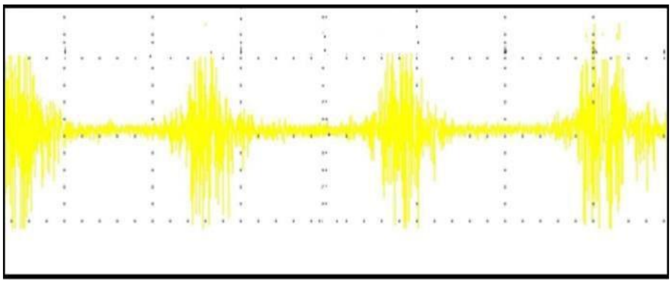

Figure 3. Acquired signal from the EMG conditioning circuit.

III. EMG SIGNAL PROCESSING

Electromyogram plays a vital role in the control of prostheses through the identification of different body movements [5]. Due to its complexity and non-linearity, appropriate signal processing tools are utilized to differentiate muscular activities corresponding to various hand motions [5]. Fig.4 shows the different stages in signal processing. Single channel data analysis is done in this work due to its simplicity and less effort. The wavelet transform is utilized to analyze and extract the features for better classification accuracy.

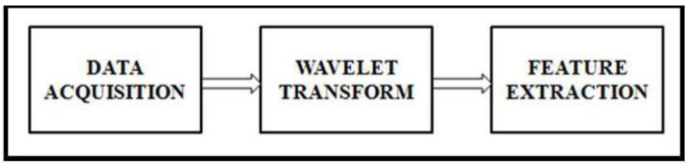

Figure 4. Various stages in EMG signal processing.

A. Data Acquisition

Single channel data acquisition is performed using the BioRadio acquisition device of GreatLakeNeuroTechnologies. It records the signals by placing surface electrodes over Flexor Carpi Radialis muscle on the right forearm in a bipolar configuration(see Fig.5(a)). The electrodes were separated by a distance of 20mm. The gain and the sampling frequency are set to 1000 and 1000Hz respectively. The device allows an inbuilt bandpass filtering of the signals to the 10-500Hz frequency range. The acquired EMG signals are used to discriminate the main two daily life upper limb motions. The motions under study are wrist flexion and forearm supination as shown in the Fig.5(b and c). The experiment was conducted for eight subjects in the age group of 20-25 years. The duration of each movement is 10sec with a transition period of 2sec at the beginning and ending. The subjects were allowed for a rest period of 2min between each trial (for a total of 8 trials) to avoid muscle fatigue.

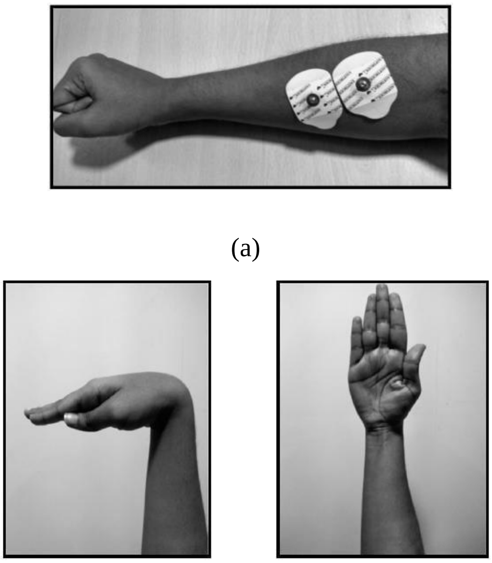

(a)

(b) (c)

Figure 5. (a) Electrode placement (b) Wrist flexion (c) Forearm supination

B. Wavelet transform

Transformation of the raw signal is done to analyze the signal with the information that is not readily available in the raw form. Since the signal is non-stationary whose frequency content constantly changes with time, the wavelet transform is chosen over the other due to its time-frequency analysis and multiresolution property [9].

Transformation of a signal with a suitable wavelet basis function into subsets of different scales is done using Discrete Wavelet Transform (DWT) [9]. The DWT of a signal x(n) is computed using (1):

$$C(a,b)=\sum_{n\varepsilon Z} x[n]\varphi_{a,b}[n] \quad (1)$$

where a is the dilation or scale, b is the translation and $\varphi_{a,b}[n]$ is the wavelet basis function which is expressed by (2)

$$\varphi_{a,b}[n]=\frac{1}{\sqrt{a}}*\left(\frac{n-b}{a}\right) \quad (2)$$

In this process, the signal is carried out through successive low pass and high pass filtering followed by down sampling. The high pass filter coefficients are called details whereas the low-pass filter coefficients are called approximations [1]. The number of samples is reduced by half and hence provides good frequency resolution. Four mother wavelets in the Daubechies family were selected to be evaluated in this study. They include db3,db4,db5, and db6. The decomposition level was set to four. Finally, it yields approximation coefficient (cA4) at level 4 and detail coefficients (cD1,cD2,cD3 and cD4) at levels 1,2,3 and 4 respectively. Fig.6 explains the procedure of wavelet decomposition of a signal S.

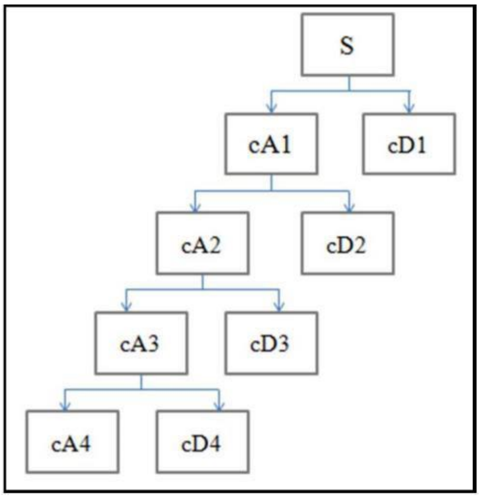

Figure 6. Wavelet decomposition tree at Level 4

C. Feature Extraction

Feature extraction is an essential method to obtain the useful information from the EMG signals. It identifies the characteristic (feature) from the signal so as to recognize the desired motion. A signal can make use of a large number of features to extract the information content. Some of them include mean absolute value, median frequency, standard deviation, phase coherence value, waveform length, and root mean square [2]. To obtain a direct correlation with the muscle activity, the selected features for EMG feature extraction in this study are the root mean square (RMS), Variance and Energy of the wavelet coefficients. All the feature values of the wavelet coefficients were extracted from levels 1 to 4 for all the specified Daubechies wavelets.

IV. RESULTS AND DISCUSSIONS

The subjects performed movements such as wrist flexion and forearm supination in order to evaluate the performance of the proposed system. A high-quality signal was obtained from the designed conditioning circuit. Signals were collected from eight subjects using the acquisition device. Fig.7 and Fig.8 show the original signal for wrist flexion and forearm supination respectively and their various decomposition levels using db6 as the mother wavelet.

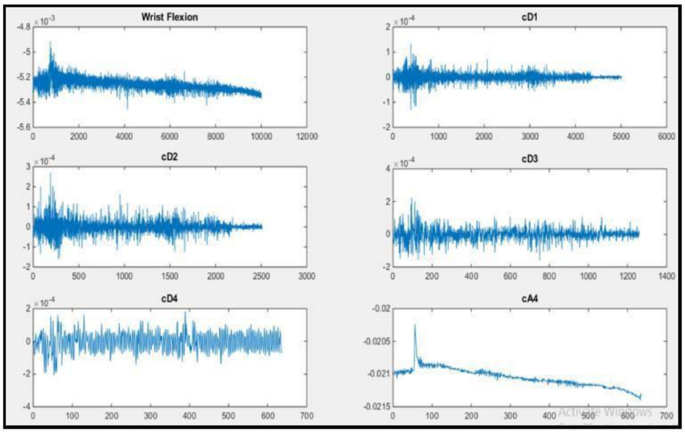

Figure 7. EMG signal of forearm supination and the wavelet coefficient subsets.

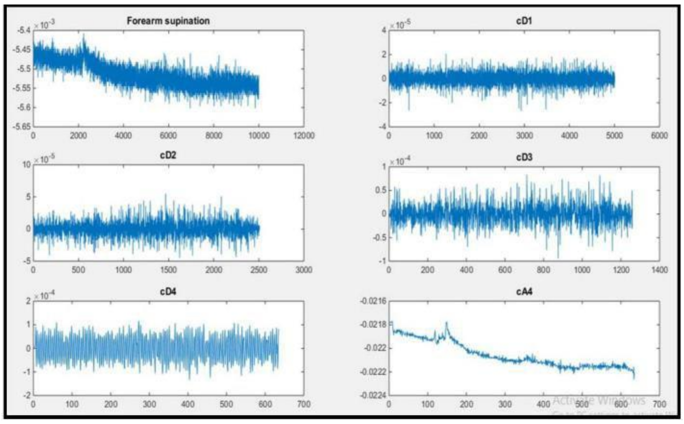

Figure 8. EMG signal of forearm supination and the wavelet coefficient subsets.

RMS, Variance, and Energy features were extracted and plotted for each level of all the wavelets used. From the results, it is seen that RMS feature produce better results when compared to the other two features in class separability point of view. Variance and energy features can, therefore, be discarded since none of them have enough separable distance to distinguish accurately between the two different kinds of motion (see Fig.9).

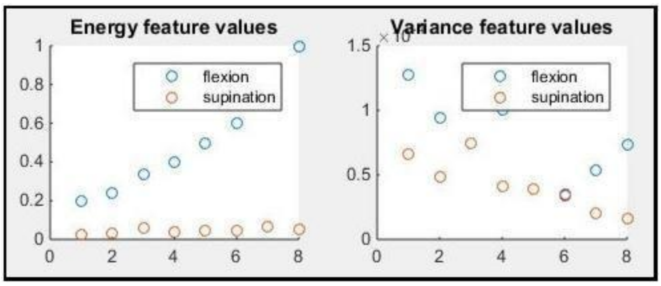

Figure 9. Scatter plot of Energy and Variance feature values using db6 wavelet decomposition.

Fig.10,11,12 and 13 shows the scatter plot of RMS feature values at different levels for db3,db4,db5 and db6 wavelets respectively.

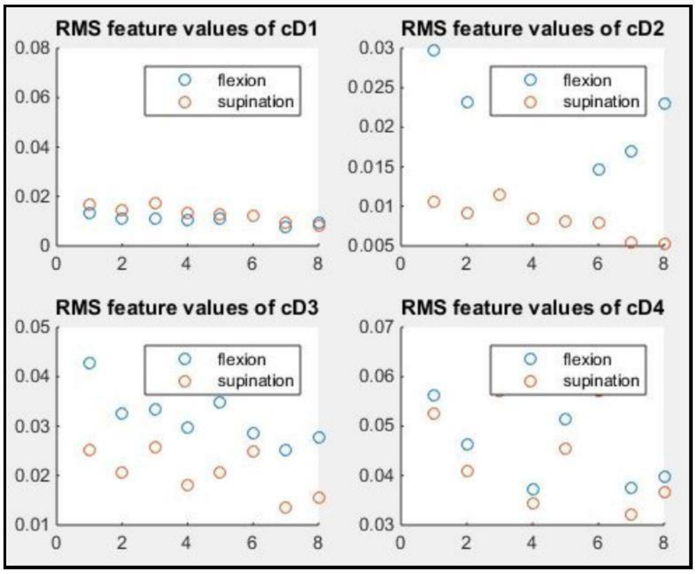

Figure 10. Scatter plot of RMS feature values using db3 wavelet decomposition.

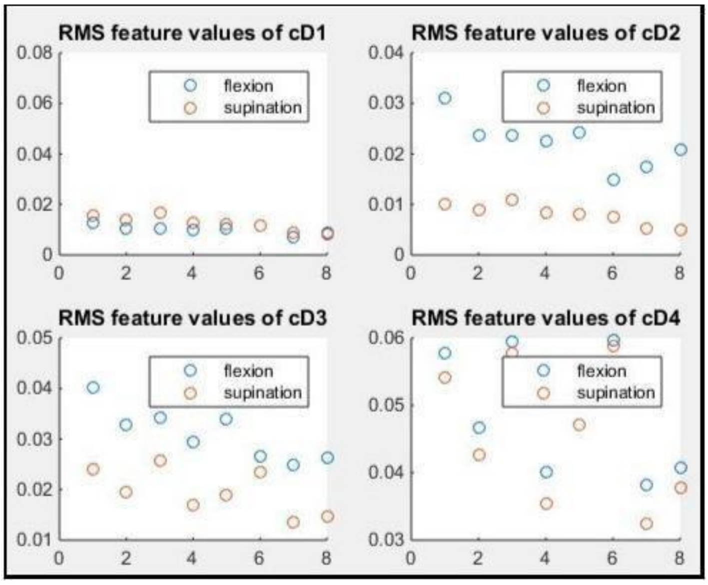

Figure 11. Scatter plot of RMS feature values using db4 wavelet decomposition.

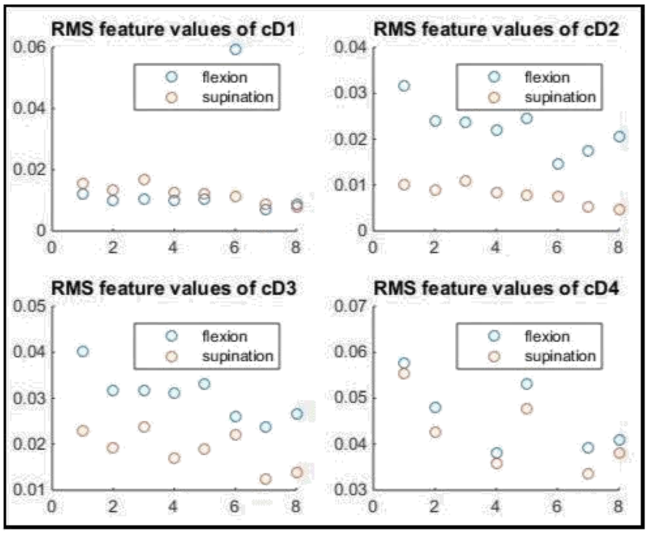

Figure 12. Scatter plot of RMS feature values using db5 wavelet decomposition.

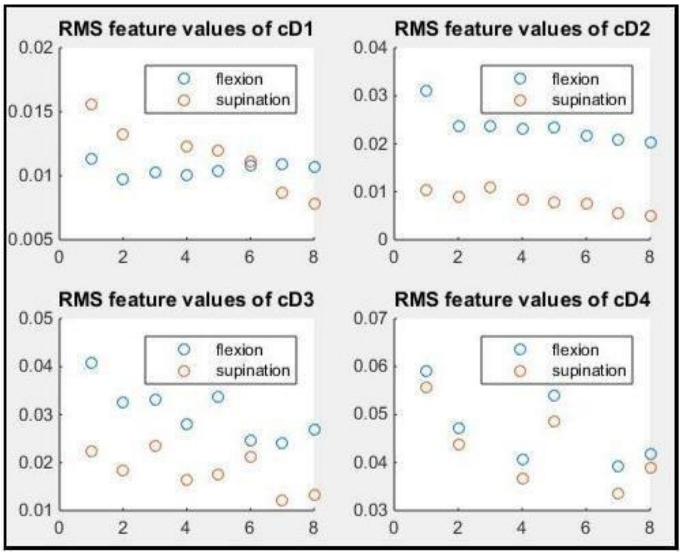

Figure 13. Scatter plot of RMS feature values using db6 wavelet decomposition.

V. CONCLUSION

This paper puts an effort to design a system that utilizes the EMG signals through single channel acquisition to identify between the two commonly used upper limb motions. The design of the analog front-end played a vital role to obtain an EMG signal with good quality. The scatter plots of RMS feature values for different mother wavelets shows that the second level detail coefficients of db6 wavelet provide a better result with high recognition. The future scope is to expand the work for other movements like wrist extension, hand close, hand open and forearm pronation using multi-channel data measurement. A number of other features can also be extracted to improve the classification accuracy.

ACKNOWLEDGMENT

We thank everyone who has helped in completing this work. Special thanks to the people for their assistance during data acquisition.

REFERENCES

[1] C. Garg, Y. Narayan, and L. Mathew, "Development of a software module for feature extraction and classification of EMG signals," *2015 Commun. Control Intell. Syst.*, vol. 1, pp. 250–254, 2015.

[2] K. Sharmila, T. V. Sarath and K. I. Ramachandran, "EMG Controlled Low Cost Prosthetic Arm," *2016 IEEE Distributed Computing, VLSI, Electrical Circuits and Robotics (DISCOVER)*, pp. 169–172, 2016.

[3] S. Guo, M. Pang, B. Gao, H. Hirata, and H. Ishihara, "Comparison of sEMG-Based Feature Extraction and Motion Classification Methods for Upper-Limb Movement," *Sensors (Basel).*, vol. 15, no. 4, pp. 9022–9038, 2015.

[4] R. Chowdhury, M. Reaz, M. Ali, A. Bakar, K. Chellappan, and T. Chang, "Surface Electromyography Signal Processing and Classification Techniques," *Sensors*, vol. 13, no. 9, pp. 12431–12466, 2013.

[5] S. M. Mane, R. A. Kambli, F. S. Kazi, and N. M. Singh, "Hand Motion Recognition from Single Channel Surface EMG Using Wavelet & Artificial Neural Network," *Procedia Comput. Sci.*, vol. 49, pp. 58–65, 2015.

[6] J. Wang, L. Tang, and J. E. Bronlund, "A pattern recognition system for myoelectric based prosthesis hand control," *Proc. 2015 10th IEEE Conf. Ind. Electron. Appl. ICIEA 2015*, pp. 830–834, 2015.

[7] S. Franco, *Design with operational amplifiers and analog integrated circuits*, 4th ed. New York: McGraw-Hill, pp.87-92, 2015.

[8] P. Konrad, "Noraxon: The ABC of EMG," *Signal Processing*, no. April, pp. 10–15, 2005.

[9] F. Duan, L. Dai, W. Chang, Z. Chen, C. Zhu, and W. Li, "SEMG-Based Identification of Hand Motion Commands Using Wavelet Neural Network Combined with Discrete Wavelet Transform," *IEEE Trans. Ind. Electron.*, vol. 63, no. 3, pp. 1923–1934, 2016.

[10] V. Nivitha Varghees and K. I. Ramachandran, "A Wavelet Based Heart Sound Delineation Algorithm for Digital Stethoscope," *International Conference on Applications of Fractals and Wavelets (ICAFW-2015)*, pp. 1-15, 2015.

ISBN 978-1-5386-4473-7
IEEE sponsored 4th International Conference on Biosignals, Images and Instrumentation, SSNCE, Chennai. ICBSII 2018 – 22nd-24thMar'18

ECG-Based Secure Healthcare Monitoring System in Body Area Networks

Shanthapriya.R
Department of ECE
SSN College of Engineering
Chennai, India
shanthaarona@gmail.com

Vaithianathan.V
Department of ECE
SSN College of Engineering
Chennai,India
vaithianathanv@ssn.edu.in

***Abstract*— Body Area Networks (BANs) plays a major role in the field of patient-health monitoring. It is profoundly important to join the universal figuring with versatile well-being innovation utilizing remote sensors to screen the prosperity of perpetual patients, for example, cardiovascular, Parkinson and epilepsy patients. In Body Area Network, every sensor will be small in size, lightweight and give secure health monitoring. Physiological signals of patient, such as heartbeat, temperature, ECG signs are checked utilizing sensors and they ought to be transmitted securely to the distinct location. Subsequently, security is an important issue in portable wellbeing (m-Health) applications, particularly if a patient has a humiliating malady. In this paper polynomial based curve is generated and steganography technique has been used for secure health monitoring which provides data confidentiality and authentication to maintain the privacy of a patient.**

Keywords— wireless body Area networks; m-Health; security; authentication; confidentiality; steganography.

I. INTRODUCTION

BAN is an emerging innovation by the fast advancement in remote sensor systems and biomedical designing procedures [1]–[2]. It comprises of various BAN gadgets (embedded or wearable sensors) and BAN controller. They are intended in screening physical parameters like temperature, pulse, ECG signals from different parts of the body and also it stores and processes individual health information (e.g. patient history, vital signs, etc.), and it raises various privacy and wellbeing concerns. In wireless networks, there exist two kinds of threads [3].

1. Unapproved information-access: An intruder can access patient's medical data which is stored in the controller or hack the data when it is transmitted by means of wireless communication, without getting approval from the patients. The assault raises noteworthy privacy concerns (e.g., some patients don't like to share their medical data to an insurance agency).
2. Message alteration: Intruder can alter the messages (such as time, arrangement, content, request and so on) created inside the BAN before they are carried to a receiver or - modify the message substance being transmitted from BAN to external entity (e.g., doctor). This assault brings up huge protection concerns- i.e., wrong diagnosis of the patient or it can crash the life-saving gadgets, such as an automated implantable cardioverter-defibrillator (AICD).

Health monitoring is very important to the patient which provides quality life during critical situation. BAN is mainly used to diagnose the chronic diseases such as cardiac, Parkinson and epilepsy [4]-[5]. For example, sports persons may check their heart rate or pressure level throughout running. Even healthy patients utilize BAN for checking any sort of sickness in their body. It is often used to detect cardiovascular diseases, observe ECG signal, depression, old individual's observance, and aldohexose level observance. The major concern within BAN is to protect the data from hackers because the patient's medical data is carried to the receiver through wireless link.

In this paper, we develop a polynomial based curve for secure mechanism that provides integrity, authenticity, confidentiality and privacy of the patient. The polynomial curve achieves the security by embedding the secret information into it and thereby the information inside the polynomial is maintained securely and transmitted to the receiver without losing its integrity and authenticity.

II. BODY AREA NETWORK

Body area networking consists of various wireless sensors to be placed on the individuals for enabling continuous monitoring of signals. Each BAN have controller which is used to store and send the data during emergency situation. The vital signs are estimated with the help of sensors placed in the various parts of the human body and it has to be carried safely to the controller. BAN controller will send the medical data to the physician for further analysis.

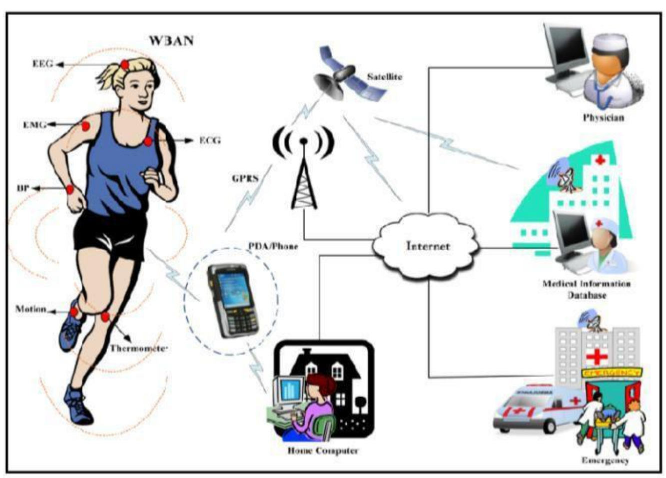

Fig.1. Body Area Network Architecture [6]

In Fig.1, vital signs such as ECG signal, EMG and temperature are gathered with the help of sensors placed in different parts of the body. The data gathered by the sensor is put into the BAN controller. The BAN controller broadcast the restorative information to doctor's facility server and put the signals in a database for later analysis.

The intruder might get the restorative information and try to alter the therapeutic data which affect the patient's health. Likewise intruder might attempt to modify the medications endorsed by a specialist. By HIPAA act the patient's secret data and therapeutic information should to be kept secret. Consequently the security is the real concern in WBAN. Eavesdropping must be eluded in wireless medium thereby integrity of the information ought to be maintained. When the sensors are kept in various parts of body, numerous requirements arises when compared to ordinary sensor systems because BAN sensors are smaller in size and have few imperatives such as restricted memory, moderate power and low computation and correspondence rate. The basic requirements in executing the BAN are [7].

1. Necessities incorporate during the arrangement of tiny sensors on the body should be at least 2-3 meters separation since it conveys short range.
2. Intervention between hub and controller should be maintained a strategic distance.
3. Data send by the transmitter should reach the destination without losing its integrity is a real issue in wireless medium.

Various security requirements in WBANs are

1. **Information Confidentiality**: It is one of the most essential issue in WBANs. Secured data must be protected from exposure and should not release patient's fundamental data to outside/neighboring systems.
2. **Information Integrity**: Intruder may change patient's information by manipulating few sections or adding few packets to the received signal. The packets can later be sent to a facilitator. Altered information is extremely unsafe particularly if a patient is in emergency condition.
3. **Data Freshness**: The adversary might in some case gather information and forward it later utilizing the previous key with a specific goal to baffle the organizer. Data carried by a receiver should be new and nobody can forward old messages.
4. **Accessibility**: It suggest effective accessibility of patient's data by a doctor. Adversary might focus on accessibility of WBAN by catching/hacking specific hub, result in death toll.

III. Related Work

A few key administration scheme and distribution plan have created to give security in WBAN. But at the same time security is a noteworthy issue in WBAN. The planning on key administration and distribution is unpredictable in WBAN. Ordinary protection and secure mechanisms may not be suitable for WBAN. The key distribution technique [8] and asymmetric crypto frameworks are not suitable for WBAN because of constrained sensor resources.

In symmetric encryption, identical key is utilized for encryption and decryption. The person wearing sensors (on body) will screen information by any mean time and need to monitor the information at all the time. The quantity of key may additionally expanded. But it will complicate the key administration process. In public key encryption, different keys are used for encryption and decryption. It requires calculation overhead. The sensor gadgets have requirements such as processing speed, memory estimate and Vitality. The vitality, memory efficient and light weight cryptography calculations are suitable for WBAN.

In PSKA scheme [9]. Fuzzy vault has been created to lock the secret values into it. The vault can be unlocked by using other set of values on the receiver side. To provide security extra chaff points are added to the original values. But extra chaff Points causes unnecessary overhead. The IBE plan is proposed in [10]. The open key can be created from an arbitrary string. In the event if more than n mystery keys are discharged, the expert mystery key is vulnerable against programmer's assault.

Key distribution plan is proposed in [11], examined the issue of synchronization and it has been overwhelmed by key refreshment module. It delineates the turn of every hub for its refreshment. Three mystery keys such as correspondence, managerial and essential keys are utilized. The BS issues a new key refreshment plan occasionally which is difficult in to find the key.

IV. Proposed Work

The health care applications get to be vital plan in numerous nations of world. The recent improvement in remote sensor hubs will have vital part in healthcare applications. Recent advances in sensor gadgets are equipped for gathering various signals from the body and process the signal, and then transfer it to base station. A WBAN is a system of bio sensors intended to deliver the information to remote clients. Advances in communication and figuring innovations have changed the therapeutic framework from paper script to electronic information.

The Electronic-healthcare gives awesome adaptability to patients and social insurance suppliers. The design of WBAN is exceptionally complex. Since, the important medicinal information is exchanged to the remote clients through web. In this section the work is proposed towards wireless patient monitoring. The organization of sensor hubs should fulfill all protection requirements without giving the security and privacy of the patient. Otherwise it creates major problem to patient's. The recent advances in remote communication, allows the sensor (wearable or implantable) to exchange data in wireless medium to the base station without influencing the everyday activity of a person. The following Fig.2. shows the schematic diagram for secure health monitoring in WBAN.

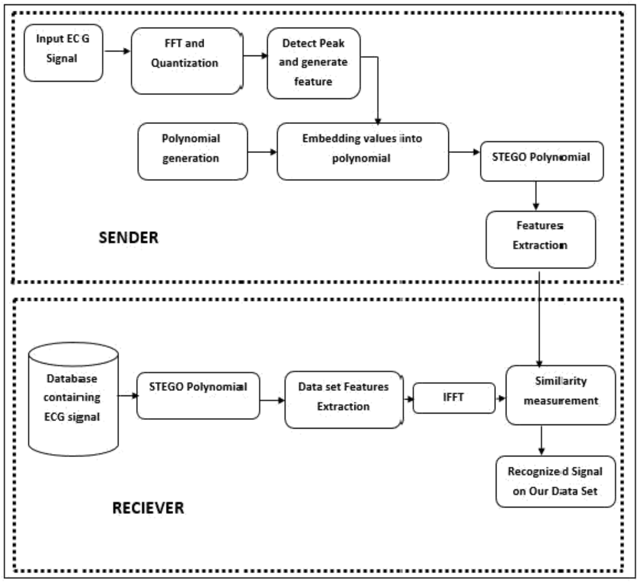

Fig.2. Block Diagram of BAN Transmitter and Receiver.

A. Polynomial curve

The objective is to design a secure healthcare monitoring system in wireless body area network that gives a trade-off between privacy and security. To achieve security higher order polynomial is used to generate a curve because there is no explicit formula for solving higher order polynomial. For this purpose we used the concept of polynomial based curve which embeds the secret information into it and make the information secure, thereby protecting the patient's data from hackers.

The n^{th} order of the polynomial is represented in the form of $p(x) = b_n x^n + b_{n-1} x^{n-1} + \ldots + b_0$ where n denotes the order of the polynomial. To generate a higher order polynomial curve, the following steps has to be proceeded:

1. Consider x as a linearly spaced vector in an interval and Y can be any function (sin, tan, or cos) or values.
2. Using *polyfit (x, y, n)* function the coefficients of the polynomial can be found, where n represents the order of the polynomial.
3. The Coefficients are concatenated to form an equation and it can be evaluated using *polyval ( )*.

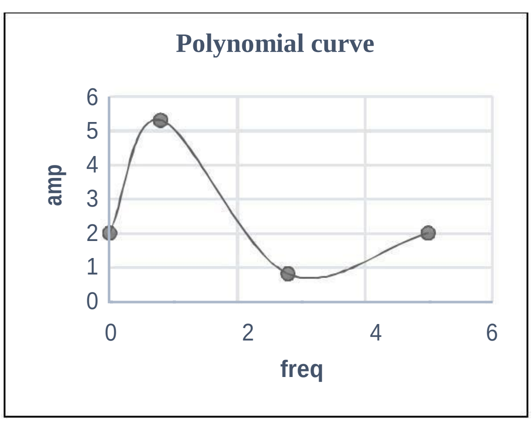

Fig.3. Polynomial curve

Example 1: Let x be linearly spaced vector in the interval [1, 6] and y=sin(x) where the order of the polynomial be 2. The coefficients of the polynomial formed for the example are 0.3581,-2.2367 and 2.5545. The equation can be framed with the help of coefficients $p(x) = 0.3581x^2 - 2.2367x + 2.5545$. The model polynomial curve for the proposed work is shown in the fig.3.

B. Stego Polynomial

Steganography is the art of covered communication, which keeps the presence of a message, secret [12]-[14]. It is an elective tool for protection and security, which may suppress and anticipate pointless consideration of third parties. Steganography algorithm is used to embed the secret information into the generated polynomial curve and it forms a Stego polynomial which is nothing but a cover media.

C. Transmitter

1. ECG signal is taken as an input signal.
2. FFT is applied to change the signal from original domain (space) or time to frequency domain.
3. Quantization process is applied to detect the peak points.
4. Peak points are converted into binary to form a feature vector.
5. When the features are produced, the higher order polynomial curve is generated by the sender.
6. Obtained feature vectors (input signal) are embedded into the polynomial curve that forms a STEGO polynomial is shown in fig 4.
7. Feature extraction is done to exact the input signal from STEGO polynomial for similarity measurement.

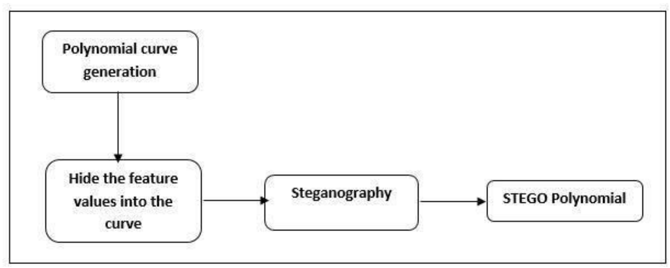

Fig.4. Hiding process

D. Receiver

1. Receiver check for the similarity measurement in the data set.
2. If the transmitted data matches with the data present in the data set, then the information will be sent to the doctor along with patient's data (medical information) for further analysis.

V. RESULTS AND DISCUSSION

The ECG signal from the patients are safely transmitted and received by the following procedure:

A. Input signal

Electrocardiogram (ECG) is most widely recognized organic signs which play a critical part in the analysis of heart diseases. Abnormalities in the patient body can be easy sensed by monitoring the ECG signal. Input ECG signal is taken from MIT-BIH database is shown in fig 5.

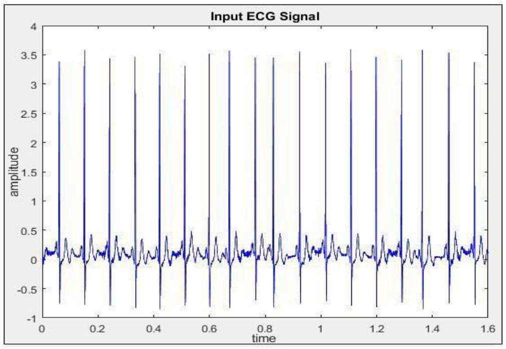

Fig.5. ECG signal

B. Fast Fourier transforms (FFT) and quantization

Fast Fourier transform converts a signal from its original domain (space or time) to frequency domain. FFT is used for two reasons: 1) stable and easy to detect 2) they portray a subject's physiology exceptionally well [15]. Quantization process converts large set of input values to small set. The original input signal is sampled and rounded to obtain quantized signal is shown in fig 6. The distinction between input signal and quantized signal helps in detecting the peak values. The obtained signals are converted to binary string and linked together with peak values to form features. Collected features are grouped to form feature vector.

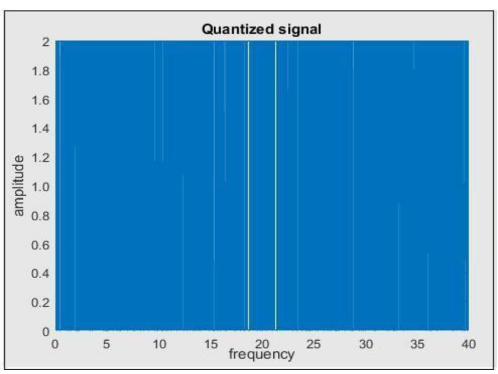

Fig. 6. Quantized signal

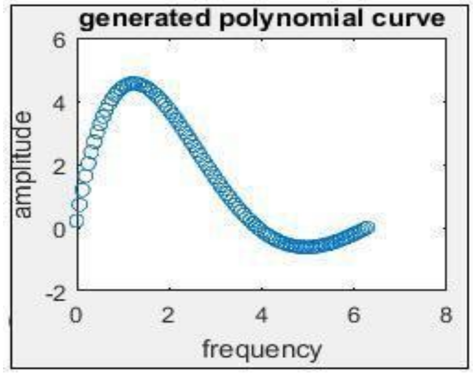

Fig.7. Generated Polynomial

C. Polynomial generation and hiding process

Once the features are created a polynomial curve is generated to hide the features into it thereby the information inside the curve is safe and provides secure transmission. The generated curve is shown in fig 7 and hidden value inside the curve is shown in fig 8.

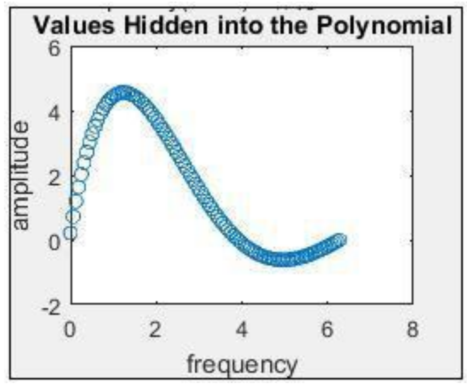

Fig.8. values hidden into the polynomial

D. Database and checking process

Input ECG signals are collected from MIT-BIH Arrhythmia database [16]. This database, provides online signals by PhysioNet, is a result of the venture between BIDMC and MIT, and most widely applied databases for research purposes. The database is made up of 48 half-hour fragment of two-channel (two leads) ambulatory ECG recordings. The input feature values and the loaded data are checked in order to find the similarities. If any match arises the corresponding patient's data will be displayed along with their current ECG signal. Retrieved ECG signal is shown in fig.9.

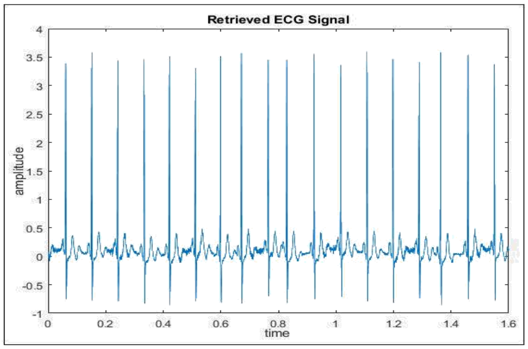

Fig.9. Retrieved signal

VI. Performance Evaluation

A. Error Reduction and Enhanced signal

When the hiding capacity of the system is low the error rate will be high. In order to reduce the error rate hiding capacity of the system must be increased is shown in fig 10.

Due to increase in the error rate at low hiding capacity the PSNR value will be low. The quality of the received signal can be improved by increasing the hiding capacity of the system, which results in enhanced PSNR value is shown in fig 11.

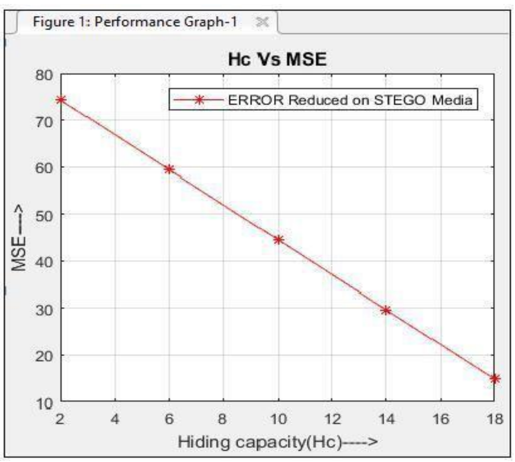

Fig.10. Error reduced on STEGO media

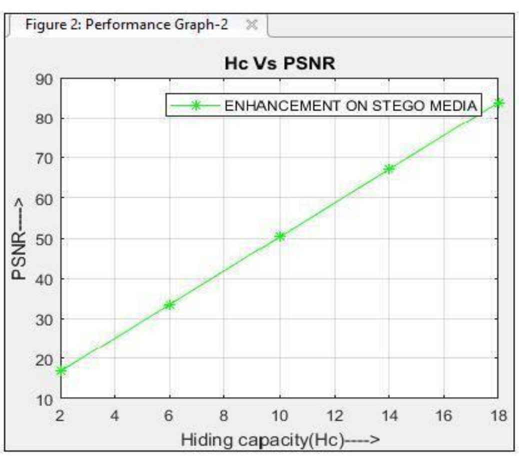

Fig.11. Enhanced signal

VII. Conclusion

The Wireless Body Area Network is a rising and future promising innovation that will change individuals' healthcare revolutionarily. Information security and protection in WBANs and WBAN-related e- healthcare frameworks is a huge zone, and there still remain various extensive issues and challenges which is difficult to overcome. In this paper, polynomial based techniques have been used for secure data transmission. Our proposed system will reduce the error rate and additionally increases the PSNR value. Performance of the proposed system can be further increased by using other transformations.

References

[1] R. Schmidt, T. Norgall, J. Morsdorf, J. Bernhard, and T. vonderGrun, "Body area network (BAN)-a key infrastructure element for patient centered medical applications," *Biomedizinische Technik/Biomedical Engineering*, vol. 47, no. s1a, 2002.

[2] L. Schwiebert, S. Gupta, and J. Weinmann, "Research challenges in wireless networks of biomedical sensors," in *MobiCom*, 2001.

[3] Chunqiang Hu, Nan Zhang, Hongjuan Li, Xiuzhen Cheng, and Xiaofeng Liao, "Body Area Network Security: A Fuzzy Attribute-Based Signcryption Scheme" in IEEE journal on selected areas in communications/supplement, vol.31, No.9, sept 2013.

[4] J. Penders, J. vande Molengraft, L. Brown, B. Grundlehner, B. Gyselinckx, and C. V. Hoof, "Potential and challenges of body area networks for personal health," in *EMBC*, 2009.

[5] M. Al Ameen, J. Liu, and K. Kwak, "Security and privacy issues in wireless sensor networks for healthcare applications," *J. Medical Syst.*vol. 36, 2012.

[6] Al Dulaimi, Layth Adnan & Ahmad, R.Badlishah & Hassnawi, L & Ehkan, Phaklen & Shihab, Israa. (2017). Performance Comparison of Different MAC Protocols over Wireless Body Area Networks (WBAN). Australian Journal of Basic and Applied Sciences. 11. 34-40.

[7] M. Li, W. Lou, and K. Ren, "Data security and privacy in wireless body area networks," *TWC*, vol. 17, no. 1, pp. 51–58, 2010J. Clerk Maxwell, A Treatise on Electricity and Magnetism, 3rd ed., vol. 2. Oxford: Clarendon, 1892, pp.68-73.

[8] Mohammed MANA, Mohammed FEHAM and Boucif AMAR BENSABER, "SEKES (Secure and Efficient Key Exchange Scheme for wireless Body Area Network)", IJCSNS International Journal of Computer Science and Network Security, Vol. 9, No. 11, November 2009.

[9] Krishna K. Venkatasubramanian, Ayan Banerjee, and Sandeep Kumar S. Gupta*, "PSKA: Usable and Secure Key Agreement Scheme for Body Area Networks "*IEEE Transactions on Information Technology in Biomedicine, Vol. 14, No. 1, January 2010.

[10] Shinyoung Lim, Tae Hwan Oh Young B.Choi Tamil Lakshman," *Security Issues on Wireless Body Area Network for Remote Healthcare Monitoring* "978-0-7695-4049-8/10, 2010 IEEE .

[11] Jinyuan Sun, Yuguang Fang, *"Privacy And Emergency Response In E-Healthcare Leveraging Wireless Body Sensor Networks* Xiaoyan Zhu 2010 IEEE IEEE Wireless Communications • February 2010.

ISBN 978-1-5386-4473-7

[12] Clair, Bryan. "Steganography: How to Send a Secret Message." 8 Nov. 2001 www.strangehorizons.com/2001/20011008/steganograph y.shtml.

[13] Dai Y., Liu G., and WangBreaking Z., "Predictive-Coding- Based Steganography and Modification for Enhanced Security", IJCSNS International Journal of Computer Science and Network Security, vol.6 no. 3b, March 2006.

[14] N. Provos and P. Honeyman, "Hide and seek: An introduction to steganography," Security and Privacy, IEEE, vol.99, no.3, pp.32-44, 2003.

[15] Krishna K. Venkatasubramanian, Ayan Banerjee and Sandeep K. S. Gupta, "Plethysmogram-based Secure Inter-Sensor Communication in Body Area Networks"IEEE 2008.

[16] Azariadi, Dimitra, Vasileios Tsoutsouras, Sotirios Xydis, and Dimitrios Soudris. "ECG signal analysis and arrhythmia detection on IoT wearable medical devices" 5th International Conference on Modern Circuits and Systems Technologies (MOCAST), 2016.

ISBN 978-1-5386-4473-7

Hidden Markov model-based Sign Language to Speech Conversion System in TAMIL

Aiswarya V, Naren Raju N, Johanan Joy Singh S, Nagarajan T, Vijayalakshmi P
SSN College of Engineering
Chennai

Abstract—***Quick-eared and articulately speaking people convey their ideas, thoughts, and experiences by vocally interacting with the people around them. The difficulty in achieving the same level of communication is high in the case of the deaf and mute population as they express their emotions through sign language. An ease of communication between the former and the latter is necessary to make the latter an integral part of the society. The aim of this work is to develop a system for recognizing the sign language, which will aid in making this necessity a reality. In the proposed work an accelerometer-gyroscope sensor-based hand gesture recognition module is developed to recognize different hand gestures that are converted to Tamil phrases and an HMM-based text-to-speech synthesizer is built to convert the corresponding text to synthetic speech.***

I. INTRODUCTION

Speech and language are the primary media of communication for the human race which enables them to move about with their everyday activities with ease. However, the vocally and hearing-impaired population is deprived of this medium thus making it difficult for them to completely be a part of the dominant unimpaired society. The deaf and mute use sign language to express their emotions and views unlike their normal counterparts who are natural language speakers. Sign language chiefly uses hand movements, facial expressions and movements of the eyebrows and head to convey their intended message. The people who benefit from the usage of the sign language are the ones who can interpret the same whereas, it is highly difficult for a person who is not trained in the sign language to understand the same. Hence, a translator that is capable of interpreting different hand gestures/signs and to convert it to speech is necessary to make communication between an untrained unimpaired listener and impaired speaker feasible.

The sign language to text conversion module is basically a hand gesture recognition module. Hand-gesture recognition involves recognizing the dynamic gesture by comparing it with pre-defined metrics of the trained models. Hand-gesture recognition systems find their application in areas such as character-recognition, home automation, robotic arm controllers and much more. Hand gesture recognition systems use sensors to sense a dynamic hand movement and based on the types of sensors used, the gesture recognition systems are classified into vision-based gesture recognition systems and glove-based gesture recognition systems.

Vision-based gesture recognition systems: In a vision-based approach, the sensor used is a camera for capturing the image/video of the static/dynamic gesture performed and the captured information is directed to the image processing unit which processes the images through different filtering and image processing techniques. Salient features for training are extracted from the images and then the gestures are recognized using various image recognition algorithms during the testing phase.

M. Hasan et al [2] proposed an USB camera-based machine learning approach using a k-NN algorithm where the nearest possible neighbors are grouped together and a Support Vector Machine (SVM) classifier is used for classifying 16 gestures. K. K. Dutta et al [3] proposed a double handed sign language translator using a Logitech web camera sensor with minimum Eigenvalue algorithm for translating English alphabets. M. Ahmed et al [5] proposed a novel technique of implementing a translator using a Kinect sensor for depth sensing of the whole body. Here, the sensor recognizes the gestures by calculating the distance between the spinal cord and joints. Though all the vision-based techniques are natural and are economical to an extent, its performance is strongly influenced by external factors such as lighting conditions and background color. Their immobility and complicated algorithms is a big turn-down as well.

Glove-based gesture recognition system: It involves using wearable sensors that can capture the physical movement of the hand. Some of the glove-based sensors used are copper glove-based sensors, flex sensors [6] [7], tactile sensors and MEMS [1] [4] sensors. The biggest advantage of using a glove-based sensor is its precise data collection ability and its portability. Algorithms such as the State Estimation algorithm and k-means clustering [8] are used in combination with glove-based sensors but have resulted in extreme time consumption and increased computational complexity. Therefore, in this paper, a robust, easily compatible and a mobile translator is proposed for facilitating effective communication between the deaf and mute and the hearing and vocally unimpaired population. The sign language to speech conversion system developed here consists of a sign language to text conversion module and a text-to-speech synthesis module.

The proposed system and its modules are described in section II. The process of gesture recognition and sign-language-to-text conversion followed by the process of text-to-speech synthesis is discussed in section III. Performance of the sensor-based gesture recognition system is analyzed, and the results are discussed in section IV.

ISBN 978-1-5386-4473-7

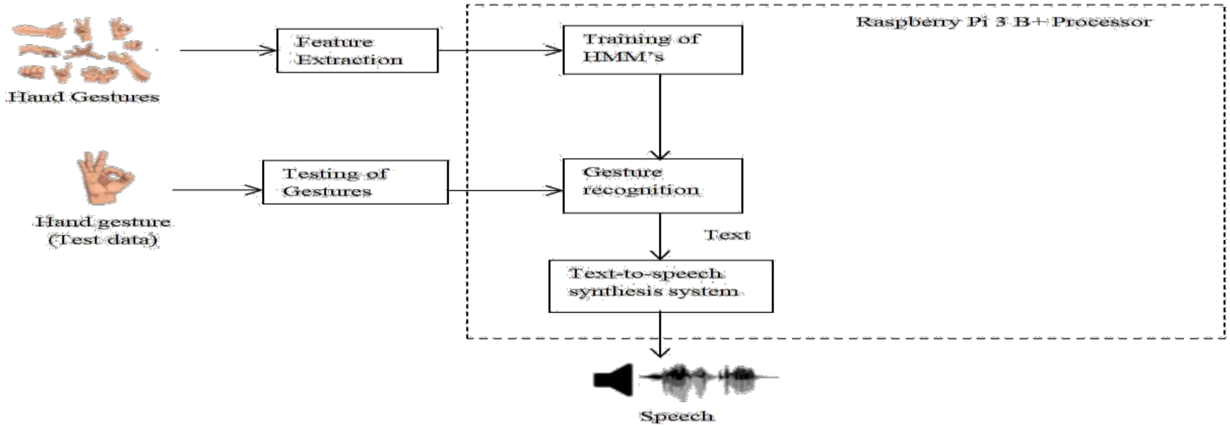

Fig.1 Sign Language to Speech Translation System

II. PROPOSED SYSTEM AND ITS MODULES

This section addresses the implementation techniques required to build the proposed system. The proposed system is a hidden Markov model-based sign language to speech conversion system. It uses a glove -based approach consisting of a 6 -axis MEMS sensor for sensing dynamic hand movements (refer to Fig.1) and is interfaced to the digital ports of a raspberry pi (3B$^+$) that hosts the entire device.

The sensor 'MPU6050', is a 6-axis dual sensor device consisting of a gyroscope and an accelerometer. The sensed data is characterized by 6 feature vectors that are further used for training the models.

The translator operates in 3 modes mainly:

- **Training mode** – involves storing the features in the database and building models using hidden Markov modeling technique.
- **Testing phase** – involves comparing the generated features from the test data with the trained model and generating the corresponding text in Tamil.
- **Translation mode** – involves synthesizing speech in Tamil for the text corresponding to the gestures recognized.

A. MPU6050 sensor

The MPU6050 (refer to Fig.2) sensor combines a 3-axis gyroscope and a 3 -axis accelerometer on the same silicon die, together with an onboard Digital Motion Processor (DMP), which processes complex 6-axis motion fusion algorithms.

Fig.2. MPU6050

The 3-axis coordinates of the accelerometer capture the acceleration of the motion and the 3-axis coordinates of the gyroscope capture the rotation of the hand in a particular direction. These coordinates represent values corresponding to rotational shift and accelerated shift with respect to position.

B. Raspberry Pi

A raspberry pi (refer to Fig.3) is a single board computer that is used for processing multiple tasks simultaneously. The chip's lightweight and low cost makes it affordable and portable. The pi has 40 General Purpose Input Output (GPIO) pins.

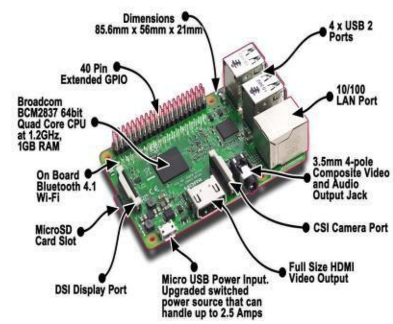

Fig.3. Raspberry Pi

The pi has a processor of 1.2 GHz, 64/32-bit quad-core ARM Cortex-A53 and a memory of 1GB RAM at 900MHz.The pi is equipped with onboard Wi-Fi, an audio jack for playing the synthesized speech, 4 USB ports for supporting other input/output devices and a MicroSD card slot for storing the database. This single module is sufficient for training and testing thereby making it a suitable choice for the proposed system.

Using the above hardware, the proposed system is developed to take the hand-gesture as input, recognize the text corresponding to the gesture and in turn convert the recognized text into synthetic speech in Tamil thus resulting in an end-to-end communication system.

ISBN 978-1-5386-4473-7

Table 1. Gestures in the conversational domain

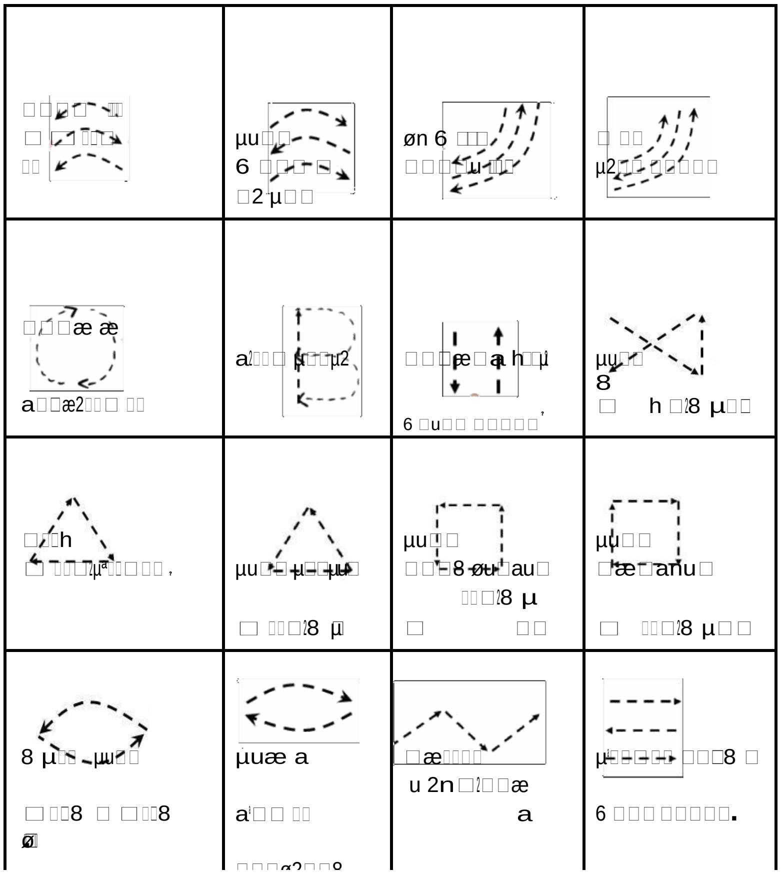

III. SIGN LANGUAGE TO SPEECH CONVERSION

The proposed Sign Language to Speech Translation (SLATS) system discussed in earlier sections makes use of a hidden Markov model (HMM) based modules for sign language recognition system and text-to-speech conversion. The hidden Markov model is a statistical model in which the system is assumed to follow a Markovian process with finite hidden states. The advantage of hidden Markov modeling technique is its ability to determine the sequence of occurrence of states in a gesture by using the transitional probability metric. The most probable sequence is determined by the Viterbi Algorithm. HMM has been widely used in many applications, such as speech recognition, activity recognition from video, gene finding and gesture tracking. The extracted features corresponding to each gesture are used to train the hidden Markov models.

The total number of gestures chosen in this current work is 16 and 16 hidden Markov models are trained. HMMs are used to synthesize speech in the text-to-speech synthesis unit which is unlike existing sign-to-speech converters where pre-recorded audio files are played back. Hence, the proposed conversion system is capable of handling a large vocabulary using a text-to-speech synthesizing unit.

A. Sign language to text conversion

Text conversion involves mapping the recognized gestures to its corresponding TAMIL texts. The number of gestures chosen for training is 16 in the conversational domain. Each gesture lasts for 3 seconds and around 90 examples are used for training and 10 examples for testing. So, a total of 100 examples are collected from 3 individuals. Each of the 16 gestures depicts 16 different Tamil phrases. Sixteen models are trained, one for each gesture in the training phase and during the testing phase a dynamic gesture is sensed by the sensor and the gesture is recognized by comparing it with the models trained. The recognized gesture is mapped to a Tamil text.

B. HMM-based text-to-speech synthesis system

A Text-to-speech (TTS) synthesis system converts any given text to its corresponding speech. The Tamil text obtained after recognition is fed to a text-to-speech synthesizer that provides a voice to the gesture made. This HMM-based TTS system also involves a training phase and a synthesis phase.

Training phase: Five hours of speech data is collected from a male speaker in a laboratory environment at a sampling rate of 16 KHz. Text from short stories forms the text corpus required for speech data collection. Feature vectors derived from the collected speech data is used to train the phoneme level HMMs.

Synthesis phase: In synthesis phase, each text sentence is converted to a pentaphone sequence. A sentence-level HMM is then generated by concatenating the appropriate phoneme-level HMMs. Specialized parameter generation algorithms are used to determine the spectral and excitation parameters. Finally, a vocal output characterized by the determined parameter values is synthesized with a source-filter model and is heard via a loudspeaker.

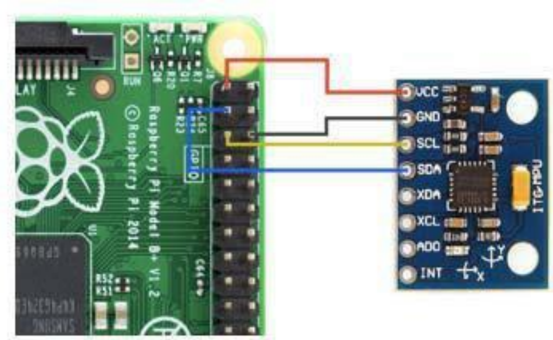

Fig.4. Interfacing MPU6050 with Raspberry Pi

The interfacing of MPU6050 with raspberry pi and the Sign Language to Speech conversion system is depicted in the Fig.4 and Fig.5 respectively.

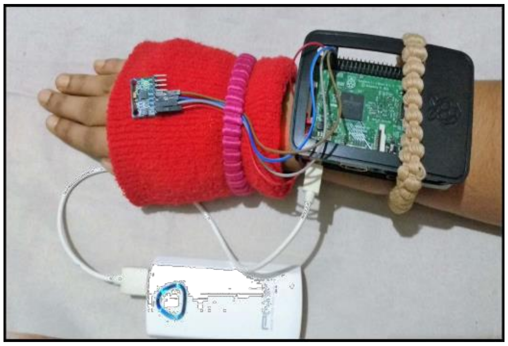

Fig.5. Sign Language to Speech Translator

IV. RESULTS AND ANALYSIS

The testing phase involves performing a gesture that captures the motion-related features and comparing it with the 16 logical HMMs. The output of testing is shown in Fig.6. This Tamil text is fed to a TTS synthesizer to produce a voice output.

==============================***

Read 12 physical / 16 logical HMMs

Read lattice with 6 nodes / 7 arcs

Created network with 10 nodes / 11 links

File: gesture_recognition_htk/data/test/hi56.htk

□□□ □ □□ □□□□□□□ == *[30 frames]*

==============================***

Fig.6.Sign language to Text Conversion

In the proposed work the system is trained for a set of 16 gestures (Table 1) in the conversational domain. Each gesture was tested 10 times in real time and also with test datasets, and the accuracy of the recognition system was found to be **87.5% and 100%** respectively. The overall performance of the translator achieves an average score of **80-90%.** The performance of the proposed system during online testing depends on the orientation of the hand during its dynamic movement. Hence, the performance can be improved by placing the hand in the right orientation to avoid any misinterpretation of the gestures.

V. CONCLUSION

Communication between the deaf and mute and their normal counterparts is very difficult when the latter is not trained in sign language. Therefore, to overcome this problem, a sign language to speech conversion system is proposed. The conversion system is basically an HMM-based hand gesture recognition system that recognizes dynamic hand gestures and converts them to Tamil text. This text is fed to a text-to-speech synthesizer which gives the system a voice. The system developed follows a glove-based approach which makes it a very portable, light weighing and power saving device. This work can be further developed by training with as many gestures as required.

References

[1] B.D.Jadhav, Nipun Munot, Madhura Hambarde, Jueli Ashtikar "Hand Gesture Recognition to Speech Conversion in Regional Language "*IJCSN International Journal of Computer Science and Network*, Volume 4, Issue 1, February 2015,pp.161-166.

[2] M. Hasan, T. H. Sajib and M. Dey, "A machine learning based approach for the detection and recognition of Bangla sign language," *2016 International Conference on Medical Engineering, Health Informatics and Technology (MediTec), Dhaka*, 2016,pp.1-5.

[3] K. K. Dutta, Satheesh Kumar Raju K, Anil Kumar G S and Sunny Arokia Swamy B, "Double handed Indian Sign Language to speech and text," *2015 Third International Conference on Image Information Processing (ICIIP)*, Waknaghat, 2015, pp.374- 377.

[4] Kiran R,"Digital Vocalizer System for Speech and Hearing impaired",in proc of *The International Journal of Advanced Research in computer and communication Engineering*, volume 4, Issue 5, May 2015,pp.81-84.

[5] M. Ahmed, M. Idrees, Z. ul Abideen, R. Mumtaz and S. Khalique, "Deaf talk using 3D animated sign language: A sign language interpreter using Microsoft's kinect v2,"*2016 SAI Computing Conference (SAI)*, London, 2016, pp. 334-335.

[6] P.Vijayalakshmi and M. Aarthi, "Sign language to speech conversion," *2016 International Conference on Recent Trends in Information Technology (ICRTIT)*, Chennai, 2016, pp. 1-6.

[7] K.Abhijith Bhaskara, Anoop G.Nair,K Deepak Ram,Krishnan Ananthanarayanan and H.R. Nandhi vardhan ,"Smart Gloves for hand gesture recognition"2016 International Conference on Robotics and Automation for Humanitarian Applications (RAHA) ,2016,pp.1-6.

[8] T. H. S. Li, M. C. Kao and P. H. Kuo, "Recognition System for Home-Service-Related Sign Language Using Entropy-Based K - Means Algorithm and ABC-Based HMM," in *IEEE Transactions on Systems,Man, and Cybernetics: Systems*,vol.46,no.1, Jan.2016,pp.150-162

[9] https://github.com/raspberrypi

[10] https://www.youtube.com/watch?v=ZqXnPcyIAL8.

[11] www.raspberrypi.org/documentation/configuration/raspi-config.md

ISBN 978-1-5386-4473-7
IEEE sponsored 4th International Conference on Biosignals, Images and Instrumentation, SSNCE, Chennai. ICBSII 2018 – 22nd-24thMar'18

Computational Investigation of Stroke Lesion Segmentation from Flair/DW Modality MRI

K. Revanth, T.D. Varsha shree, N. Sri Madhava Raja, V. Rajinikanth

Department of Electronics and Instrumentation Engineering,
St.Joseph's College of Engineering,
OMR, Chennai 600119, India.
Email: revanth.k.h@gmail.com

***Abstract*— Brain stroke (BS) is one of the dangerous diseases in human community, which causes the temporary or permanent disability and also death. Hence, in clinical level, the screening procedure BS is usually done using with brain images. MRI is a widely considered imaging procedure to record the internal organs of human body for clinical analysis purpose. This paper presents a soft computing procedure to examine the BS from the MRI of Diffused Weigh (DW) and Flair. This paper implements the combination of thresholding and Localized Active Contour (LAC) segmentation procedure to extract the stroke section. The evaluation of the stroke section if done using Haralick texture features. This paper also provides a performance evaluation of DW and Flair images. The outcome of this research confirms that, flair modality supports better result compared with the DW.**

Keywords—Brain stroke; diffused weigh; flair modality; thresholding; segmentation; Haralick features.

I. INTRODUCTION

In medical domain, imaging practices are widely considered to record the abnormalities in internal or external organs to keep the record, such as the nature of the disease, cause for the disease, infection rate, severity and evolution with respect to time. These images are also considered to obtain the initial opinion from the doctors before planning a treatment process to limit or cure the disease [1-6].

After getting the medical image, a dedicated image evaluation procedure is to be implemented on the image in order to extract the abnormal region, which provides the essential information regarding the disease. In the imaging literature, a considerable number of procedures are implemented by the researchers to extract and examine the infected region from a class of imaging methods [7-12].

This paper considers the examination of brain stroke recorded using MRI of Flair and DW modalities. From the literature, it can be noted that, MRI and CT are widely considered to record and abnormalities in brain, like stroke and tumor. Initially, the MRI is to be examined to localize the abnormal section, to examine the volume/infected area and also to assess the severity. The accuracy of the evaluation procedure is increased by implementing the combination of the thresholding operation and segmentation task. To have the better thresholding, Bacterial Foraging Optimization (BFO) is considered. The considered MRI images are RGB scaled pictures and a thresholding is implemented to get the best thresholds from the R, G, B levels. The outcome of the thresholding procedure is then considered to implementation a region extraction task based on Active Contour (LAC) segmentation. Finally, the texture features of the extracted lesion is examined by computing the Haralick features (GLCM) which can be considered to test and train the classifier unit in future. The results of this study confirm that, the Flair modality MRI offers better outcome compared with the MRI recorded with DW modality. The average simulation time taken for both the cases is approximately similar.

II. METHODOLOGY

This part of the paper provides the details of methods implemented to extract and evaluate the stroke section of the considered MRI dataset. In the proposed work, two stage procedure widely discussed in the recent imaging literature are adopted [5,8,13-15].

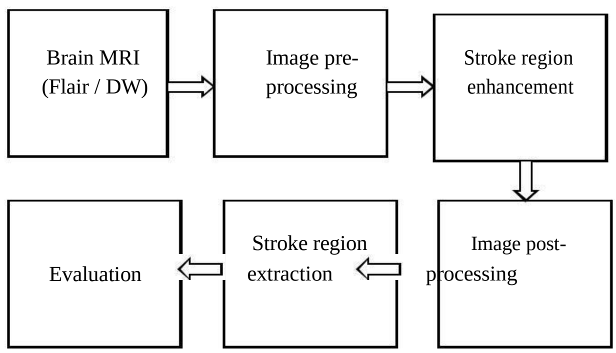

Fig 1. Various stages in the proposed approach

Fig 1 depicts a block diagram representing the various stages existing in the proposed approach. The two stage approach involves in; (i) Pre -processing method to improve the region of interest (ROI) and (ii) Post-processing procedure to extract the ROI. Finally, the proposed approach is validated based on the stroke evaluation procedure implemented by means of Haralick function. In this work, the 2D brain images of Radiopedia database [16] is considered for the evaluation. A total 20 normal and 20 abnormal MRimages are considered for study.

ISBN 978-1-5386-4473-7

A. Pre-processing

As discussed in the earlier works [8, 13 -15], the pre-processing stage is normally considered to enhance the abnormality in the test picture. This stage implements Tsallis entropy based procedure to improve the visibility of stroke section in Flair/DW modality images based on the pixel grouping concept. The previous work confirms the superiority of the Tsallis entropy based procedures on various image processing applications and the mathematical expression of Tsallis function can be accessible from [17-21]. The main process in the thresholding operation is, adjusting the picture's threshold value till the maximum value of entropy is reached.

$$f(T)_{max} = argmax \left[S_q^A(T) + S_q^B(T) + S_q^C(T) + (1-q).S_q^A(T).S_q^B(T)S_q^C(T) \right] \quad (1)$$

Eqn. (1) represents the maximal Entropy based on the threshold level 'T' [19,20]. A tri-level thresholding process separates the test image into background, brain section and the stroke region.

In order to speed up the thresholding processing, the optimization exploration is executed based on the BFO algorithm. A detailed theoretical assessment of the BFO can be found in [22,23]. For tri-level thresholding search, the BFO parameters are chosen as; number of bacteria is 25, dimension of exploration is 3, total number of iteration is fixed as 1000 and the stopping criteria is chosen as $f(T)_{max}$.

B. Post-processing

After the segregation, the stroke region can be easily mined by implementing a segmentation process. Various possible segmentation methods for the stroke extraction is clearly discussed in the recent paper of Rajinikanth and Satapathy [24]. In this paper, the localized active contour (AC) proposed by Chan and Vese [25,26] is adopted. The limitation of this procedure is, it requires the initial bounding box in order to extract the ROI based on an adaptable boundary, which will adjust till all the similar pixel groups are identified and extracted. The AC is initially proposed to mine a section based on the user's choice [27]. The recent biomedical imaging works confirms the superiority of the AC over other segmentation techniques [13, 15]. In the proposed work, AC is initialized inside the brain region to extract the stroke section from Flair/DW modality MRI.

C. Feature extraction

Finally, the texture features of the mined region are extracted using the Haralick function widely known as the Gray Level Co-occurrence Matrix (GLCM) [28,29]. The previous image processing works confirm that, GLCM features are normally used to extract vital information from the ROI. After extracting these features, a classifier system is to be constructed to classify the MRI dataset of stroke lesion into normal, mid and severe, which will help the doctor to identify the treatment process to be followed to cure the disease [30].

III. Results and Discussion

The experimental investigation and the corresponding outcome are presented in this section. The proposed work is implemented using MATLAB 7 software and the necessary brain MRI dataset considered in this paper is obtained from the Radiopedia image database [16]. The test images have a pixel dimension of 630 x 630 pixels and these MRI images are in RGB scale format, hence the initial pre-processing procedure called the thresholding is directly implemented in RGB scale. The RGB scale thresholding is more complex compared with the gray scale thresholding due to three different histogram regions [31,32].

TABLE I. SAMPLE TEST IMAGES CONSIDERED IN THIS STUDY

Pseudo name	MRI stroke pictures: DWI	MRI stroke pictures: Flair
Slice1	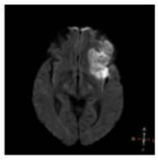	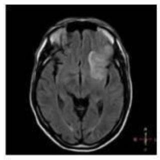
	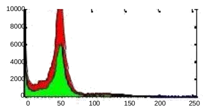	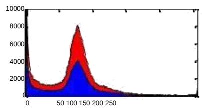
Slice2	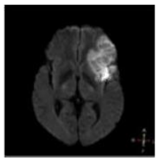	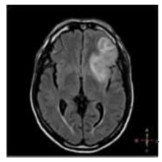
Slice3	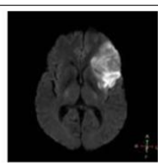	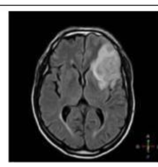
Slice4	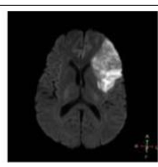	
Slice5	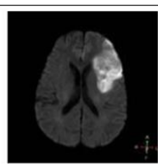	
Slice6	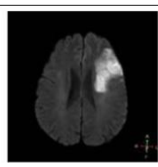	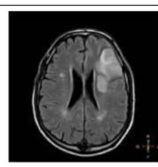

Slice7	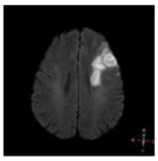	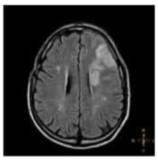
Slice8	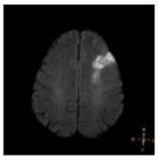	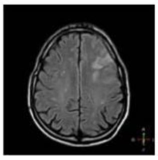

Table 1 presents the RGB scaled MRI images recorded using the Flair and DW modalities. Flair image visibility is more and it does not have any skull section. Hence, the proposed tool can be easily implemented and it does not require any skull stripping procedure [24]. The visibility of stroke section of DW modality picture is not perfect compared with the Flair and the DW image also contains the skull section. From this, it is clear that, extraction of ROI is complex in DW image compared to Flair.

This table also shows the histogram of slice1 to confirm that, these images falls in RGB class. Proposed image processing procedure is initially tested on Slice1 of Flair and DW MRI and the corresponding results are presented in Fig 2. Fig 2 (a) and (e) depicts the tri-level thresholded image of Slice1 based on the BFO algorithm and Tsallis entropy. From these images, it can be noted that, tri-level thresholding procedure enhances the stroke lesion by grouping the similar pixel levels. Also, it divides the entire image cluster into three classes, such as background, brain section and stroke lesion. Fig 2 (b) and (f) presents the initial bounding box assigned manually in AC to extract the stroke region. When the time/iteration increases, the box is allowed to shrink towards the ROI, after identifying all the possible similar image pixel which belongs to the stroke, AC section stops as in Fig. 2 (c) and (f) . The extracted ROI section by the proposed approach is shown in Fig.2 (d) and (h) and this ROI are then considered to extract the texture features based on GLCM. The computation time (CPU run time; sec) of the entire procedure is recorded and for Slice1 picture, it is found that, 173.18sec for Flair and 178.41 sec for DW modality.

Similar procedure is repeated for other slices of Flair/DW existing in the chosen dataset and the corresponding results are clearly presented in Table II. From this Table, it is clear that, proposed procedure is directly implemented on the RGB scale picture and the final outcome also confirms that, this tool is very efficient in extracting the ROI completely without any deviation. Similar work recently done by Rajinikanth and Satapathy [24], considers a gray scale image to examine the stroke lesion of the Flair/DW modality. Hence the proposed technique can be used to extract the abnormality from the complex test images, irrespective of its color scale.

The main aim of the proposed research work is to evaluate the performance image processing tool on various modality brain MRIs. From the experimental outcome, it is confirmed that, proposed procedure is a semi-automated approach, which perfectly extracts the ROI from the Flair and DW modality pictures. Moreover, this approach does not require any skull stripping procedure as previously discussed in many of the brain MRI examination approaches. In the medical image processing literature, classification is a proven procedure to examine the test pictures based on its texture features. After extracting the ROI from a chosen MRI images, its texture features are then extracted using the Haralick function discussed in [28, 29]. The Haralick function computes the vital shape and engineering features based on the length, width and orientation of the ROI. In future, these features can be considered to train and test the classifier units to segregate the test images into various classes for the automated segregation and detection of the stroke based on its harshness.

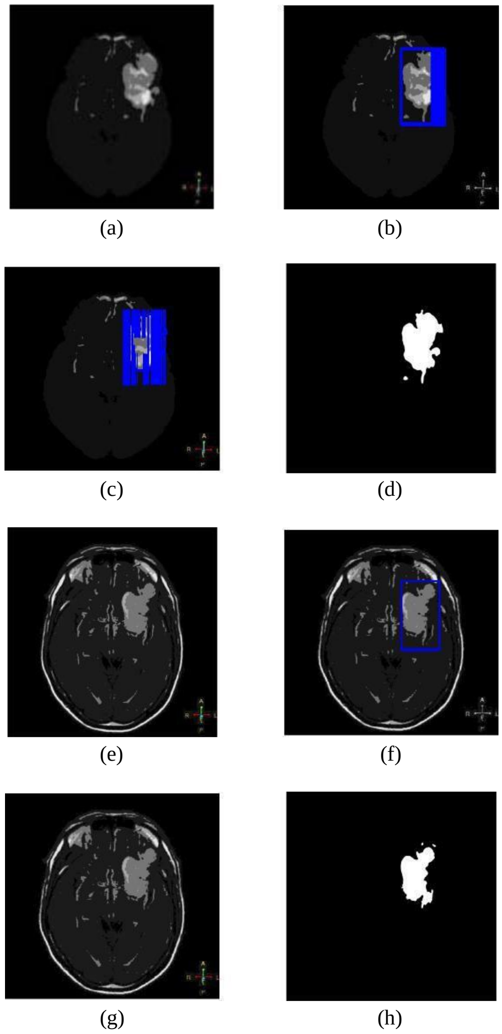

Fig 2. Implementation of proposed tool on Slice1 test picture (a) and (e) Represents outcome of pre-processing section of Flair and DW respectively, (b) and (f) shows the initial bounding box of active contour, (c) and (g) presents the converged active contour boundary and (d) and (h) presents the extracted stroke section.

TABLE II. RESULT OBTAINED WITH THE CHOSEN MRI DATASET

	Thresholded images		Segmented images	
	DWI	Flair	DWI	Flair
Slice1	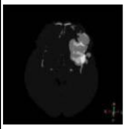	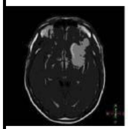		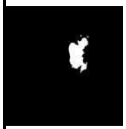
Slice2	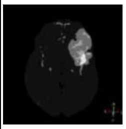	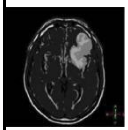		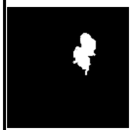
Slice3	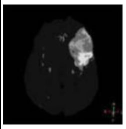	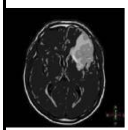	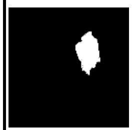	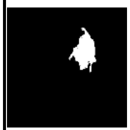
Slice4	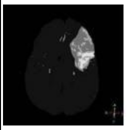	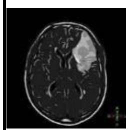		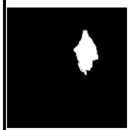
Slice5	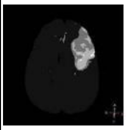	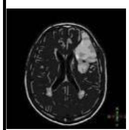		
Slice6		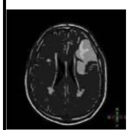	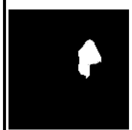	
Slice7		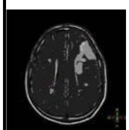		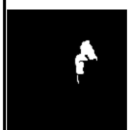
Slice8		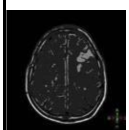	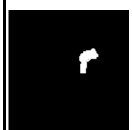	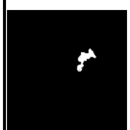

The proposed paper considers a two stage image processing technique guided by a heuristic search. In this work, performance of the work of Flair and DW modality brain MRI is evaluated using the average CPU time. The Flair modality offers better CPU time compared with DW modality, which confirms that, proposed approach may give better throughput when used to examine the Flair modality. The throughput can also be increased by reducing the size of the test picture. Since, the imaging literature confirms that gray scale images and images with nominal size are less complex than the RGB and large sized images. The main objective is to extract and evaluate the stroke section, hence, in the proposed work, the image quality measures are not computed for the pre-processing stage as discussed in the work [32 -34]. Finally, the texture features are computed for the all the 2D test pictures and the average values are clearly presented in Table III. Selective features, like homogeneity, energy, entropy and correlation or all the GLCM features existing in the table III can be then considered to train the classifier system built using a dedicated soft computing procedure. The future scope of the proposed work is as follows;
(i) Implementing the proposed work on the benchmark ISLES database [35], (ii) Validation of the proposed work with other related works existing in the literature, and (iii) Proposing an automated classifier unit to segregate the MRI image into various disease classes using a classifier system.

TABLE III. AVERAGE GLCM FEATURES AND THE CPU TIME

Feature name	Flair MRI	DW MRI	CPU time (sec)	
			Flair	**DW**
Homogeneity	0.5734	0.5627	151.29	158.36
Energy	0.3835	03892		
Entropy	0.2217	0.3725		
Correlation	0.9584	0.9442		
Variance	0.7184	0.7229		
Contrast	0.1063	0.1094		
IMC1	-0.4926	-0.5118		
IMC2	0.6278	0.6327		
Sum Average	1.6372	1.6627		
Sum Variance	4.2254	4.1864		
Sum Entropy	0.3826	0.4417		
MCC	0.2864	0.2861		

IV. CONCLUSION

This paper implements a two stage analysis to extract the stroke section from the Flair/DW modality brain MRI. The initial stage implements a tri-level thresholding based on the BFO algorithm and Tsallis entropy and the next stage employs an active contour methodology to mine the infected region.
The initial pre-processing stage is implemented directly on the RGB scaled 630 x 630 sized test image in order to test the performance of the proposed approach. The experimental result of this paper confirms that, proposed procedure is very efficient in extracting the stroke lesion in both Flair and DW modality based MRI. In order to assess the throughput of proposed technique, the run time is computed and the average runtime of 151.29 sec and 158.36 sec are obtained for Flair and DW images respectively. Finally, the GLCM features for the stroke section is then computed and in future, these texture features can be considered to design an automated classifier unit which assist the doctors to segregate the patient's image database to identify the severity during the treatment planning procedure.

REFERENCES

[1] G. Garg and M. Juneja, A Survey of Prostate Segmentation Techniques in Different Imaging Modalities, Current Medical Imaging Reviews, vol.14, no.1, pp.19-46, 2018. doi : 10.2174/1573405613666170504145842.

[2] K. Sharma and J. Virmani, A decision support system for classification of normal and medical renal disease using ultrasound images: A decision support system for medical renal diseases, International Journal of Ambient Computing and Intelligence (IJACI), vol.8, no.2, pp. 52-69, 2017. doi: 10.4018/IJACI.2017040104

[3] Y. Hu, H. Li, Z. Li and D. Hu, Hepatic Tumors: Diagnosis and Therapeutic Effect Evaluation of Diffusion- Weighted Imaging, Current Medical Imaging Reviews, vol. 14 , no. 2 , pp. 172 - 178 , 2018. doi : 10.2174/1573405613666161221155922.

[4] K. Manickavasagam, S. Sutha and K, Kamalanand, An automated system based on 2D empirical mode decomposition and k-means clustering for classification of Plasmodium species in thin blood smear images, BMC Infectious Diseases, vol.14, no.3, pp.1, 2014.

[5] T.K. Palani, B. Parvathavarthini, K. Chitra, "Segmentation of brain regions by integrating meta heuristic multilevel threshold with Markov random field," Current Medical Imaging Reviews, vol.12, no.1,pp. 4-12, 2016.

[6] H.M. Warner, R. Batty, A.R. Hart, S.R. Mordekar, A. Raghavan, F. Williams and D.J.A. Connolly, CT and MR Imaging of the Encephalopathic Child, Current Medical Imaging Reviews, vol.14, no.2, pp. 196-206, 2018. doi : 10.2174/1573405613666170504152118.

[7] Y. Zhou, X. Yang, W. Yang, W. Shi, Y, Cui and X.Chen, Recent Progress in Automatic Processing of Skeletal Muscle Morphology Using Ultrasound: A Brief Review, Current Medical Imaging Reviews, Vol.14, no.2, pp. 179-185, 2018. doi : 10.2174/1573405613666170126155934.

[8] N.S.M.Raja, V. Rajinikanth, S.L. Fernandes, S.C. Satapathy, "Segmentation of breast thermal images using Kapur's entropy and hidden Markov random field," Journal of Medical Imaging and Health Informatics, vol.7, no.8, pp. 1825-1829, 2017.

[9] K. Kamalanand, S. Ramakrishnan, "Effect of gadolinium concentration on segmentation of vasculature in cardiopulmonary magnetic resonance angiograms," Journal of Medical Imaging and Health Informatics, vol. 5, pp.1–5, 2015.

[10] M. A. Belarbi, S. Mahmoudi and G. Belalem, PCA as dimensionality reduction for large-scale image retrieval systems, International Journal of Ambient Computing and Intelligence (IJACI), vol.8, no.4, pp. 45-58, 2017. doi: 10.4018/IJACI.2017100104.

[11] R. Vishnupriya, N.S.M. Raja, V. Rajinikanth, "An efficient clustering technique and analysis of infrared thermograms," Third International Conference on Biosignals, Images and Instrumentation (ICBSII), IEEE, pp.1-5, 2017. DOI: 10.1109/ICBSII.2017.8082275.

[12] N. Dey, V. Rajinikanth, A.S. Ashour and J.M.R.S. Tavares, Social group optimization supported segmentation and evaluation of skin melanoma images, Symmetry, vol.10, no.2, pp. 51, 2018. doi:10.3390/sym10020051.

[13] V. Rajinikanth, S.C. Satapathy, S.L. Fernandes, S. Nachiappan, "Entropy based Segmentation of Tumor from Brain MR Images–A study with Teaching Learning Based Optimization," Pattern Recognition Letters, vol.94, pp.87-95, 2017. DOI: 10.1016/j.patrec.2017.05.028.

[14] V. Rajinikanth, N.S.M. Raja, K. Kamalanand, "Firefly Algorithm Assisted Segmentation of Tumor from Brain MRI using Tsallis Function and Markov Random Field," Journal of Control Engineering and Applied Informatics, vol.19, no.3, pp. 97-106, 2017.

[15] V. Rajinikanth, N.S.M. Raja, S.C. Satapathy, S.L. Fernandes, "Otsu's multi-thresholding and active contour snake model to segment dermoscopy images," Journal of Medical Imaging and Health Informatics, vol.7, no.8, pp.1837–1840, 2017.

[16] Cerebral infarction database (Case courtesy of Dr Ahmed Abd Rabou, Radiopaedia.org, rID: 25281)

[17] C.Tsallis, Possible generalization of Boltzmann-Gibbs statistics, Journal of Statistical Physics, vol. 52, no.1, pp.479–87, 1988.

[18] S. Sarkar, S. Das, S. Paul, S. Polley, R. Burman and S.S. Chaudhuri, Multi-level image segmentation based on Fuzzy - Tsallis entropy and differential evolution. In. IEEE International Conference on Fuzzy Systems (FUZZ), (2013). doi: 10.1109/FUZZ-IEEE.2013.6622406.

[19] V. Rajinikanth, S.L. Fernandes, B. Bhushan, N.R.Sunder, "Segmentation and analysis of brain tumor using Tsallis entropy and regularised level set," Lecture Notes in Electrical Engineering, vol.434, pp. 313-321, 2018.

[20] V. S. Lakshmi, S.G. Tebby, D. Shriranjani, V. Rajinikanth, "Chaotic cuckoo search and Kapur/Tsallis approach in segmentation of t.cruzi from blood smear images," International Journal of Computer Science and Information Security (IJCSIS), vol.14, CIC 2016, pp. 51-56, 2016.

[21] K.S. Manic, R.K. Priya, and V Rajinikanth, "Image multithresholding based on Kapur/Tsallis entropy and firefly algorithm," Indian Journal of Science and Technology, vol.9, no.12, 89949, 2016.

[22] K. M. Passino, Biomimicry of bacterial foraging for distributed optimization and control, IEEE Control Systems Magazine, vol. 22, no. 3, pp. 52–67, 2002.

[23] V. Rajinikanth and K. Latha, Controller parameter optimization for nonlinear systems using enhanced bacteria foraging algorithm, Applied Computational Intelligence and Soft Computing, vol. 2012, Article ID 214264, 12 pages, 2012. doi:10.1155/2012/214264.

[24] V. Rajinikanth and S.C. Satapathy, Segmentation of ischemic stroke lesion in brain MRI based on social group optimization and Fuzzy-Tsallis entropy, Arabian Journal for Science and Engineering, pp.1-14, 2018. doi: 10.1007/s13369-017-3053-6.

[25] T.F. Chan and L.A. Vese, Active contours without edges, IEEE T. Image Process., vol.10, no.2, pp.266-277 , 2001.

[26] T.F. Chan and L.A. Vese, Active contour and segmentation models using geometric PDE's for medical imaging. Geometric Methods in Bio-Medical Image Processing, pp.63-75, 2002. doi.10.1007/978-3-642-55987-7_4.

[27] N. Salman, Image segmentation and edge detection based on Chan-Vese algorithm, The International Arab Journal of Information Technology, vol.3, no.1, pp. 69-74, 2006.

[28] R.M. Haralick, K. Shanmugam, and I. Dinstein, Textural features for Image classification, IEEE Transactions on Systems, Man, and Cybernetics, vol.3, no.6, pp. 610–621, 1973.

[29] K. Manickavasagam, S. Sutha and K. Kamalanand, Development of systems for classification of different plasmodium species in thin blood smear microscopic images, Journal of Advanced Microscopy Research, vol.9, no.2, pp. 86-92, 2014.

[30] S. Hemalatha and S. Margret Anouncia, Unsupervised segmentation of remote sensing images using fd based texture analysis model and ISODATA, International Journal of Ambient Computing and Intelligence (IJACI), vol.8, no.3, pp. 58-75, 2017. doi: 10.4018/IJACI.2017070104.

[31] N.S.M. Raja, V. Rajinikanth and K. Latha, Otsu Based Optimal Multilevel Image Thresholding Using Firefly Algorithm, Modelling and Simulation in Engineering, vol.2014, paper id.794574, 2014.

[32] S.C. Satapathy, V. Sri Madhava Raja, V. Rajinikanth et al. Neural Comput & Applic (2016). https://doi.org/10.1007/s00521-016-2645-5.

[33] N.S.M. Raja, P.R.V Lakshmi and K.P. Gunasekaran, Firefly Algorithm-Assisted Segmentation of Brain Regions Using Tsallis Entropy and Markov Random Field, Lecture Notes in Networks and Systems , vol.7, pp. 229-237, 2018.

[34] T.D.V. Shree, K. Revanth, N.S.M. Raja and V.Rajinikanth, A Hybrid Image Processing Approach to Examine Abnormality in Retinal Optic Disc, Procedia Computer Science, vol.125, pp. 157-164, 2018.

[35] ISLES 2015 (www.isles-challenge.org)

ISBN 978-1-5386-4473-7
IEEE sponsored 4th International Conference on Biosignals, Images and Instrumentation, SSNCE, Chennai. ICBSII 2018 – 22nd-24thMar'18

Analysis of Parkinson's disease SPECT images using Geometric measures and Orthogonal Moments

Sivaranjini S, Sujatha C M
Department of Electronics and Communication Engineering,
CEG Campus - Anna University, Chennai – 600025, Tamil Nadu, India.

***Abstract*—Parkinson's disease being a neurodegenerative disorder commonly seen in older age group has become an alarming health issue. The reduced dopaminergic activity in the striatum region leads to serious complications when not diagnosed at the early stage. Symptomatic changes can be seen in these patients which includes both motor and non motor indications. In this work, an attempt is made to discriminate between the normal and Parkinson's disease subjects by morphological changes in the striatum. SPECT neuroimaging modality has been used for this study. DAT SPECT images were downloaded and analyzed. The striatum region on both the left and right hemispheres is segmented. Geometrical changes seen in the segmented region is quantified by various parameters. Geometric features such as area, axis length, extent and circularity measures show significant changes differentiating between normal and Parkinson's disease. The orthogonal image moments extracted from the striatum discriminates between HC and PD with higher significant values. Thus the experimental results show a decreased dopamine activity region on the striatum in Parkinson's disease patients.**

Keywords- Parkinson Disease; SPECT; geometric features; Zernike moments.

I. INTRODUCTION

Parkinson's Disease (PD) is a severe progressive neurodegenerative disorder. It is characterized by degeneration of dopamine producing neurons in the striatum region comprising the caudate nucleus and putamen. Striatum appearing in the subcortical basal ganglia of the forebrain regulates various aspects of motor and cognitive functions [1]. Common indications of PD are seen in impairment of motor functions which is extended to non motor symptoms such as dementia progressing to cognitive decline, depression, sleep disturbances, olfactory disorders, apathy, etc [2, 4]. These manifestations find greater significance with the quality of life measures being deteriorated. The symptoms start appearing when 60% of the dopaminergic neurons start declining only after which an appropriate treatment measure is possible [3]. The annual mortality rate due to PD has been increased by 45% in the recent years [5] with an average increase of 1.4% all over the world [6]. Hence early detection of PD is required with efficient analysis even with subtle signs to decide on the beneficial treatment measures.

Various neuroimaging modalities like SPECT, MRI, PET, Transcranial Sonography, etc. [7, 8] are being used for the diagnoses of PD when prominent manifestations of the disease appear. Diagnostic uncertainty during the early or premature stages of PD can immensely be avoided by the use of SPECT imaging modality compared to the former neuroimaging techniques [9]. Reduction in the binding of the radiotracer used in SPECT neuroimaging indicates dopamine transporter degeneration in PD [10]. Analysis of the morphological changes in the four striatal regions namely the right caudate nucleus, left caudate nucleus, right putamen and the left putamen is required to indicate the loss or dysfunction in the dopamine system. The binding of the radiotracer in the striatum region is obtained from the count densities of the four striatal regions known as the Striatal Binding Ratio (SBR) [14]. The visual interpretation on the SPECT images is the general assessment approach used by physicians. Hence an automated analysis is required to quantify the intensity changes in the striatal regions.

Shape based analysis is essential to acquire information on the morphological changes of the striatum. Quantification of the shape based measures is done to capture the information that can be used to differentiate between Healthy Control (HC) and PD group [11]. Based on the theory of the orthogonal polynomials, moments are derived to capture the global information of the image [12]. These moments are being used in the recent years to give better feature extraction results [13].

In this work, the striatum region of both the right and the left hemispheres are segmented from the SPECT images of HC and PD subjects. From the segmented regions geometric features and Zernike moments are extracted. These feature values are interpreted to show the variation in the shape defining the regions of decreased dopamine activity levels in HC and PD images. This paper is indexed as: Section II expounds on the methodology used in the analysis, Section III presents the results obtained from the simulation and the interpretation of the simulated results and Section IV provides the conclusion of the proposed work.

II. METHODOLOGY

A. Image Database

Single Photon Emission Computed Tomography (SPECT) images with 123I-Ioflupane radiopharmaceutical commonly called as $DaTSCAN_{TM}$ from Parkinson's Progression Markers Initiative (PPMI) database is used for the analysis of PD patients [14]. PPMI database is being used widely to identify the progression biomarkers in PD. SPECT images of HC and

ISBN 978-1-5386-4473-7

PD with a count of 10 images each is utilized for this study. Totally 91 slices for each patient is available in the database out of which the 42nd slice is being considered for this study. This slice selection criterion is based on the higher activity region based on the higher uptake 123I-Ioflupane in the striatum. The PPMI database provides preprocessed images for researchers to carry out the necessary analysis. These images are subjected to segmentation to identify the regions of maximum activity.

B. Segmentation

The striatal regions of elevated activity are to be segmented to analyze the differences in the morphological features between the HC and PD group. Both the left and the right striatum are segmented by image binarization method. The variation in the intensity levels in the image is used. An optimal threshold value of 0.67 is chosen based on various trials for binarization is used for all the images under study.

C. Feature Extraction

Geometric features from the segmented regions are used to quantify the results for the analysis procedure. The feature obtained from the right and the left striatum region is averaged to find the total quantification parameter for each subject. The geometric features such as area, convex area, filled area, solidity, extent, tortuosity, perimeter, major axis length, minor axis length, form factor, compactness and circularity are obtained from the segmented regions.

Zernike moments from the image are extracted by computing the radial polynomials, followed by Zernike basis functions and projecting the image onto the Zernike basis functions to compute Zernike moments [15]. The radial polynomial is given by

$$R_{n,m} = \sum_{s=0}^{(n-|m|)/2} (-1)^s \frac{(n-s)!}{s!((\frac{n-|m|}{2})-s)!((\frac{n-|m|}{2})-s)!} (\rho)^{n-2s} \quad (1)$$

The orthogonal Zernike moments of an N x N image in the discrete form can be expressed as

$$Z_{n,m} = \frac{n+1}{\lambda_n} \sum_{c=0}^{N-1} \sum_{r=0}^{N-1} f(c,r) R_{n,m} \rho_{cr} e^{-jm\theta_{cr}} \quad (2)$$

The transformed distance or magnitude in the above expression can be defined as

$$\rho_{cr} = \frac{\sqrt{(2c-N+1)^2+(2r-N+1)^2}}{N} \quad (3)$$

where c and r are the column and the row numbers of the respective image. These moments can be separated into higher and lower order moments based on the values of n and m in equation 2, called as order of the moments.

III. RESULTS AND DISCUSSION

The representative set of SPECT images for HC is shown in fig. 1(a-b) and for PD is shown in the fig. 2(a-b). The segmented left and the right striatum regions are presented in fig.1 (c-d) for HC and in fig. 2 (c-d) for PD. The striatum is lobe shaped in healthy control whereas it is circular in Parkinson's disease. The striatum changes from lobe shaped to circular shape due to the disease progression.

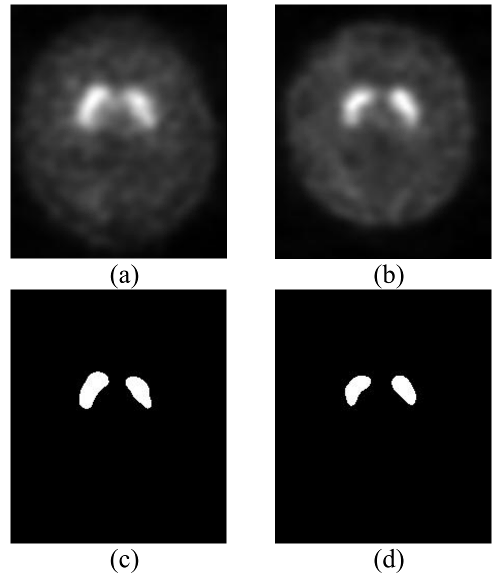

Fig.1 (a - b) representative sets of healthy control SPECT images and their corresponding segmented striatum region (c-d)

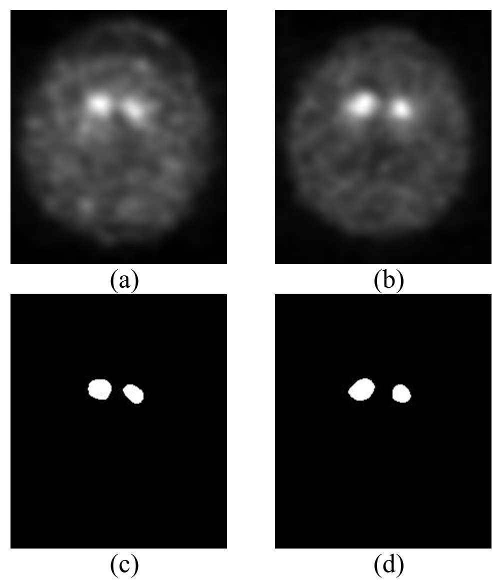

Fig.2 (a-b) representative sets of Parkinson's disease SPECT images and their corresponding segmented striatum region (c-d)

The reduction in the dopamine transporter levels evidenced by the circular segmented reduced striatum region can be seen in PD images. This indicates an adequate loss of dopaminergic activity in these patients. The striatal feature values extracted from the both the left and the right striatum region are given in table 1. The decremented mean values of the area measures and the major axis length indicate a decreased dopaminergic activity in PD compared to HC subjects.

TABLE I: Geometric Features of HC and PD subjects.

Features	HC	PD
Area	0.70 ± 0.16	0.60 ± 0.19
Convex area	0.69 ± 0.15	0.60 ± 0.19
Filled area	0.70 ± 0.16	0.60 ± 0.19
Solidity	0.96 ± 0.03	0.99 ± 0.004
Extent	0.82 ± 0.06	0.89 ± 0.03
Perimeter	0.81 ± 0.10	0.74 ± 0.14
Major Axis Length	0.81 ± 0.10	0.77 ± 0.14
Minor Axis Length	0.84 ± 0.09	0.73 ± 0.13
Form Factor	0.84 ± 0.06	0.91 ± 0.03
Tortuosity	0.95 ± 0.02	0.93 ± 0.03
Compactness	0.84 ± 0.06	0.93 ± 0.04
Circularity	0.84 ± 0.06	0.91 ± 0.03

The minor axis length, solidity, extent, form factor and circularity of the PD subjects are increased with respect to the healthy control. There is a remarkable increase in the mean extent and circularity feature value of PD subjects related to HC. This indicates decreased dopamine levels evidenced by the morphological changes in the striatum. These changes can be observed from the scatter plots of extent and circularity feature values in fig.3

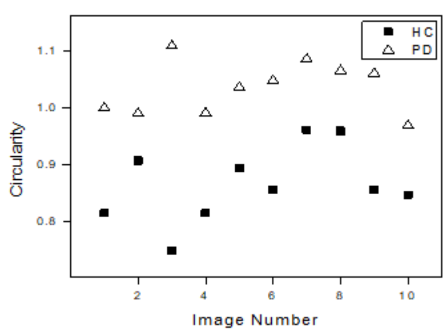

(a)

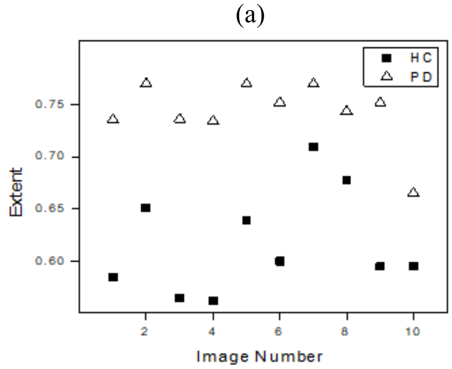

(b)

Fig.3 Scatter plot for Geometric features of HC and PD group.

The Zernike moments are extracted from the segmented HC and PD subject SPECT images. A total of 64 moments with 32 lower order moments and 32 higher order moments have been obtained from the segmented regions. The Zernike moments along with the significance values (p-value) are given in table 2. Variation in the geometry of the striatum region is better evidenced between HC and PD subjects given by good significance values as given in fig.4. Due to the lower computation complexity in the lower order moments they show better significant values than the higher order moments. This indicates reduced uptake of DAT radiotracer showing reducing levels of dopamine.

TABLE II: Zernike moments extracted from segmented HC and PD SPECT images.

Moments	HC	PD	p-value
A(4,2)	0.71 ± 0.19	0.54 ± 0.22	0.00031
A(6,2)	0.70 ± 0.18	0.57 ± 0.25	0.000062
A(8,0)	0.57 ± 0.26	0.74 ± 0.20	0.000478
A(8,2)	0.69 ± 0.16	0.55 ± 0.30	0.000009
A(9,3)	0.66 ± 0.16	0.73 ± 0.22	0.00208
A(10,0)	0.67 ± 0.18	0.75 ± 0.17	0.00366
A(10,2)	0.70 ± 0.14	0.46 ± 0.30	0.000002
A(11,3)	0.73 ± 0.21	0.70 ± 0.16	0.000803
A(14,6)	0.64 ± 0.25	0.74 ± 0.18	0.00142
A(15,3)	0.71 ± 0.30	0.82 ± 0.20	0.000184
A(16,0)	0.32 ± 0.29	0.55 ± 0.22	0.000095

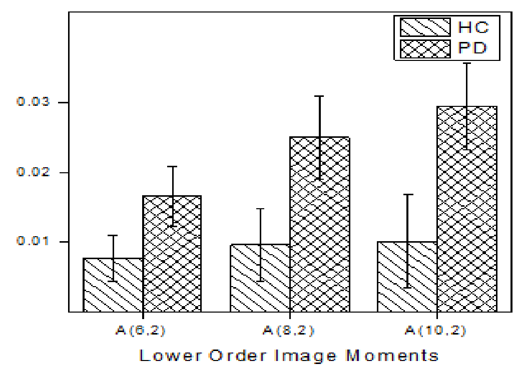

(a)

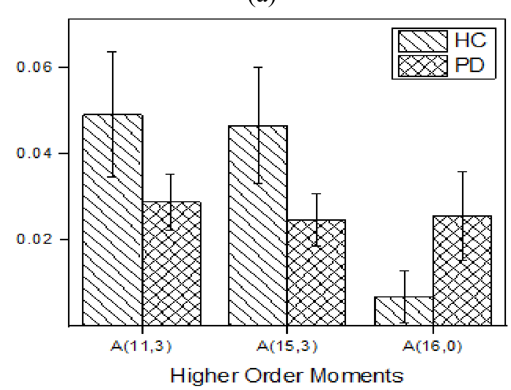

(b)

Fig. 4 Significant Zernike moments of HC and PD represented as bar graph.

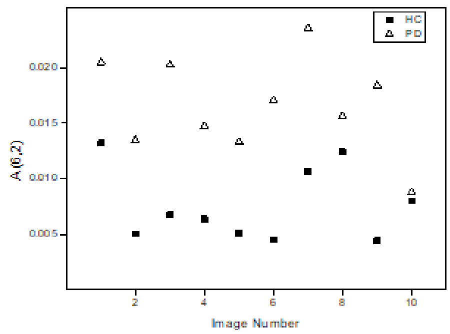

(a)

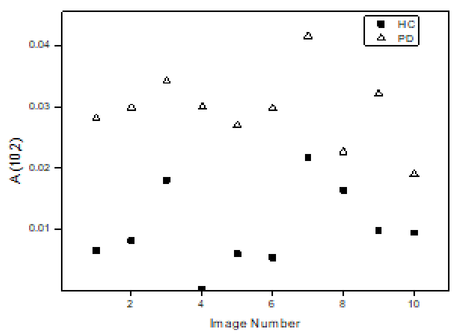

(b)

Fig. 5 Scatter plot representation of A (6, 2) and A (10, 2) Zernike moments.

IV. CONCLUSION

An early diagnosis of Parkinson's disease is essential to improve the management strategies and treatment measures in the disease process. 123I-Ioflupane SPECT imaging plays a significant role in determining the dopaminergic levels in PD patients. In this work, an attempt has been made to analyze striatum region to indicate the reduced dopamine levels in PD group. The striatum region in the SPECT images of HC and PD group is segmented and the geometric features are extracted. Significant feature values such as area, axis length, extent and circularity are interpreted to indicate decreased uptake of DAT radiotracer. Thus the reduced dopamine transporter levels in PD are seen when compared to healthy control. The Zernike image moments extracted from the segmented image indicate prominent variations in the geometry of the striatum region discriminating between the two groups. Thus the stratified decrease in the dopamine activity levels can be seen by the shape based analysis.

REFERENCES

[1] Jean-Sebastien Provost, Alexandru Hanganu, OuryMonchi, "Neuroimaging studies of the striatum in cognition PartI: healthy individuals", Frontiers in Systems Neuroscience, vol. 9, no. 140, 2015.

[2] K Ray Chaudhuri et al., "Non-motor symptoms of Parkinson's disease: diagnosis and management", The Lancet Neurology, vol. 5, no. 3, pp. 235 – 245, 2006.

[3] R. Prashanth, Sumantra Dutta Roy, Pravat K. Mandal, Shantanu Ghosh, "High-Accuracy Classification of Parkinson's Disease Through Shape Analysis and Surface Fitting in 123I-Ioflupane SPECT Imaging", IEEE Journal of Biomedical and Health Informatics, vol. 21, pp. 794-802, 2017.

[4] Siepel et al., "Cognitive Executive Impairment and Dopaminergic Deficits in De Novo Parkinson's Disease", Movement Disorders, vol. 29, no. 14, 2014

[5] Global Burden of Disease Study (ghdx.healthdata.org).As of 2013; refreshed July 2016.

[6] Dorsey ER, Constantinescu R, Thompson JP, et al., "Projected number of people with Parkinson diseases in the most populous nations, 2005 through 2030", Neurology, vol. 68, pp. 384–388, 2007.

[7] Provost et al., "Neuroimaging studies of the striatum in cognition Part I: healthy individuals", Frontiers in Systems Neuroscience, vol. 9, pp. 1-13, 2015.

[8] Dag Aarsland et al., "Cognitive impairment in Parkinson's disease and dementia with Lewy bodies" Parkinsonism and Related Disorders, vol. 22, pp. 144-148, 2016.

[9] Conrado et al, "Dopamine Transporter Neuroimaging as an Enrichment Biomarker in Early Parkinson's Disease Clinical Trials: A Disease Progression Modelling Analysis", Clinical and Translational science, vol. 11, issue 1, 2018.

[10] Dukart et al., "Distinct Role of Striatal Functional Connectivity and Dopaminergic Loss in Parkinson's Symptoms", Frontiers in Aging Neuroscience, vol. 9, pp. 1-10, 2017.

[11] R. Prashanth, S. Dutta Roy, P. K. Mandal, and S. Ghosh, "Shape features as biomarkers in early Parkinson's disease", in Conf Proc 6th Int IEEE/EMBS Conf Neural Eng (NER), pp. 517 – 520, 2013.

[12] Alireza Khotanzad , Yaw Hua Hong, "Invariant Image Recognition by Zernike Moments", IEEE Transactions on Pattern Analysis and Machine Intelligence, vol.12, issue 5, pp. 489-497, 1990.

[13] P. Bhaskara Rao, D.Vara Prasad, Ch.Pavan Kumar, "Feature Extraction Using Zernike Moments", International Journal of Latest Trends in Engineering and Technology (IJLTET), vol. 2, no. 2, 2013.

[14] K. Marek, D. Jennings, S. Lasch et al., "The Parkinson Progression Marker Initiative (PPMI)," Progress in Neurobiology, vol. 95, no. 4, pp. 629-635, 2011.

[15] Amir Tahmasbi, Fatemeh Saki, Shahriar B. Shokouhi, "Classification of benign and malignant masses based on Zernike moments", Computers in Biology and Medicine, vol. 41, No. 8, pp. 726-735, 2011.

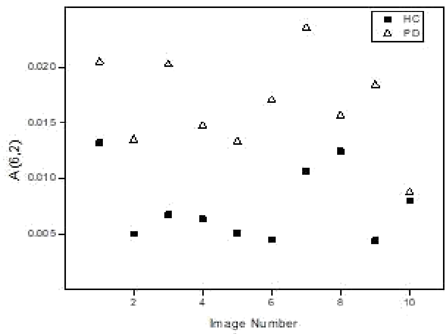

(a)

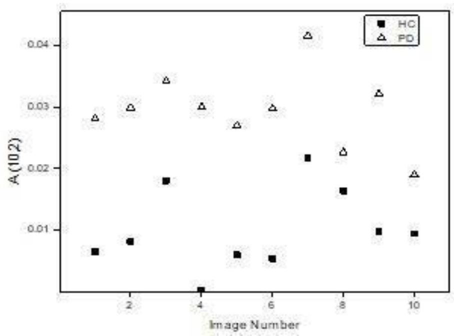

(b)

Fig. 5 Scatter plot representation of A (6, 2) and A (10, 2) Zernike moments.

IV. CONCLUSION

An early diagnosis of Parkinson's disease is essential to improve the management strategies and treatment measures in the disease process. 123I-Ioflupane SPECT imaging plays a significant role in determining the dopaminergic levels in PD patients. In this work, an attempt has been made to analyze striatum region to indicate the reduced dopamine levels in PD group. The striatum region in the SPECT images of HC and PD group is segmented and the geometric features are extracted. Significant feature values such as area, axis length, extent and circularity are interpreted to indicate decreased uptake of DAT radiotracer. Thus the reduced dopamine transporter levels in PD are seen when compared to healthy control. The Zernike image moments extracted from the segmented image indicate prominent variations in the geometry of the striatum region discriminating between the two groups. Thus the stratified decrease in the dopamine activity levels can be seen by the shape based analysis.

REFERENCES

[1] Jean-Sebastien Provost, Alexandru Hanganu, OuryMonchi, "Neuroimaging studies of the striatum in cognition PartI: healthy individuals", Frontiers in Systems Neuroscience, vol. 9, no. 140, 2015.

[2] K Ray Chaudhuri et al., "Non-motor symptoms of Parkinson's disease: diagnosis and management", The Lancet Neurology, vol. 5, no. 3, pp. 235 – 245, 2006.

[3] R. Prashanth, Sumantra Dutta Roy, Pravat K. Mandal, Shantanu Ghosh, "High-Accuracy Classification of Parkinson's Disease Through Shape Analysis and Surface Fitting in 123I-Ioflupane SPECT Imaging", IEEE Journal of Biomedical and Health Informatics, vol. 21, pp. 794-802, 2017.

[4] Siepel et al., "Cognitive Executive Impairment and Dopaminergic Deficits in De Novo Parkinson's Disease", Movement Disorders, vol. 29, no. 14, 2014

[5] Global Burden of Disease Study (ghdx.healthdata.org).As of 2013; refreshed July 2016.

[6] Dorsey ER, Constantinescu R, Thompson JP, et al., "Projected number of people with Parkinson diseases in the most populous nations, 2005 through 2030", Neurology, vol. 68, pp. 384–388, 2007.

[7] Provost et al., "Neuroimaging studies of the striatum in cognition Part I: healthy individuals", Frontiers in Systems Neuroscience, vol. 9, pp. 1-13, 2015.

[8] Dag Aarsland et al., "Cognitive impairment in Parkinson's disease and dementia with Lewy bodies" Parkinsonism and Related Disorders, vol. 22, pp. 144-148, 2016.

[9] Conrado et al, "Dopamine Transporter Neuroimaging as an Enrichment Biomarker in Early Parkinson's Disease Clinical Trials: A Disease Progression Modelling Analysis", Clinical and Translational science, vol. 11, issue 1, 2018.

[10] Dukart et al., "Distinct Role of Striatal Functional Connectivity and Dopaminergic Loss in Parkinson's Symptoms", Frontiers in Aging Neuroscience, vol. 9, pp. 1-10, 2017.

[11] R. Prashanth, S. Dutta Roy, P. K. Mandal, and S. Ghosh, "Shape features as biomarkers in early Parkinson's disease", in Conf Proc 6th Int IEEE/EMBS Conf Neural Eng (NER), pp. 517 – 520, 2013.

[12] Alireza Khotanzad , Yaw Hua Hong, "Invariant Image Recognition by Zernike Moments", IEEE Transactions on Pattern Analysis and Machine Intelligence, vol.12, issue 5, pp. 489-497, 1990.

[13] P. Bhaskara Rao, D.Vara Prasad, Ch.Pavan Kumar, "Feature Extraction Using Zernike Moments", International Journal of Latest Trends in Engineering and Technology (IJLTET), vol. 2, no. 2, 2013.

[14] K. Marek, D. Jennings, S. Lasch et al., "The Parkinson Progression Marker Initiative (PPMI)," Progress in Neurobiology, vol. 95, no. 4, pp. 629-635, 2011.

[15] Amir Tahmasbi, Fatemeh Saki, Shahriar B. Shokouhi, "Classification of benign and malignant masses based on Zernike moments", Computers in Biology and Medicine, vol. 41, No. 8, pp. 726-735, 2011.

ISBN 978-1-5386-4473-7
IEEE sponsored 4th International Conference on Biosignals, Images and Instrumentation, SSNCE, Chennai. ICBSII 2018 – 22nd-24thMar'18

Examination of Digital Mammogram using Otsu's Function and Watershed Segmentation

S.P. Sachin raj, N. Sri Madhava Raja, M.R. Madhumitha, V. Rajinikanth

Department of Electronics and Instrumentation Engineering,
St.Joseph's College of Engineering,
OMR, Chennai 600119, India.
Email: nsrimadhavaraja@stjosephs.ac.in

***Abstract*— Breast malignancy is one of dangerous illness among the women community and premature detection may facilitate to provide the appropriate treatment to diminish/eliminate breast cancer. Digital Mammogram (DM) is a commonly approved imaging scheme to record and scrutinize the breast cancer. This paper implements a novel hybrid approach based on the combination Otsu's multi-thresholding and Water Shed Segmentation (WSS) to mine the suspicious sections from the DM. Initially, the multi-level thresholding using the Bat Algorithm (BA) driven Otsu with a bi-, tri- and four-level thresholding is implemented to pre-process the DM. Afterward, a marker controlled WSS is implemented to mine the infected division of DM. The mined section is then evaluated using the Haralick texture feature in order to know the severity of the disease by examining its texture feature. In this paper, DM dataset with dense, medium, low and normal breast regions are analyzed independently with the proposed approach. The experimental result of this paper confirms that, proposed method is very proficient in extracting the breast malignancy from the considered DM database.**

Keywords—Digital mammogram; Bat algorithm; Otsu; Water shed segmentation; GLCM features.

I. INTRODUCTION

Medical image examination is essential to identify the nature, location and severity of the disease in internal and external organs. Due to its need, a considerable amount of imaging procedures, such as Computed Tomography (CT), Magnetic Resonance Imaging (MRI), X-ray, Thermal Imaging (TI) , dermoscopy, and digital microscopic images are widely implemented in clinics to record the picture of the infected regions [1-8]. In medical domain, these imaging procedures are chosen based on the disease to be analyzed.

Breast cancer is a dangerous disease widely affects the women community irrespective of their race. This cancer is mainly affects the women due to several reasons. Initial screening practice is widely adopted by the doctors in order to identify the disease in its early stage [9-11].

Digital mammogram is one of the cost effective procedures widely adopted to record the abnormality in breast section. In most of the medical centers, X-ray machines are existing to identify the abnormality in internal organs. Similar procedure ac be considered to record the abnormality in breast section.

The recorded X-ray picture is then evaluated by an expert member, to confirm the presence of the cancer, infection size, infected area and its severity level.

Due to its significance, X-ray examination is widely carried by the researchers. Garma and Hassan discussed about the texture feature extraction and classification of mammogram in to normal and abnormal [12]. This method also attains 95.7% of accuracy in their work. Marias et al. [13] proposed a computer based approach to examine the abnormal section. Babu and Rajamani [14] discussed about an evolutionary approach based DM image examination scheme. Singh et al. [15] discussed about the classification of DM images using the Support Vector Machines (SVM) based on its shape and texture features. Srivastava et al. [16] also proposed a computer based approach to examine DM images. The work of Jenifer et al. [17] proposes an automated scheme based on neural network and extracted the Gray Level Co-occurrence matrix (GLCM) to classify images in to various classes into, fatty- benign, fatty-malignant, glandular-benign, glandular-malignant, dense-benign and dense-malignant. With a comparative analysis, they confirmed that, their approach offered better values of sensitivity (100%), specificity (98%) and accuracy (99.7%).

From the previous works, it is noted that, heuristic algorithm assisted biomedical image processing approach will offer enhanced results [18-22]. Hence, in this paper a recent heuristic procedure called Bat Algorithm (BA) [23] is considered to examine the DM image database. The implemented technique is the combination of a multi-level thresholding based on the BA and Otsu's thresholding and segmentation based on the Watershed. The advantage of the thresholding and segmentation procedures are confirmed with the image quality measures and the GLCM values respectively.

II. METHODOLOGY

This section provides the details regarding the methods adopted to examine the Digital Mammogram (DM). Fig 1 depicts the stages involved in DM examination. Initially, the 2D DM is extracted from the mini-MIAS and it is then thresholded with CBA+Otsu. The outcome of thresholding is then processed with the watershed algorithm and the region of interest (ROI) is extracted. Finally, the GLCM features for the ROI are extracted. Based on the GLCM values, it can be classified into benign and malignant.

ISBN 978-1-5386-4473-7
IEEE sponsored 4th International Conference on Biosignals, Images and Instrumentation, SSNCE, Chennai.

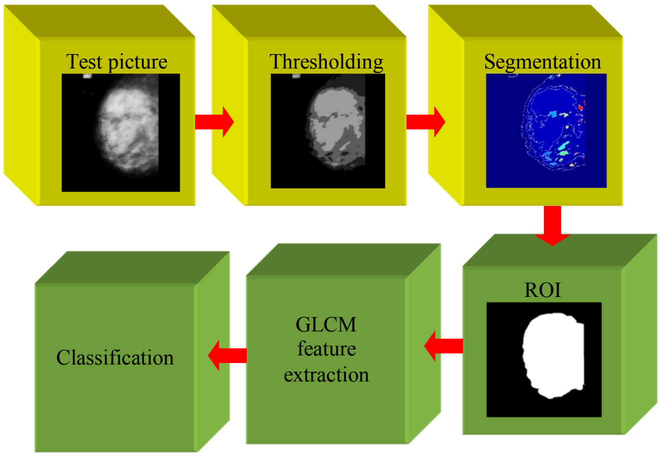

Fig 1. Mammagram examination procedure implemented in this paper

A. Image dataset

Digital mammogram (DM) is normally recorded using X-ray on a chosen breast section. 2D DM pictures considered in this paper are obtained from the benchmark mini-MIAS database more than 50 in both malignant and benign subjects are considered [24, 25]. This dataset has a gray scaled 2D DM with major category as benign and malignant and sub classification as fatty, fatty-glandular and dense-glandular. This work considers the mini-MIAS and segregates the DM images into four classes, like normal, low, medium and dense based on the size of the irregularity.

B. Bat algorithm

The BA was initially projected by imitating the tracking events of microbats [26]. BA contains subsequent arithmetical equations [20]:

$$E_i^{(k+1)} = F_i^{(k)} + (E_i^{(k)} - G).H_i \qquad (1)$$

$$F_i^{(k+1)} = F_i^{(k)} + E_i^{(k+1)} \qquad (2)$$

$$H_i = H_{min} + (H_{max} - H_{min}).\beta^1 \qquad (3)$$

where $E_i^{(k+1)}$ and F_i^{k+1} symbolize the rapidity and location of the bat, H_{min} is the least frequency and H_{max} is utmost frequency.

From Eqn.1, it is prominent that, rapidity renewal depends predominantly on frequency renewal. Throughout the heuristic exploration, fresh result for every agent produced as in the subsequent relation:

$$X_{new} = X_{old} + \varepsilon A^t \qquad (4)$$

where ε = arbitrary digit of the range [-1,1] and A is the intensity of bats' discharged sound throughout the investigation of a new area. Chaotic BA (CBA) discussed in [20] is considered in this paper. The CBA is responsible to discover the optimal threshold for the DM based on Otsu's function.

C. Otsu's function

Otsu's technique is a common used thresholding procedure since 1979 to process the gray/RGB scaled pictures [27-31] Otsu's multi-thresholding is adopted in this paper to threshold the DM. Let us consider that there are thresholds , such as t_1, t , and t , which partition the input picture into separate sections, such as C_0 (gray levels of range 0 to t_1-1), C_1 (gray levels of range t_1 to t_2-1) and, C_m (gray levels of range t_{m-1} to L-1). Where L = 256.

Objective value for this multi- thresholding can be expressed as;

$$J_{max} = \sigma_0 + \sigma_1 + \ldots + \sigma_m \qquad (5)$$

More aspect regarding the Otsu is existing in the literature. Eqn.4 is known as the Otsu's between class variance function which supports the exploration process of Chaotic BA search.

D. Segmentation

Segmentation operation is used to extract the ROI based on the Marker Controller Watershed Algorithm (MCWS) discussed in [8]. MCWS is the mixture of the Sobel edge recognition, morphological maneuver, and mining. Comprehensive arithmetical explanation of MCWS considered here can be found in earlier works [33].

E. Feature extraction

The geometrical properties of the ROI are extracted using the Haralick feature (GLCM) discussed in [34]. These features can be considered to train and test the classifier system in future to classify the DM in to benign and malignant. After the classification, the doctor will examine the images once again to take the decision for the possible treatment planning to cure the breast cancer [35].

III. Results and Discussion

This section of the paper presents the experimental outcome and its discussion. Initially, the DM pictures of the size 1024 x 1024 pixels are collected from the mini-MIAS dataset [24]. These images are in the form of the gray scale, and the sample DM images considered for the discussion is shown in Table 1. For the examination, DM pictures with dense, medium, low and normal images are initially evaluated using the proposed approach. All the simulation works are executed using the Matlab 7 (Release 14) software.

Firstly, BA and Otsu's function based thresholding is implemented. In order to find the optimal threshold value for the chosen image, the values are arbitrarily varied and the corresponding image quality measures and the segmented abnormalities are recorded. In this work, threshold values are varied like 2, 3 and 4 and the corresponding results are recorded.

Fig 2 depicts the sample DM and its gray histogram. Based on the chosen threshold value, the BA+Otsu's search explores the threshold level and enhances the abnormal section in DM. The results of *Th*= 2, 3 and 4 are presented in Table II. After thresholding, the abnormal section is then extracted using the watershed procedure. Table II also depicts the results of watershed and the extracted ROI. Table III shows the picture excellence measures to fix the *Th* value. When the *Th*=4, the picture quality measures such as Root Mean Square Error (RMSE), Peak Signal to Noise Ratio (PSNR in dB), Normalized Cross-Correlation (NCC), Average Difference (AD), Structural

ISBN 978-1-5386-4473-7

Content (SC), Normalized Absolute Error (NAE) are found to be excellent, hence in this paper, the threshold level is chosen as four. Similar procedure is applied for other test pictures considered in this work.

Table I. Sample test images chosen for the experimental work

Type	Left region	Right region
Dense	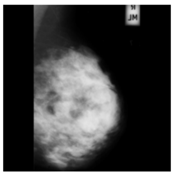	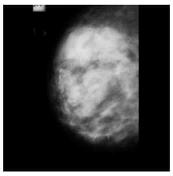
Medium	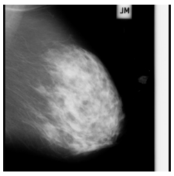	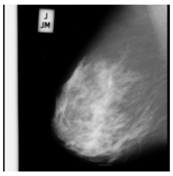
Low	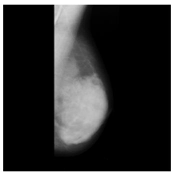	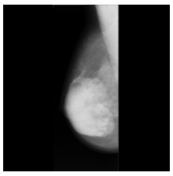
Normal	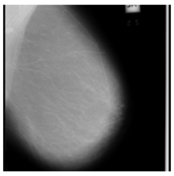	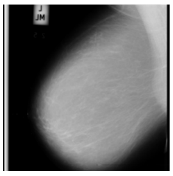

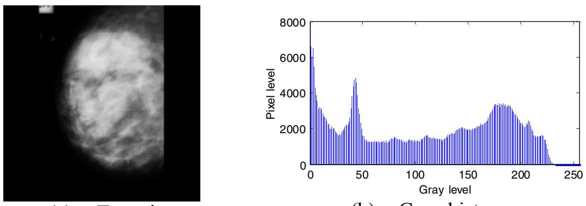

(a) Test picture (b) Gray-histogram

Fig 2. Sample DM picture and its histogram

Table II. Outcome for Threshold = 2, 3, and 4

Th	Test picture	Detected boundary	Morphological treatment	Extracted section
2		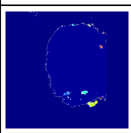	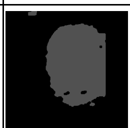	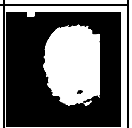
3		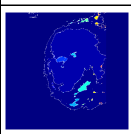	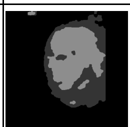	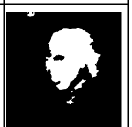
4	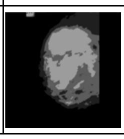	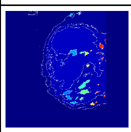	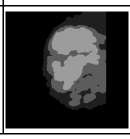	

Table III. Image quality measures for the sample DM

Parameter	2	3	4
Iteration no.	382	571	726
RMSE	47.4440	30.1162	21.7723
PSNR(dB)	14.6072	18.5548	21.3727
NCC	0.4784	0.6974	0.7837
AD	26.2929	16.9963	12.1480
SC	3.9578	1.9455	1.5880
NAE	0.5256	0.3398	0.2429

Proposed experiment is repeated for the other images of the dataset and the corresponding outcomes are recorded. If, *Th*=4, the image enhancement is superior and it clearly separates the abnormality from background and the breast tissue region. Table V presents the outcome for the left and right regions of DM. From this table, it is clear that, proposed approach offers superior outcome for the dense and medium breast irregularity. For the low and normal case, the abnormality level is very minimal or nil. First column of this table presents the considered test images and the second and third columns depict the thresholded and segmented images. From these results, it is clear that, proposed technique is efficient in extracting the abnormal section in dense, medium and low abnormalities and for normal cases, the outcome is good. From Table V, it can be observed that, proposed CBA+Otsu offers better thresholding result for the left and the right breast pictures for all the cases considered in this paper. Similarly, watershed segmentation is also presents the better result on extracting the abnormal sections of the test pictures adopted in this study. The result also confirms that, this approach is efficient in extracting the tumor section effectively from the breast X-ray pictures. After extracting the ROI from the DM, the texture features are then extracted using the GLCM features. Table IV presents the texture properties obtained for the dense, medium and low abnormality regions. In this study, it is noted that, for normal case, there is no outcome from the considered DM.
After extracting the GLCM features of all the pictures (total picture = 60), the values are considered DM are grouped into benign (early phase) and the malignant (acute phase) and the average values of these pictures are presented in table IV.

Table IV. GLCM features for the dataset

Feature	Benign	Malignant
Autocorrelation	1.8651	1.5013
Contrast	2.9411e-03	4.1688e-03
Dissimilarity	2.912e-03	4.1699e-03
Energy	0.5862	0.7165
Entropy	0.6209	0.4782
Homogeneity	0.9985	0.9979
IMF1	-0.9669	-0.9428
IMF2	0.8291	0.7576
Sum average	2.5778	2.3356
Sum variance	4.6558	4.0152

ISBN 978-1-5386-4473-7

Table V. Results obtained for the sample DM

	Original picture	Thresholded	Segmented section
Dense	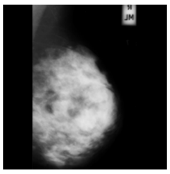	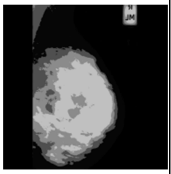	
	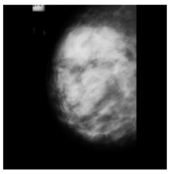	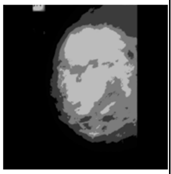	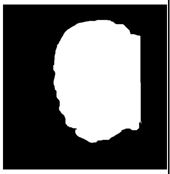
	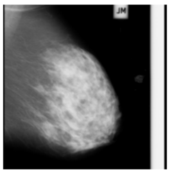	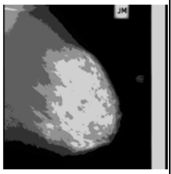	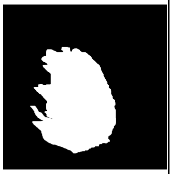
	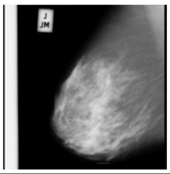	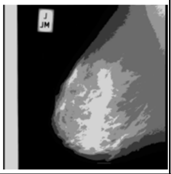	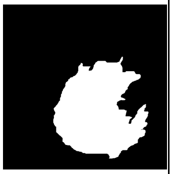
	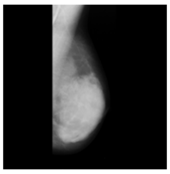		
	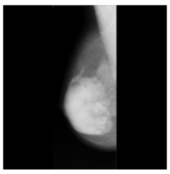	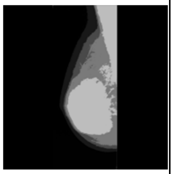	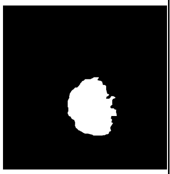
Normal	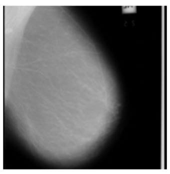		Not Applicable
	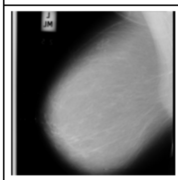	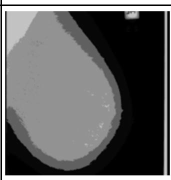	Not Applicable

IV. CONCLUSION

In this paper, a technique is proposed based on the combination of multi-thresholding and Watershed Segmentation (WS) to examine the Digital Mammogram (DM) dataset of mini-MIAS. Initially, CBA+Otsu based thresholding is implemented to enhance the abnormal section from the DM. later; the improved section is extracted using the WS. Later, the texture properties of the extracted section is computed based on the GLCM. In this work pictures, like dense, medium, low and normal images are examined using the proposed approach and is classified into benign and malignant based on its GLCM values. The results of this study confirm that, proposed approach is efficient in mining the abnormal section from the DM. In future, the proposed approach is to be compared against the related approaches already proposed by the researchers and a classifier system is to be implemented to classify the DM dataset into various disease classes. Further, validations with their corresponding ground truths can also be compared to estimate the efficacy of the segmentation.

REFERENCES

[1] T.K. Palani, B. Parvathavarthini, K. Chitra, "Segmentation of brain regions by integrating meta heuristic multilevel threshold with Markov random field," Current Medical Imaging Reviews, vol.12, no.1,pp. 4-12, 2016.

[2] H.M. Warner, R. Batty, A.R. Hart, S.R. Mordekar, A. Raghavan, F. Williams and D.J.A. Connolly, CT and MR Imaging of the Encephalopathic Child, Current Medical Imaging Reviews, vol.14, no.2, pp. 196-206, 2018. doi : 10.2174/1573405613666170504152118.

[3] Y. Zhou, X. Yang, W. Yang, W. Shi, Y, Cui and X.Chen, Recent Progress in Automatic Processing of Skeletal Muscle Morphology Using Ultrasound: A Brief Review, Current Medical Imaging Reviews, Vol.14, no.2, pp. 179-185, 2018. doi : 10.2174/1573405613666170126155934.

[4] G. Garg and M. Juneja, A Survey of Prostate Segmentation Techniques in Different Imaging Modalities, Current Medical Imaging Reviews, vol.14, no.1, pp.19-46, 2018. doi : 10.2174/1573405613666170504145842.

[5] K. Sharma and J. Virmani, A decision support system for classification of normal and medical renal disease using ultrasound images: A decision support system for medical renal diseases, International Journal of Ambient Computing and Intelligence (IJACI), vol.8, no.2, pp. 52-69, 2017. doi: 10.4018/IJACI.2017040104

[6] Y. Hu, H. Li, Z. Li and D. Hu, Hepatic Tumors: Diagnosis and Therapeutic Effect Evaluation of Diffusion- Weighted Imaging, Current Medical Imaging Reviews, vol. 14 , no. 2 , pp. 172 - 178 , 2018. doi : 10.2174/1573405613666161221155922.

[7] V. Rajinikanth, S.C. Satapathy, S.L. Fernandes and S. Nachiappan, "Entropy based Segmentation of Tumor from Brain MR Images–A study with Teaching Learning Based Optimization," Pattern Recognition Letters, vol.94, pp.87-95, 2017. DOI: 10.1016/j.patrec.2017.05.028.

[8] V. Rajinikanth, and S.C. Satapathy, "Segmentation of Ischemic Stroke Lesion in Brain MRI Based on Social Group Optimization and Fuzzy-Tsallis Entropy," Arabian Journal for Science and Engineering, pp.1-14, 2018. Doi: 10.1007/s13369-017-3053-6.

[9] N.S.M.Raja, V. Rajinikanth, S.L. Fernandes, S.C. Satapathy, "Segmentation of breast thermal images using Kapur's entropy and hidden Markov random field," Journal of Medical Imaging and Health Informatics, vol.7, no.8, pp. 1825-1829, 2017. doi: https://doi.org/10.1166/jmihi.2017.2267.

[10] A.man Gautam, V. Bhateja, A.Tiwari, and S.C. Satapathy, "An improved mammogram classification approach using back propagation neural network," Advances in Intelligent Systems and Computing , vol.542, pp. 369-376, 2018. Doi: 10.1007/978-981-10-3223-3_35.

[11] A. Tiwari, V. Bhateja, A. Gautam, and S.C. Satapathy, ANN-Based Classification of Mammograms Using Nonlinear Preprocessing, Lecture Notes in Electrical Engineering, vol. 434, 2017. doi: 10.1007/978-981-10-4280-5_39.

[12] F.B. Garma, and M.A. Hassan, "Classification of Breast Tissue as Normal or Abnormal Based on Texture Analysis of Digital Mammogram," Journal of Medical Imaging and Health Informatics, vol.14, pp. 647–653, 2014. doi: https://doi.org/10.1166/jmihi.2014.1310.

[13] Marias et al., A mammographic image analysis method to detect and measure changes in breast density," European Journal of Radiology, vol. 52, no.2, pp.276–282, 2004. Doi: 10.1016/j.ejrad.2004.02.014.

[14] P. Babu, and V. Rajamani, "Evolutionary Algorithm Based Optimized Histogram Modification for Contrast Enhancement of Mammogram Images," Journal of Medical Imaging and Health Informatics, Vol. 6, no.2, pp. 518–525, 2016. Doi: https://doi.org/10.1166/jmihi.2016.1693.

[15] B. Singh, V.K. Jain, and S. Singh, "Mammogram Mass Classification Using Support Vector Machine with Texture, Shape Features and Hierarchical Centroid Method," Journal of Medical Imaging and Health Informatics, Vol. 4, no.5, pp. 687–696, 2014. DOI: 10.1166/jmihi.2014.1312.

[16] S. Srivastava, N.Sharma1, S.K. Singh, and R. Srivastava, "Quantitative Analysis of a General Framework of a CAD Tool for Breast Cancer Detection from Mammograms," Journal of Medical Imaging and Health Informatics, vol. 4, no.5, pp. 654–674, 2014. doi: https://doi.org/10.1166/jmihi.2014.1304.

[17] S. Jenifer, S.Parasuraman, and A. Kadirvel, "An Efficient Biomedical Imaging Technique for Automatic Detection of Abnormalities in Digital Mammograms," Journal of Medical Imaging and Health Informatics, vol. 4, no.2, pp. 291-296, 2014. doi: https://doi.org/10.1166/jmihi.2014.1246.

[18] V. Rajinikanth, S.L. Fernandes, B. Bhushan, N.R.Sunder, "Segmentation and analysis of brain tumor using Tsallis entropy and regularised level set," Lecture Notes in Electrical Engineering, vol.434, pp. 313-321, 2018. Doi: 10.1007/978-981-10-4280-5_33.

[19] V. Rajinikanth, N.S.M. Raja and K. Kamalanand, "Firefly Algorithm Assisted Segmentation of Tumor from Brain MRI using Tsallis Function and Markov Random Field," Journal of Control Engineering and Applied Informatics, vol.19, no.3, pp. 97-106, 2017.

[20] S.C. Satapathy, N.S.M. Raja, V. Rajinikanth, A.S. Ashour and N. Dey, "Multi-level image thresholding using Otsu and chaotic bat algorithm," Neural Computing and Applications, 2016. doi:10.1007/s00521-016-2645-5.

[21] N. Dey, V. Rajinikanth, A.S. Ashour, and J.M.R.S. Tavares, "Social Group Optimization Supported Segmentation and Evaluation of Skin Melanoma Images," Symmetry, vol.10, no.2, pp.51, 2018. doi:10.3390/sym10020051.

[22] K.S. Manic, R.K. Priya and V. Rajinikanth, "Image Multithresholding based on Kapur/Tsallis Entropy and Firefly Algorithm," Indian Journal of Science and Technology, vol.9, no.12, pp.89949, 2016.

[23] P. Anitha, S. Bindhiya, A. Abinaya, S.C. Satapathy, N.Dey and V. Rajinikanth, "RGB image multi-thresholding based on Kapur's entropy — A study with heuristic algorithms," In. Second International Conference on Electrical, Computer and Communication Technologies (ICECCT), IEEE, 2017. DOI: 10.1109/ICECCT.2017.8117823.

[24] http://peipa.essex.ac.uk/info/mias.html

[25] J. Suckling et al. "The Mammographic Image Analysis Society Digital Mammogram Database, " Exerpta Medica. International Congress Series, 1069, pp375-378, 1994.

[26] X.S.Yang, "Bat algorithm: literature review and applications", Int. J. Bio-Inspired Computation, vol. 5, no. 3, pp. 141–149, 2013.

[27] N.S.M. Raja, V. Rajinikanth and K. Latha, "Otsu Based Optimal Multilevel Image Thresholding Using Firefly Algorithm," Modelling and Simulation in Engineering, vol.2014, paper id.794574, 2014.

[28] V. Rajinikanth, N.S.M.Raja, S.C. Satapathy and S.L. Fernandes, "Otsu's Multi-Thresholding and Active Contour Snake Model to Segment Dermoscopy Images," Journal of Medical Imaging and Health Informatics, vol.7, no.8, pp. 1837-1840, 2017. Doi: https://doi.org/10.1166/jmihi.2017.2265.

[29] T.D.V. Shree, K. Revanth, N.S.M. Raja and V.Rajinikanth, A Hybrid Image Processing Approach to Examine Abnormality in Retinal Optic Disc, Procedia Computer Science, vol.125, pp. 157-164, 2018.

[30] N.S.M. Raja, V. Rajinikanth and K. Latha, Otsu Based Optimal Multilevel Image Thresholding Using Firefly Algorithm, Modelling and Simulation in Engineering, vol.2014, paper id.794574, 2014.

[31] K. Manickavasagam, S. Sutha and K. Kamalanand, Development of systems for classification of different plasmodium species in thin blood smear microscopic images, Journal of Advanced Microscopy Research, vol.9, no.2, pp. 86-92, 2014.

[32] R. Vishnupriya, N.S.M. Raja, V. Rajinikanth, "An efficient clustering technique and analysis of infrared thermograms," Third International Conference on Biosignals, Images and Instrumentation (ICBSII), IEEE, pp.1-5, 2017. DOI: 10.1109/ICBSII.2017.8082275.

[33] K. Manickavasagam, S. Sutha and K, Kamalanand, An automated system based on 2D empirical mode decomposition and k-means clustering for classification of Plasmodium species in thin blood smear images, BMC Infectious Diseases, vol.14, no.3, pp.1, 2014.

[34] K. Manickavasagam, S. Sutha and K. Kamalanand, Development of systems for classification of different plasmodium species in thin blood smear microscopic images, Journal of Advanced Microscopy Research, vol.9, no.2, pp. 86-92, 2014.

ISBN 978-1-5386-4473-7

DETERMINATION OF CONCENTRATION FOR CONGO RED DYE USING COLOUR IMAGE ANALYSIS.

Vinitha.N,
Dept. of Chemical Engg,
SSNCE, Chennai
vinitha.gethzie@gmail.com

Pavendan.K
Dept. of Chemical Engg,
SSNCE, Chennai
pavendank@ssn.edu.in

Gopinath K.P
Dept. of Chemical Engg,
SSNCE, Chennai
gopinathkp@ssn.edu.in

Abstract--In this study, Digital images are the main source of information and they are obtained from digital camera which is of low cost when compared to calorimetric discovery. This method involves RGB which consist of Red, Green and Blue colour and Grayscale image analysis consist of Black and White which is used to determine the concentration of the Congo red dye. In this RGB colour image and Grayscale images are equally cropped in square shape using Adobe Photoshop to obtain RGB histogram and Grayscale histogram. From this image analysis, histogram shows the exact accuracy of colour present in the image. The output values obtained from the RGB analysis is used to predict the unknown concentrations of the dyes.

***Keywords:** congo red, RGB analysis, Histogram, Concentration.*

I. INTRODUCTION

Dyeing industry is one of the largest water polluting industries and removal of dye from waste water plays an important role in industrialized countries [1]. Many dyes are available and dying process has been carried out in many countries for more than 5000 years [2],[3].Because of the toxicity of the dye and their perceivability in surface water, removal of them has been considered [4].The dyes coming out of the industries contain many chemicals and compounds and it requires proper treatment before it is discharged into water body. But, the effluents are difficult to treat because they are highly variable in composition [5] Release of dye from industries is the major reason for water pollution [6]. Dyes are mainly delivered from dress materials, beautifying agents, paper, calfskin and pharmaceuticals [7]. Various dyes present in the environment may cause severe health issues in human and also animals [8]. It is important for dye releasing industries to use proper steps to control them [9]. Congo red is a azo dye which is soluble in water and its organic compound, obtained as a red colour solution; its solubility is higher in various solvents [10]. Digital images are sources of chemical information [11]. It is utilized as a part of histology to recolor collagen [12]. The image has 256 levels of intensities [13]. The RGB colour image analysis is the source of the three primary colours, red, green, and blue [14] .The RGB image has detailed representations of images when it is captured under LED lighting conditions [15]. A histogram represents the set with realized values of some random variable is obtained using the data from the finite sample. It is highly soluble in aqueous solution and it has a complex aromatic structure [16-19].

II. STEPS INVOLVED IN ANALYSIS

2.1 Preparation of dye solutions

Congo red, is the sodium salt of benzidinediazo-bis-1-naphthylamine-4-sulfonic acid; Chemical Formula: $C_{32}H_{22}N_6Na_2O_6S_2$, Molar mass: 696.665g mol^{-1}, λ_{max}: 497nm was supplied by Sri Hari Chemicals (India). Stock solution of Congo Red dye was prepared by dissolving the 100mg of dye powder in 100ml of distilled water.

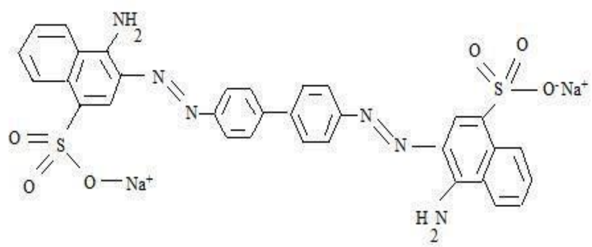

Fig.1.1 Structure of Congo Red

2.2 Apparatus and software

Determination of Congo Red was performed directly on a 12-well plate containing 12 vessels. Automatic pipettes were used to transfer the samples solutions to the transparent 12-well plate. For capturing of images, a Smartphone camera iphone 6s with 12 megapixels resolution was used. The 12 -well plate was placed in a cardboard box with the same dimensions, top opening for placing LED light is used for focusing the plate with dimensions of 15 × 1.0 × 0.1 cm with a current consumption ranged from 20 to 100 mA.

ISBN 978-1-5386-4473-7

Apparatus

- Iphone 6s
- Micro pipettes
- Cardboard box
- LED lights

Software

- RGB colour analysis -Matlab7.1
- Image processing -Excel2007
- Cropping of images - Adobe Photoshop CS4

2.3 Photographic Procedure

Dye samples were prepared by dilutions of (100 mg/L) of dye with pure distilled water. The stock arrangements were set in a transparent 12 well plate to keep up the same natural light and photographic conditions. Colours were obtained from a delegate well plate. Images were transferred to a computer and it is cropped using Adobe Photoshop programming. The RGB analysis and grayscale analysis were measured using Matlab's tool software.

2.4 RGB model and histogram

A digital image is a collection of information data which are collected in the form of pixels which corresponds to the nearest neighbourhood of the pixels [20]. The Image data of each and every pixel consist of three colours namely red, green, and blue, which has different methods to form the wide cluster of colour. This is known as the RGB model [21]. Histograms are the pictorial representation of the image in detail showing the amount of pixels present in the red, Green and Blue colour [22]. It is easy to implement with low complexity [23].

III. RESULTS AND DISCUSSIONS

3.1. Pre-processing of colour Image

Colour image from the Iphone6s camera was saved in a compact flash card and transferred to the computer using card reader and the obtained image is cropped using Adobe Photoshop software. Histogram is useful for visual data presentation [24]. The average R, G and B colour values were analyzed using Matlab software. Figure 1 shows the Congo Red is present in various concentrations. Table 1 shows the RGB colour histogram for each well solution. The specific image area was selected as shown in Table 2 which in a cropped image with 124 x 109 dimensions. Further, it shows that the original colour image is converted into grayscale image to obtain the grayscale histogram.

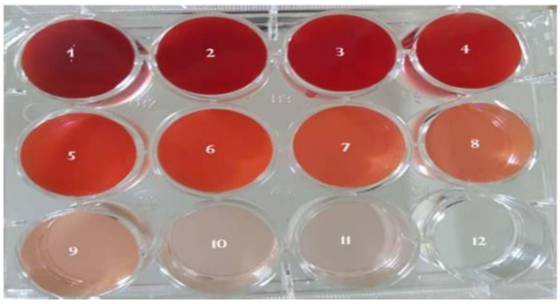

Fig3.1.1 Congo Red Dye in transparent 12 well plate.

Congo Red	Congo Red- RGB Histogram	Grayscale Histogram
A1 	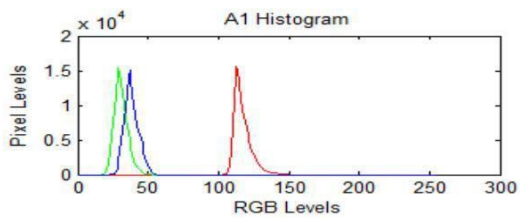	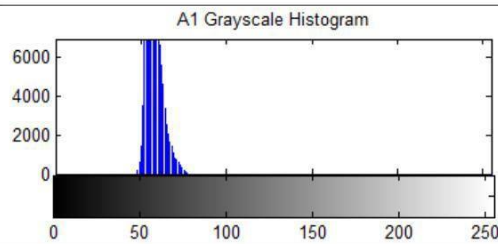
A2 	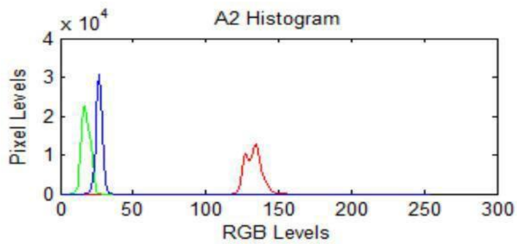	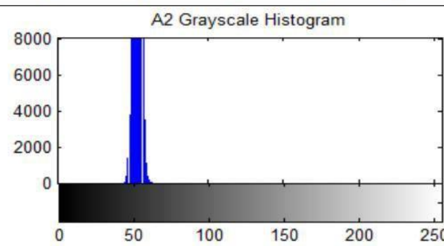

ISBN 978-1-5386-4473-7

A3

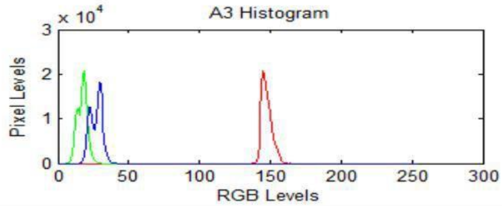

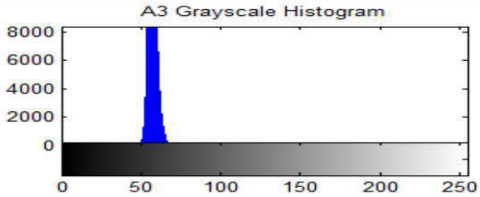

A4

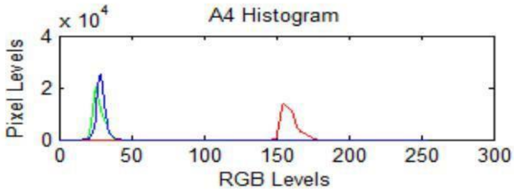

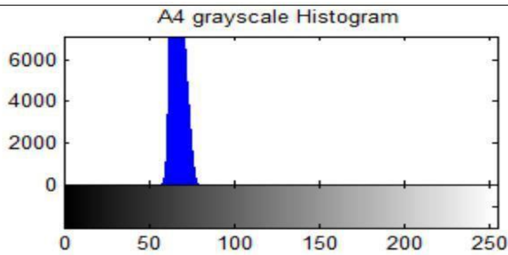

B1

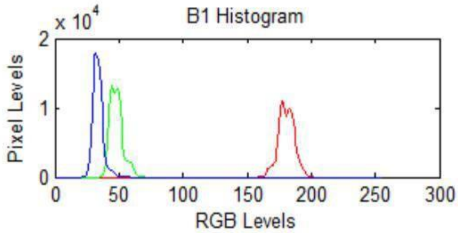

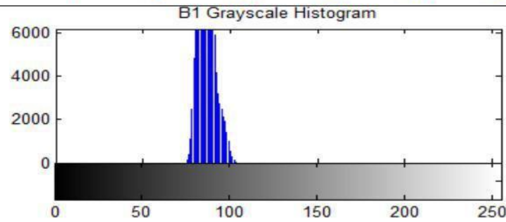

B2

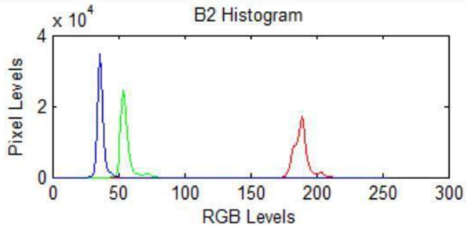

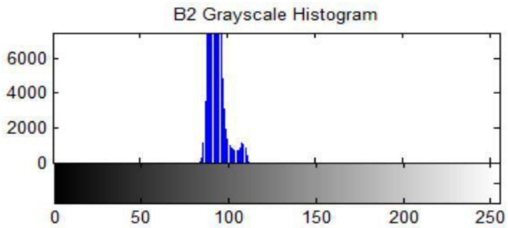

B3

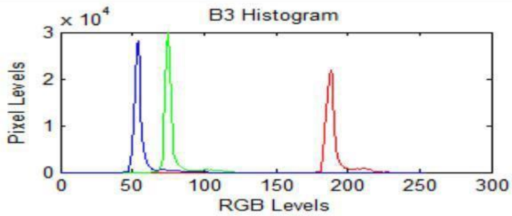

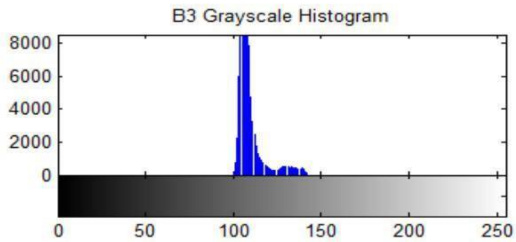

B4

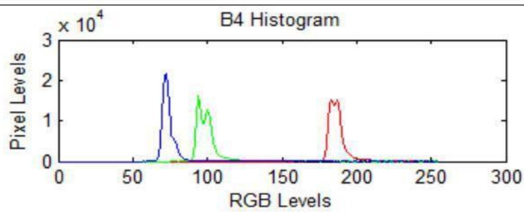

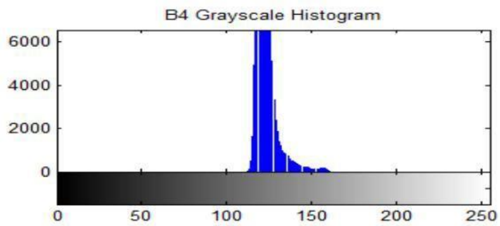

C1

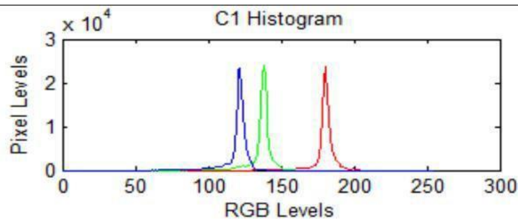

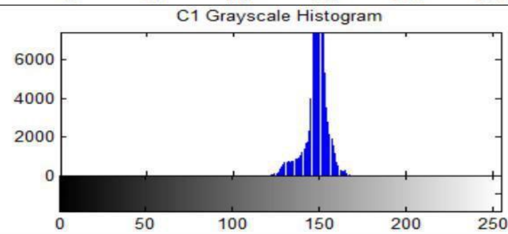

ISBN 978-1-5386-4473-7

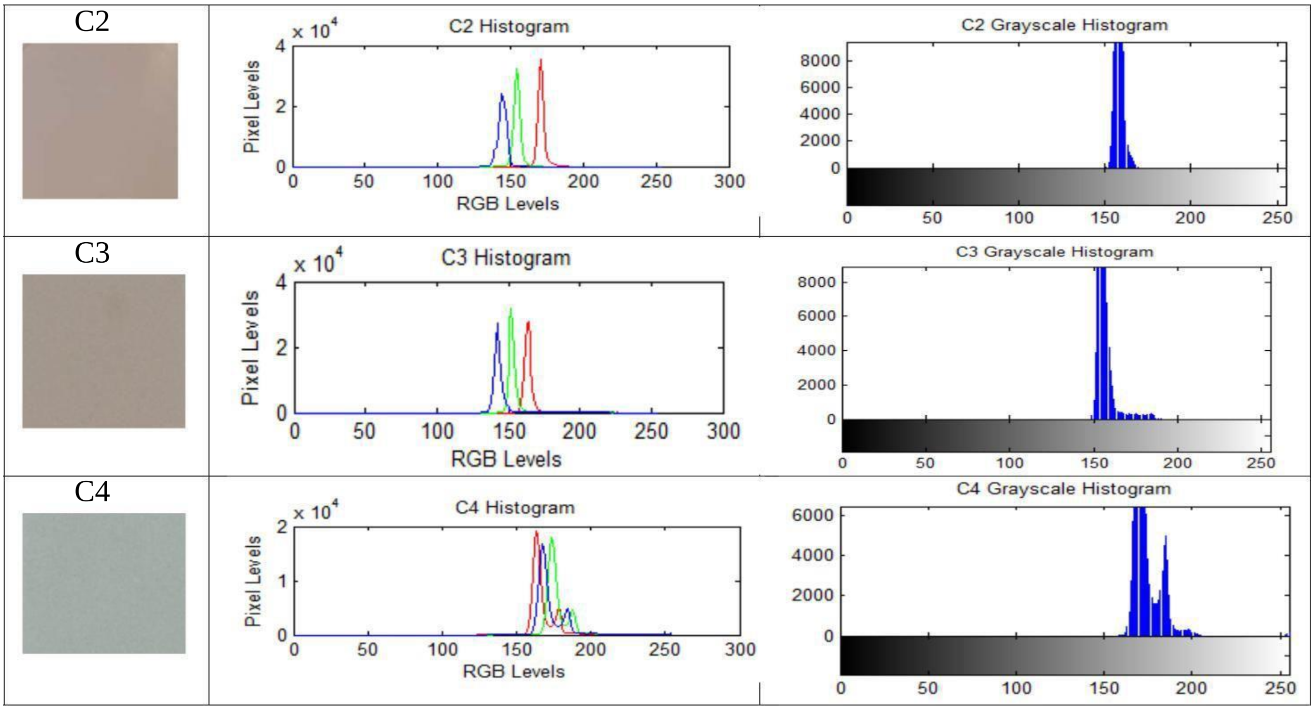

3.2 Concentration Vs grayscale intensity

Figure 2 shows the graphical plot between predicted concentrations (mg\L) vs Average Grayscale coordinates. Such relation curve decreases gradually with respect to increase in concentration. This curve describes line using an equation $y=150.851e^{-0.001x}$ and whose corresponding R^2 value 0.929.

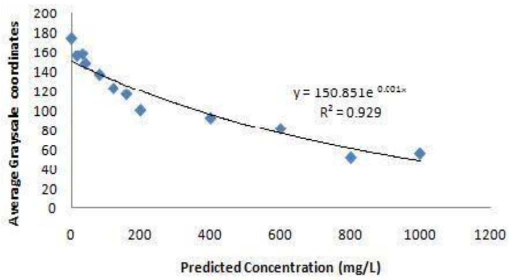

Fig3.2.1 For various concentrations from 0 to 1000 mg/L grayscale Intensity values is obtained from Matlab software.

3.3 Concentration Vs RGB values

The below Fig.3 shows Predicted concentration mapped against average RGB coordinates. Such graph includes distinct curves in Red, Blue and Green. Among such curves Red coordinates are higher in values.

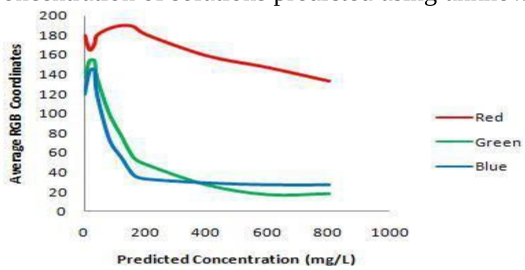

Fig. 3.3.1 For various concentrations from 0 to 1000 mg/L RGB values is obtained from Matlab software.

3.4 Unknown Image coordinates Vs Unknown concentration

In experimental setup, different unknown concentration of solutions predicted using unknown image coordinates whose relation decreases linearly as shown in below Fig.4.

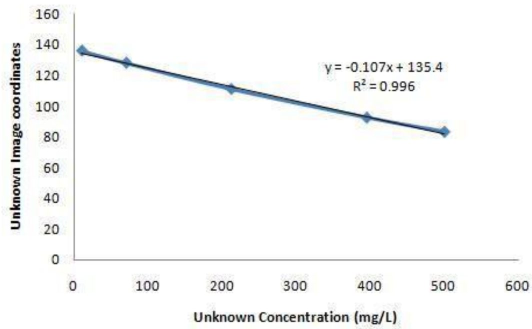

Fig. 3.4.1 Graphical plot between Unknown Concentration (mg\L) Vs Unknown Image coordinates

IV. CONCLUSION

A fast and low cost method for quantitative colour image analysis of Methylene blue, Naphthol b green, Congo red in aquatic samples has been proposed [25]. This method gives the exact information of the histograms obtained from digital image and it is fast, easy procedure, require small amount of sample and it is simple to execute. In this method histogram for RGB images, were used to describe the digital images. The expensive equipment can be replaced by the image analysis for the removal of dyes from wastewater. Furthermore, the easiest colour image analysis using RGB histogram and Grayscale histogram is comparable with more expensive method of UV-visible spectrophotometry. Histogram is the easiest method to analyze an image with low cost dye sample.

V. REFERENCES

[1] S.E Rizk & Mostafa M.Hamed, "Batch sorption of iron complex dye Naphthol green B from waste water on charcoal, kaolinite and tafla", journal Desalination and water Treatment. vol.56 (2015) pp.1536-1546.

[2] Deepika Bhatia, Neeta Raj.Sharma, joginder singh & Rameshwar S.Kanwar, "Biological method for textile dye removal from waste water: A review", journal critical reviews in environmental science and Technology. vol.47 (2017) pp.1836-1876.

[3] Papita Das Saha & Keka sinha," Natural dye from bixa seeds as a potential alternative to synthetic dyes for use in textile industry, Desalination and Water Treatment. Vol.40 (2012) pp.298-301.

[4] Sze-Mun Lam, Jin-Chung Sin, Ahmad Zuhairi Abdullah & Abdul Rahman Mohamed, "Degradation of wastewater containing organic dyes photocatalysed by zinc oxide: A review", Desalination and Water Treatment. Vol.41 (2012) pp. 131-169.

[5] J.S Do and M.L Chen.., Decolourization of dye- containing solutions by electrocoagualtion, J. of Appl. Electrochemistry.vol 24 (1990) pp.785-790.

[6] Pradeep Kumar, Ruchika Agnihotri, Kailas L.Wasewar, Hasan Uslu & Changkyoo Yoo, "Status of adsorption removal of dye from textile industry effluent", Desalination and water Treatment. Vol.50 (2012) pp.226-244,.

[7] H Zollinger (1991). "Color chemistry. Synthesis, properties and applications of organic dyes and pigments", 2nd revised edn. VCH, New York.

[8] A. Mittal, V.Thakur, V.Gajbe "Adsorptive removal of toxic azo dye Amido Black 10B by hen feather". Environ Sci Pollut Res.(2012). doi: 10.1007/s11356-012-0843-y.

[9] K.Y.Foo & B.H.Hameed, An overview of dye removal via activated carbon adsorption process, Desalination and water Treatment. Vol.19 (2010) pp 255-274.

[10] Klaus Hunger, Peter Mischke, Wolfgang Rieper, Roderich Raue, Klaus Kunde, Aloys Engel: "Azo Dyes" in Ullmann's Encyclopedia of Industrial Chemistry, Wiley-VCH, Weinheim (2005). doi:10.1002/14356007.a03_245

[11] P. Geladi, S. Wold & K. H. Esbensen, Anal. Chim. Acta. Vol.191 (1986) pp. 473–480.

[12] J. A. Kiernan, Histological and Histochemical Methods: Theory and Practice, 4th edition.

[13] Levkowitz, Haim, and Gabor T. Herman. GLHS: a generalized lightness, hue, and saturation color model. CVGIP: Graphical Models and Image Processing. Vol.55 (1983) pp. 271-285.

[14] Mohammad-Hossein Sorouraddin , Masoud Saadati , Fariba Mirabi, "Simultaneous determination of some common food dyes in commercial products by digital image analysis", journal of food and drug a n a l y s i s xxx 1e6 2015.

[15] X. Xu, W. Li, D. Xu," Distance metric learning using privileged information for face verification and person re-identification", IEEE Trans. Neural Netw. Learn. Syst vol.26 (2012) pp. 3150-3162.

[16] A. Mahapatra, B.G. Mishra, G. Hota, Ceramics. International., vol.39 (2013) pp. 5443.

[17] S. Kaur, S. Rani, V. Kumar, R.K. Mahajan, M. Asif, I. Tyagi, V.K. Gupta,J. Ind. Eng. Chem., vol 26 (2015) pp. 234.

[18] A. Mahapatra, B.G. Mishra, G. Hota, Ceramics International., vol.39 (2013) pp. 5443.

[19] K. Ahmadi, M. Ghaedi, A. Ansari, Comparison of nickel doped Zinc Sulfide and/or palladium nanoparticle loade d on activated carbon as efficient adsorbents for kinetic and equilibrium study of removal of Congo red dye Spectrochim. ActaMol.Biomol.Spectrosc.vol.136 (2013) pp.1441–1449.

[20] P. Facco, F. Bezzo , M. Barolo , Mukherjee & R, Romagnoli JA. Monitoring roughness and edge shape on semiconductors through multiresolution and multivariate image analysis. AlChE J; 55:1147e60,(2009).

[21] Geladi PLM, Grahn HF & Burger JE. Multivariate images, hyperspectral imaging: background and equipment. Techniques and applications of hyperspectral image analysis. Chichester, UK: John Wiley & Sons, Ltd; 2007. p. 1e15

[22] Marina A. Dominguez, María E. Centurión Departamento de Química," Application of digital images to determine color in honey samples from Argentina",INQUISUR (UNS-CONICET), Universidad Nacional del Sur, Av. Alem 1253 (B8000CPB), Bahía Blanca, Buenos Aires, Argentina.

[23] Xuewen Wang & Lixia Chen, "An effective histogram modification scheme for image contrast enhancement", Signal processing; Image Communication.vol 58 pp187-198, 2017.

[24] S.I.Bityukov, A.V.Maksimushkina & V.V.Smirnova, "Comparison of histograms in physical research, Nuclear Energy and Technology". Vol.2 (2016) pp.108-113.

[25] B.H. Hameed & I.A.W. Tan, "Nitric acid-treated bamboo waste as low – cost Adsorbent for removal of cationic dye from aqueous solution", Desalination and Water Treatment.vol.21 2010 pp.357-363.

ISBN 978-1-5386-4473-7
IEEE sponsored 4th International Conference on Biosignals, Images and Instrumentation, SSNCE, Chennai. ICBSII 2018 – 22nd-24th Mar'18

Raman Monte Carlo simulation of tooth model with embedded sphere for different launch beam configurations

Subitcha Jayasankar, Vijitha Periyasamy, Snekhalatha Umapathy* and Manojit Pramanik*

Abstract — **The Monte Carlo simulation of light transport in multi- layered tissue is utilized to implement Raman scattering. The unique molecular signature of Raman spectroscopy makes it a highly potential technique for many medical applications including structural analysis of tooth. To provide an environment for the developmental defect of dentine such as dentinogenesis imperfecta, an embedded sphere is introduced in the simulation medium to model the dentine in the layer of enamel. Simulations are carried out for photons launched as pencil beam and broad beams of radius 0.1 cm, 0.2 cm, and 0.3 cm to study the best illumination pattern for the detection of dentine in the tooth. High-performance computing supercomputers are used to run the simulations in parallel, and the results are averaged for computational efficiency. The spatial location of generation of Raman photons is shown in two-dimension and one-dimension. The Raman photon intensity from the object (signal) and layer (noise) is recorded independently and the signal-to- noise is plotted. The signal intensity from the embedded sphere is high for 0.1 cm broad beam. The reproducibility of the broad beam is illustrated by performing the simulation for best illumination radius with different offsets from the origin along the x-axis.**

I. INTRODUCTION

To gain an insight into the behavior of light in any biological medium, studying the light-tissue interaction and simulating the light transport is of high importance in today's emerging world of optical diagnostics. A computational method called Monte Carlo (MC) method serves this purpose by random sampling of a physical quantity. The MC method can simulate the transport of light photons in a turbid medium with very high accuracy with the availability of high-end computational facilities. This makes the MC method a gold standard technique for simulating the transport of photons in multi-layered biological tissues [1]. Currently, MC method is used for wide range of biomedical applications in the field of optics for example, optimizing light delivery in photoacoustic imaging based on fluence distribution or absorption map, to estimate the depth of scan for optical coherence tomography, to estimate the optical properties of the medium using diffuse reflectance spectroscopy and identification of object using Raman scattering [2].

Absorption, reflectance, transmittance and scattering events occur during the light-tissue interaction. During each scattering event, the scattered light consists of both Rayleigh and Raman scattered photons. The generation of Raman scattered photons are fractional (10^{-6}) at every scattering site and it is dependent on the optical properties of the medium under simulation, which represents the composition of the material at the molecular level [3, 4]. The unique Raman signature helps in various biological applications such as detecting breast cancer from the calcifications, the margin of a breast tumor, monitoring the effects of various agents on the skin, determination of atherosclerotic plaque composition, rapid identification of pathogenic microorganisms and continuous patient monitoring (blood analysis) [5-7].

In order to provide a simulation environment for the real world medical applications, a sphere embedded object can be introduced in the medium to provide a more realistic approach towards simulation using MC. To quote an example, tumors and lymph nodes can be modeled using a sphere in the medium. One such application of the MC simulation of Rayleigh scattered photons in a medium with embedded sphere was utilized to optimize the delivery of light in photoacoustic imaging of sentinel lymph node [8]. Also, the Raman scattering was simulated using Monte Carlo for the identification of explosive material inside a cuboid container [9]. Another method used for simulating irregular or inhomogeneous medium involved the use of a technique called Mesh-based Monte Carlo (MMC) where the medium is modeled using meshes or given as dimensional input for the geometries. The technique was computationally expensive, very time consuming and involved a lot of post-processing for decoding the output. The introduction of embedded objects in Monte Carlo simulation of Multi-layered tissues has proved to be faster and advantageous than MMC [10]. The conventional MC can also be easily modified for different applications as per the requirement of the user. Hence, the introduction of embedded objects for Monte Carlo simulation of Raman scattering will help one to choose a better tool for faster and efficient simulation model

This work was supported by NTU-India connect research internship.
Subitcha Jayasankar is in Department of Biomedical Engineering, SRM Institute of Science And Technology, Kattankulathur, Kancheepuram District, Tamil Nadu 603203, India. (email: subijayasankar@gmail.com). This work is done as a part of her research internship in School of Chemical and Biomedical Engineering, Nanyang Technological University, Singapore 637459. Vijitha Periyasamy is in School of Chemical and Biomedical Engineering, Nanyang Technological University, Singapore 637459 (email: vijitha@ntu.edu.sg). Corresponding authors: Snekhalatha Umapathy is in Department of Biomedical Engineering, SRM Institute of Science And Technology, Kattankulathur, Kancheepuram District, Tamil Nadu 603203, India. (email: snehalatha.u@ktr.srmuniv.ac.in). Manojit Pramanik is in School of Chemical and Biomedical Engineering, Nanyang Technological University, Singapore 637459 (email: manojit@ntu.edu.sg)

ISBN 978-1-5386-4473-7

for their required application. However, the introduction of low probability event of Raman scattering in the Monte Carlo simulation has made it an intensive and time-consuming process again.

Currently, Raman spectroscopy is widely used for the classification of sound and carious enamel in the tooth. The calcium hydroxyapatite in the tooth gives the strong signal from the tooth which changes with demineralization, enabling early detection of caries [11,12]. In addition to detection of caries, Raman spectroscopy is also widely used for the detection of developmental disorders of the tooth such as dentinogenesis imperfecta which affects the morphological structure of tooth because of demineralization [13]. The genetic factors associated with the developmental disorders are studied using Raman spectroscopy [14]. Developing a tooth model for simulating Raman scattering will prove to be helpful in expectation of the results in such experiments and also in detecting the structural abnormalities. In this work, the simulation of Raman scattering events is carried out for a tooth, which is modeled with the embedded sphere to mimic the presence of dentine in a layer of enamel. The simulation demonstrates the efficiency of the illumination in detecting the presence of a structure inside a medium such as dentine underneath the enamel which will be very useful detecting the structural abnormalities inside the tooth. This simulation will enable one to choose the required illumination geometry to efficiently analyze the structures in the tooth non-invasively.

II. SIMULATION SETUP

The MC simulation for multi-layered tissue developed by Wang *et al.*, was modified to implement Raman scattering with embedded objects [15]. The flowchart of the simulation is shown in the Fig. 1. The trajectory of the photon launched from the surface is dependent on the scattering coefficient (μ_s) and absorption coefficient (μ_a) and scattering anisotropy (g). The dimensionless step size (s) taken by the photon depends on the scattering coefficient. At the end of every step size, the photon undergoes scattering which is Rayleigh. To implement Raman scattering, at every Rayleigh scattering site a pseudo Random number which ranges from 0 to 1 is generated to check if it the photon is converted to Raman with the probability 10^{-6}. The introduction of the embedded sphere in the Raman scattering MC simulation requires the distance to be calculated from the photon to the boundary of the sphere, in addition to the distance calculation to the layer boundary. In order to account for the dependency of the Raman signal strength on the area of illumination, and reproducibility of the spectrum the launch model of the photons is also modified here to accommodate the simulation for a broad beam [16, 17]. In this simulation, the initial angle of each photon in the broad beam is dependent on the numerical aperture (NA) of the lens used to focus the light (NA=0.66) and the refractive index of the medium (n=1.6)
[18]. The code is modified to record the diffusely reflected Raman photons as well as the Raman photon intensity from the object and layer separately. The number of Raman photons generated is also recorded separately for object and layer.

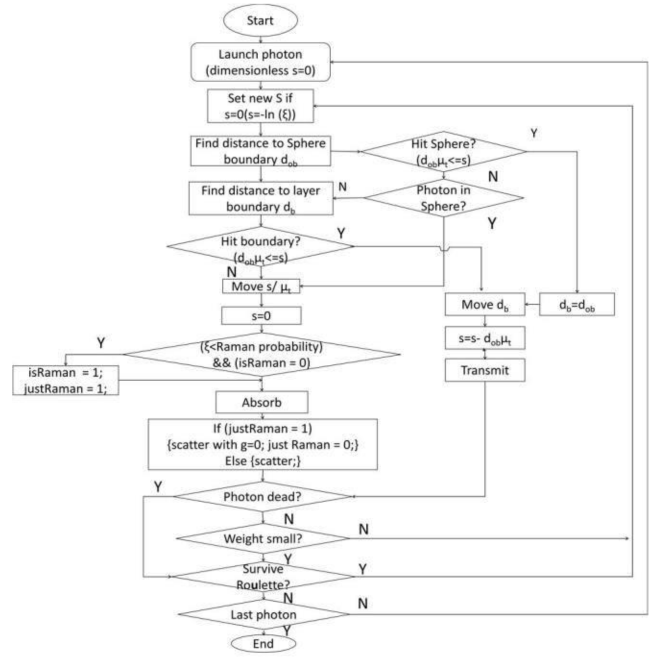

Figure 1. Flowchart showing the Raman Monte Carlo simulation of light in multi-layered tissue with embedded objects

A. Properties of simulation model:

As mentioned below, the optical properties used in this simulation correspond to that of the teeth where the layer takes the properties of the enamel and the object assumes the optical properties of the dentine found beneath it. The dentine is modeled using the embedded sphere to portray the presence of curvatures of the dentine in the buccolingual direction of molar teeth. The optical properties used here correspond to 633nm, which is the most commonly used wavelength for Raman spectroscopy of tooth [19, 20]. For enamel, μ_a and μ_s are chosen as 0.4 cm^{-1} and 15 cm^{-1} respectively. For the sphere, μ_a and μ_s are 3 cm^{-1} and 260 cm^{-1} respectively. The scattering anisotropy g is 0.7 for enamel and 0.9 for dentine. The dimensions of the simulation medium are selected carefully to agree with the nominal dimension of enamel and dentine of an adult molar tooth. As the thickness of the dentine in the molars ranges from 0.44 cm to 0.9 cm, the embedded sphere takes the diameter of 0.6 cm to portray a generalized model of the dentine in the molars [21, 22]. The simulation is carried out for a pencil beam of 10^{10} photons from the origin and a broad beam of different radius launched from the origin to cover the entire region of the sphere on the medium.

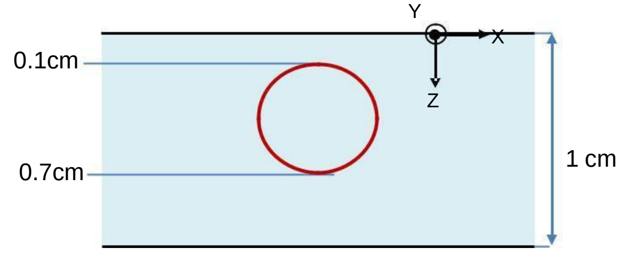

Figure 2. Dimensions of the simulation medium embedded sphere

The dimension of the medium and the beam are shown in the Fig. 2. The different radius of the broad beam is used here to evaluate the best mode of beam configuration for the detection of the object.

III. RESULTS AND DISCUSSION

All the simulations were run in high-performance computing facility by National Supercomputing Centre (NSCC) .The petascale computer is built on an x86 architecture, with 128 nodes and about 30,000 cores with 6TB RAM. To reduce the computational time, the multiple simulation outputs obtained for a lesser number of photons are averaged to get a result for a higher number of photons efficiently. This technique reduces the result acquisition time drastically. The signals from the tooth are compared with different from the object and the layer is separated and plotted across depth. The signal intensity varies for different illumination radius of the broad beam. Fig. 4 illustrates the ability of the broad beam to distinguish an object from the layer. For a pencil beam, though there is a significant signal from the object, the signal intensity from the layer is also quite high. So, in the total Raman intensity obtained there is a domination of signal from the layer and not from the object. But in the case of the broad beam there is higher signal intensity from the object. Both the top boundary and the bottom boundary is completely distinguished using the 0.1 cm broad beam. Also, the signal intensity from the layer is very low.

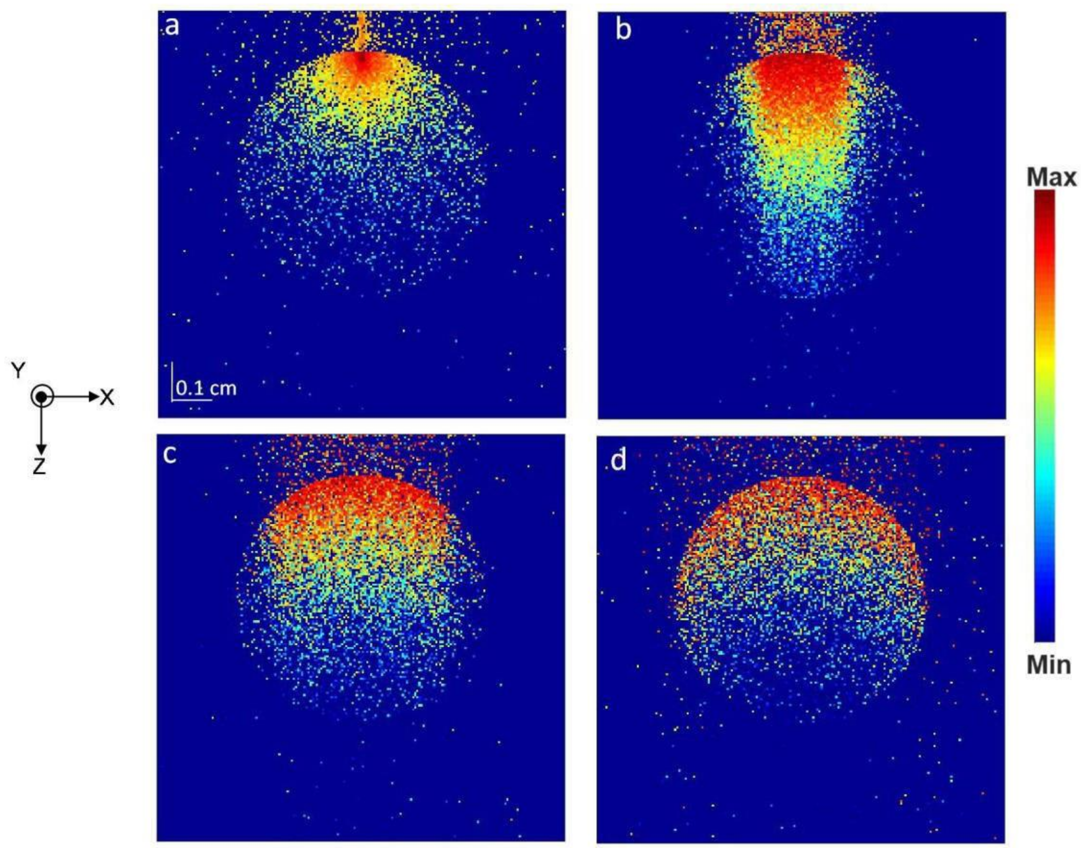

Figure 3 Raman photon generation in the tooth medium with embedded sphere for different illumination beam.
(a) Pencil beam (b) Broad beam r = 0.1 cm (c) Broad beam r = 0.2 cm (d) Broad beam r = 0.3 cm

configurations of illumination such as a pencil beam and a broad beam of different radius (r) of illumination such as 0.1 cm, 0.2 cm, and 0.3 cm. The spatial location of the generation of the Raman photons is shown in 2 dimensions in the XZ plane for the tooth model in Fig. 3.

Fig. 4 shows the Raman photon intensity for the simulation carried out with a pencil beam and a broad beam of different radius. It can be seen from the figure that the Raman signal was high from the boundary of the sphere when compared with the signal from the layer. The Raman photon intensity

So in the total Raman intensity obtained there is a major signal contribution by the object. This can be attributed to the optimal spread of the light over the object in the medium. As the beam radius increases to 0.2 cm and 0.3 cm, though there is a high signal from the object, the signal from the layer is also quite high. The signal intensity also reduces towards the bottom boundary for the 0.2 cm and 0.3 cm broad beam. The increase in beam radius increases the illumination of the beam on the layer in addition to the object which increases the signal from the layer. So for an object of radius 0.3 cm located in the medium, a light beam

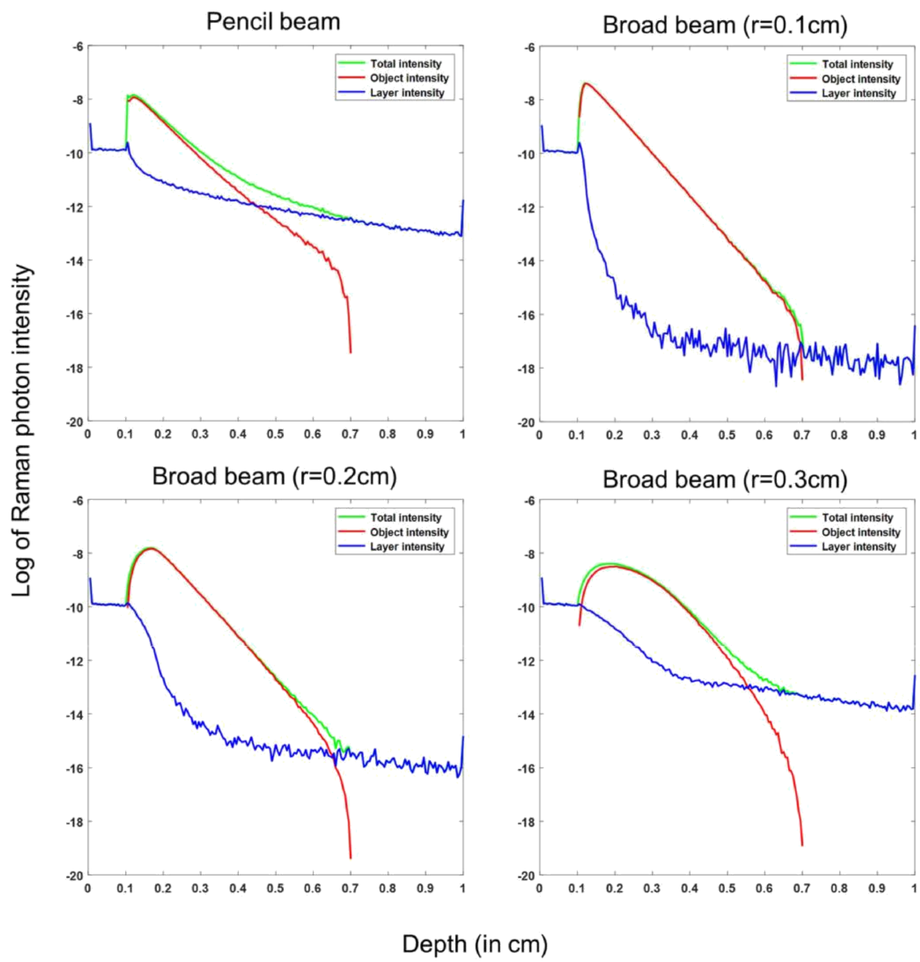

Figure 4 Raman photon intensity across depth in total, object and layer separately.

of radius 0.1 cm provides best signal intensity from the object of interest. There are evidence which show that the dominating Raman signal will be obtained from the layer near the illumination [23]. In the backscattering collection geometry, the signal from the top layer (in our case enamel) dominates, but the dependency of the signal with the material properties makes it possible to get a stronger signal from the object embedded below, in case of our simulation medium, the dentine.

TABLE I. PERCENTAGE OF RAMAN PHOTONS GENERATED IN TOTAL, OBJECT AND LAYER

Launch beam configurations	Total Raman photons (%)	Raman photons from object (%)	Raman photons from layer (%)
Pencil beam	0.02	68	32
Broad beam (r=0.1cm)	0.04	95.48	4.52
Broad beam (r=0.2cm)	0.039	93.43	6.57
Broad beam (r=0.3cm)	0.034	87.99	12.01

The Raman photon intensity is directly proportional to the total number of Raman photons generated in the medium.

The percentage of Raman photons generated was calculated from the formula (Total Raman photons generated / Total number of photons for simulation)*100. The Raman photons generated in the object and the Raman photons from the layer are recorded separately from the simulation. The percentage of Raman photons from the dentine (object) is calculated using the formula (Raman photons from the object/ Total number of Raman photons from the complete simulation medium)*100. The percentage of Raman photon generation varies for different launch beam configuration as shown in Table 1.

The percentage of Raman photons generated is high for broad beam than pencil beam. The increase in the percentage for 0.1 cm broad beam is because of the optimal spread of the illumination beam over the object with high scattering co-efficient which increases the multiple scattering events, which in turn increases the Raman photon generation. Though in a pencil beam the photon density is very high in a single line the initial area of contact of the light beam over the object is very less. As the total Raman photon generation is high for the 0.1 cm broad beam, 95.48% of the Raman photons are from the object which is very high, leading to better detection of object in the medium.

To successfully detect the presence of a sphere object under the medium, a strong signal from the object of interest is required. Signal to noise ratio is plotted as a function of depth for different illumination configuration, considering the Raman photon intensity from the sphere as the required signal and the Raman photon intensity from the layer as the noise. Fig. 5 depicts that the SNR from 0.1 cm broad beam is the highest and the lowest SNR is obtained from the pencil beam where the noise is high.

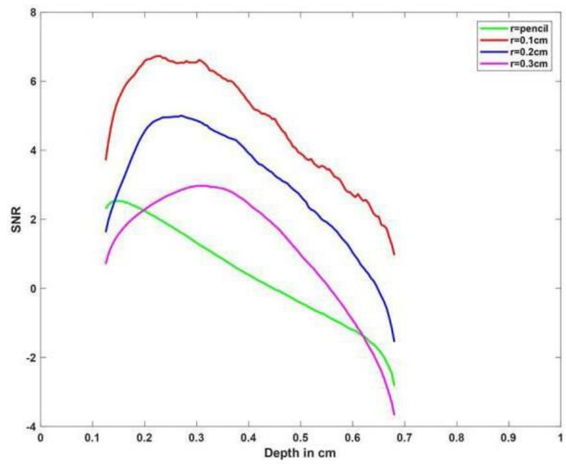

Figure 5 SNR as a function of depth for Raman photon intensity from object and layer

To illustrate reproducibility of the results with broad beam even with slight offset of the beam from the original region of interest, the simulation is repeated with slight offset of the beam from the origin. The offset considered here is 0.05 cm and 0.1 cm for the best broad beam illumination geometry of radius 0.1 cm. It can be seen from Figure 6 that there is no significant difference in spatially shifting the beam by 0.05 cm. However there is difference in signal when the beam is shifted by 0.1 cm. Any offset which is smaller than the beam radius has considerable reproducibility.

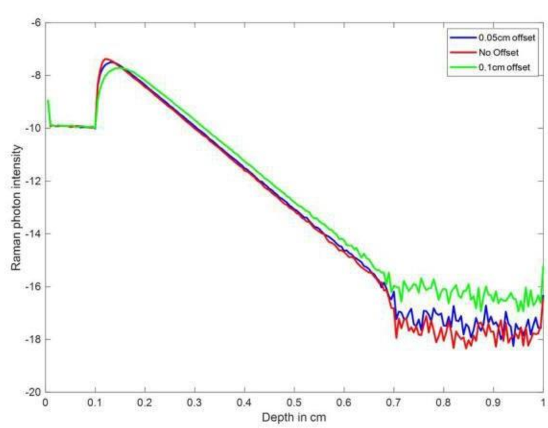

Figure 6 Raman photon intensity for broad beam of 0.1cm radius launched from origin, 0.05 cm offset from origin in x-axis and 0.1 cm offset from origin in x-axis.

IV. Conclusion

This work illustrates the implementation of Raman scattering and embedded object in the Monte Carlo simulation of light in tooth model. Utilizing different illumination model, the simulation mainly focuses on the identification of the object from the medium using Raman scattered photons. Results show that changing the illumination model to broad beam is useful in detecting the object inside the medium. The signal from the dentine will be useful in detecting the severity of the dental disorders from the amount of demineralization and help us in classifying the type of developmental disorder at an early stage. This will help in improving the aesthetics and function of the tooth by providing appropriate treatment. The broad beam also proves to produce reproducible results for offsets less than the beam radius. This method of simulating an embedded sphere inside the medium will be useful in detecting the abnormalities in the structure of dentine inside the teeth.

Acknowledgment

The authors would like to thank National Supercomputing Centre, Singapore for giving us access to their computing resources.

References

[1] B. C. Wilson, "A Monte Carlo model for the absorption and flux distributions of light in tissue" *Med. Phys.*, vol. 10, no. 6, 1983, pp. 824-830.

[2] Vijitha Periyasamy and Manojit Pramanik, "Advances in Monte Carlo simulation for light propagation in tissue" *IEEE Rev. Biomed. Eng.*, 2017, to be published.

[3] C. V. Raman, K. S. K. "A change of wave-length in light scattering" *Nature*, 121, 619, Apr. 1928

[4] Richard L. McCreery, "Raman spectroscopy for chemical Analysis" *John Wiley & Sons Inc. USA,* 2005.

[5] Kenny Kong, Catherine Kendall, et al., "Raman spectroscopy for medical diagnostics - from in-vitro biofluid assays to in-vivo cancer detection" *Adv. Drug Deliv. Rev.*, vol. 89, 2015, pp. 121-134.

[6] Pavel Matousek and Nicholas Stone. "Development of deep subsurface Raman spectroscopy for medical diagnosis and disease monitoring" *Chem. Soc. Rev.,* vol. 45, 2016, pp. 1794–1802.

[7] Matthew D. Keller, Robert H. Wilson, et al., "Monte Carlo model of spatially offset Raman spectroscopy for breast tumor margin analysis" *Appl. Spectrosc.*, vol. 64, no. 6, 2010, pp. 607–614.

[8] Periyasamy, V. and Pramanik, M. "Monte carlo simulation of light transport in tissue for optimizing light delivery in photoacoustic imaging of the sentinel lymph node" *J. Biomed. Opt*, vol 18, no. 10, 2006, p. 106008.

[9] Vijitha Periyasamy, Sanchita Sil et al., "Experimentally validated raman monte carlo simulation fora cuboid object to obtain raman spectroscopic signatures for hidden material" *J. Raman Spectrosc.*, vol. 46, 2014, pp. 669–676.

[10] Vijitha Periyasamy, and Pramanik, M. "Monte carlo simulation of light transport in turbid medium with embedded object-spherical, cylindrical, ellipsoidal, or cuboidal objects embedded within multilayered tissues" *J. Biomed. Opt*, vol. 19, no. 4, 2014 p. 045003, 2014.

[11] Mohanty B, Dadlani D, Mahoney D and Mann AB. "Characterizing and identifying incipient carious lesions in dental enamel using micro-Raman spectroscopy" *Caries Res,* vol. 47, 2013, pp. 27-33.

[12] El-Sharkawyi Y. H. "Detection and Characterization of Human Teeth Caries Using 2D Correlation Raman Spectroscopy." *J Biomed Phys Eng.* www.jbpe.org, 2016

[13] Ravikumar Ramakrishnaiah, Ghufran ur Rehman, et al., "Applications of Raman spectroscopy in dentistry: Analysis of tooth structure" *Appl. Spectrosc. Rev.*, vol. 50, no. 4, 2015, pp. 332–350.

[14] V. Renugopalakrishnanl, R. Garduño-Juárez, Juan Carlos Hernández Guerrero, Patricia N. Casillas Lavín and K. Ilangovan, "An Integrated, Holistic Experimental and Theoretical Approach Applied to the Derivation of the 3D Structure of Bovine Amelogenin implicated in Amelogenesis imperfecta, a Molecular Disease Characterized by a Single Point Mutation" *Rev. Soc. Quím. Méx*. vol. 43, No. 1, 1999

[15] Lihong Wang, Steven L. Jacques, and Liqiong Zheng. "Mcml - monte carlo modeling of light transport in multi-layered tissues" *Comput Methods Programs Biomed.*, vol. 47, 1995, pp. 131–146. .

[16] Seok Chan Park, Minjung Kim, Jimin Park, Hoeil Chung, Hea Yeon Kim, "Wide area illumination Raman scheme for simple and nondestructive discrimination of seawater cultured pearls" *J. Raman Spectrosc.*, vol. 40 no. 12, 2009, pp. 2187-2192.

[17] Jaejin Kim, Jintae Han, Jaegeun Noh, and Hoeil Chung., "Feasibility of a Wide Area Illumination Scheme for Reliable Raman Measurement of Petroleum Products" *Appl. Spectrosc.*, vol. 61, no. 7, 2007, pp. 686-693

[18] Peter Naglič, Franjo Pernuš, Boštjan Likar, and Miran Bürmen, "Limitations of the commonly used simplified laterally uniform optical fiber probe tissue interface in Monte Carlo simulations of diffuse reflectance" *Biomed. Opt. Express,* vol. 6, no.10, 2015, p. 3973.

[19] Daniel Fried, Richard E. Glena, John D. B. Featherstone, and wolf seka., "Nature of light scattering in dental enamel and dentin at visible and near-infrared wavelengths" *Appl. Opt.*, vol. 34, no. 7, 1995, pp. 1278-1285.

[20] Ahmed L. Abdel Gawad, Yasser H. El-Shakawy and Ashraf F.El-Sherif., "Classification of human teeth caries using custom non-invasive optical imaging system" *Laser Dent Sci.*, vol. 1, pp. 73-81, 2017

[21] Yongji Fu, and Steven L. Jacques, "Monte carlo simulation for light propagation in 3d tooth model" *Proc. of SPIE.*, Optical Interactions with Tissue and Cells XXII, 2011, 78971N

[22] E.I. Tolstykh · M.O. Degteva · V.P. Kozheurov E.A. Shishkina · A.A. Romanyukha · A. Wieser P. Jacob., "Strontium metabolism in teeth and enamel dose assessment: analysis of the Techa river data" *Radiat Environ Biophys.*, vol. 39, 2000, pp. 161–171.

[23] Sanchita Sil & Siva Umapthy., "Raman spectroscopy explores molecular structural signatures of hidden materials in depth: Universal Multiple Angle Raman Spectroscopy" *Sci. Rep.*, vol. 4, no. 5308, 2014.

ISBN 978-1-5386-4473-7

Applications of magnetic nanoparticles in hyperthermia and its characterization studies

C.L. Annapoorani[1] and Nisha shree

[1]Assistant Professor, Department of Biomedical Engineering, Jerusalem College of Engineering, Chennai – 600100.

***Abstract*— Magnetic hyperthermia is considered as a therapeutic way since they exhibit hysteresis property and dissipate heat when placed under the magnetic flux area. As per ampere's law, the sum of elements in the magnetic field is equal to the permeability in the electric current enclosed in the loop area. Thus, it transforms high frequency electromagnetic energy to heat. When hyperthermia is applied, the cancerous cells get devastated due to their local increase in temperature. The Cobalt ferrite magnetic nanoparticles were considered for hyperthermia applications to destroy tumor cells locally. The magnetic nanoparticles were synthesized using co-precipitation method and were coated with polyacrylic acid as it exhibited toxic properties when it was subjected to analysis. Thus, it was characterized using SEM, XRD, VSM and FTIR. Also, the magnetic nanoparticles were tested for its cellular uptake. By suspending the magnetic nanoparticles into the aqueous environment where the brine shrimp larvae were habituated, the cellular uptake was studied with respect to time. It is implied that the cells were subjected to necrosis. This can be measured in several different ways such as assessing cell viability.**

I. INTRODUCTION

Nanotechnology is the science of small things that are less than 100nm in size. Nanomaterials have a variety of potential applications including medical, industrial and military areas. Magnetic nanoparticles usually react to varying magnetic field gradients. Magnetic nanoparticles are comprised of elements such as iron, nickel, cobalt and their chemical compounds. The magnetic nanoparticles find more applications in biomedical sciences, tissue specific targeting, magnetic resonance imaging and so on. Hyperthermia may be defined more as raising the temperature of a part of the body above normal temperature. Magnetic fluids are highly used in all the clinical applications. It has been developed for the cancer treatment for several decades. The magnetic nanoparticles are injected into the tumor area and their subsequent heating in an alternating magnetic field.

II. OBJECTIVES

To study the toxicity by inducing necrosis or apoptosis using magnetic nanoparticles in brine shrimp cells. Also, to analyse if the magnetic nanoparticles can induce artificial fever in the body cells. Depending upon the applied temperature and heating period, tumor cell killing which is stated as necrosis happens. Our aim is to get a stable ferrofluid solution by dispersing surfactant coated $CoFe_2O_4$ MNPs into deionized water. In this regard, we have chosen a polymer, Polyacrylic acid (PAA) as the surfactant. A pre-calculated quantity of poly acrylic acid (PAA) was added to the CFO solution as a coating material.

III. SYNTHESIS

Composition of Cobalt chloride and ferric chloride was used to prepare magnetic nanoparticles by co-precipitation method.

Co - precipitation method:
Co-precipitation method (Kandpal, N.D et al., 2014) is a convenient way to synthesize ferrites from aqueous ferritic solution with the addition of an alkaline solution at room ambience (Balakrishnan, P et al., 2015). The co-precipitation approach has been used widely used to produce ferrite nanoparticles of controlled sizes and magnetic properties.

Surfactant – poly acrylic acid:

- 5gm of poly acrylic acid is dispersed in 10ml of water.
- 1.5 gm of poly acrylic acid is dispersed in 10ml
- 1.25 gm of poly acrylic acid is dispersed in 10ml of water.

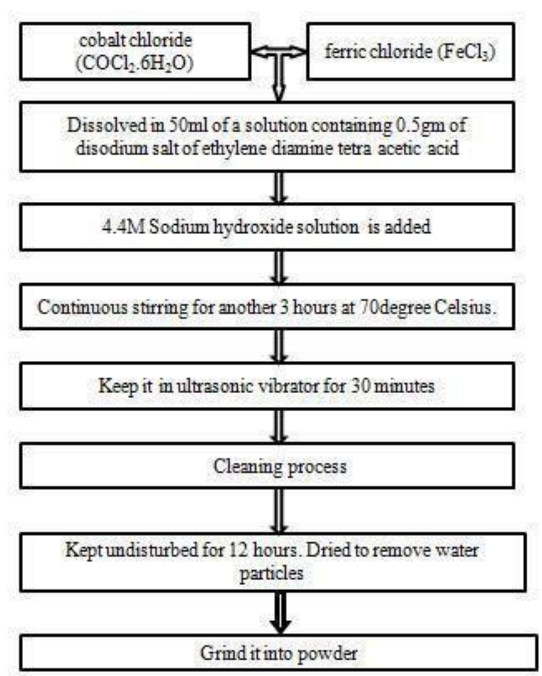

Fig. 1: Synthesis process

ISBN 978-1-5386-4473-7

IV. HYPERTHERMIA

The magnetic moments present in the cells in a disoriented manner when subjected to an external magnetic field (Lao, L.L et al., 2004). As the external field changes its alignment, the magnetic moment will align randomly. This produces dissipation leads to heating.

Solenoid:

The magnetic field is generated (Krause et al., 1994) along a straight length of current-carrying wire. It is usually weak even with a high current passing through it. However, if several number of coils in the wire are wound together along the same axis producing a coil of wire, (He, X et al., 2004) the resultant magnetic field will become concentrated and stronger.

Hyperthermia setup:

Hyperthermia (Hafeli, U et al., 1997) setup consists of copper coil windings which is used to produce magnetic field when there is an application of electric current (Ampere's law). The coil windings are made in a such a way that it can form an aperture in between as shown in fig. 2. The beaker with ferrofluid (magnetic nanoparticles in distilled water) is placed inside the aperture. A thermometer is placed inside the beaker to measure the temperature rise of the respective samples (Rosensweig R.E et al., 2002)

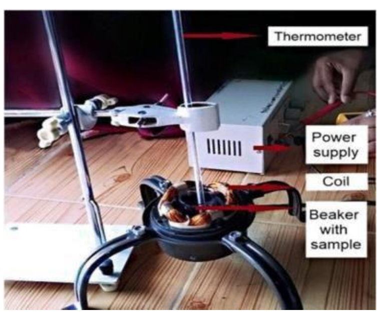

Fig. 2: Hyperthermia setup

Brine shrimp cells:

Artemia salina is the biological name of brine shrimp cells. It belongs to the genus of aquatic crustaceans. Artemia is a primitive arthropod with a segmented body along with appendages. Artemia is used as a test specimen for its utilisation in toxicological assays. In a pollution research test, the brine shrimp larvae are said to possess an extensive use as a test specimen and determine its cellular uptake.

V. CELLULAR UPTAKE

Cellular uptake is the abbreviation used for the exposure concentration of a toxic substance lethal to half of the test animals. In this test, 0.1gm of synthesized magnetic nanoparticle (both coated and uncoated), 5 Brine shrimp larvae were taken in a vial as shown in fig. 3. Freshly prepared sodium chloride solution (19gm in 500 ml) is added to it and kept undisturbed for 24 hours. The mortality rate was studied by counting the number of alive larvae in the vial.

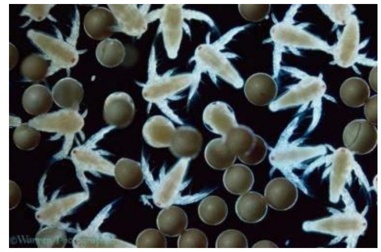

Fig. 3: Brine shrimp eggs & larvae

VI. RESULTS AND DISCUSSIONS

1. X-Ray Diffraction (XRD):

The structure of the obtained $CoFe_2O_4$ powders was studied by means of the X-ray powder diffraction technique. Fig. 4 shows the representative pattern obtained at room temperature for synthesized powder. The XRD spectrum exhibited broadened diffraction peaks that implied the nanocrystalline nature of the powder. The average crystallite size (d) of the cobalt ferrite powder was calculated using Scherrer's formula.

$$KZ / \beta \cos\theta$$

Where K is shape factor irrespective of dimension, Z is the wavelength, β is the line broadening at half of the maximum intensity and θ is Bragg angle. The mean crystallite sizes of the $CoFe_2O_4$ magnetic nanoparticles that are synthesized lie under the range of 25.41 nm and 30.64 nm.

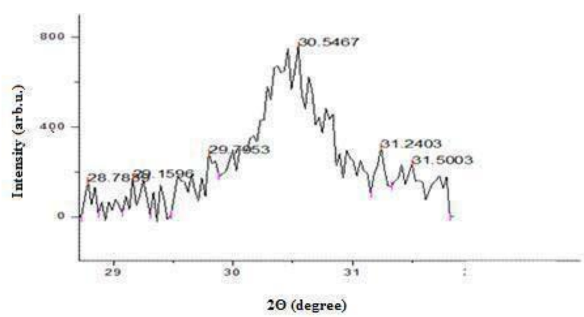

Fig. 4: X-Ray Diffraction-uncoated sample

XRD patterns were recorded using X-ray diffractometer with a step size of 0.016^{o} per second. Fig.5 shows the XRD patterns of poly acrylic acid coated $CoFe_2O_4$ nanoparticles synthesized with 1 mL, 3 mL, 5 mL and 10 mL of poly acrylic acid (PAA) (Kyung Kim et al., 2003). Phase of Cobalt ferrite is confirmed by comparing the obtained XRD pattern with standard JCPDS pattern (22-1086). No other phases were determined other than $CoFe_2O_4$ and the samples consists of pure phase. Lattice parameter that was measured is 8.3 Å.

ISBN 978-1-5386-4473-7

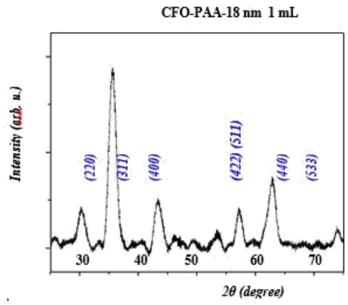

Fig. 5: PAA coating

2. Scanning electron microscope (SEM):

The surface morphology of $CoFe_2O_4$ powder is studied using SEM. The morphology of the crystals, particles size is studied by a scanning electron microscopy. The annealing temperature increases and the particles size decreases simultaneously. From the morphology, it is interesting to note that when temperature increases the shape does not change but affects only the radius of the nanoparticles.

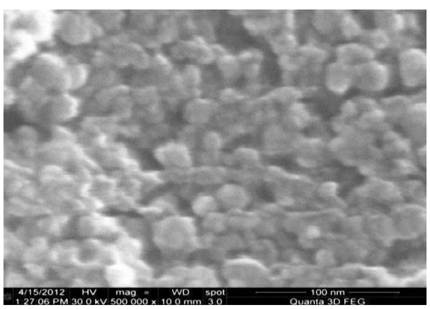

Fig. 6: SEM image

3. Vibrating sample magnetometer (VSM):

Magnetic characterization of the samples was performed by VSM at room ambience with a maximum applied magnetic field of ±15kOe. Fig. 7 shows hysteresis loop of test sample. It can be observed that sample reveal typical paramagnetic behaviour. The paramagnetic behaviour of the prepared nanocrystals is clearly shown by coercivity , saturation magnetization and remanence magnetization.

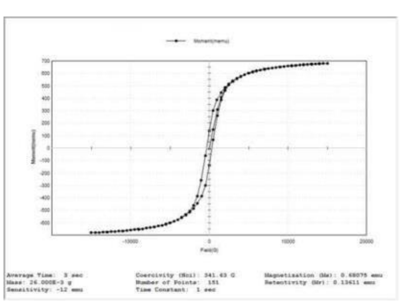

Fig. 7: VSM graph

4. Particle size analysis (PSA):

This instrument measures the particle size through sedimentation principle. Particle size versus concentration plots will be recorded. Particle size and distribution is important to get the first band information of sizes of the nanomaterials prepared. The instrument works under the centrifugal force principle. The cobalt ferrite nanoparticles coated with poly acrylic acid at various concentration, shows almost the same particle diameter. This shows that the nanoparticles produced, are almost similar in size.

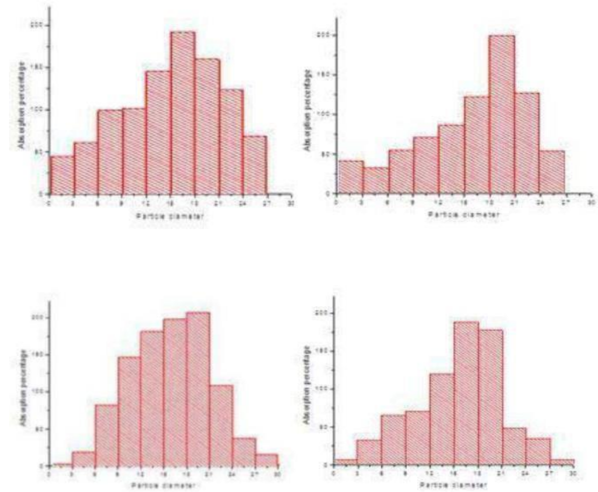

Fig. 8 (a,b,c,d): distribution of particles in the medium in the range of 12 - 20 nm.

5. Fourier transform infrared spectroscopy (FTIR):

FTIR measurements were performed using Perkin Elmer Spectrum FT-IR instrument by making a semi-transparent pellet made using a small amount of $CoFe_2O_4$ nanoparticles and KBr in the spectral region from 450 to 4000 cm^{-1}. FTIR spectroscopy is a very powerful tool to investigate the structure and phase of chemical compounds. The information about the bonding of Co-O and Fe-O in octahedral and tetrahedral sites of the inverse spinel structure in CFO can be obtained by FTIR spectra. Fig. 9 shows the FTIR spectra of as prepared CFO-PAA nanoparticles. A broad band at 3842-3378 cm^{-1} observed corresponds to -OH stretching vibration mode.

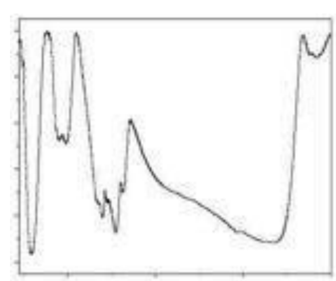

Fig. 9: FTIR results for PAA-coated CFO Magnetic nanoparticles

ISBN 978-1-5386-4473-7

The bands at 1634-1547 cm^{-1} assigned to the symmetry and anti-symmetry stretching vibration mode. The bands at the 1399-1328 cm^{-1} are assigned to C-O bending vibration. The two strong bands at 976-900 cm^{-1} are assigned to C-H bending vibration. The bands at 590 cm^{-1} for all CFO-PAA MNPs are corresponding to the lattice vibration of octahedral and tetrahedral sites in inverse – spinel structures.

6. Hyperthermia studies:

The heat generation of cobalt ferrite MNPs (Li, G.C. et al., 1995) and influence of colloidal concentration and particle size on heating rate under various DC magnetic field ranging from 30 mT to 70 mT was studied using magnetic hyperthermia setup. The magnetic field was obtained from the current passing through the copper coil is given by

$$B = \mu_s n I$$

where 'I' is the current in ampere and 'n' is the number of coil turns per unit length and μ_o is the free space permeability. The temperature profile was taken for 60 minutes using thermometer. Fig. 10 (a,b,c) show the temperature profile of ferrofluid with 19 nm particles for four different concentration (a) 10g/L, (b) 5g/L, (c) 2.5g/L and (d) 1.25g/L. Similar experiments were carried out using ferro fluids of nanoparticle sizes 18 nm (Fig.) and 16 nm (Fig.) at four different concentrations.

Hyperthermia study results for CFO-PAA 1 studies

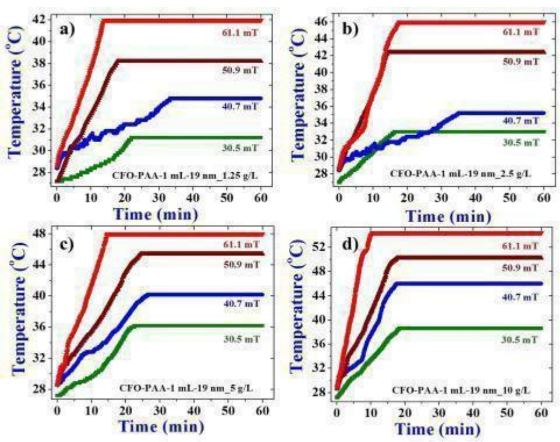

Hyperthermia study results for CFO-PAA 2 studies

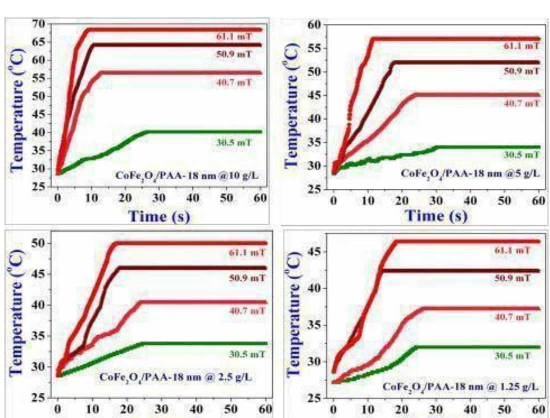

Hyperthermia study results for CFO-PAA 3 studies

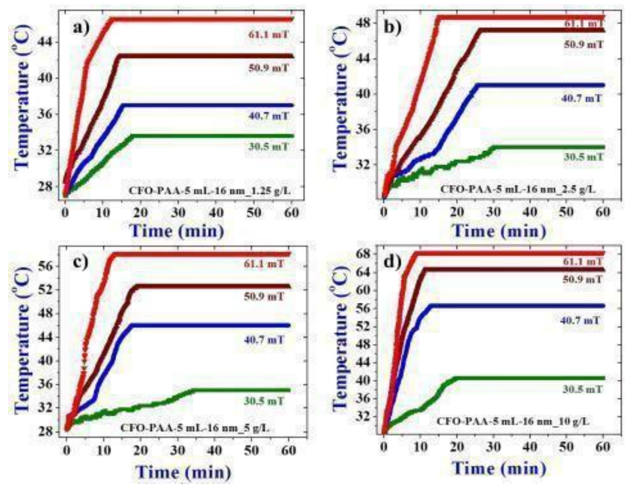

Fig. 10 (a,b,c): Hyperthermia study results

CONCLUSION:

Thus, the magnetic nanoparticles that are synthesized show a good result in the hyperthermia analysis. a maximum of 68°C is obtained. with this it can be concluded that the magnetic nanoparticles that are injected intra arterially, can be subjected to magnetic flux, which can induce artificial fever and is used to treat tumor cells lysis.

REFERENCES

[1] Balakrishnan, P. & Veluchamy, P. Synthesis and Characterization of CoFe2O4 Magnetic Nanoparticles using Sol-Gel Method, (2015).

[2] Chakrabarti, S. Mandal, S. K. and Chaudhuri, S, Nanotechnology, 16: 506 (2005).

[3] Hafeli, U. Schütt, W. Teller, J and Zborowski, M. Plenum Press, 3: 569-595 (1997).

[4] He, X. McGee, S. Coad, J.E. Schmidlin, F. Iaizzo, P.A. Swanlund, D.J. Kluge, S. Rudie, E. Bischof, J.C. Int. J. Hyperthermia, (2004).

[5] Krause and Felix, R. Magnetic Fluid Hyperthermia, Scientific and Clinical Applications of Magnetic, Magnetism and Magnetic Materials, Cambridge University Press, Cambridge (1994).

[6] Kandpal, N.D. Sah, N. Loshali, R. Joshi, R and Prasad, J. Co-precipitation method of synthesis and characterization of Iron Oxide nanoparticles, journal of scienetific and industrial research, 73: 87-90 (2014).

[7] Kyung Kim and Maria Mikhaylova, Starch-Coated Super paramagnetic Nanoparticles as MR Contrast Agents, Chem. Mater., 15: 4343–4351 (2003).

[8] Lao, L.L. and Ramanujan, R.V. "Magnetic and Hydrogel Composite Materials for Hyperthermia Applications", J. Mater.Sci.Mater. Medicine, 15: 1061-1064 (2004).

[9] Li, G.C. Mivechi, N.F and Weitzel, "Hyperthermia classic article commentary: Re-induction of hsp70 synthesis: an assay for thermotolerance", G. Int., J. Hyperthermia, 11(4): 459-88 (1995).

[10] Rosensweig R.E, "Heating magnetic fluid with alternating magnetic field" J.Magn. Magn. Mater. 252: 370-374 (2002).

[11] Svoboda, J, "Magnetic Techniques for the Treatment of Materials", Kluwer Academic Publishers, Dordrecht, The Netherlands (2004).

ISBN 978-1-5386-4473-7
IEEE sponsored 4th International Conference on Biosignals, Images and Instrumentation, SSNCE, Chennai. ICBSII 2018 – 22nd-24thMar'18

Computational Analysis of Respiratory Tract with 2D And 3D Models

S.M.Umarani ,M.E
Assistant professor, Department of ECE, Hindustan Institute of technology and science, HITS
Padur, Chennai, India
uma912010@gmail.com

P.Archana,M.E
Assistant professor, Department of ECE, Hindustan Institute of technology and science, HITS
Padur, Chennai, India
archanaveni@gmail.com

***Abstract*—One of the most unique systems in the human body is human respiratory system . Being suited with the task of gas exchange across the respiratory surface, each aspect of the human lungs plays an interconnected role in ensuring that this process is carried out effectively and efficiently. The primary function of the respiratory system entails the intake of oxygen into the body and the expulsion of carbon dioxide from the body. The pathway by which the air enters to the nasal cavity passes to the trachea to the bronchi then to the bronchioles and finally to alveolus. Analysis of respiratory tract is important to study the mechanical process during inspiration and expiration. This analysis can provide an insight about the input and output parameters involved during Inspiration and Expiration. With the help of computational studies such details about the analysis of respiratory tract can be investigated in detail. Laminar viscous model has been used to depict the real time scenario. The pressure and velocity parameters were analysed to get the results.**

Keywords— Respiratory tract, laminar, 2D, 3D model (key words)

I. INTRODUCTION

Human respiratory system play an very important role in breathing mechanism as well as gas exchange. The human respiratory system mainly consists of two important zones namely the respiratory zone and conducting zone [6], seen in Fig.1. The conducting zone is built by many sections which includes nasal cavity, pharynx, larynx, trachea, bronchi and bronchioles. From the numerical modelling point of view, it can be divided into the extra thoracic region, tracheobronchial region, and the alveolar region. The tracheobronchial region and alveolar region can be assigned to intrathoracic region. The extra thoracic region includes nasal cavity, oral cavity, pharynx, larynx and trachea which forms the upper respiratory system. The tracheobronchial tree starts from generation 0 (trachea) to generation 23^{rd} (alveoli). Conducting zone is from generation 0 –generation 16^{th} and respiratory zone is from generation 17^{th} to generation 23^{rd} where the gas exchange takes places Fig.2. The need of this work is that, the respiratory tract is responsible for conducting the pathway for air to enter and exit the lungs. So that, the efficient modelling of respiratory tract can make us understand the processes involved during inspiration and expiration. So that the pressure difference, velocity, volume and flow rate can be understood from the model designed.

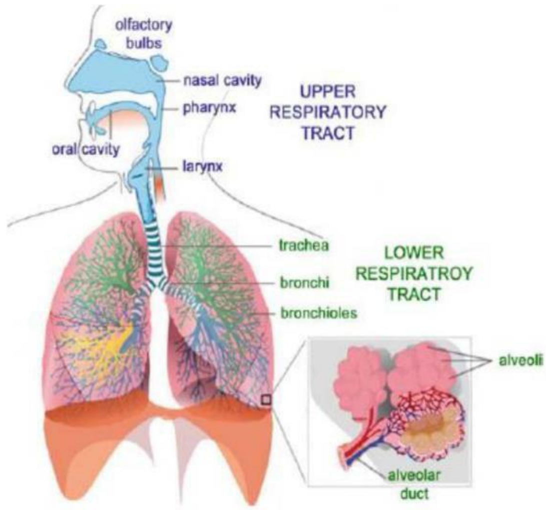

Fig 1: Schematic diagram of the Entire Respiratory System [6]

II. LITERATURE REVIEW

During inspiration, the air passes through the nostrils and the nasal cavity to the larynx. Then the larynx, it flows through the trachea to the primary bronchi. These bronchi are split into secondary bronchi and secondary to tertiary and so on. The number of branches along the path which denotes the bifurcation of branching nodes (sometimes called generation number). The last generation of tubes end in bunches of tiny round air sacs has observed 23^{rd} generations of conducting airways ranging from the trachea until the terminal bronchioles in normal human respiratory system. In view of the fact that each person has a different geometry of the lungs (depending on age, gender, body composition, weight, height) for calculation purposes, several generalized models of the lung are used. The simplest model of the lungs is a Weibel symmetrical model, i.e. all ways from trachea to alveoli are the same and all branching are at the same angle. The commonly used anatomical model of the lower airways was developed by Weibel [3]. In this unidimensional model, weibel indicates the directions of bifurcation, which designed as such the trachea(generation 0) as kept the first airway and assumptions are made that each airway leads to two symmetrical branches (regular dichotomy). The model developed by Weibel gives a minimum of 23^{rd} bronchial generations, which is describes the lengths and diameters [3].

ISBN 978-1-5386-4473-7

Zhang and Kleinstreuer presented a model based on the weibel geometric data and used the finite volume method which analyze the particle deposition in the human upper airway at different breathing flow rates [4]. They showed that the airway deformation can affect airflow field and particle deposition pattern.

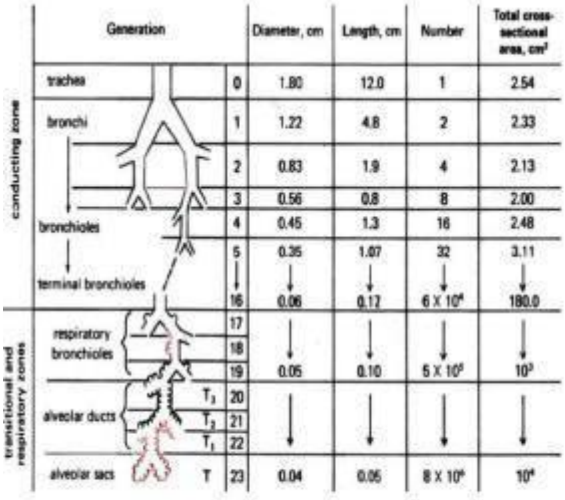

Fig 2: Branching Airways (Redrawn from Weibel 1963) [10]

Gemci et al [2] used the generation 17^{th} lung model of Schimdt et al. (2004). They studied the inhalation process from trachea (generation 0) to generation 17^{th} (the terminal bronchioles), with quasi steady-state simulations. An equal and constant pressure condition at all flow outlets (corresponding to areas not modelled) has been considered in this paper.

Liu et al [8] studied the inspiratory flow characteristics by using volume controlled method for three generation airway (5^{th} to 7^{th}) of weibel [3] model for both in plane and off plane geometry with mouth –air breathing rate ranging from 0.27-2.16 l/s. The pressure drop in both model has been studied.

Luo et al [9] studied the turbulent flow characteristics in airway during particle deposition using dimensions of Schlesinger and lipmannet al model. He compared the particle deposition and velocity contour laminar LES and k-w model.

Computational modelling is considered to be use of physics, mathematics and computer science to study about the behaviour of complex systems by computer simulation. Modelling is needed in the area of medicine to understand the operation of functional system of human body [14]. The model construction and simulation of the model is analysed by adjusting these variables and observing the changes that affect the outcomes predicted by the model. The results of simulation model help us to understand what will happen to the in the real system that is being observed in response to changing conditions. Computational Fluid Dynamics (CFD) has become a recent method for numerically studying various patterns of pressure, flow and resulting particle deposition and particle transport through the airways. Previous studies says that an anatomically accurate geometry is more enough for a understanding of airway flow thoroughly.

This paper shows the construction and analysis of 2D (3 generations) and 3D (one generation) respiratory tract and also its validation in the model implementation. The main aim and purpose of this work is to determine the characteristics of respiratory tract thus obtaining a thorough insight of its role in breathing mechanism, thus to analyse the physiological functions of respiratory tract during normal respiratory conditions with help of a model and to evaluate the mechanical properties from the results derived from the model.

III. MATERIALS AND METHODS

A simple human airway model geometry which was described by Weibel [3] is being used. The Software which is being used in this paper is Ansys 15.0. The 2D and 3D respiratory tract model were designed in ANSYS Design Modeller. Further, the meshing operation which plays an important role in numerical study is done by segmenting the geometry into small cells in which the flow equation will be solved which was performed in ANSYS mesh. The next step involves the numerical simulation of the meshed models. The meshed models were computationally analysed in ANSYS FLUENT 15.0 using the laminar viscous model. The contour of total pressure and velocity were taken.

A. 2D Respiratory model

The 2D respiratory tract model was designed with 3 generations fig.5, which was then meshed with 5297 nodes and 4928 elements of square grids shown in fig.6. The pressure profile and velocity profile is shown in Fig.11 and Fig.12.

B. 3D Respiratory model

The 3D respiratory tract model was designed with one generation as shown in Fig .7 which was then meshed with 3811 nodes and 17020 elements of tetrahedral grids as shown in Fig.8. The size of the mesh is consistent with size of the boundary layer and descending from high-order to low-order generations. The pressure profile and velocity profile is shown in Fig.13 and Fig.14.

The 2D and 3D model of the respiratory tract is designed using Ansys design modeller with reference to Weibel [3]. The CFD simulation can be done by using the measured values of velocity and pressure profile of 2D model. Ansys -Fluent Solver has been used for the numerical simulation which is inbuilt function. Second order upwind numerical scheme were used for the discretization of various terms in transport equation. Semi -Implicit Method for Pressure Linked Equations (SIMPLE) algorithm was enabled in Fluent for velocity-pressure coupling. The flow behavior in human airways shows both laminar and turbulent. In this work, the flow is solved for Laminar. For the laminar model, the boundary conditions are that the velocity, no slip condition at the wall is satisfied, the inlet velocity is uniform and outlets shows zero pressure.

The 2D and 3D respiratory tract model is modelled according to the dimensions of Weibel's[3] model shown in fig.2, The geometric properties with the dimensions is listed in table.1

A. INPUT PARAMETERS

The input parameters such as boundary conditions, geometric properties and material properties are listed in the below tables.

1. Boundary conditions

The boundary conditions are very important to specify as it gives the relation between inlet and outlet in which is obtained from the literature survey. The inlet is pressure inlet with pressure value less than atmospheric pressure in pascal. The outlet is considered as pressure outlet with uniform pressure, assumed to be Zero and no slip boundary is considered here.

Table 1: Boundary conditions

BOUNDARY CONDITIONS	***VALUES***
Inlet pressure	*101234.3 pascal*
Inlet turbulent intensity	*5%*
Outlet pressure	*0 pascal*
Wall	*No slip*

2. Geometric properties

The geometric property is the dimensions of both 2D and 3D respiratory tract model which has been used.

Table 2:Design parameters-Respiratory tract

GENERATION	***LENGTH (mm)***	***DIAMETER (mm)***	***RADIUS OF CURATURE(mm)***
Trachea(0)	*120*	*18*	*34.2*
1st generation	*47.6*	*12.2*	*14.64*
2nd generation	*19*	*8.3*	*7.47*
3rd generation	*7.6*	*5.6*	*6.72*
4th generation	*13*	*4.5*	*-*

3. Material Properties

Table 3:Respiratory tract model

PROPERTY	***VALUES***
Density	*1.29(kg/m^3)*
Material	*Air(incompressible)*
Viscosity	*1.81e-5(kg/ms)*

The inlet of the geometry is assumed to be a pressure inlet. The exits are both in left and right side of geometry which is assumed to be pressure outlet with pressure less than the atmospheric pressure. The fluid is considered as incompressible air and properties are given in the table.

IV. RESULTS AND DISCUSSIONS

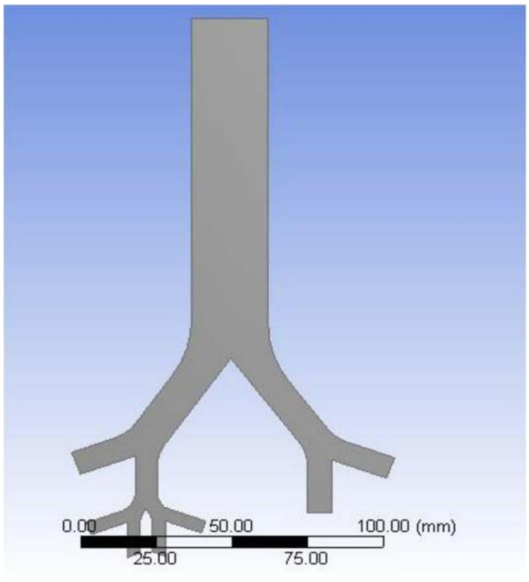

Fig 4:2D Respiratory tract

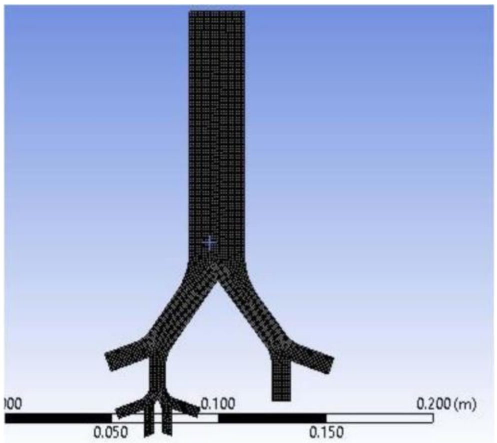

Fig 5: Meshed output of 2D Respiratory tract

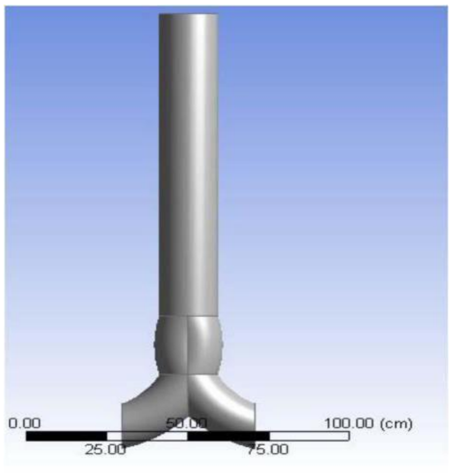

Fig.7 3D respiratory tract model

Figure 4 and 5 represents the 2D respiratory tract model and meshed output respectively, in which 2 D model has three generations. The geometric properties which are used to design the model is the table1 above.

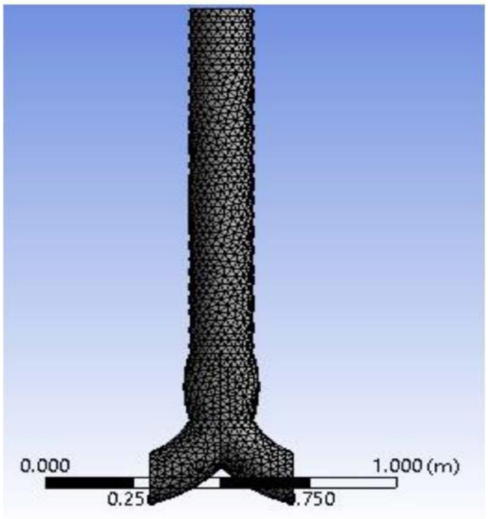

Fig.8: Meshed output of 3D respiratory tract model

Figure 7 and 8 represents the 3D respiratory tract model and meshed output respectively, in which 3 D model has only one generation. The geometric properties which are used to design the model is the table1 above.

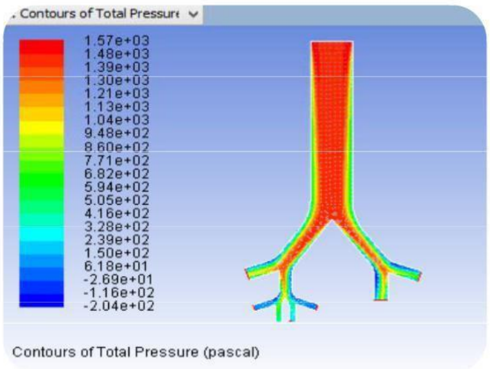

Fig.11.Pressure Profile of 2D Respiratory tract model

The numerical computation to the model is with the pressure and velocity distribution in the airways. In the 2D respiratory tract and 3D respiratory tract model simulations, the flow pattern obtained using the laminar models. Laminar flow is considered because from literature for normal airway, the flow in trachea is always laminar.

Pressure drop behavior in the bifurcating airways plays an vital role in the respiratory process Figure 11. The respiratory process can only take place when the alternative contraction and expansion of the respiratory muscles overcomes the pressure drop due to viscous loss which make them continually and normally perform the process. Some analyses t to establish the relation between the pressure drop and Reynolds number has been carried out ,ranging from laminar to turbulent cases with and without wall roughness in straight and curved tubes.

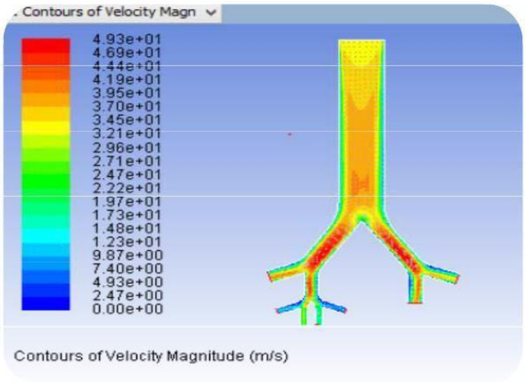

Fig.12: Velocity profile of 2D respiratory tract model

The result of velocity distribution of 2D respiratory tract model is displayed on Figure.12 due to the no-slip condition applied at the wall, the outside surface has zero velocity. It can be seen from Figure.12 that the velocity decreased with the generations.

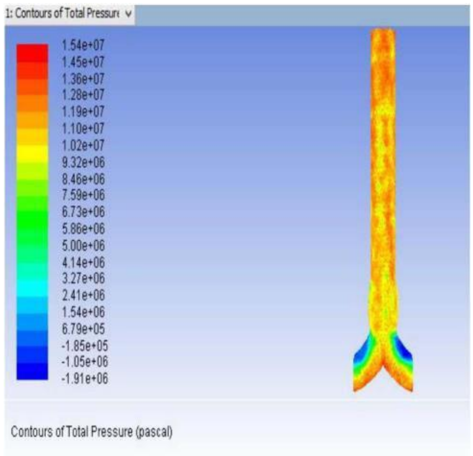

Fig.13.Pressure profile of 3D respiratory tract model

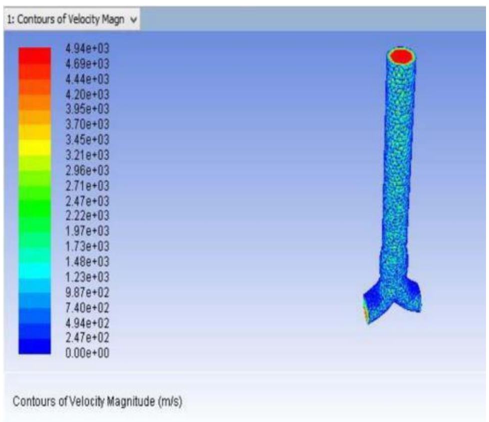

Fig.14.Velocity profile of 3D respiratory tract model

During the respiratory process, the pressure drop plays an important role in bifurcating airways. Pressure drop in the respiratory tract is displayed in figure.13 the pressure profile shows that the higher pressure is seen at the bifurcating point compared to others.

Velocity profile of 3D respiratory tract model is displayed in figure 14.from the profile, the velocity seems to be very less in the outer wall whereas it seems to have higher velocity in the center of airway.

CONCLUSION

This paper reveals 2D and 3D model of respiratory tract designed by following the Weibel's[3] (1963) symmetrical model. The 2D model consists of trachea with 3 generation of airways and 3D model consists of trachea with only one generation of airway. These 2D and 3D respiratory tract model were analysed by Ansys fluent software under laminar viscous model conditions.

The model has been meshed using tetrahedral cells which give satisfactory results with respect to the geometry.

The 2D and 3D respiratory tract model with the pressure and velocity profiles can be validated. The sudden increase in pressure can be seen in both the model at the bifurcating point. The decrease in velocity is seen in the outer surface of both the model then the inner surface.

FUTURE WORK

Further investigation can be carried out by modelling the whole respiratory tract from generation 4 to generation 23 (alveoli) and analysis of the same can be obtained in order to investigate specific diseases.

ACKNOWLEDGMENT

I like to thank my guide and well wishes who helped to start my research paper.

REFERENCES

[1] Ramana M. Pidaparti1, Matthew Burnette, Rebecca L. Heise, Angela Reynolds,"Analysis for stress environment in the alveolar sac model" (2013).

[2] Gemci, T., Ponyavin, V., Chen, Y., Chen, H., & Collins, R. ,"Computational model of airflow in upper 17 generations of human respiratory tract". *Journal of Biomechanics*, *41*, 2047–2054,2008.

[3] Weibel, E.R.,. "Morphometry of the Human Lung", Academic Press, New York, Springer, Berlin. 1963

[4] Z. Zhang and C. Kleinstreuer, "Airflow structures and nano-particle deposition in a human upper airway model", *Journal of Computational Physics* 198 (2004), 178–210.

[5] Taherian S and Rahai H.R. "CFD Modeling and Analysis of Pulmonary Airways/Particles Transport and Deposition", *41st AIAA Fluid Dynamics Conference and Exhibit 27 - 30 June 2011,Honolulu, Hawaii*

[6] J. Tu et al, Chapter 2 "The Human Respiratory System *Computational Fluid and Particle Dynamics in the Human Respiratory System",* Biological and Medical Physics, Biomedical Engineering, © Springer Science+Business Media Dordrecht (2013),

[7] Luo, H. Y. & Liu, Y.,. "Modeling the Bifurcating Flow in an CT-Scanned Human Lung Airway". *Journal of Biomechanics*, 41(12), pp. 2681-2688. 2008

[8] Y. Liu, R.M.C. So, C.H. Zhang, "Modeling the bifurcating flowing a human lung airway", *Journal of Biomechanics 35 (2002) 465–473*

[9] X.Y. Luo, J.S. Hinton, T.T.Liew, K.K. Tan,"LES modelling of flow in a simple airway model", *Medical Engineering & Physics 26 (2004) 403–413*

[10] Shyan-Lung Lin ,Nai-Ren Guo,Chuang-Chien Chiu(2010), "Modeling and Simulation of Respiratory control with Labview" Journal of Medical and Biological Engineering, 32(1): 51-60 Dec

[11] Levitzky, M.G., "*Pulmonary Physiology"*., New York: McGraw-Hill. 1991

[12] Hiroko Kitaoka(2012), "Construction of the Human Lung and Air Flow Analysis" *Forma*, 27, S21–S27, April 30

[13] Devdatta, V.K.Katiyar, "Pratibha Mathematical Modelling of Respiratory System: A Review" - Indian Journal of Biomechanics: Special Issue (NCBM 7-8 March) 2009

[14] National institute of biomedical imaging and bioengineering, National institutes of health, Computational modelling, www.nibib.nih.gov.

Special Thanks to our Sponsors

IEEE

GENTECH
Genetics & Technology

Bionics Biomedical Systems,
Chennai

Proceedings of the

4th International Conference on Bio Signals, Images and Instrumentation (ICBSII 2018)

Biomedical Engineering is a field of study that integrates two dynamic professions, Medicine and Engineering. It has recently established itself as an independent field with the objective of assisting medicine towards the betterment of society, through research.

Being an interdisciplinary science, it has associations with various other subjects such as Electrical Engineering, Mechanical Engineering, Chemical Engineering and Biotechnology. The spectrum of Bio-medical research aims to unite these disciplines in synergy, leading to new possibilities thus enabling the development of technology that could save lives.

The 4th International Conference on Bio Signals, Images and Instrumentation (ICBSII-2018) was conceived with the thought of bringing together scientists, engineers and researchers from various domains all over the world.it has been a platform where some of the greatest minds of the country and abroad could interact, exchange ideas and work together towards a common goal.

Research papers were received from diverse areas such as Physiological Modeling, Medical Imaging, Medical Robotics, Biomechanics, Biomedical Instrumentation and Nano-materials amounting to a total of 69 papers. After a rigorous review process by an expert review committee, 29 papers that displayed quality in idea and work were selected for final presentation at the conference.

This conference is the fruit of a vision of the Management, faculty and students of the Department of Biomedical Engineering, SSN College of Engineering in association with the Centre for Healthcare Technologies (CHT), a multi-disciplinary R&D centre, who worked unanimously towards materializing it and were instrumental in its success.

The Department of Biomedical Engineering, since its inception in 2005, has been a pioneer in the field of biomedical technology, instrumentation, and administration. The department has excellent infrastructure, experienced faculty members and motivated students. Department also has several foreign collaborations which includes Birmingham University, UK, Drexel University, Philadelphia, USA, Neolight LLC, USA, Wildbox Technologies Pvt Ltd., Singapore and several industries such as L&T Medical System, Texas Instruments, National Instruments, Chettinad Hospitals and Sri Ramachandra Medical College. To add feather to the crown, the department has conducted three International conferences (ICBSII) in 2013, 2015, 2017 and two national conferences (NCABES) in 2014, 2016.